Subband Investigation of Continuous Volcanic Tremor

Joshua P. Jones

A dissertation
submitted in partial fulfillment of the
requirements for the degree of

Doctor of Philosophy

University of Washington

2009

Program Authorized to Offer Degree:

Department of Earth and Space Sciences

In presenting this dissertation in partial fulfillment of the requirements for the doctoral degree at the University of Washington, I agree that the Library shall make its copies freely available for inspection. I further agree that extensive copying of the dissertation is allowable for scholarly purposes, consistent with "fair use" as prescribed in the U.S. Copyright Law. Request for copying or reproduction of this dissertation may be referred to ProQuest Information Learning, 300 North Zeeb Road, Ann Arbor, MI 48106-1346, 1-800-521-0600, to whom the author has granted "the right to reproduce and sell (a) copies of the manuscript in microform and/or (b) printed copies of the manuscript made from microform."

Signature _____

Date _____

University of Washington

Abstract

Subband Investigation of Continuous Volcanic Tremor

Joshua P. Jones

Chair of the Supervisory Committee:

Professor Emeritus Stephen Malone

Department of Earth and Space Sciences

This research analyzes subbands of continuous volcanic tremor in an attempt to better understand the properties of its (potentially many) seismic sources, and particularly to understand the changing spectral content of continuous volcanic tremor. A new method for analyzing volcanic tremor is presented, which uses properties of undecimated wavelet packet transforms to decompose, and recover signals from, continuous multichannel data. The method preserves many standard properties that are used to characterize tremor in the volcanological literature, such as wavefield polarization and seismic energy. Tests on synthetic data show that

signals can be recovered in very noisy environments. Using data from Mt. Erebus (Antarctica), Erta 'Ale (Ethiopia), and Mt. Etna (Italy), this method suggests that continuous volcanic tremor generally has multiple, simultaneously active seismic sources, and that not all of these sources are persistent. At Erebus, several signals are recovered, including at least two low-frequency signals from isotropic, non-volcanic sources, and a high-frequency signal of probable volcanogenic origin. At Erta 'Ale, several signals can be seen that suggest continuous tremor was simultaneously generated by magma flow in a conduit, degassing at a system of fumaroles, gas bubbles coalescing in the shallow, active lava lake, and degassing in a crater that formerly held a lava lake. The spectral transitions seen at Erta 'Ale in 2002 are resolved using this method, and result from secondary signals introduced during rapid convection. These secondary signals can be explained entirely by cooled surface crust sinking at the edges of the active lava lake. At Mt. Etna, the background tremor is shown by this method to undergo virtually no changes in response to unrest. However, changing low-frequency signals can be recovered from the Etna data before and during the paroxysm of 23-24 Nov 2006, which suggest that decomposing tremor into subbands could recover precursors to volcanic unrest that cannot be easily detected by conventional means.

TABLE OF CONTENTS

Page

LIST OF FIGURES

Page

LIST OF TABLES

Page

ACKNOWLEDGEMENTS

The author wishes to express his gratitude for the gracious and extended support of the University of Washington Department of Earth and Space Sciences. Special thanks are due to Professor Don Percival of the University of Washington Applied Physics Laboratory and Professor Anthony Qamar of the University of Washington Department of Earth and Space Sciences for many illuminating discussions. The author thanks Professor Andy Harris of the University of Hawai'i for discussions and loan of radiometers; Professor Jeff Johnson of the University of New Hampshire for the loan of acoustic microphones; Dr. Susanna Falsaperla of INGV-Catania for Mt. Etna data; and Professor Rick Aster of the New Mexico Institute of Mining and Technology for Mt. Erebus data and discussions. Special thanks to the staff of Red Jackal Tours, Addis Ababa, Ethiopia, for solving many challenging logistics problems, and to Jim Ramey of the Pacific Northwest Seismic Network, for extensive troubleshooting and equipment testing, without whose assistance this research would have been impossible. The author also wishes to thank his family and friends for their encouragement, support, and patience.

DEDICATION

To my father, who taught me to dream; to my grandfather, who inspired me to think; and to Marniy, for too many reasons to enumerate.

Introduction

Seismic data is the most common tool used in volcano monitoring. A fundamental goal in both volcanology and seismology is to understand the relationship between measurable properties of volcanic systems, such as their seismic signals, and physical changes at the volcanoes themselves. The term "volcanic tremor", as formally defined by Konstantinou and Schlindwein (2002), refers to a broad class of quasi-continuous seismic signals, whose relationship to volcanic processes has been the subject of increasing interest over the last several decades (e.g. McNutt, 1996; Aki, 1992). Any understanding of volcanic tremor must therefore necessarily begin with a review of its observed properties and their significance to the complex problem of understanding volcanic activity.

Several classification schemes have been proposed in the literature for volcanic tremor. Two of the best known examples are Power et al. (1994) and Minakami (1960). As a result, the class of signals called "volcanic tremor" is very broad. Volcanic tremor is often subdivided using terms that characterize its appearance and/or frequency content (e.g. Konstantinou and Schlindwein, 2002, Table I). The term variously describes observed signals with frequencies from as low as 0.02 Hz (de Martino et al., 2005) to 5+ Hz (e.g. Patanè et al 2008); observed ground velocities from as low as a few $\mu m\ s^{-1}$ at basaltic volcanoes (e.g. Carniel et al., 2003), to strong enough to feel (e.g. Fehler 1983); and durations ranging from

several tens of minutes to several tens of years (e.g. Carniel et al. 2003, Jones et al. 2006). For these reasons, restricting a detailed study to one specific sub-category of tremor signals makes the general problem of understanding *all* tremor far more tractable.

Because volcanic tremor usually lacks clear onsets or phases, relating measured amplitudes to seismic source properties – and thus, quantitatively comparing tremor at different volcanoes – can be difficult. Generally, the former requires enough additional information to constrain a source model. As perhaps the best-known example, when tremor location can be constrained, and site amplification can be estimated in some way, one can use the "reduced displacement" of Aki and Koyanagi (1981) to relate observed tremor amplitude to seismic moment rate (e.g. Arenal - Benoit and McNutt 1997, Shishaldin – Thompson et al. 2002). Ripepe et al. (1996) used infrasonic data to relate tremor displacement to pressure changes induced in magma by forced coalescence of gas bubbles. Thus, any study of volcanic tremor is best restricted to a group of volcanoes with similar eruptive behaviors, where seismic and non-seismic observations suggest similar tremor source mechanisms.

To simplify the terminology of this work, I adopt the following conventions. Recall first that a measured seismic signal can be written as the filtering of a source time series S(t) by a "path effect" filter P(t) and a "receiver effect" filter R(t) ,

$X(t) = S(t) * P(t) * R(t)$ (Lay and Wallace, 1995). By “input data” I refer to such filtered time series *X(t)*, i.e. the observed seismograms, except where specifically indicated. The term "recovered signal", on the other hand, refers to a signal (call this Y(t)) which is recovered from *X(t)* by mathematical means. It is not true that *Y(t)* is the direct expression of some seismic source *S(t)*, though it will be demonstrated that recovered signals sometimes have properties that can constrain seismic source processes.

To further simplify the terminology of this work, I use “high frequency” tremor to mean any observed signal *X(t)* whose peak spectral energy lies at frequencies above 1 Hz, “low frequency” as any observed signal *X(t)* with peak spectral energy of 0.1 Hz < f < 1 Hz, and “very low frequency” tremor as any signal *X(t)* with peak spectral energy below 0.1 Hz. I use the term “continuous tremor” for a signal *X(t)* which persists for durations greater than 60 min with little amplitude fluctuation, and "spasmodic tremor" as that with significant bursts superimposed on an otherwise continuous background signal. My use of the terms “monochromatic” and “harmonic” tremor follow the convention of Konstantinou and Schlindwein (2002): "harmonic" tremor refers to tremor whose spectrum features a fundamental frequency and higher order overtones, while "monochromatic" tremor shows a single sharp spectral peak. Other terms used to describe volcanic tremor will be introduced as needed.

Continuous, High Frequency, Inharmonic Tremor

Of the many seismic signals categorized as “volcanic tremor”, continuous, high-frequency tremor is among the least studied and least understood. The specific case of harmonic tremor has several models that describe its behavior at specific volcanoes (e.g. Chouet 1992, Julian 1994); however, this type of tremor is relatively rare compared to the inharmonic case, and is therefore not the subject of this research. Examples of volcanoes exhibiting continuous, inharmonic tremor include, but are not limited to, Ambrym, Vanuatu (Carniel et al. 2003); Bromo, Indonesia (Gottschämmer and Surono 2000); Deception Island, Antarctica (Almendros et al. 1997); Erta ‘Ale, Ethiopia (Harris et al. 2005, Jones et al. 2006); Kilauea, Hawai’i, USA (Goldstein and Chouet 1994); St. Helens, USA (Hofstetter and Malone 1986) Stromboli, Italy (Ripepe et al. 2002); Vatnajökull, Iceland (Konstantinou 1996); Villarrica, Chile (Calder et al. 2004); and White Island, NZ (Sherburn et al. 1998).

In the case of high viscosity magmas, with explosive eruptions, continuous inharmonic tremor has been modeled as the superposition of discrete low-frequency seismic events (e.g. Hofstetter and Malone 1986, Fehler 1983); however, even here there is some controversy, for as Konstantinou and Schlindwein (2002) remark, theoretical frequency domain modeling of tremor spectra and low-frequency earthquakes has suggested that many physical mechanisms can identically explain their similarity (Nishimura et al. 1995). In the other "end member" case, at low

viscosity, basaltic magmas where explosive eruptions are rare, successful models that characterize continuous tremor are generally less ambiguous about possible source mechanism, but are also restricted to very specific systems. Examples include Harris (2008) for Erta 'Ale, Ethiopia, Ripepe et al. (2002) for Stromboli, Italy, and Rymer et al. (1998) for Masaya, Nicaragua.

The case of continuous, inharmonic tremor is therefore interesting for two principal reasons. First, because volcanic systems can be extraordinarily complex, a serious effort to better understand even one sub-category of volcanic tremor must be restricted to the simplest volcanic systems at which that class of signals is observed. Basaltic volcanoes are generally thought to have the simplest magmatic system geometry (see e.g. Harris 2008, Ripepe et al. 2002, Harris and Stevenson 1997, Rymer et al 1998, Harris et al. 1999). Observing such “end member” cases might therefore allow volcanologists to better understand relationships between meaningful changes in different data, and between observed data and (changes in) eruptive activity. Second, the cause of continuous, inharmonic tremor at these volcanoes is not well understood. Even fundamental questions about the nature of these signals are generally not answerable on a broad scale, such as:

- Can (any part of) continuous, inharmonic tremor be associated with changes in eruptive behavior?

- What signals comprise the continuous tremor? How many seismic sources does the tremor have? Do these seismic sources have distinct spectral or temporal characteristics that can be recovered from the composite data?
- What physical processes are associated with these recoverable signals?

Each of these fundamental questions has been investigated to some degree. I now briefly review some important papers relevant to each.

Regarding the first question, the association of tremor with changes in eruptive behavior is not new, and extends to many classes of tremor signals; in fact this qualitative correlation often seems implicitly included in the definition of "tremor". In recent years, an abundance of new evidence suggests that continuous, inharmonic tremor has multiple or varying source processes, even at simple, relatively quiescent basaltic systems. For example, Ripepe et al. (2002) at Stromboli, Carniel et al. (2003) at Ambrym, Vanuatu, and Jones et al. (2006) at Erta 'Ale, Ethiopia, all found spectral transitions that suggested either a changing or additional seismic source $S(t)$ affecting the observed data. Similarly, Gottschämmer and Surono (2000) for Bromo, Indonesia and Jones et al. (2006) at Erta 'Ale, Ethiopia, found characteristic changes in tremor epicenters that seemingly corresponded to changes in eruptive behavior; these were specifically the amplitude of tremor in the former case, and the amplitude and spectral content of tremor in the latter case. Further, continuous tremor at Erta 'Ale exhibited spectral characteristics that corresponded roughly to

the rate of lava lake convection (Harris 2008, Harris et al. 2005). Such findings lead to still more fundamental questions about the nature of these signals, e.g.:

1.) Are there sources of seismic signals whose measurable, recoverable properties correspond in some way to changes in eruptive behavior?
2.) What do these tell us about physical sources of the tremor, and their use (if any) as a predictor of changes in volcanic activity?

Regarding the second question, numerous studies have attempted to constrain the possible sources of continuous, inharmonic tremor, via various forward and inverse methods. Specific cases relevant to this research include polarization studies, spectral analysis, and tremor locations.

Spectral analysis is perhaps the most common means of interpreting continuous, inharmonic tremor. Some of the more representative examples include Ambrym, Vanuatu (Carniel et al. 2003); Deception Island, Antarctica (Almendros et al. 1997); Erta ‘Ale, Ethiopia (Harris et al. 2005, Jones et al. 2006); Etna, Italy (e.g. Patanè et al. 2008); Kilauea, Hawai’i, USA (Goldstein and Chouet 1994, Aki and Koyanagi 1981), Stromboli, Italy (Ripepe et al. 1996); and White Island, New Zealand (Sherburn et al. 1998). Such studies typically report spectral content estimated using the Maximum Entropy Method of Burg (1967), which assumes only a stochastic time series. They can be quite useful for examining the influence of site effects (e.g. Goldstein and Chouet 1994), and identifying changes in long-term behavior of

volcanic systems (Carniel et al. 2003). However, spectral analysis methods in general, and FFT based methods in particular, are inappropriate if the observed data *X(t)* are non-stationary. In the case of tremor with changes in spectral content, such as Erta ‘Ale, Ethiopia (Harris et al. 2005), such a possibility cannot be ignored.

Polarization studies use interpretations of the well-known covariance matrix (Jurkevics 1988, Vidale 1986, Montalbetti and Kanasewich 1970) to constrain the seismic wavefield of 3-component data. This, also, has many uses, but is not without some controversy. For example, at Mt. Etna, Ferrucci et al. (1990) determined that the tremor consisted of P waves, while Wegler and Seidl (1997) reported primarily Love/SH waves at Etna in complicated overlapping patterns. Similar polarization studies of the seismic wavefield found predominantly S waves in the tremor of Arenal, Costa Rica (Benoit and McNutt 1997), and P waves at Stromboli, Italy (Falsaperla et al. 1998). Wave field polarization studies can be quite useful in eliminating some possible tremor sources. However, inherent in their assumptions is the notion that the entire frequency range being studied is generated by (the same) seismic source. Some recent studies (e.g. Ripepe et al., 2002, for Stromboli) suggest this is not always true.

Because tremor lacks clear onsets, one cannot constrain its source region using techniques from classical seismology. In other words, the traditional approach of using a velocity model to invert travel times for an origin point is totally

inapplicable. Obviously, the process of locating tremor is fundamental to understanding its source process: one can either relate tremor locations to meaningful geophysical sources (Furumoto et al. 1992, Kawakatsu et al. 2000), or observe how changes in tremor location correspond to changes in eruptive behavior (Jones et al. 2006, Gottschämmer and Surono 2000). I now briefly discuss some of the more common techniques that use seismic amplitude, seismic energy, or statistical properties of volcanic tremor to estimate its source location.

For two reasons, I do not include methods of spatial correlation coefficients (Aki 1957) in this discussion of tremor location techniques. First, the spatial correlation method assumes that the wavefield is mostly comprised of surface waves, while studies of high-frequency continuous tremor (see above) suggest that this is *not* the case. Second, spatial correlation does not locate a tremor centroid, or source region, although Chouet et al. (1998) showed that one can constrain a source region by applying this method to determine the source direction of a wavefield that impinges upon multiple seismic arrays.

Every method that can constrain a tremor centroid assumes that tremor propagates through a homogeneous medium, i.e. the complex velocity structure of volcanoes is not (and cannot easily be) taken into account. Tremor location techniques further assume that seismic amplitude decays in some way with distance, and do not account for absorption, scattering, and phase conversions. Researchers compensate

for the possibility of multiple sources (or correlated noise) by preprocessing data with a bandpass filter. Filtering parameters are determined using either outside information or *ad hoc* assumptions about the frequencies where a seismic source *S(t)* dominates.

Amplitude based location techniques (Patanè et al. 2008, di Grazia et al. 2006, Battaglia et al. 2005), assume that tremor amplitude decays according to some power law, and a grid search is performed to find the point at which observed amplitude decay best fits the calculated amplitude values. Misfit is determined based on the goodness of fit (R^2) obtained for each point. Patanè et al. (2008) use RMS amplitudes instead of average values to minimize the effects of transients. The exponent of amplitude decay that minimizes misfit is also sometimes a grid search parameter.

Energy based location techniques (Jones et al. 2006, Gottschämmer and Surono 2000) are a variant on methods that use amplitude, and assume that the seismic source decays as a body wave. Here the observed quantity is the "energy" of the velocity component seismograms, i.e.

$$E \equiv \int_{t_1}^{t_2} A^2 dt \qquad (1)$$

The measured quantity is the isotropic source power, which can be explicitly written

$$P = 4\pi R^2 \rho v e^{\kappa R} E \qquad (2)$$

Here density is ρ, phase velocity is v, (scalar) absorption coefficient is κ, and distance from the source is R. There are two possible refinements to this method. One refinement, which greatly increases computational efficiency, forms an overdetermined least-squares problem to invert for corrections to a trial location that minimize the difference between mean source power $\overline{P}$ and source power P_i at each seismic station,

$$\frac{\partial P_i}{\partial x_j} = 4\pi\rho v x_j e^{\kappa R}\left(2+\kappa R\right)E \qquad (3)$$

This was the method I adopted in Jones et al. (2006). The other refinement solves the problem using a three-dimensional grid, rather than least squares inversion, but takes an additional step that allows explicit computation of the χ^2 misfit; that method will be discussed in detail in this work.

Statistical methods of tremor location implicitly assume that some statistical measure of signal coherency is maximized in certain time windows because of phases arriving from a (single) source, which can be approximated by (or averaged to) a single "best fit" grid point. Researchers commonly use the semblance of Neidel and Taner (1971), which, for T total samples from a seismogram $X_k(t)$, recorded by station k out of K total stations, is defined

$$S \equiv \frac{\sum_{t=1}^{T}\left(\sum_{k=1}^{K} X_k(t)\right)^2}{K\sum_{t=1}^{T}\sum_{k=1}^{K} X_k^2(t)} \qquad (4)$$

One can calculate source-receiver travel times by changing the source location over a 3D grid, and evaluate S using the time delays associated with each grid point. The grid point that maximizes *S* is then said to be the tremor hypocentroid. The notion of semblance was be extended to the specific case of an isotropic source by Kawakatsu et al. (2000), in which case the semblance is implicitly weighted by the wavefield rectilinearity. Here, if data are rotated into a (body wave) azimuth and incidence angle (Jurkevics 1988), and one uses *R(t), V(t)* and *T(t)* to denote the rotated radial, vertical, and tangential components, then the "radial" or "waveform" semblance is defined as

$$S \equiv \frac{\sum_{t=1}^{T}\left(\sum_{k=1}^{K} R_k(t)\right)^2 - K\left(\sum_{k=1}^{K} V_k^2(t) + \sum_{k=1}^{K} T_k^2(t)\right)}{K\sum_{t=1}^{T}\sum_{k=1}^{K} R_k^2(t)} \qquad (5)$$

The radial semblance is commonly used to estimate the location of low frequency and very low frequency tremor, where the size *T* of the sample window is chosen to include only a few wavelengths of data (Almendros et al., 2002, Kawakatsu et al., 2000). The semblance of Neidel and Taner (1971) is more commonly used for high frequency data, where scattering and phase conversions can violate the assumption of a rectilinear wavefield.

There are, of course, natural objections to every method of examining volcanic tremor. First and foremost, large volcanic data sets demand efficient processing methods that accurately characterize the changing time-frequency content of the recorded signals. In the case of volcanic tremor, and specifically inharmonic, continuous volcanic tremor, one must consider the very real possibility of multiple discrete signals (e.g. explosions, hybrids, local transients) superimposed on a continuous background signal, or even multiple source signals being continuously generated. For such problems, where the notion of statistical stationarity may not apply, Fourier analysis may be inappropriate. It is similarly problematic to rely on techniques that assume the seismic wavefield has a single source signal $S(t)$, particularly when a wealth of evidence suggests this is not always true. I therefore take the following methodical approach, in order to better understand the properties, causes, and relationships of continuous, inharmonic, volcanic tremor.

First, I derive analysis methods which preserve many of the standard parameters (cf. Konstantinou and Schlindwein 2002) used to constrain the source(s) of volcano-seismic signals, but which are applicable to a seismic record comprised of *multiple* sources whose *composite* is the observed multichannel data. My methods employ a top-down, adaptive preprocessing algorithm to filter multichannel volcano-seismic data by selecting and grouping sub-bands of data in the wavelet domain based on the similarity and relative energy of their principal components. Wavelet transforms do *not* assume signal stationarity, and, as shall be shown, the subband analysis technique developed can recover signals from very noisy

environments. Using this method, I examine representative tremor samples from Erta 'Ale, Ethiopia, to demonstrate how many seismic sources can be simultaneously active, even at quiescent systems. I examine data from Erebus, Antarctica, to demonstrate the resolution and limitations of the algorithm. Finally, I examine sample data from Mt. Etna, Italy, to investigate the applicability of this method in detecting signals associated with volcanic unrest. Because of the useful properties of undecimated wavelet transforms, I am able to recover signals $Y(t)$ that constrain seismic sources $S(t)$ associated with such diverse geologic features as convecting lava lakes, fumaroles, and magmatic conduits. In at least one case, recovered signals detected using my method could even have been precursors to volcanic unrest.

Notes to Chapter I

Aki, K., 1957. Space and time spectra of stationary stochastic waves, with special reference to microtremors. *B. Earthq. Res. Inst. Tokyo Univ.* 25, 415-457.

Aki, K., 1992. State of the art in volcanic seismology. In: Gasparini, P., Scarpa, R., Aki, K. (Eds.), Volcanic Seismology. *IAVCEI Proc. Volcanol.* 3, 3-10.

Aki, K., Koyanagi, R.Y., 1981. Deep volcanic tremor and magma ascent mechanism under Kilauea, Hawaii. *J. Geophys. Res.* 86, 7095-7110.

Almendros, J., Ibanez, J.M., Alguacil, G., Del Pezzo, E., Ortiz, R., 1997. Array tracking of the volcanic tremor source at Deception Island, Antarctica. *Geophys. Res. Lett.* 24, 3069-3072.

Battaglia, J., K. Aki, Ferrazzini, V., 2005. Location of tremor sources and estimation of lava output using tremor source amplitude on the Piton de la Fournaise volcano: 1. Location of tremor sources, *J. Volcanol. Geotherm. Res.*, 147, 268-290.

Benoit, J., McNutt, S.R., 1997. New constraints on the source processes of volcanic tremor at Arenal volcano, Costa Rica, using broadband seismic data. *Geophys. Res. Lett.* 24, 449-452.

Burg, J.P., 1967. Maximum entropy spectral analysis. In: Childers (Ed.), Modern Spectral Analysis. New York: IEEE Press, pp. 34-41.

Calder, E.S., Harris, A.J.K., Peña, P., Pilger, P., Flynn, L.P., Fuentealba, G., Moreno, H., 2004. Combined thermal and seismic analysis of the Villarrica volcano lava lake, Chile. *Revista Geológica de Chile* 31(2), 259-272.

Carniel, R., Di Cecca, M., Rouland, D. 2003. Ambrym, Vanuatu (July-August 2000): spectral and dynamical transitions on the hours-to-days timescale. *J. Volcanol. Geotherm. Res.* 128, 1-13.

Chouet, B.A., 1992. A seismic model for the source of long period events and harmonic tremor. In: Gasparini, P., Scarpa, R., Aki, K. (Eds.), Volcanic Seismology. *IAVCEI Proc. Volcanol.* 3, 133-156.

Chouet, B., 1996. Long-Period volcano seismicity: its source and use in eruption forecasting. *Nature* 380, 309-316.

Chouet, B.A., De Luca, G., Milana, G., Dawson, P., Martini, M., Scarpa, R., 1998. Shallow velocity structure of Stromboli volcano, Italy, derived from small aperture array measurements of Strombolian tremor. *B. Seism. Soc. Am.* 88, 653-666.

De Martino, S. Falanga, M., Scarpa, R., Godano, C., 2005. Very-long-period volcanic tremor at Stromboli, Italy. *B. Seism. Soc. Am.*, 95:1186-1192.

Di Grazia, G., S. Falsaperla, Langer, H., 2006. Volcanic tremor location during the 2004 Mount Etna lava effusion, *Geophys. Res. Lett*., 33, L04304, doi:10.1029/2005GL025177.

Falsaperla, S., Langer, H., Spampinato, S., 1998. Statistical analyses and characteristics of volcanic tremor on Stromboli Volcano (Italy). *B. Volc.* 60(2), 75-88.

Fehler, M.C., 1983. Observations of volcanic tremor at Mt. St Helens volcano. *J. Geophys. Res.* 88, 3476-3484.

Ferrucci, F., Godano, C., Pino, N.A., 1990. Approach to the volcanic tremor by covariance analysis: Application to the1989 eruption of Mt Etna (Sicily). *Geophys. Res. Lett.* 17, 2425-2428.

Furumoto, M., Kunitomo, T., Inoue, H., Yamada, I., Yamaoka, K., Ikami, A. Fukao, Y., 1990. Twin sources of high-frequency volcanic tremor of Izu-Oshima Volcano, Japan. *Geophys. Res. Lett.* 17(1): doi: 10.1029/89GL03678. issn: 0094-8276.

Goldstein, P., Chouet, B., 1994. Array measurements and modeling of sources of shallow volcanic tremor at Kilauea volcano, Hawaii. *J. Geophys. Res.* 99, 2637-2652.

Gottschämmer, E., Surono, I., 2000. Locating tremor and shock sources at Bromo Volcano. *J. Volcanol. Geotherm. Res.* 101, 199-209.

Harris, A.J.L., 2008, Modeling lava lake heat loss, rheology, and convection, *Geophys. Res. Lett.*, 35, L07303, doi:10.1029/2008GL033190.

Harris, A.J.L., Carniel, R., Jones, J., 2005. Identification of variable convective regimes at Erta Ale Lava Lake. *J. Volcanol. Geotherm. Res.*, 142, 207-223.

Harris, A.J.L., Flynn, L.P., Rothery, D.A., Oppenheimer, C., Sherman, S.B., 1999. Mass flux measurements at active lava lakes: Implications for magma recycling. *J. Geophys. Res.* 104 (B4), 7117-7136.

Hofstetter, A.S., Malone, S.D., 1986. Observations of volcanic tremor at Mt. St Helens in April and May 1980. *B. Seism. Soc. Am.* 76, 923-938.

Jones, J., Carniel, R., Harris, A.J.L., Malone, S., 2006. Seismic characteristics of variable convection at Erta `Ale lava lake, Ethiopia, *J. Volcanol. Geotherm. Res.* 153, 64-79.

Julian, B.R., 1994. Volcanic tremor: nonlinear excitation by fluid flow. *J. Geophys. Res.* 99, 11859-11877.

Jurkevics, 1988. Polarization analysis of three-component array data. *B. Seis. Soc. Am.* 78, 1725-1743.

Kawakatsu, H., Kaneshima, S., Matsubayashi, H., Ohminato, T., Sudo, Y., Tsutsui, T., Uhira, K., Yamasato, H., Legrand, D., 2000. Aso94: Aso seismic observation with broadband instruments. *J. Volcanol. Geotherm. Res.* 101, 129-154.

Konstantinou, K.I., Schlindwein, V., 2002. Nature, wavefield properties and source mechanism of volcanic tremor: a review. *J. Volcanol. Geotherm. Res.* 119, 161-187.

Lay, T., Wallace, T.C., 1995. Modern global seismology. New York: Academic press.

McNutt, S.R., 1996. Seismic monitoring and eruption forecasting of volcanoes : A review of the state-of-the-art and case histories. In: Scarpa, Tilling (Eds.), Monitoring and Mitigation of Volcanic Hazards. Springer, Berlin, pp. 100-146.

Minakami, T., 1960. Fundamental research for predicting volcanic eruptions (Part 1). *B. Earthq. Res. Inst. Univ. Tokyo* 38, 497-544.

Montalbetti, J.F., Kanasewich, K.R., 1970. Enhancement of teleseismic body phases with a polarisation filter. *Geophys. J. R. Astron. Soc.* 21, 119-129.

Neidel, N., Tanner, M.T., 1971. Semblance and other coherency measures for multichannel data. *Geophys.* 36, 483-497.

Nishimura, T., Hamaguchi, H., Ueki, S., 1995. Source mechanisms of volcanic tremor and low-frequency earthquakes associated with the 1988-89 eruptive activity of Mt Tokachi, Hokkaido, Japan. *Geophys. J. Int.* 121, 444-458.

Patanè, D., Di Grazia, G., Cannata, A., Montalto, P., Boschi, E. 2008. The shallow magma pathway geometry at Mt. Etna volcano. *Geochem. Geophys. Geosys.* 9, doi: 10.1029/2008GC002131.

Power, J.A., Lahr, J.C., Page, R.A., Chouet, B.A., Stephens, C.D., Harlow, D.H., Murray, T.L., Davies, J.N., 1994. Seismic evolution of the 1989-90 eruption sequence of Redoubt volcano, Alaska. *J. Volcanol. Geotherm. Res.* 62, 69-94.

Ripepe, M., Poggi, P., Braun, T., Gordeev, E., 1996. Infrasonic waves and volcanic tremor at Stromboli, *Geophys. Res. Lett.* 23(2), 181–184.

Ripepe, M., Gordeev, E., 1999. Gas bubble dynamics model for shallow volcanic tremor at Stromboli, *J. Geophys. Res.* 104(B5), 10,639–10,654.

Rymer, H., van Wyk de Vries, B., Stix, J., Williams-Jones, G., 1998. Pit crater structure and processes governing persistent activity at Masaya Volcano, Nicaragua. *B. Volc.* 59, 345-355.

Sherburn, S., Scott, B.J., Nishi, Y., Sughihara, M., 1998. Seismicity at White Island volcano, New Zealand: a revised classification and inferences about source mechanism. *J. Volcanol. Geotherm. Res.* 83, 287-312.

Thompson, G., McNutt, S.R., Tytgat, G., 2002. Three distinct regimes of volcanic tremor associated with the eruption of Shishaldin Volcano, Alaska 1999. *B. Volc.* 64(8), 535-547.

Vidale, J., 1986. Complex polarization analysis of particle motion. *B. Seis. Soc. Am.* 76(5), 1393-1405.

Wegler, U., Seidl, D., 1997. Kinematic parameters of the tremor wavefield at Mt. Etna (Sicily). *Geophys. Res. Lett.* 24, 759-762

I. Subband Decomposition and Reconstruction of Multichannel Data

Background and Motivation

Large volcanic data sets demand efficient processing methods that accurately characterize the changing time-frequency content of the recorded signals. In the particular case of volcano-seismic data, each seismogram can be a composite waveform generated by many seismic sources, including quasi-continuous sources with superimposed transients. This research seeks an alternate means of characterizing seismic data that can isolate regions of the frequency spectrum where different sources dominate the energy.

The idea that volcano-seismic data has multiple sources is not new. However, in recent years, an abundance of evidence has arisen that suggests volcanogenic data can come from multiple sources, which are active at similar frequencies during the same time periods. Perhaps the best example comes from Stromboli, Italy, where Acenerse et al. (2004) determined that low frequency explosion seismograms consist of three mathematically independent components, with non-overlapping frequencies, corresponding to three separate regions of the conduit system. The best-studied example, however, is volcanic tremor, which is observed only near active volcanoes, and can last tens of minutes to tens of years (Konstantinou and Schlindwein 2002, Chouet 1996). For this particular class of volcano-seismic signal, Ripepe et al. (2002) for Stromboli, Italy, Carniel et al. (2003) for Ambrym, Vanuatu, and Jones et al. (2006) for Erta ‘Ale, Ethiopia, found

spectral transitions (and, in the latter case, corresponding changes in tremor epicentroids) that suggested either a changing source mechanism, or additional seismic sources generating signals that affect the seismic wave field. In the last example, we discovered that continuous tremor at Erta ‘Ale exhibited spectral characteristics that changed with the rate of lava lake convection, and that these changes occurred on scales as short as a few tens of minutes (Jones et al. 2006, Harris et al. 2005).

The ability to quantitatively divide the frequency spectrum of multichannel data into regions dominated by different recoverable signals would enable us to answer several fundamental questions about volcano-seismic data in general, namely:

3.) How many seismic sources comprise volcanic tremor? Do they change over time?

4.) Over what frequency ranges does each signal dominate?

5.) Is it necessarily true that a signal from a single seismic source dominates all parts of the spectrum where seismic energy is high?

Having no wish to rewrite volcano seismology to focus on an entirely new set of mathematical parameters, such a method should preserves many of the standard parameters (a good review of which is given in Konstantinou and Schlindwein, 2002), used to constrain the source(s) of volcanic tremor, but which is applicable to a seismic record comprised of *multiple* sources whose *composite* is the observed multichannel data. Ideally such a method should recover some of these

standard parameters about each input. Common examples of parameters used to interpret volcanic tremor include the polarization of 3-component data (e.g. Jurkevics 1988, Vidale 1986, Montalbetti and Kanasewich 1970), and the signal amplitude and energy, which can be used to locate the tremor centroid (e.g. Patanè et al. 2008, Gottschämmer and Surono 2000). Alternate means of locating tremor (e.g. Furumoto et al. 1992, Kawakatsu et al. 2000) are equally applicable if one can recover signals from each station whose coherency is maximized in certain time windows because of phases arriving from a (single) source.

Subband Decomposition and Reconstruction

It can be challenging to isolate which sources comprise the (composite) tremor data without making *ad hoc* assumptions. For example, for data comprised of transients superimposed on a continuous background signal, the notion of statistical stationarity may not even apply, which could potentially render Fourier analysis inappropriate. Thus the goal is a means of preprocessing volcano-seismic data sets which makes as few assumptions about the content of the data as possible.

We begin with only the following assumption: That there exists a subband (or subbands) of the frequency spectrum where seismic energy at some stations is dominated by a single recoverable signal. From this assumption, we develop a simple, efficient, "top-down" algorithm based on the undecimated (a.k.a. "maximal overlap") discrete wavelet packet transform (Percival and Walden 2000, Walden and Cristan 1998). Our algorithm makes use of top-down "best basis" methods

(Coifman and Wickerhauser 1992) which are similar to an algorithm proposed for medical by Oweiss and Anderson (2007). We follow a simple 4-step procedure:

1.) Determine the wavelet basis in which a single principal component most strongly dominates each wavelet packet.
2.) Hierarchically cluster the wavelet packets using information about the content of the signals of each.
3.) Inverse transform and sum, thereby filtering the input data to frequencies where the same signal dominates the seismic energy.
4.) Repeat step 3 for each recovered signal seen in the data.

Wavelet Decomposition and Representation

For purposes of this paper we use the following variation on standard notation: Assume that non-boldface variables (e.g. N) refer to scalars, and boldface variables (e.g. $\mathbf{h}$) refer to vectors. Assume that *uppercase* boldface variables (e.g. $\boldsymbol{X}_t$) refer to vectors of (or derived from) a single data channel with N data points, and that uppercase boldface variables with a bar (e.g. $\overline{\mathbf{X}}_\mathbf{t}$) refer to matrices of (or derived from) multi-channel data, having K channels and N data points.

Let us first review some relevant principles of wavelet transforms for a single time series $\boldsymbol{X}_t$, i.e. a single data channel at a single seismic station. The discrete wavelet transform of an input time series $\boldsymbol{X}_t$ to some level J is an orthonormal transform that uses a sequence of filtering operations to obtain wavelet coefficients $\boldsymbol{W}_j$ and scaling coefficients $\underline{\boldsymbol{V}}_j$, associated with weighted differences on

scales of $\tau_j = 2^{j-1}$. Whereas each DFT coefficient is associated with a particular frequency, each wavelet coefficient $\boldsymbol{W}_j(t)$ can be thought of as the difference in adjacent averages of $\boldsymbol{X}_t$ on scales of $\tau_j = 2^{j-1}$, centered about some time t. For a more in-depth review of the meaning of wavelet and scaling coefficients, see e.g. Percival and Walden (2000), Chapter 4.

The Discrete Wavelet Transform, or DWT, captures information about both the frequency and temporal content of the input data; this is contrasted with Fourier transforms, which characterizes the amplitude and phase of the frequency content. We can succinctly write $\boldsymbol{W}_j$ and $\boldsymbol{V}_j$ as circularly filtered convolutions of $\boldsymbol{X}_t$ with a wavelet filter $\mathbf{h}_l$ or scaling filter $\mathbf{g}_l$ using the recursion relations

$$\boldsymbol{W}_j(t) = \sum_{t=0}^{L-1} \mathbf{h}_l \boldsymbol{V}_{j-1,2t+1=l \bmod N_j - 1} \qquad \boldsymbol{V}j(t) = \sum_{t=0}^{L-1} \boldsymbol{g}_l \boldsymbol{V}_{j-1,2t+1=l \bmod N_j - 1} \qquad (1)$$

and by definition $\boldsymbol{V}_0 \equiv \boldsymbol{X}_t$. Here l is the index of the coefficient in a filter ($\mathbf{h}_j$ or $\boldsymbol{g}_j$), L is filter width, and N is the length of the input vector $\boldsymbol{X}_t$. A complete description of the DWT is given in Strang (1993), with detailed discussion in Daubechies (1992) and Chui (1997). Wasserman (1997) previously used the DWT to characterize and locate volcanic tremor at Stromboli.

A common variant on the discrete wavelet transform is the so-called maximal overlap discrete wavelet transform (MODWT), also called the undecimated, stationary, translation invariant, or shift invariant DWT (Greenhall 1991, Shensa 1992, Percival and Guttorp 1994, Coifman and Donoho 1995, Nason and Silverman 1995, Liang and Parks 1996, Percival and Mojfeld 1997). The

MODWT carries out filtering steps nearly identical to the DWT, only with no decimation (down sampling by 2) at each successive level j. Several useful mathematical properties of the MODWT are described in Walden and Cristan (1998) and Percival and Walden (2000). Here, we list only those relevant to this research:

I. Because the MODWT does not downsample, the sample length N for the input time series $\boldsymbol{X}_t$ need not be a power of 2. (Percival and Guttorp 1994)

II. Inverse transforming the MODWT creates so-called "detail" coefficients or "details" D_j and "smooths" S_J that form a multi-resolution analysis of $\boldsymbol{X}_t$; that is,

$$\boldsymbol{X}_t = \boldsymbol{S}_J + \sum_{j=1}^{J} \boldsymbol{D}_j$$

III. D_j and S_J are associated with zero phase filters (Percival and Mojfeld 1997); thus, each wavelet coefficient vector $\boldsymbol{W}_j$ forms a subband of the frequency range [0 f_n]. Further, for the Daubechies (1992) “least asymmetric” class of wavelet and scaling filters, the MODWT wavelet coefficients can easily be shifted to align in time with features in the original time series. (McCoy et al. 1995)

IV. The MODWT preserves energy. For a MODWT of an input time series $\boldsymbol{X}_t$ to any level J, $\|\boldsymbol{V}_J\|^2 + \sum_{j=1}^{J} \|\boldsymbol{W}_j\|^2 = \|\boldsymbol{X}_t\|^2$ (Percival and Walden 2000). This property is not shared by the detail coefficients, which follows from (II) and the Schwarz inequality.

V. Wavelet transforms can estimate the time-varying cross-correlation of 3-component seismic data in a subband, and hence its polarization. (Anant and Dowla 1997, Lily and Park 1995)

The maximal overlap discrete wavelet packet transform (MODWPT) of Walden and Cristan (1998) generalizes the MODWT by recursively filtering an input time series $\boldsymbol{X}_t$ with all possible combinations of the (rescaled) wavelet filter $\mathbf{h}_l$ and scaling filter $\mathbf{g}_l$, without down sampling $\mathbf{W}_{j,n}$ by 2 at each successive level j. A sample selection of filters used to create the MODWPT to level j=2 is given in Fig. 1.1, along with their squared gain functions at unit sampling frequency. Observe that, for data sampled Δ times per second, each wavelet packet $\boldsymbol{W}_{j,n}$ is associated with frequencies in the nominal passband

$$\frac{\Delta * n}{2^{j+1}} < f \le \frac{\Delta * (n+1)}{2^{j+1}} \qquad (2)$$

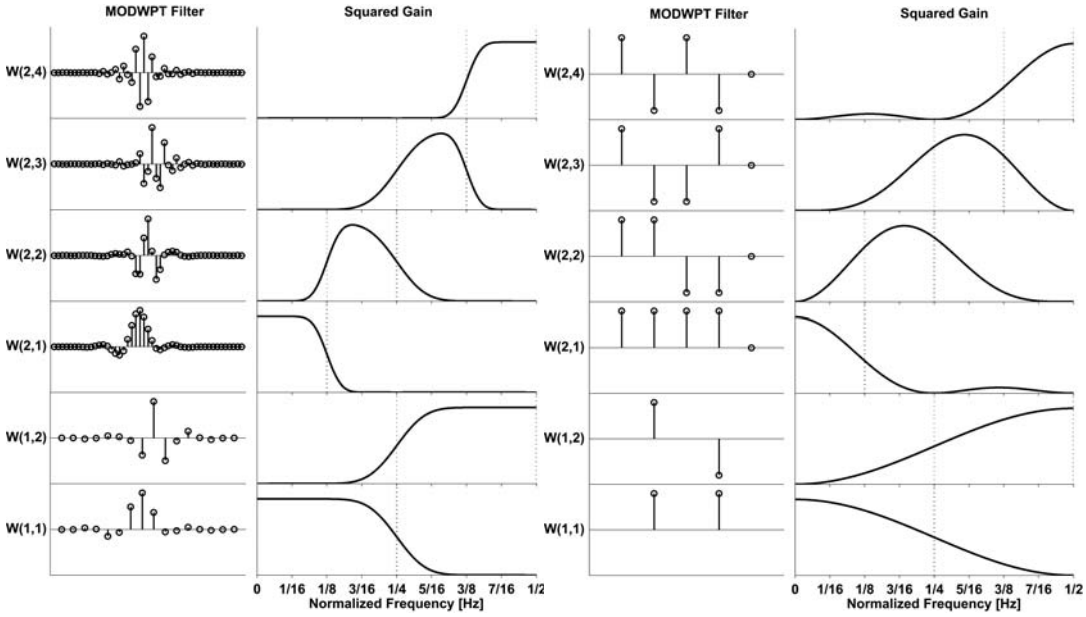

Figure 1.1. Wavelet packet filters and corresponding squared gain functions that create a MODWPT to level $j = 2$. **Left:** The LA16 wavelet. **Right:** The Daubechies-2 or 'Haar' wavelet.

It is clear from Fig. 1.1 that the MODWPT forms an overcomplete representation of the frequency range [0 f_n]. The idea behind the MODWPT is thus to compute a generalized, highly redundant table of non-decimated wavelet packet vectors $\widetilde{\boldsymbol{W}}_{j,n}$. For each successive level j of the MODWPT, one filters each wavelet packet $\widetilde{\boldsymbol{W}}_{j-1,n}$ with (rescaled wavelet or scaling) coefficients $\widetilde{\mathbf{u}}_{n,l} \equiv \mathbf{h}_{n,l} / \sqrt{2}$ (or $\widetilde{\mathbf{u}}_{n,l} \equiv \mathbf{g}_{n,l} / \sqrt{2}$ depending on sequency) to create vectors $\widetilde{\boldsymbol{W}}_{j,2n}$ and $\widetilde{\boldsymbol{W}}_{j,2n+1}$, respectively. At each successive level j, we can write the equivalent recursive filtering operation to obtain $\widetilde{\boldsymbol{W}}_{j,n}$ as

$$\widetilde{\boldsymbol{W}}_{j,n}(t) = \sum_{l=0}^{L_j-1} \widetilde{\mathbf{u}}_{n,l} \widetilde{\boldsymbol{W}}_{j-1,\left\lfloor \frac{n}{2} \right\rfloor, t-2^{j-1} l \bmod N_{j-1}} \tag{3}$$

where we define $\widetilde{\boldsymbol{W}}_{0,0} \equiv \boldsymbol{X}_t$. Using this more general notation, the MODWT coefficients W_j (and corresponding detail coefficients D_j) correspond to wavelet packets $\widetilde{\boldsymbol{W}}_{j,1}$ for any level j. The "scaling coefficients" V_J and corresponding "smooths" S_J correspond to wavelet packet $\widetilde{\boldsymbol{W}}_{J,0}$ and its inverse transformed detail coefficients $D_{J,0}$. For convenience, as the rest of this manuscript deals exclusively with the MODWPT, we will abbreviate $\widetilde{\boldsymbol{W}}_{j,n}$ as $\boldsymbol{W}_{j,n}$ and henceforth assume non-decimation.

Percival and Walden (2000) showed that any complete partition of the frequencies $[0, f_N]$ using wavelet packets $\boldsymbol{W}_{j,n}$ is an orthonormal transform. Thus, any MODWPT basis shares properties I-V of the MODWT. The collection of all wavelet packets for all levels $1 \le j < J$ is called a wavelet packet (WP) table.

Wavelet Basis Selection for Multichannel Data Using the MODWPT

We can extract many different orthonormal transforms from a WP table. Many algorithms and cost functionals have been devised to determine the “best” wavelet packet basis for single channel data, a problem first addressed by Coifman and Wickerhauser (1992). Such algorithms select parts of the wavelet packet tree

that evaluate the characteristics of input data $\boldsymbol{X}_t$ using some cost functional $m(\boldsymbol{W}_{j,n})$, which is associated with each wavelet packet vector $\boldsymbol{W}_{j,n}$. The wavelet basis that satisfies

$$\min_{C} \sum_{(j,n)\in C} m(\boldsymbol{W}_{j,n}) \tag{4}$$

is the “best” representation of the data in the wavelet domain. Several such algorithms are described in the literature; the best known and most widely used is Wickerhauser (1994).

Unfortunately, algorithms applicable to a single input time series are not necessarily appropriate for multichannel data. For real seismic data, the data channels containing the highest energy naturally have the highest associated cost, and therefore most significantly affect the calculation. In the ideal case of a single seismic source recorded by multiple receivers, with no glitches, transients, or additive noise, wavelet packet vectors are weighted for each station by the same power law as the falloff rate of the energy in the frequency range of equation (2). One natural problem, however, is that the “best basis” determined by such algorithms can be skewed by one channel of bad data.. Another is that, with multiple sources having different relative energies at each station, summing costs for each node of the wavelet packet table over each data channel are not necessarily appropriate.

The problem of determining a "best" wavelet decomposition for multichannel data was partially addressed by Oweiss and Anderson (2007), who

derived a multichannel cost functional relating the eigen decomposition of each wavelet packet $\overline{W}_{j,n}$ to that of $\overline{\mathbf{X}}_{\mathbf{t}}$. Such an approach is designed to guarantee that the "best basis" is also the best fit of the wavelet packet transform to the input data, and is suitable for problems with broadband sources whose spectra span [0 f_n]. However, multiple studies of continuous volcanic tremor (e.g. Jones et al. 2004, Gottschämmer and Surono 2000, Konstantinou and Schlindwein 2002), and generally almost any other volcano-seismic data set (e.g. Sherburn et al. 1998, McNutt 1996), suggest that real seismic sources often generate energy in a relatively narrow frequency band, and generally do *not* span the frequency range [0 f_n]. Thus, for volcano-seismic data sets, it is *not* necessarily true that the eigen decomposition of the covariance matrix of $\overline{\mathbf{X}}_{\mathbf{t}}$ is a suitable match to *every* subband.

Rather than approaching the problem of wavelet basis selection with the expectation that each $\overline{W}_{j,n}$ will match the eigen decomposition $\overline{\mathbf{X}}_{\mathbf{t}}$, we approach this problem with the expectation that we can find a wavelet decomposition of $\overline{\mathbf{X}}_{\mathbf{t}}$ whose subbands $\overline{W}_{j,n}$ are each nearly dominated by a single principal component (a notion widely assumed in volcano-seismological literature, as suggested by the references above).

Here we define a cost functional with this goal in mind for data from K seismic stations. Whereas conventional cost functionals seek to minimize an information cost, our goal is to select a basis based on the expectation that a single

principal component dominates (each part of) our observation matrix $\overline{\mathbf{X}}_\mathbf{t}$ in some subband of [0 f_n]. We can quantify this expectation by making note of the following properties of the principal components, i.e. eigenvalues $\lambda_{j,n,k}$ and eigenvectors $v_{j,n,k}$ of the covariance matrix of each wavelet packet (Pearson 1901):

A. For Gaussian data, the eigenvectors of the covariance matrix of each $\overline{W}_{j,n}$ point in the "direction" (in *K*-space) of the independent components, i.e. each eigenvector represents the relative strength of each independent component at each seismic station. Even for non-Gaussian or multi-modal Gaussian data, principal components analysis (PCA) de-correlates the axes of the independent components. (Hyvärinen et al. 2001).

B. The relative eigenvalues of the covariance matrix of each $\mathbf{W}_{j,n}$ correspond to the relative energies of the independent components. (see e.g. Shaw 2003)

The use of these properties is best illustrated with two conceptual examples. First, an eigenvector aligned almost exactly in *K*-space to a single station, whose corresponding eigenvalue is very large, could represent a local transient at that station. On the other hand, if the energies of the eigenvalues of one subband are nearly equal, and the eigenvectors seem randomly oriented, the subband is probably dominated by white noise.

Principal components analysis can produce erroneous results when trace data are out of phase, as the maxima at one station may align in time with the minima of another station. For this reason, and following from property V of wavelet coefficients, one can align the multichannel wavelet packet coefficients in a least-squares sense following the algorithm of Vandecar and Crosson (1990), prior to computing their principal components. This introduces some potential for cycle skipping, however, which must be controlled by carefully choosing a maximum lag for each pair of stations. We remark that this slows the algorithm slightly, because unshifted coefficients are needed to compute successive levels of $\mathbf{W}_{j,n}$ in iterative algorithms (e.g. Mallat 1999).

From these properties of principal components analysis, we can now define a cost functional based on how well a single principal component dominates a subband $\mathbf{W}_{j,n}$. For K stations, when $\lambda_{j,n,1}$ is large relative to $\lambda_{j,n,2}, \ldots \lambda_{j,n,K}$, we expect the ratio

$$\frac{\sum_{k=2}^{K} \lambda_{j,n,k}}{\lambda_{j,n,1}}$$

to be small. Recalling from (2) that each $\mathbf{W}_{j,n}$ is associated with a normalized bandwidth of approximately $\Delta/2^{j+1}$, we can define a cost functional directly from the above ratio, which accounts explicitly for this bandwidth:

$$M(\mathbf{W}_{j,n}) \equiv \frac{\sum_{k=2}^{K} \lambda_{j,n,k}}{\lambda_{j,n,1}(2^{j+1})} \qquad (5)$$

This cost functional behaves similarly to the entropy-based cost functional of Coifman and Wickerhauser (1992) and Wickerhauser (1994), but is bounded by $0 \leq M(\mathbf{W}_{j,n}) < (K\text{-}1)/2^{j+1}$. However, it must be noted that, like the cost functional of Oweiss and Anderson (2007), this is no longer a true optimization problem, as the principal components of the input data are not necessarily inherited by each subband.

In fact this cost functional is best suited for almost the opposite situation, provided that we apply one additional constraint when selecting a wavelet basis. Using this cost functional in traditional "best basis" type algorithms determines those wavelet packets $\mathbf{W}_{j,n}$ which are most dominated by a single principal component. However, it is not necessarily true that the *same* seismic source (or equivalently the *same* principal component) will dominate each $\mathbf{W}_{j,n}$. In fact, due to the notorious complexity of tremor sources, it is likely that some $\mathbf{W}_{j,n}$, and their associated frequencies (2) will be dominated by very different seismic sources than others.

Thus, we constrain our basis selection algorithm in the following way. The similarity of the most energetic principal component in each wavelet packet is easily quantifiable by measuring the distance $d(\cdot)$ between eigenvectors $\mathbf{v}_{j,n,k}$, $\mathbf{v}_{j,n+1,k}$, corresponding to adjacent wavelet packets $\mathbf{W}_{j,n}$ and $\mathbf{W}_{j,n+1}$. Note, however, that the distance between eigenvectors must account for a possible sign change. Thus we compute distance from the trigonometric formula

$$d\left(v_{j,n,k}, v_{j,n+1,k}\right) = \sqrt{2 - 2\left|v_{j,n,k} \cdot v_{j,n+1,k}\right|} \quad (6)$$

If this distance falls below some predetermined threshold δ, we say that the dominant principal component of each is the same. Thus, we apply the following constraint when selecting a basis. At each parent node $\mathbf{W}_{j,n}$ in the wavelet packet tree, for wavelet levels $1 \leq j < J$, we replace child nodes $\mathbf{W}_{j+1,2n-1}$, $\mathbf{W}_{j+1,2n}$ with their parent node $\mathbf{W}_{j,n}$ if the following two criteria are met:

1. $M(\mathbf{W}_{j,n}) \leq M(\mathbf{W}_{j+1,2n-1}) + M(\mathbf{W}_{j+1,2n})$

2. $d(\mathbf{v}_{j+1,2n-1,1}, \mathbf{v}_{j+1,2n,1}) < \delta$

By proceeding down (or up) the wavelet packet table, we use this conditional basis selector to determine the subband decomposition in which the subbands are most dominated by one principal component each.

Wavelet Packet Clustering and Signal Reconstruction

If subbands in the wavelet basis can be grouped in some way, then summing the (inverse transformed) detail coefficients $\mathbf{D}_{j,n}$ of each cluster of subbands enables us to reconstruct our original observation matrix $\mathbf{X}_t$, filtered to those frequency bands where each recovered signal dominates. This provides us with a powerful preprocessing tool, as standard analysis methods (e.g. amplitude-based centroid location) act under the fundamental assumption that the energy in (some subband of) data is dominated by a single seismic source. Because we have already selected a wavelet basis using the first principal component $v_{j,n,1}$ of each subband, and

constrained our wavelet basis selection routine using the distance $d(\mathbf{v}_{j,n,1}, \mathbf{v}_{j,n+1,1})$ between the principal components of each subband, it is natural to group wavelet packets using hierarchical clustering (Jain et al. 1999), and the same threshold δ used as a constraint on the basis selection above.

This final step -- clustering, reconstruction, and summation -- essentially treats the wavelet filters $\mathbf{u}_{n,l}$ as orthogonal zero-phase filter banks. To see why this is possible, recall from Walden and Cristan (1998) that wavelet filters $\mathbf{u}_{n,l}$ are orthogonal, and consider the single-channel case $\boldsymbol{X}_t$. From Percival and Walden (2000) we have a convenient way to define the wavelet detail coefficients $\boldsymbol{D}_{j,n}$ for a single channel $\boldsymbol{X}_t$ in terms of the circular cross-correlation of wavelet filters with their corresponding wavelet packets $\boldsymbol{W}_{j,n}$:

$$\boldsymbol{D}_{j,n}(t) \equiv \sum_{l=o}^{L_j-1} \mathbf{u}_{j,n,l} \boldsymbol{W}_{j,n,t+l \bmod N} \tag{7}$$

where we define

$$\mathbf{u}_{j,n,l} \equiv (2^{-j/2}) \sum_{k=0}^{L-1} \mathbf{u}_{n,k} \mathbf{u}_{j-1,\left\lfloor \frac{n}{2} \right\rfloor, l-2^{j-1}k} \tag{8}$$

i.e. $\mathbf{u}_{j,n,l}$ is defined as the wavelet packet filter that directly creates $\boldsymbol{W}_{j,n}$ by circular convolution with $\boldsymbol{X}_t$. Percival and Walden (2000) have already shown that each wavelet detail vector $\boldsymbol{D}_{j,n}$ is equivalent to $\boldsymbol{X}_t$ convolved with a zero-phase bandpass filter. The idea that we can create a filtered time series merely by summing detail coefficients follows from expressing $\boldsymbol{X}_t$ as the sum of those detail coefficients $\boldsymbol{D}_{j,n}$

whose $\boldsymbol{W}_{j,n}$ belong to the best basis; expressed using (5), and noting from (6) that the detail coefficients are created from orthonormal $u_{n,l}$, we have

$$\boldsymbol{X}_t = (2^{-j/2}) \sum_{j=1}^{J} \sum_{n=0}^{2^j-1} \left(\sum_{l=o}^{L_j-1} \left(\sum_{k=0}^{L-1} \mathbf{u}_{n,k} \mathbf{u}_{j-1,\left\lfloor \frac{n}{2} \right\rfloor, l-2^{j-1}k} \right) \boldsymbol{W}_{j,n,t+l \bmod N} \right) \tag{9}$$

The desired result follows from taking the DFT of both sides of (8), multiplying each by its complex conjugate, and noting that cross terms vanish due to orthogonality of $\mathbf{u}_{n,k}$. The optimal passband of each detail coefficient $\boldsymbol{D}_{j,n}$ is, again, given by (2).

Algorithm Description

We now describe the algorithm that uses our cost functional to compute an iterative, top-down, wavelet decomposition of an observation matrix $\mathbf{X}_t$, clusters subbands $\mathbf{W}_{j,n}$ using the dominant principal component of each subband, and returns $\mathbf{X}_t$ filtered to those frequencies where each recovered signal dominates (we'll call this $\mathbf{X}_t'$). We first describe its use for single-component data, then discuss how to generalize to the case of 3-component data.

Step 1. Iterative, top-down wavelet decomposition. For each level j, beginning with j=1 (and recalling from above that we defined $\mathbf{W}_{0,0} \equiv \mathbf{X}_t$):

1. Compute wavelet packet coefficients $\mathbf{W}_{j,n}$ for each channel at each station. In practice, this not computed directly using the convolution of equation (3),

but is obtained using more efficient means, e.g. the pyramid algorithm of Mallat (1999).

2. Compute principal components $\mathbf{v}_{j,n,1}$ and "cost" $M(\mathbf{W}_{j,n})$ of the (possibly circularly shifted) wavelet packet coefficients.
    a. *For single-component data*, compute the principal components of the vertical component of each station.
    b. *For three-component data*, polarization filter the data, and compute the principal components of the most energetic (i.e. z') component from each station.
3. Compare the costs of the sum of each pair of "children" nodes, $M(\mathbf{W}_{j+1,2n})$ and $M(\mathbf{W}_{j+1,2n+1})$, with the cost of their parent node, $M(\mathbf{W}_{j,n})$.
    a. If $M(\mathbf{W}_{j+1,2n}) + M(\mathbf{W}_{j+1,2n+1}) > M(\mathbf{W}_{j,n})$, and $d(\mathbf{v}_{j+1,2n,1}, \mathbf{v}_{j+1,2n+1,1}) < \delta$, mark $\mathbf{W}_{j,n}$ as a member of the “best basis”, and do not compute wavelet packet coefficients for its children nodes.
    b. Otherwise, replace the cost of $\mathbf{W}_{j,n}$ by the sum of the costs of the children nodes, and continue down the wavelet packet table.
4. Repeat steps 1-3 as we move down the WP table, computing wavelet packet coefficients for those nodes whose parents do not belong to the best basis.
5. Stop either when an arbitrary level $j=J$ has been reached, or when there are no further “child” nodes available.

Step 2. Hierarchical clustering. In this step, we cluster the wavelet packets $\mathbf{W}_{j,n}$ belonging to the best basis. We use the distance $d(\cdot)$ given in (6) to measure the similarity between eigenvectors $\mathbf{v}_{j,n,1}$ of each $\mathbf{W}_{j,n}$. To determine whether the input data $\mathbf{X}_t$ is a good match to some subband of the data, the first eigenvector of the original observation matrix (i.e. $\mathbf{v}_{0,0,1}$) is included in clustering for comparison purposes.

Step 3. Signal reconstruction. Inverse transform each $\mathbf{W}_{j,n}$ in each cluster using (5) to create detail coefficients $\mathbf{D}_{j,n}$; summing $\mathbf{D}_{j,n}$ over all j,n corresponding to a cluster yields the filtered output $\mathbf{X}_t'$.

With regards to volcanoseismic data in particular, the following specific steps are performed to separate the subbands of K stations of 3-component data:

A.) Data are loaded and detrended. Instrument response is deconvolved, then reconvolved with a common filter.

B.) For each subband n at wavelet level j :

1) Wavelet coefficients $\mathbf{W_{j,n}}$ are computed via the pyramid algorithm of Mallat (1999).

2) For 3-component data, the method of Jurkevics (1988) is used to calculate the 3x3 covariance matrix from inner products of the 3 components. A similar method was used in Lilly and Park (1995) and Anant and Dowla (1997).

3) Eigenvalues and eigenvectors are computed for each 3-component station. Rectilinearity and planarity are computed as defined in Jurkevics (1988).

4) Define Z' at a given station/subband as $\mathbf{W_{j,n}}$ rotated into the eigenvector corresponding to the largest eigenvalue. This eigenvector is multiplied by -1 (if necessary) to force the vertical component to be positive.

5) Define R and T following the convention of Jurkevics (1988) by rotating into the azimuth of Z'. This ensures that detail coefficients $\mathbf{D_{j,n}}$ formed from R and T are always aligned identically relative to Z'.

6) Align Z' coefficients in time using the method of Vandecar and Crosson (1990) if each Z' wavelet packet vector correlates to at least one other Z' wavelet packet vector at a level of $r\,(1\text{-}p) \geq 0.1$. Here r is the maximum cross-correlation computed over a range of lag times determined from the estimated phase velocity and inter-station distance. p is probability of that maximum arising from random chance. A maximum of one under-constrained channel is allowed per subband.

7) The (possibly aligned) Z' are now used to calculate the K x K covariance matrix of the principal components. The total cost of this subband n at wavelet level j is given by equation (5).

8) The eigenvector $v_{j,n,1}$ corresponding to the largest eigenvalue $\lambda_{j,n,1}$ is saved, as is the cost and polarization.

9) Successive "child" nodes of each $\mathbf{W_{j,n}}$ are computed (if necessary) from the (unaligned) unrotated wavelet coefficients corresponding to the "parent" node. The (unaligned) rotated wavelet coefficients are used to form the detail coefficients $\mathbf{D_{j,n}}$.

For a matrix $\mathbf{X}_t$ with K stations and N data points, and wavelet packets grouped into P clusters, the algorithm returns P filtered sets of $3K$xN outputs $\mathbf{X}_t'$. Since this algorithm works from the top down, it is almost never necessary to compute a full MODWPT. In an ideal case, where one seismic source completely dominates a wide subband of the frequency spectrum, and there are not many stations included, real time implementation is possible on modern computing equipment. However, the lack of decimation when computing the DWPT does not allow the $O(KN)$ efficiency of Oweiss and Anderson (2007).

Tracking Signal Invariance using Principal Components

Implicit in this method is that the invariance of recovered signals $\mathbf{X}_t'$ can be tracked over time by examining the principal components of their constituent subbands. If all principal eigenvectors $v_{j,n,1}$ of the wavelet packets $W_{j,n}$ whose detail coefficients $D_{j,n}$ form a recovered signal $\mathbf{X}_{t1}'$ cluster to all principal eigenvectors $v_{j,n,1}$ of a recovered signal $\mathbf{X}_{t2}'$ from a later period, and the frequencies of their nominal passbands in (2) overlap, then it follows from the definition of a recovered signal that $\mathbf{X}_{t1}'$ and $\mathbf{X}_{t2}'$ are the same. This property is potentially useful for

determining the difference between whether a recovered signal $\mathbf{X}_t'$ changes over time, or whether there are merely different secondary signals superimposed upon regions of its source spectrum.

Applicability and Limitations

The method outlined above is naturally applicable to problems where the time-frequency content of data is similar at every station. It would thus be well-suited to narrow aperture array studies. However, it has natural limitations. First, particularly energetic broadband noise (such as wind noise) at one station can decouple the principal components of other stations. This is also true for significant data glitches. Second, this approach becomes less appropriate as intrinsic attenuation and geometrical spreading increasingly affect the frequency content of each station. To see why this is true, consider the double convolution that creates a seismogram from a single source function, $X(t) = S(t) * P(t) * R(t)$ (Aki and Richards, 2002). Even if the receiver functions *R(t)* can be neglected or deconvolved from each seismogram, path effects *P(t)* change the frequency content of each station. This is especially problematic in volcanic environments, where path effects are notoriously complex (e.g. Harrington and Brodsky 2007). So, for stations whose source-receiver distances vary greatly, subbands will be clustered using a "master station" approach: that is, each cluster of subbands is determined entirely by the station whose seismic energy in each subband is highest.

Now, recall that a non-volumetric source function *S(t)* (or even a volumetric source function in an inhomogeneous medium) generates at least two distinct phase arrivals (*P* and *S*) in the far field, and even a volumetric source has a transverse near-field term (Aki and Richards 2002). In the most general case, PCA decouples the axes of the mathematically independent inputs; however, these independent components are *any* signal whose mathematical properties (e.g. arrival time, frequency content) are different. Now, because the radiation patterns of *P* and *S* differ -- e.g. the orientation of the maximum energy of each phase is rotated 45° -- their relative amplitudes at each station also differ. Therefore one feature of this algorithm is that it could recover two (or more) signals for each unique source -- one for each region of the frequency spectrum in which a different seismic phase dominates the energy.

Performance Testing with Synthetic Data

Because this algorithm has been developed with volcanic tremor in mind, it is instructive to illustrate its ability to recover quasi-continuous signals under various circumstances that mimic real volcanogenic signals. To this end, two sets of Monte-Carlo simulations are performed using synthetic data buried in Gaussian noise. A sample of such data is given in Fig. 1.2. Both tests use the LA-16 wavelet, which offers a good balance between linear phase and compact length (Daubechies 1992), and whose detail coefficients are nearly perfect bandpass filters (Fig. 1.1a). MODWPT coefficients are computed to level $J = 7$. All tests use a clustering

threshold of $d = 0.3$ to group the principal eigenvectors $v_{j,n,1}$ of each $\mathbf{W}_{j,n}$. This is equivalent to a maximum average angle in K-space of $\theta = 17°$ between members of any two wavelet packet clusters.

In both sets of Monte-Carlo simulations, the inputs are three sinusoids of unit amplitude. The first test evaluates the algorithm's ability to recover signals as background noise becomes more energetic. The second test evaluates the algorithm's sensitivity to the number of channels, or stations, present. In both tests, the inputs are 3 sinusoids at $f = 1.5$ Hz, $f = 1.8$ Hz, and $f = 3.6$ Hz, sampled at 50 Hz for 81.92 sec. The first two sources differ in frequency by only slightly more than the passband width of each wavelet packet at level $J=7$ (from eqn. 2, ~0.195 Hz). Their closely spaced spectral peaks test the algorithm's sensitivity, while the third sinusoids tests whether the algorithm falsely detects harmonics when two sources are really unique.

For all tests, input amplitudes at each "station" (i.e. channel) are scaled by a random multiplier chosen from a normal distribution with $\mu = 1$ and $\sigma = 0.5$. Sinusoids are phase shifted randomly in each channel by -2π to 2π radians. Thus the randomly generated parameters of each simulation are Gaussian white noise and amplitude and phase of each of 3 inputs in each data channel. We restrict our $Kx3$ matrix $\mathbf{S}$ of input scale factors so that $\max(\mathrm{rms}(\mathrm{cov}(\mathbf{S})-\mathbf{I})) < 0.3$. Thus the amplitude falloff of one input is never proportional to another.

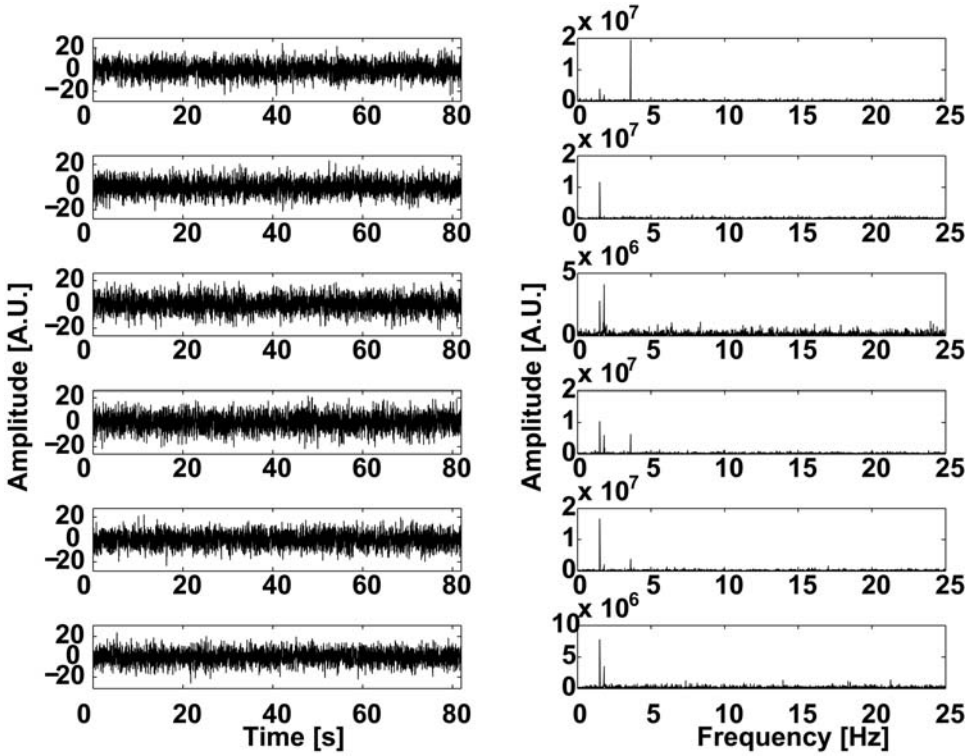

Figure 1.2. Sample synthetics and Fourier power spectra for three sinusoids at f = 1.5 Hz, f = 1.8 Hz, and f = 3.6 Hz, randomly phase shifted and masked by Gaussian white noise of 6x unit amplitude. Signal scaling is described in the text.

For the first set of simulations, 6 data channels (equivalent to "stations") are generated. Noise in each channel is multiplied by a scaling factor that increases from 0.1 to 100 in increments of $10^{0.2}$. 100 Monte-Carlo simulations are performed for each scale factor, making 1600 total simulations. The algorithm recovers each sinusoid independently in 1589/1600 tests (i.e. 99.3% success rate), without clustering them together. However, we remark that control tests of pure Gaussian white noise, containing no sinusoidal input, also recover each band independently in >95% of tests. A far more appropriate measure of *SDR*'s signal recovery ablity is the RMS error between the output signal $\mathbf{Y}_t$ that contains each sinusoid, and each

(scaled, shifted) input sinusoid $\mathbf{X}_t$. With 6 channels and 3 signals, each simulation produces 18 RMS values. A shaded intensity plot of $\log_{10}$(RMS) vs. noise scaling factor is given in fig. 1.3. Because the median amplitude of each input sinusoid is unity, this plot suggests that *SDR* recovers signals even when noise amplitude is almost an order of magnitude larger than input signal amplitude.

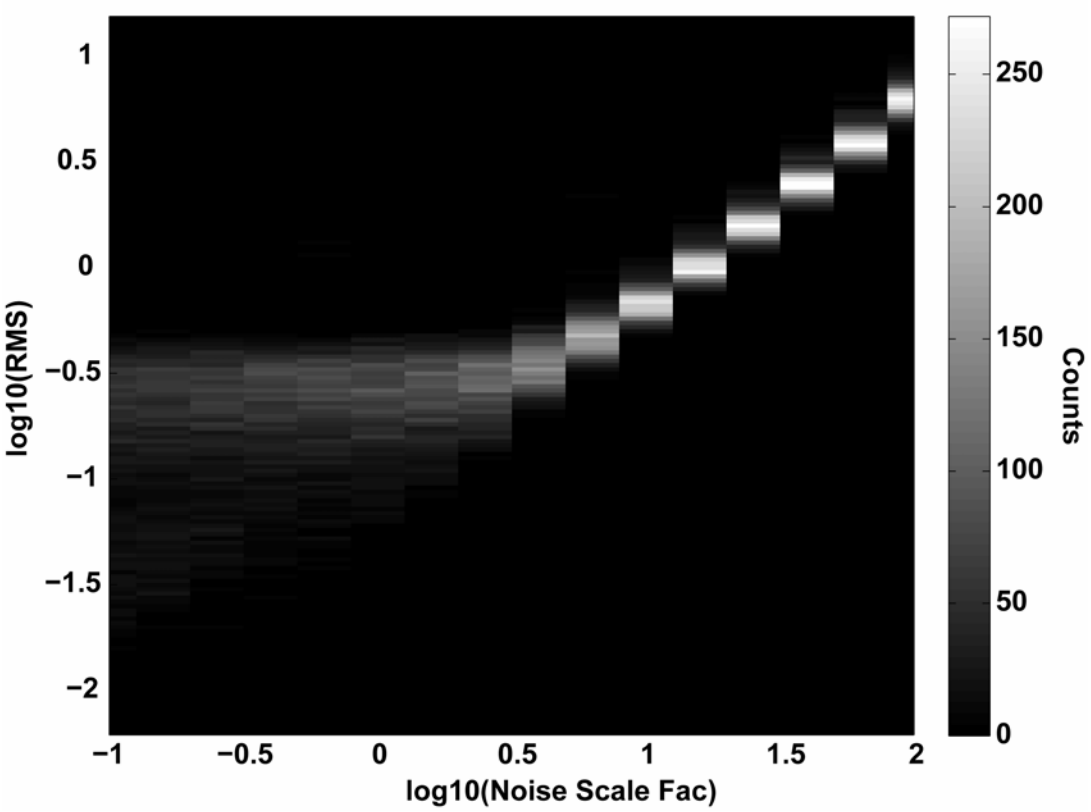

Figure 1.3. Shaded intensity plot of $\log_{10}$(RMS) of recovered signals as a function of noise amplitude scaling factor. Input signals are sinusoids whose median amplitude is unity.

It is similarly important to investigate how the number of channels of data affects performance, as this affect the cost functional (5) and the principal eigenvectors. Thus, a second set of simulations follows a similar process to the first

for generating noise, signal scaling, and phase shifts, but varies the number of channels from 3 up to 10. 100 simulations are performed for each number of channels. In each simulation, background noise is held constant at a scale factor of 4, which (from fig. 1.3) produces typical RMS values of 0.36 ± 0.08 with 6 data channels. Fig. 1.4 shows a plot of $\log_{10}$(RMS) vs. number of channels. The mean RMS of the recovered signals, and variations in RMS, are virtually unchanged when 5 or more channels are used. However, the mean RMS of recovered signals is factor of two greater (0.67 ± 0.41) when the number of data channels is reduced to 3.

It must be re-emphasized here that sampling interval and sinusoid frequencies were carefully chosen so that wavelet coefficients on the finest scale ($J = 7$) had nominal passbands narrower than the difference between the two closest spectral peaks. *SDR* cannot be expected to recover signals whose spectral peaks are closer together than this passband. In a hypothetical worst-case scenario, multiple signals with identical spectral peaks will prove indistinguishable.

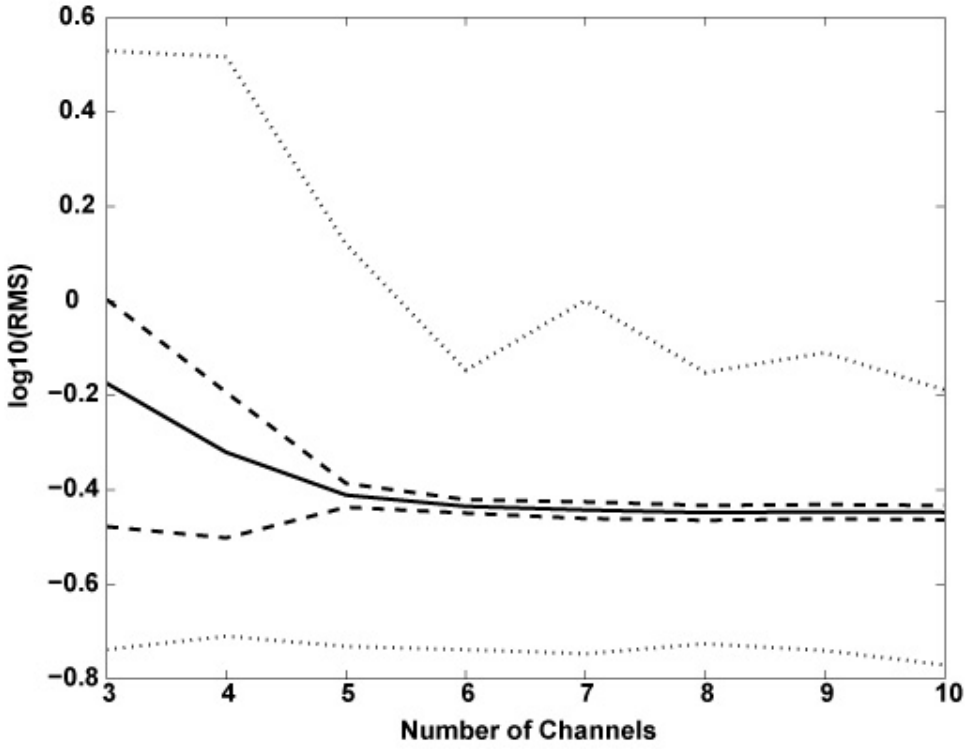

Figure 1.4. Plot of $\log_{10}$(RMS) of recovered signals as a function of number of channels used in *SDR*. Solid line indicates mean RMS of recovered signals in each set of simulations. Dashed lines indicate 2σ errors for each set of simulations. Dotted lines indicate maxima and minima of each set of simulations. Noise amplitude is held constant at a scale factor of 4. Input signals are sinusoids whose median amplitude is unity.

Performance Testing with Real Data: Erebus, Antarctica

To illustrate the use and limitations of this algorithm by example, we present a sample analysis of a half hour of continuous data recorded by the Mt. Erebus broadband seismic network. Mt. Erebus, Antarctica is a phonolitic stratovolcano which has held a persistent summit lava lake for decades (Aster et al. 2008, Giggenbach et al. 1973). The lava lake has frequent Strombolian surface eruptions

that produce VLP signals (Aster et al. 2008, Rowe et al. 2000), and short-lived tremor episodes, sometimes harmonic, with peak amplitudes of ~5 μm s^{-1} (Rowe et al. 2000, Knight et al. 1996). Erebus has been monitored by a telemetered seismic network since 1980 (Rowe et al. 2000, Kaminuma 1994, Kienle et al. 1981). It was suggested in Rowe et al. (2000) that sustained tremor could exist below the detection capabilities of the (triggered) seismic system. It is instructive to see which of these signals, if any, can be detected using *SDR*.

We begin with a 30 min segment of data recorded by 5 broadband CMG-40T (f_0 = 0.033 Hz) stations on Mt. Erebus (Fig. 1.5), beginning on 23 Jan 2006, 10:00 GMT. Raw data are shown in Fig. 1.6a. Fig. 1.6b shows a sample spectrogram of this data from the vertical component of station E1S, the closest station to the Erebus vent that was fully functional during the period examined. All data are publicly available from the IRIS archive (http://www.iris.edu). Data are sampled at 40 Hz, and horizontal components are pre-rotated so that the "1" component is radial to the Erebus vent and the "2" component is orthogonal to the radial component. Data are preprocessed by converting from counts to velocity (m s^{-1}), and a 3s cosine taper is applied to the edges of the data. *SDR* is then performed on this data sample using the LA-16 wavelet, with a clustering threshold of r = 0.3. The MODWPT is computed to a maximum wavelet level J =7, which, from the remarks of the previous section, suggests that the method can recover signals whose spectral peaks are more than 0.16 Hz apart.

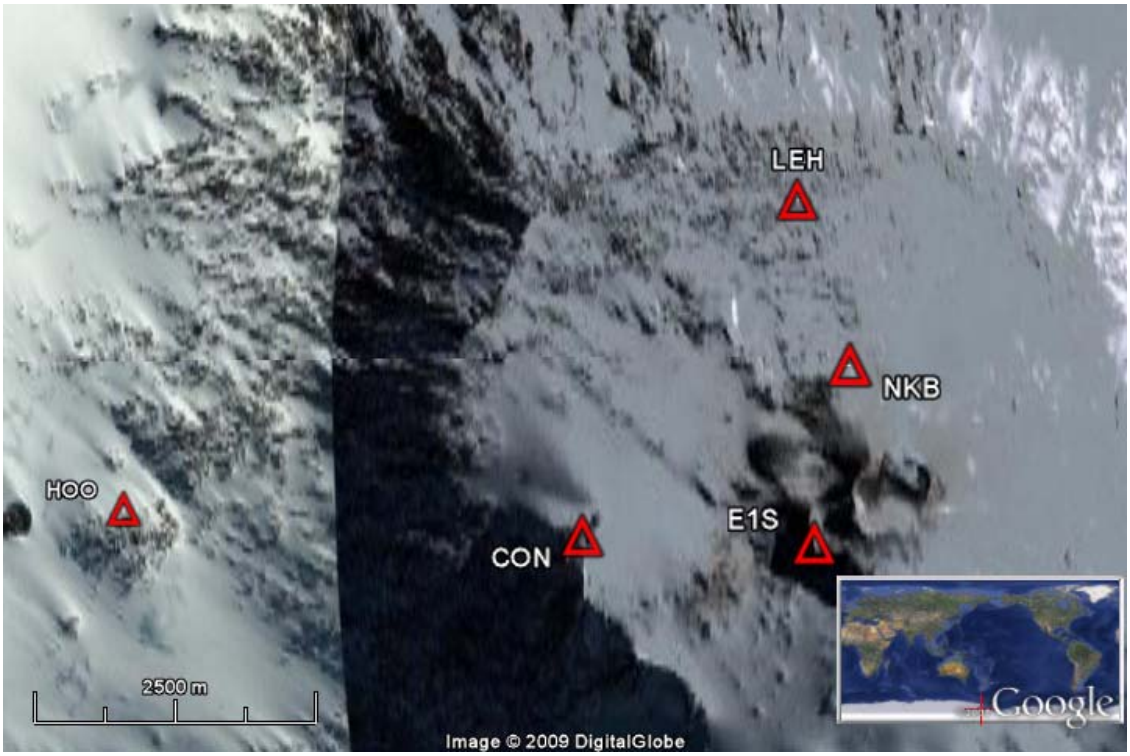

Figure 1.5. Station map of Mt. Erebus, Antarctica, showing the 5 permanent broadband stations (red triangles) at which the data sample was recorded. All stations use CMG-40T sensors (f_0 = 0.033 Hz) sampling at 40 Hz. Erebus vent is approx. 1 KM NE of station E1S and corresponds to origin of plume in photo.

Fig. 1.7a shows the wavelet basis selected to decompose the input data. Wavelet packet coefficients are shaded according to how they cluster, and arranged so that each $\mathbf{W}_{j,n}$ fills its nominal passband (from eqn. 2) at the appropriate wavelet level *j*. By convention the input data (i.e. the data shown in Fig. 1.6a) are placed on the frequency axis of Fig. 1.7a at level $j = 0$, and shaded according to how they cluster with subbands. It is obvious, from the squared gain functions of Fig. 1.1a, that some spectral leakage exists in a few wavelet packets. However, unlike Fourier-based spectral analysis, this spectral leakage is not an aliasing phenomenon, but a

consequence of wavelet filters being imperfect bandpass filters (Fig. 1.2). Thus the shaded plot in Fig. 1.7b shows the logarithmic ratio of energy *inside* each wavelet packet's passband to energy *outside* each wavelet packet's nominal passband. Wavelet packets that are not selected by the algorithm, and wavelet packets whose logarithmic spectral leakage ratio is greater than unity, are whited out in this figure.

Fig. 1.8 shows a dendrogram of the distances between principal eigenvectors $v_{j,n,1}$ of those $\mathbf{W}_{j,n}$ that form the subband decomposition in Fig. 1.7a. Each node of the dendrogram has been labeled with the passband of the corresponding wavelet packet. Clusters of wavelet packets are color-coded. The clustering of the input data is included for reference (labeled "X (0-20)"). 11 signals are recovered from this data sample. Each is described in Table 1.1, using common parameters such as polarization and energy (following the conventional definition $E \equiv \int_{t_1}^{t_2} W_{j,n,t}{}^2 dt$), the logarithmic spectral leakage fraction (defined in the preceding paragraph), and the nominal passbands of wavelet packets $\mathbf{W}_{j,n}$ whose summed detail coefficients $\mathbf{D_{j,n}}$ reconstruct each signal. The principal eigenvectors of each $\mathbf{W}_{j,n}$ are also given for reference.

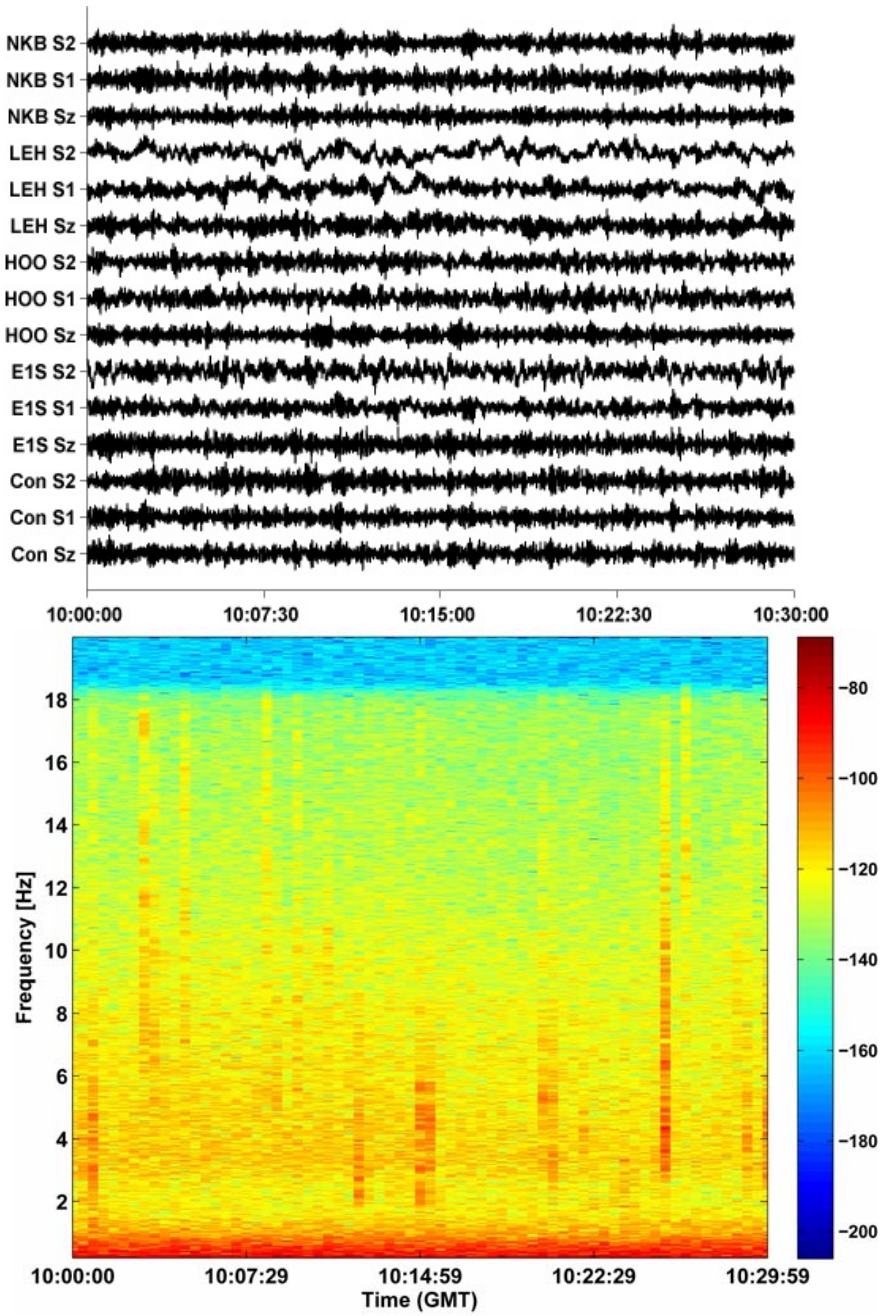

Figure 1.6. Sample data analyzed. **a.** (Top) Ampliute-normalized, detrended seismograms. Absolute amplitude scaling is removed to show detail. Sample begins on 23 Jan 2006 at 10:00 GMT. **b.** (Bottom) Spectrogram of *Z* component seismic data recorded by station *E1S*.

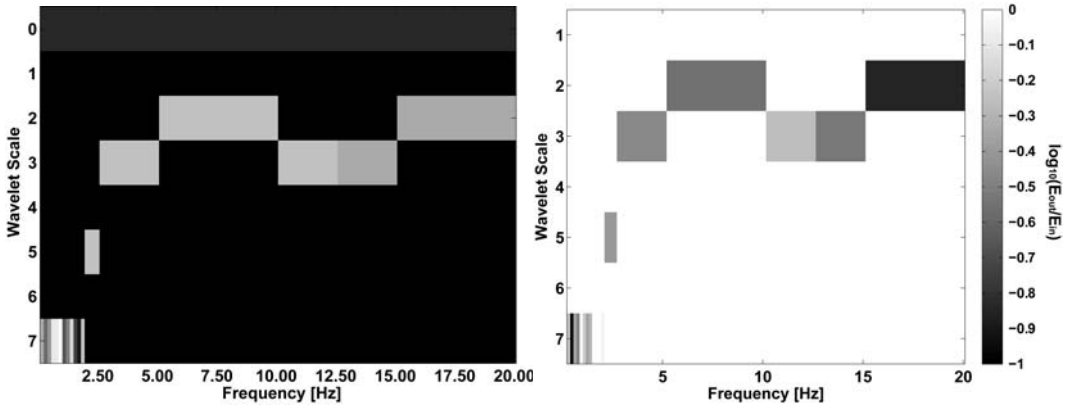

Figure 1.7. Wavelet basis selected to decompose the input data of Figure 1.6. **a.** (Left) Wavelet packets are shaded according to cluster, arranged so that each wavelet packet fills its nominal passband *n* (from equation 2 in the text) at the correct level *j*. By convention, the input data of Fig. 1.7a are placed at level $j = 0$, shaded according to how they cluster with their subbands. **b.** (Right) Spectral leakage for the wavelet basis of Fig. 1.7a, shaded in grayscale using the common log ratio of energy outside the passband to energy inside the passband. Wavelet packets that are not selected by the algorithm, or whose logarithmic leakage ratio is greater than unity, are whited out.

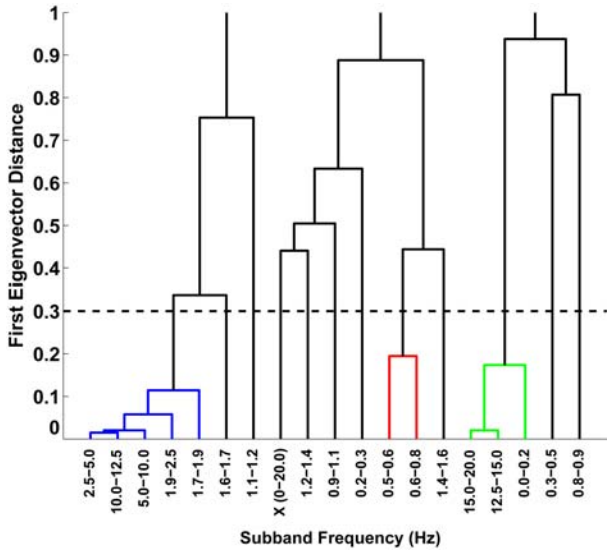

Figure 1.8. Dendrogram showing the clustering of principal components for the selected wavelet packets in Fig. 1.7a that decompose the data in Fig. 1.6a. Nodes that cluster below the Euclidean distance threshold $\rho = 0.3$ are labeled according to the nominal passband of each wavelet packet. The node corresponding to the input data $\mathbf{X}_t$ is labeled **X** (0-20).

It is illustrative to discuss some of the recovered signals in detail. Notably, no recovered signal has principal eigenvectors that fall within $\delta = 0.3$ of the principal eigenvector of the input data, an observation that nicely illustrates the importance of treating volcanogenic seismograms as composites. We further note that the greatest variation in recovered signal content is below 1.7 Hz, with many recovered signals in this range having nominal passbands only 0.16 Hz wide. For further discussion, these recovered signal will be named using the convention **ER(.)**. These numbers are a shorthand way of referencing each recovered signal, and do not correspond to any measure of e.g. principal eigenvector distance for subband clustering.

It is not necessarily true that every signal recovered by this method corresponds to a real seismic source. For example, **ER(1)** is formed from three subbands: $\mathbf{W_{7,0}}$ (nominal passband 0-0.16 Hz), $\mathbf{W_{3,5}}$ (12.5-15 Hz), and $\mathbf{W_{2,3}}$ (15-20 Hz). It is highly unlikely that a real seismic source coincidentally generates energy at periods $\tau > 6$ s and frequencies $f > 12.5$ Hz simultaneously. Inspection of the principal eigenvectors of this recovered signal (Table 1.1) reveals that these 3 subbands all lie within the clustering distance threshold $\delta = 0.3$ of the "axis" of station LEH in the 5-dimensional space defined by each station's *Z'* wavelet coefficients. Thus, this signal is not recovered from a single seismic source, but instead is formed from subbands dominated by energetic site noise at station LEH.

On the other hand, many low-frequency signals seem real. For example, wavelet packet $\mathbf{W_{7,1}}$ is the sole subband that forms recovered signal **ER(2)** (0.16-0.31 Hz). Unlike **ER(1)**, this recovered signal does not align with any station's "axis" in 5-dimensional space, though Table 1.1 suggests little signal contribution from station HOO. A plot of the *Z'* components of this recovered signal at stations CON, E1S, LEH, and NKB (Fig. 1.9a) verifies that the recovered signal contains coherent energy. The cross-correlation between stations E1S and CON, for example, attains a maximum value of $r = 0.93$, suggesting that the waveforms of this recovered signal are nearly identical at the two stations. Although the polarization of $\mathbf{W_{7,1}}$ is not rectilinear, the similarity of this signal's Z' components strongly suggests an isotropic source. The azimuths of $\mathbf{W_{7,1}}$ (Fig. 1.9b) are generally oriented N-S, and the signal energy is almost identical everywhere. Thus, this signal may be recovered from a persistent, low-frequency isotropic seismic source, but its origins are likely non-volcanic.

A similar result is obtained for recovered signal **ER(4)**, whose nominal passband is 0.47-0.78 Hz (Fig. 1.10a). The correlation coefficients at a maximum value of $r = 0.61$ between stations CON and E1S, but the azimuths of its subbands point toward a region several km from the active vent (Fig. 1.10b). Thus, the recovered signal **ER(4)** could come from a low-frequency, isotropic source, but it is unlikely that the seismic source recovered as **ER(4)** relates to eruptive activity at Erebus.

The other recovered signals are less apparent. As suggested by the data of Table 1.1, and particularly the principal eigenvectors of the subbands that form each signal, many of these signals have complex polarizations with no obvious physical interpretation.

One conspicuous signal merits further discussion. Shaded in blue in Fig. 1.7, **ER(11)** lies within the clustering distance threshold $\delta = 0.3$ of the "axis" of station E1S in the 5-dimensional space defined by each station's *Z'* wavelet coefficients. This suggests that this recovered signal contains local transients to E1S. However, an inspection of the recovered signal (Fig. 1.11a) suggests that these signals are coherent and real. Furthermore, its azimuths are clustered, and sometimes point toward the active vent (Fig. 1.11b). This recovered signal can only be interpreted as a grouping of (possibly many) seismic sources whose energy is highest at E1S. The transients in the recovered signal qualitatively resemble explosion signals described in Rowe et al. (2000), but are not preceded by VLP seismicity.

Even from this rudimentary analysis, we see immediately the value of quantitatively dividing the frequency spectrum into narrow subbands. Features such as the discrete events of Fig. 1.10a and the persistent low-frequency signal of Fig. 1.9a are not obvious in the wideband signals, nor are they easily obtainable from visual inspection, spectral analysis, or *ad hoc* bandpass filtering.

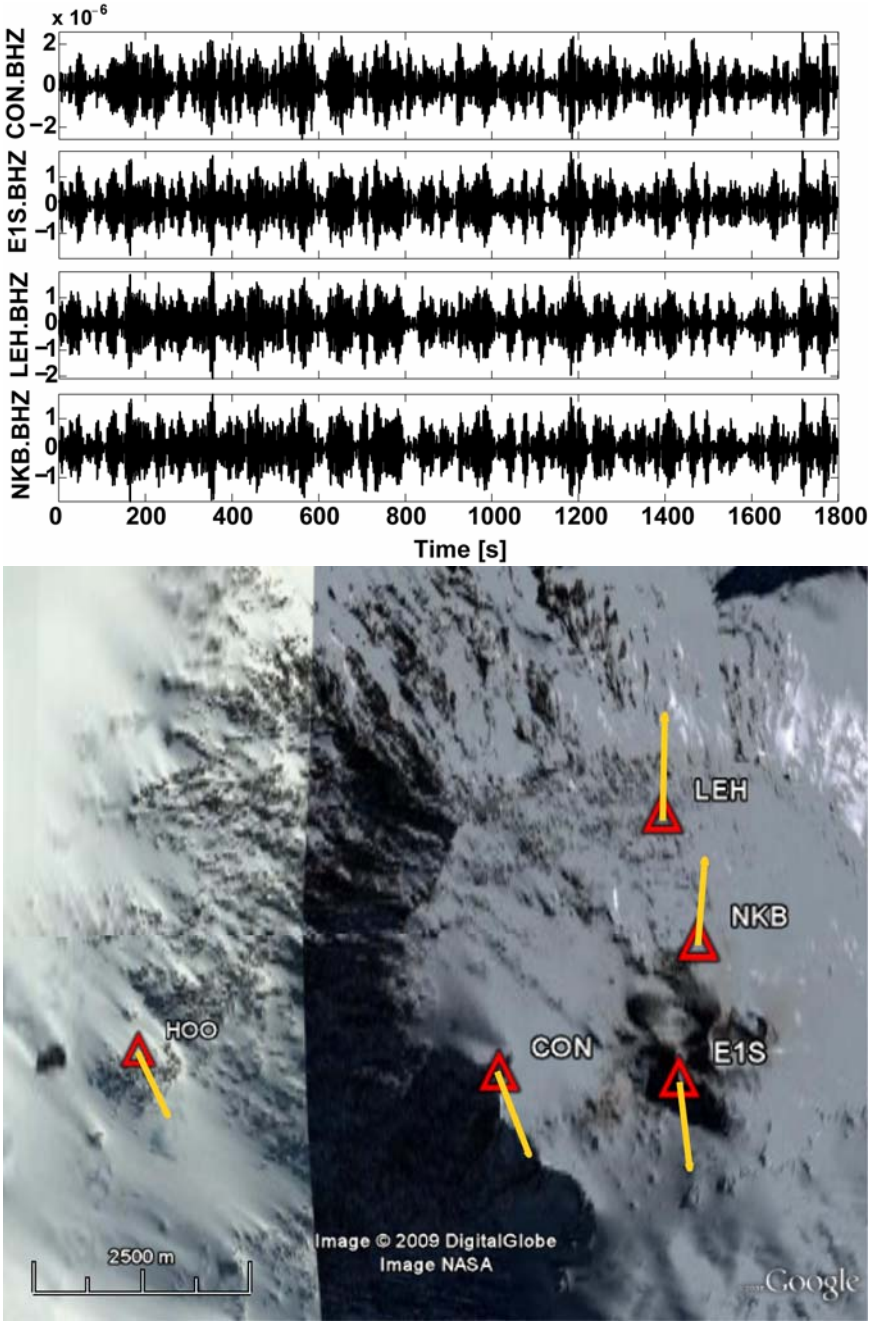

Figure 1.9. Sample data and polarization for recovered signal **ER(2)**. **a.** (Top) *Z′* components of recovered signal **ER(2)** (nominal passband 0.16-0.31 Hz), at stations CON, E1S, NKB, and LEH. **b.** (Bottom) Azimuth plots showing orientation of *Z′* components at CON, E1S, and NKB. Arrows are scaled according to the relative seismic energy at each station.

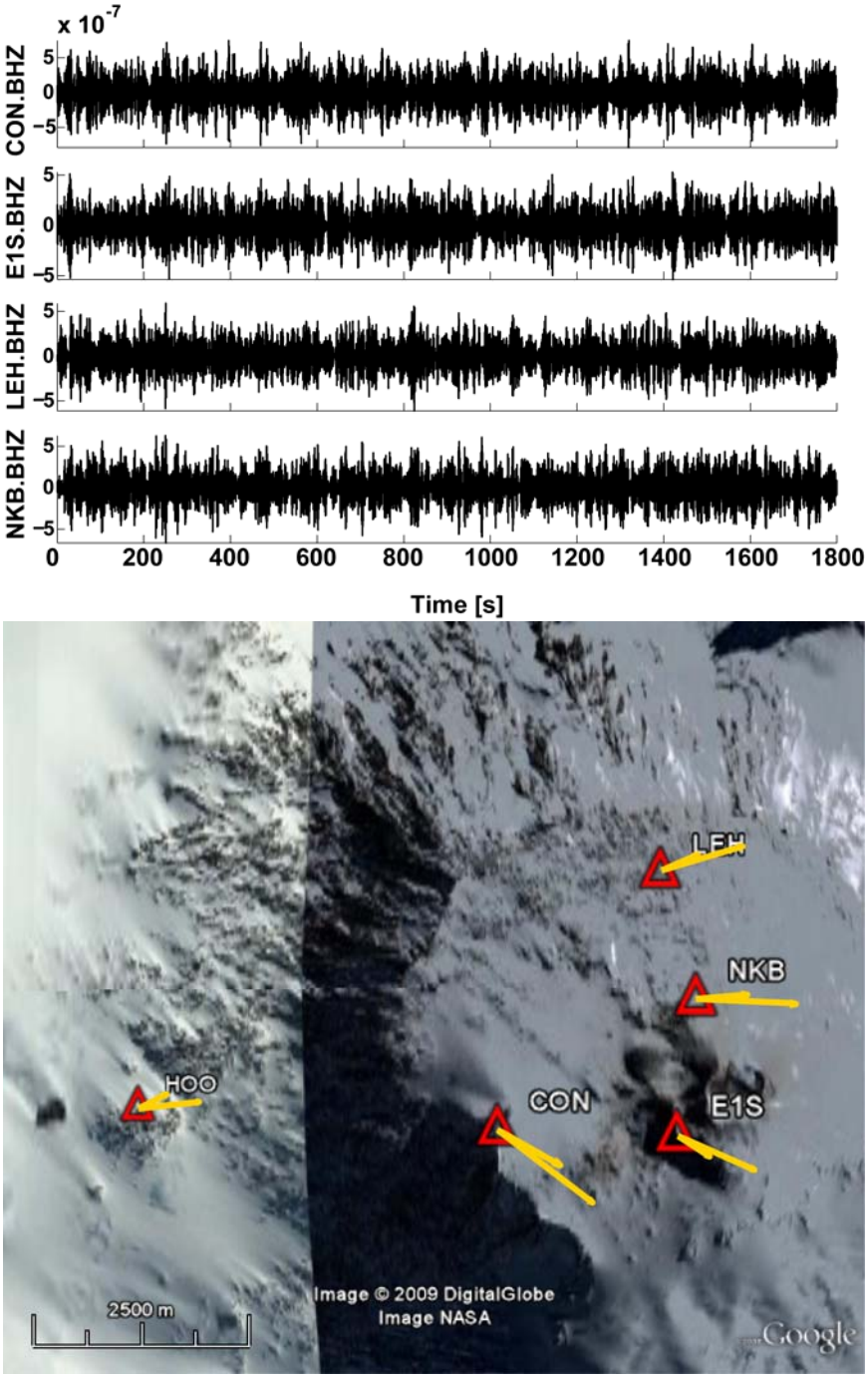

Figure 1.10. Sample data and polarization for recovered signal **ER(4)**. **a.** (Top) *Z*′ components of recovered signal **ER(4)** (nominal passband 0.47-0.78 Hz), at stations CON, E1S, NKB, and LEH. **b.** (Bottom) Azimuth plots showing orientation of *Z*′ components toward Erebus vent, at CON, E1S, and NKB. Arrows are scaled according to the relative seismic energy at each station.

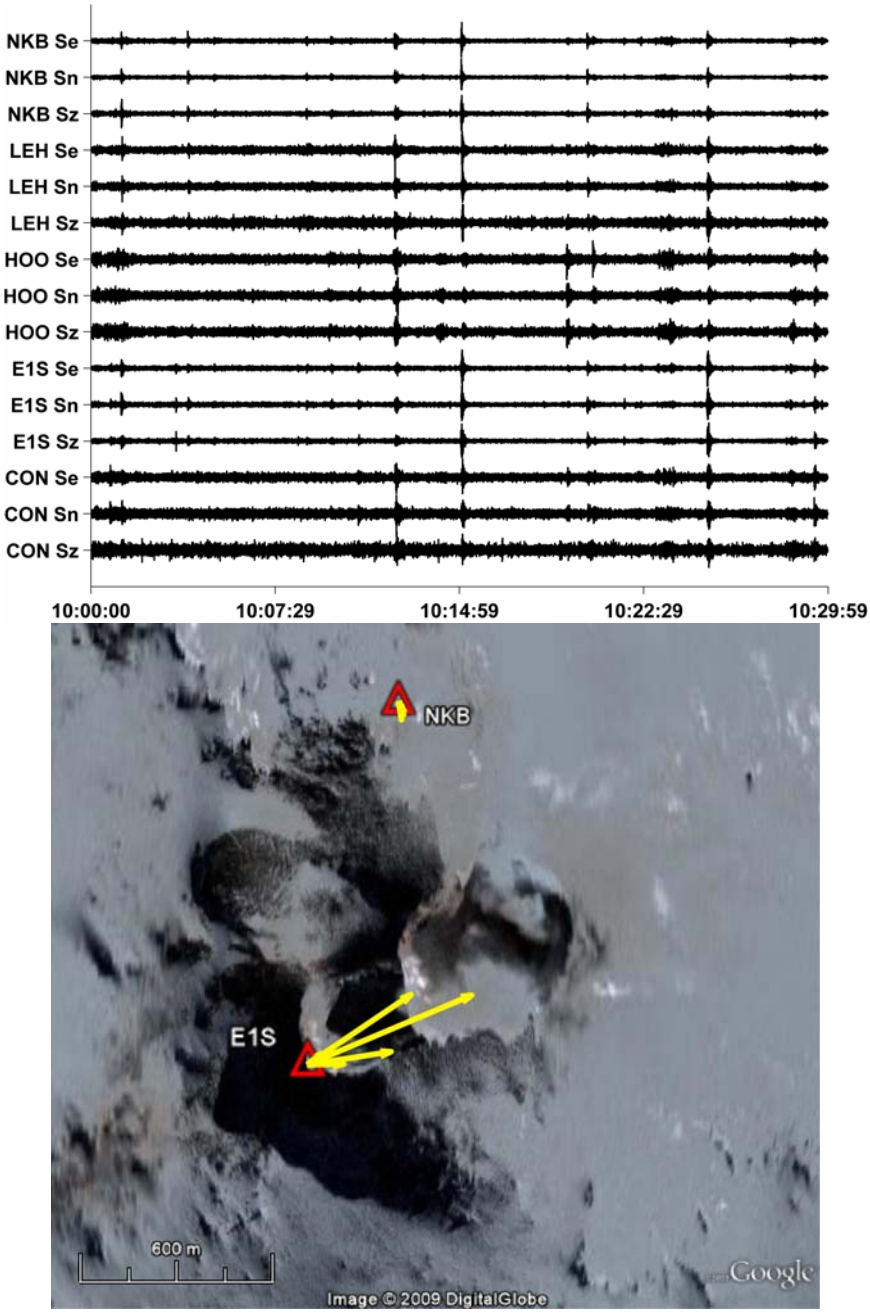

Figure 1.11. Sample data and polarization for recovered signal **ER(11)**. **a.** (Top) Trace data for recovered signal **ER(11)** (nominal passband 1.71-12.5 Hz). Amplitudes of trace data are normalized to illustrate detail. **b.** (Bottom) Azimuth compass plots showing orientation of *Z′* components at CON, E1S, and NKB. Arrows are scaled according to the relative seismic energy of each subband at each station.

Conclusions

We have developed a top-down, adaptive preprocessing algorithm that filters multichannel volcano-seismic data sets by selecting and grouping sub-bands of data in the wavelet domain, based on the similarity and relative energy of their principal components. This algorithm, called *Subband Decomposition and Reconstruction*, or SDR, is designed to select regions of the frequency spectrum that are strongly dominated by a single seismic phase or input signal. Because undecimated wavelet packet coefficients are constructed from orthogonal filters, and because the wavelet packet transform preserves energy, this method for subband decomposition and reconstruction preserves polarization and signal amplitude of each recovered signal. Thus, it allows different signals in various regions of the spectrum to be examined in a quantitative, semi-automated way.

Tests on synthetic data suggest that *SDR* can recover quasi-continuous signals that differ by an order of magnitude, even in noisy environments, provided that their spectral peaks are further apart than the bandwidth of wavelet coefficients $\mathbf{W}_{\mathbf{J,n}}$ at the highest wavelet level *J*. Tests on a half-hour data sample from Mt. Erebus are able to detect at least one coherent, continuous low-frequency signals in the band 0.16-0.31 Hz, and possibly a secondary signal at 0.47-0.78 Hz; whose polarizations suggest an isotropic source near or under the active vent. This method also detects a series of discrete high-frequency events at 1.72-12.5 Hz that resemble small Strombolian explosions. Simple examination confirms that these signals are coherent and real. We conclude that this algorithm is effectively able to detect subtle

changes in the time-frequency content of volcanic tremor, and thereby detect signals whose spectral peaks are otherwise buried in background noise (and masked by one another). Such an algorithm could allow volcanologists much greater insight into the dynamics of volcanic systems, and, as shown by tests on real data, could detect subtle signals that might help address the possibility of unrest.

Table 1.1. Recovered signals from a data sample at Mt. Erebus beginning 23 Jan 2006 10:00 GMT. Signal names use the convention **ER(n)**, described in the text. Values for eigenvectors $v_{j,n}$ correspond to the largest eigenvalue $\lambda_{j,n,1}$ of the principal components of each wavelet packet $\boldsymbol{W_{j,n}}$. $v_{j,n}$, energy (En), azimuth (Az), incidence angle (In), rectilinearity (Rc), and planarity (Pl) are sorted in columns according to station. Az and In are in degrees. Wavelet packets are designated $\boldsymbol{W_{j,n}}$ and nominal passbands f_{min} - f_{max} for each $\boldsymbol{W_{j,n}}$ are given in Hz. Cost functional M($\boldsymbol{W}$) is renormalized (multiplied by normalized bandwidth) so that $0 \le M(\boldsymbol{W}) < 5$. Spectral leakage for each subband is tabulated in the form $\log_{10}(E_{out}/E_{in})$, the base 10 logarithm of spectral energy outside the passband to spectral energy inside the passband. Relative lags of each subband at each station are given in seconds for subbands whose wavelet cross-correlations are well constrained.

Signal		Sta	CON	E1S	HOO	LEH	NKB
ER(1)							
$W_{7,0}$		$v_{7,0}$	0.06	0.15	-0.05	-0.99	-0.03
f_{min}-f_{max} (Hz)	0.00-0.16	En	1.2e-08	2.9e-08	8.6e-09	7.3e-08	6.9e-09
M($W_{7,0}$)	0.842	Az	144.24	101.59	-13.18	65.79	69.02
$\log_{10}(E_{out}/E_{in})$	-0.000	In	89.62	85.96	55.05	79.84	67.98
		Rc	0.35	0.32	0.20	0.41	0.31
		Pl	0.54	0.50	0.20	0.54	0.54
$W_{3,5}$		$v_{3,5}$	-0.01	0.02	0.00	1.00	0.00
f_{min}-f_{max} (Hz)	12.50-15.00	En	4.5e-12	4.1e-12	4.7e-13	9.3e-12	1.2e-12
M($W_{3,5}$)	1.108	Az	-29.54	-126.89	-82.21	-99.52	-11.23
$\log_{10}(E_{out}/E_{in})$	-0.000	In	29.78	39.92	61.43	85.28	53.53
		Rc	0.69	0.64	0.43	0.70	0.53
		Pl	0.70	0.58	0.31	0.70	0.40
$W_{2,3}$		$v_{2,3}$	0.00	-0.00	0.00	-1.00	-0.00
f_{min}-f_{max} (Hz)	15.00-20.00	En	5.4e-12	2.6e-12	6e-13	1.2e-11	1.3e-12
M($W_{2,3}$)	0.746	Az	-29.09	-130.86	-51.96	-98.00	-21.38
$\log_{10}(E_{out}/E_{in})$	-0.242	In	29.93	41.51	38.59	85.72	49.18
		Rc	0.75	0.55	0.35	0.68	0.63
		Pl	0.76	0.45	0.39	0.76	0.57
ER(2)							
$W_{7,1}$		$v_{7,1}$	0.66	0.48	0.14	0.31	0.47
f_{min}-f_{max} (Hz)	0.16-0.31	En	5.7e-08	2.8e-08	2.2e-08	3.4e-08	2.7e-08
M($W_{7,1}$)	0.480	Lag	-0.70	-0.82	1.40	1.02	-0.90
$\log_{10}(E_{out}/E_{in})$	-1.563	Az	-21.13	-6.50	154.75	-178.84	4.82
		In	79.23	77.85	72.65	72.02	88.62
		Rc	0.59	0.58	0.30	0.50	0.62
		Pl	0.62	0.75	0.28	0.42	0.69

Table 1.1 continued

ER(3)		*Sta*	*CON*	*E1S*	*HOO*	*LEH*	*NKB*
$W_{7,2}$		$v_{7,2}$	0.04	0.41	-0.11	0.68	0.60
f_{min}-f_{max} (Hz)	0.31-0.47	En	5.8e-09	2.7e-09	2.2e-09	3.8e-09	2.6e-09
M(W7,2)	1.678	Az	78.24	45.59	-98.18	-97.21	-72.98
$\log_{10}(E_{out}/E_{in})$	-0.356	In	89.62	85.96	55.05	79.84	67.98
		Rc	0.35	0.32	0.20	0.41	0.31
		Pl	0.54	0.50	0.20	0.54	0.54
ER(4)							
$W_{7,3}$		$v_{7,3}$	-0.75	-0.40	-0.06	-0.20	0.49
f_{min}-f_{max} (Hz)	0.47-0.62	En	2.7e-09	1.4e-09	1e-09	1.4e-09	1.7e-09
M(W7,3)	1.128	Lag	0.25	0.23	-0.93	0.42	0.03
$\log_{10}(E_{out}/E_{in})$	-0.497	Az	61.28	-122.03	-1.27	90.32	-49.42
		In	89.08	86.64	77.32	86.55	89.74
		Rc	0.61	0.58	0.37	0.57	0.55
		Pl	0.73	0.72	0.44	0.67	0.76
$W_{7,4}$		$v_{7,4}$	-0.77	-0.45	0.05	-0.27	0.36
f_{min}-f_{max} (Hz)	0.62-0.78	En	1.2e-09	6.4e-10	5.4e-10	6.7e-10	8.8e-10
M($W_{7,4}$)	1.378	Lag	-0.10	-0.35	1.18	-0.23	-0.47
$\log_{10}(E_{out}/E_{in})$	-0.012	Az	53.60	-113.07	-22.14	83.73	-56.46
		In	86.53	86.03	80.71	89.15	84.43
		Rc	0.58	0.51	0.45	0.54	0.60
		Pl	0.78	0.71	0.52	0.58	0.79
ER(5)							
$W_{7,5}$		$v_{7,5}$	0.13	-0.25	0.18	0.43	0.84
f_{min}-f_{max} (Hz)	0.78-0.94	En	3e-10	2e-10	1.5e-10	2.3e-10	3.4e-10
M($W_{7,5}$)	1.897	Lag	-0.00	-0.62	1.43	-0.25	-0.55
$\log_{10}(E_{out}/E_{in})$	-0.212	Az	77.60	-89.68	-35.23	-118.78	-47.11
		In	87.92	89.07	73.92	80.30	72.14
		Rc	0.41	0.44	0.39	0.56	0.75
		Pl	0.77	0.73	0.45	0.73	0.82
ER(6)							
$W_{7,6}$		$v_{7,6}$	0.87	0.17	0.01	-0.16	0.44
f_{min}-f_{max} (Hz)	0.94-1.09	En	1.2e-10	7.4e-11	3e-11	6.9e-11	9.3e-11
M($W_{7,6}$)	1.842	Lag	0.03	-0.25	0.70	-0.23	-0.25
$\log_{10}(E_{out}/E_{in})$	-0.352	Az	163.81	144.11	-47.50	-148.73	-47.20
		In	89.40	86.17	74.12	69.94	65.97
		Rc	0.65	0.55	0.31	0.56	0.73
		Pl	0.84	0.81	0.32	0.76	0.79
ER(7)							
$W_{7,7}$		$v_{7,7}$	0.57	-0.75	-0.01	0.21	0.27
f_{min}-f_{max} (Hz)	1.09-1.25	En	3.9e-11	3.8e-11	8.6e-12	2.2e-11	2e-11
M($W_{7,7}$)	1.851	Az	-36.01	154.24	162.82	-170.56	-50.25
$\log_{10}(E_{out}/E_{in})$	-0.283	In	85.13	83.91	79.48	63.16	62.68
		Rc	0.57	0.53	0.23	0.46	0.41
		Pl	0.76	0.82	0.31	0.60	0.42

Table 1.1 continued

ER(8)							
$W_{7,8}$		$v_{7,8}$	0.80	0.58	0.02	-0.12	0.11
f_{min}-f_{max} (Hz)	1.25-1.41	En	3.3e-11	3e-11	7e-12	1.7e-11	1.6e-11
M($W_{7,8}$)	1.740	Lag	0.57	0.03	-0.40	-0.03	-0.17
$\log_{10}(E_{out}/E_{in})$	-0.013	Az	31.27	-110.52	-123.30	-20.10	49.02
		In	86.37	83.29	83.99	70.78	53.56
		Rc	0.58	0.44	0.28	0.43	0.33
		Pl	0.75	0.82	0.33	0.59	0.41
ER(9)							
$W_{7,9}$		$v_{7,9}$	-0.54	-0.77	0.00	-0.17	0.31
f_{min}-f_{max} (Hz)	1.41-1.56	En	2.7e-11	2.8e-11	6e-12	1.4e-11	1.7e-11
M($W_{7,9}$)	2.148	Az	26.20	-179.84	-145.03	51.53	82.49
$\log_{10}(E_{out}/E_{in})$	0.052	In	86.45	88.47	87.00	68.39	53.13
		Rc	0.57	0.49	0.26	0.37	0.43
		Pl	0.77	0.87	0.34	0.62	0.52
ER(10)							
$W_{7,10}$		$v_{7,10}$	-0.33	-0.94	-0.01	0.03	0.04
f_{min}-f_{max} (Hz)	1.56-1.72	En	1.7e-11	2.6e-11	4.2e-12	8.7e-12	9.9e-12
M($W_{7,10}$)	1.433	Az	22.90	-55.41	27.94	42.01	89.54
$\log_{10}(E_{out}/E_{in})$	0.114	In	87.82	89.39	80.94	72.90	62.02
		Rc	0.52	0.58	0.30	0.35	0.42
		Pl	0.69	0.89	0.31	0.46	0.59
ER(11)							
$W_{7,11}$		$v_{7,11}$	-0.05	-1.00	0.02	0.03	0.07
f_{min}-f_{max} (Hz)	1.72-1.88	En	8.2e-12	2.1e-11	2e-12	4.1e-12	3.7e-12
M($W_{7,11}$)	1.502	Az	1.99	88.76	-137.29	73.35	-36.26
$\log_{10}(E_{out}/E_{in})$	-0.000	In	77.45	89.37	84.30	82.18	41.33
		Rc	0.54	0.69	0.34	0.32	0.32
		Pl	0.56	0.87	0.31	0.33	0.46
$W_{5,3}$		$v_{5,3}$	-0.05	1.00	0.01	0.00	0.04
f_{min}-f_{max} (Hz)	1.88-2.50	En	1.5e-11	4.8e-11	2.2e-12	5.5e-12	6.5e-12
M($W_{5,3}$)	0.566	Az	-8.43	-98.61	-140.19	-38.31	-32.26
$\log_{10}(E_{out}/E_{in})$	-0.000	In	53.26	86.70	70.98	42.39	35.05
		Rc	0.51	0.70	0.21	0.12	0.50
		Pl	0.56	0.73	0.17	0.22	0.41
$W_{3,1}$		$v_{3,1}$	0.00	1.00	-0.00	0.01	0.02
f_{min}-f_{max} (Hz)	2.50-5.00	En	2.8e-11	1e-10	1.7e-12	8.8e-12	1.1e-11
M($W_{3,1}$)	0.590	Az	-36.03	-112.93	-164.67	-121.13	-10.14
$\log_{10}(E_{out}/E_{in})$	-0.000	In	23.12	35.84	80.45	78.90	23.79
		Rc	0.67	0.69	0.25	0.20	0.55
		Pl	0.67	0.69	0.23	0.29	0.45
$W_{2,1}$		$v_{2,1}$	-0.01	1.00	0.00	-0.00	0.01
f_{min}-f_{max} (Hz)	5.00-10.00	En	1.8e-11	7.1e-11	1.3e-12	1.3e-11	8.2e-12
M($W_{2,1}$)	0.852	Az	-53.18	-123.84	-168.00	-104.29	-20.25
$\log_{10}(E_{out}/E_{in})$	-0.056	In	17.12	33.40	69.98	86.98	29.64
		Rc	0.66	0.76	0.25	0.46	0.53
		Pl	0.62	0.70	0.20	0.39	0.49

Table 1.1 continued

$W_{3,4}$		$v_{3,4}$	*-0.01*	*-1.00*	*-0.00*	*-0.01*	*-0.00*
f_{min}-f_{max} (Hz)	10.00-12.50	En	5.1e-12	9.8e-12	4.2e-13	7.3e-12	1.9e-12
M($W_{3,4}$)	0.482	Az	-35.58	-127.88	-174.50	-100.31	-10.72
$\log_{10}(E_{out}/E_{in})$	-0.000	In	25.61	37.39	73.45	86.77	50.17
		Rc	0.64	0.70	0.23	0.64	0.54
		Pl	0.57	0.62	0.27	0.58	0.47

Notes to Chapter I

Acernese, F., Ciaramella, A., De Martino, S. Falanga, M., Godano, C., Tagliaferri, R., 2004. Polarization analysis of the independent components of low frequency events at Stromboli volcano (Aeolian Islands, Italy). *J. Volcanol. Geotherm. Res.* 137, 153-168.

Aki, K., Richards, P., 2002. Quantitative seismology, 2nd ed. New York: University science books.

Anant, K.S., and Dowla, F.U., 1997. Wavelet transform methods for phase identification in three-component seismograms. *B. Seism. Soc. Am.* 87, 1598-1612.

Aster, R., Zandomeneghi, D., Mah, S., McNamara, S., Henderson, D.B., Knox, H., Jones, K., 2008. Moment tensor inversion of very long period seismic signals from Strombolian eruptions of Erebus Volcano, *J. Volcanol. Geotherm. Res. 177*, 635-647.

Carniel, R., Di Cecca, M., Rouland, D. 2003. Ambrym, Vanuatu (July-August 2000): spectral and dynamical transitions on the hours-to-days timescale. *J. Volcanol. Geotherm. Res.* 128, 1-13.

Chouet, B., 1996. Long-Period volcano seismicity: its source and use in eruption forecasting. *Nature* 380, 309-316.

Chui, C.K., 1997. Wavelets: a mathematical tool for signal processing. *SIAM*, Philadelphia, PA, USA.

Coifman, R.R., Wickerhauser, M.V., 1992. Entropy-based algorithms for best basis selection. *IEEE Trans. Inf. Theory* 38, 713-718.

Coifman, R.R., Donoho, D.L., 1995. Translation-invariant de-noising. In *Wavelets and Statistics* (Lecture Notes in Statistics, v. 103), A. Antoniadis and G. Oppenheim, eds. New York: Springer-Verlag, pp.125-150.

Daubechies, L., 1992. Ten lectures on wavelets. *SIAM*, Philadelphia, PA, USA.

Furumoto, M., Kunitomo, T., Inoue, H., Yamada, I., Yamaoka, K., Ikami, A. Fukao, Y., 1990. Twin sources of high-frequency volcanic tremor of Izu-Oshima Volcano, Japan. *Geophys. Res. Lett.* 17(1): doi: 10.1029/89GL03678. issn: 0094-8276.

Giggenbach, W.F., Kyle, P.R., Lyon, G.L., 1973. Present volcanic activity on Mt. Erebus, Ross Island, Antarctica. *Geology* 1, 135–156.

Gottschämmer, E., Surono, I., 2000. Locating tremor and shock sources at Bromo Volcano. *J. Volcanol. Geotherm. Res.* 101, 199-209.

Greenhall, C.A., 1991. Recipes for degrees of freedom of frequency stability estimators. *IEEE Trans. Inst. Measurement*, 40, 994-999.

Harrington, R.M., Brodsky, E.E., 2007. Volcanic hybrid earthquakes that are brittle-failure events. *Geophys. Res. Lett.* 34, L06308, doi:10.10129/2006GL028714.

Harris, A.J.L., Carniel, R., Jones, J., 2005. Identification of variable convective regimes at Erta Ale Lava Lake. *J. Volcanol. Geotherm. Res.*, 142, 207-223.

Hyvärinen, A., Karhunen, J, Oja, E., 2000. Independent component analysis. New York: John Wiley and Sons.

Jain, Anil, M. Narasimha Murty, and Patrick Flynn, 1999. Data clustering: A review. *ACM Computing Surveys* 31 (3), 264-323.

Jones, J., Carniel, R., Harris, A.J.L., Malone, S., 2006. Seismic characteristics of variable convection at Erta `Ale lava lake, Ethiopia, *J. Volcanol. Geotherm. Res.* 153, 64-79.

Jurkevics, 1988. Polarization analysis of three-component array data. *B. Seis. Soc. Am.* 78, 1725-1743.

Kaminuma, K., 1994. The seismic activity of Mount Erebus in 1981–1990. *In*: Kyle, P.R. (Ed.), *Volcanological and Environmental Studies of Mount Erebus, Antarctica*. Antarctic Research Series, American Geophysical Union, Washington DC, pp. 35–50.

Kawakatsu, H., Kaneshima, S., Matsubayashi, H., Ohminato, T., Sudo, Y., Tsutsui, T., Uhira, K., Yamasato, H., Legrand, D., 2000. Aso94: Aso seismic observation with broadband instruments. *J. Volcanol. Geotherm. Res.* 101, 129-154.

Kienle, J., Kyle, P.R., Estes, S., Takanami, R., Dibble, P.R., 1981. Seismicity of Mt. Erebus, 1980–81. *Antarct. J. US* 16 (5), 35–36.

Knight, R.L., Dibble, R.R., Aster, R.C., Kyle, P.R., Ameko, A.K., 1996. Digital recording of the Seismicity of Mount Erebus Volcano, November 1994–June 1996. *Antarct. J. US* 31 (2), 41–43.

Konstantinou, K.I., Schlindwein, V., 2002. Nature, wavefield properties and source mechanism of volcanic tremor: a review. *J. Volcanol. Geotherm. Res.* 119, 161-187.

Liang, J., Parks, T.W., 1996. A translation-invariant wavelet representation algorithm with applications. *IEEE Trans. Sig. Processing*, 44, 225-232.

Lilly, J.M., Park, J., 1995. Multiwavelet spectral and polarization analyses of seismic records. *Geophys. J. Int* 122, 1001-1021.

Mallat, S.G., 1999. A wavelet tour of signal processing. New York: Academic Press.

McCoy, E.J., Percival, D.B., Walden, A.T., 1995. On the phase of least-asymmetric scaling and wavelet filters. *Technical Report* TR-95-15, Statistics Section, Imperial College of Science, Technology and Medicine, London, UK.

McNutt, S.R., 1996. Seismic monitoring and eruption forecasting of volcanoes : A review of the state-of-the-art and case histories. In: Scarpa, Tilling (Eds.), Monitoring and Mitigation of Volcanic Hazards. Springer, Berlin, pp. 100-146.

Montalbetti, J.F., Kanasewich, K.R., 1970. Enhancement of teleseismic body phases with a polarisation filter. *Geophys. J. R. Astron. Soc.* 21, 119-129.

Nason, G.P., Silverman, B.W., 1995. The stationary wavelet transform and some statistical applications. In *Wavelets and Statistics* (Lecture Notes in Statistics, v. 103), A. Antoniadis and G. Oppenheim, eds. New York: Springer-Verlag, 281-299.

Oweiss, K.G., Anderson, D.J., 2007. Tracking signal subspace invariance for blind separation and classification of nonorthogonal sources in correlated noise. *EURASIP Journal on Advances in Signal Processing*, 2007 (37485).

Patanè, D., Di Grazia, G., Cannata, A., Montalto, P., Boschi, E. 2008. The shallow magma pathway geometry at Mt. Etna volcano. *Geochem. Geophys. Geosys.* 9, doi: 10.1029/2008GC002131.

Pearson, K., 1901. On lines and planes of closest fit to systems of points in space. *Philosophical Magazine* 2 (6), 559–572.

Percival, D.B., Guttorp, P., 1994. Long-memory processes, the Allan variance and wavelets. In *Wavelets in Geophyics*, E. Foufoula-Georgious and P. Kumar, *eds*. San Diego: Academic Press, 325-344.

Percival, D.B., Mojfeld, H., 1997. Analysis of subtidal coastal sea level fluctuations using wavelets. *Journ. Am. Stat. Assoc*, 92, 868-880.

Percival, D.B., Walden, A.T., 2000. Wavelet methods for time series analysis, Cambridge University Press, Cambridge, U.K.

Ripepe M., Harris, A. J. L. Carniel, R. 2002. Thermal, seismic and infrasonic evidences of variable degassing rates at Stromboli volcano, *J. Volcanol. Geotherm. Res.*118 (3-4), 285-297.

Rowe, C., Aster, R., Kyle, P., Dibble, R., Schlue, J., 2000. Seismic and acoustic observations at Mount Erebus Volcano, Ross Island, Antarctica, 1994–1998. *J. Volcanol. Geotherm. Res.* 101, 105–128.

Shaw, P.J.A., 2003. Multivariate statistics for the Environmental Sciences. Hodder-Arnold.

Shensa, M.J., 1992. The discrete wavelet transform: wedding the a Trous and Mallat algorithms. *IEEE Trans. Signal Processing*, 40, 2464-2482.

Sherburn, S., Scott, B.J., Nishi, Y., Sughihara, M., 1998. Seismicity at White Island volcano, New Zealand: a revised classification and inferences about source mechanism. *J. Volcanol. Geotherm. Res.* 83, 287-312.

Strang, G., 1993. Wavelet transforms versus Fourier transforms. *B. Am. Math. Soc.* 28(2), 288-305.

Vandecar, J.C., Crosson, R., 1990. Determination of teleseismic relative phase arrival times using multi-channel cross-correlation and least squares. *B. Seis. Soc. Am.* 80(1), 150-169.

Vidale, J., 1986. Complex polarization analysis of particle motion. *B. Seis. Soc. Am.* 76(5), 1393-1405.

Walden, A.D., Cristan, A.C., 1998. The phase-corrected undecimated discrete wavelet packet transform and the recurrence of high latitude interplanetary shock waves. *Proceedings of the Royal Society of London*, Series A, 454, 2243-2266.

Wasserman, J., 1997. Locating the sources of volcanic explosions and volcanic tremor at Stromboli volcano (Italy) using beam-forming on diffraction hyperboloids. *Phys. Earth & Plan. Int.* 104, 271-281.

II. Classification and Location of Tremor at Erta 'Ale, Ethiopia

Introduction

Erta ‘Ale is a basaltic shield volcano in the Danakil depression of northeast Ethiopia (13.60° N, 40.67° E, Fig. 2.1), with a summit 613 m a.s.l. (Barberi and Varet 1970). The summit caldera features two pit craters, the southernmost of which held a persistent, active lava lake from 1967 through late 2004 (Martini, 1969; Oppenheimer and Francis 1998; Bardintzeff et al 2004, Fig. 2.2). An active lava lake reappeared at Erta 'Ale in 2005, possibly in relation to the Danakil earthquake swarm (Yirgu et al 2005), and has persisted to the present time (Rivallin and Mougin 2008, Grandjean 2006). Lava lakes may have existed in one or both summit pit craters from a considerably earlier time, as reports of a characteristic red summit glow come from some of the first non-natives to visit Erta 'Ale in the modern era (Dainelli and Marinelli 1907).

Active summit lava lakes are of scientific interest because they offer a rare opportunity to make quasi-direct, long-term, continuous observations of magma system circulation and associated physical parameters, such as volcanic tremor, deformation, heat flux, and gas release, at the exposed upper end of a magma conduit (Le Guern, 1987; Hamaguchi et al., 1992; Kaminuma, 1994; Amelung et al., 2000; Oppenheimer and Francis, 1997; Kyle et al., 1994). Only a handful of other volcanoes have reported persistent, active summit lava lakes in the current decade: Ambrym, Vanuatu (Carniel et al. 2003); Nyamuragira and Nyiragongo, D.R. Congo,

(Bajope et al. 2006); Villarrica, Chile (Witter 2003); Erebus, Antarctica (Aster et al. 2004); and Saunders Island, S. Sandwich Islands (Patrick et al. 2004).

Figure 2.1. Location of Erta ‘Ale, Ethiopia (black crosshairs).

Figure 2.2. Comparative photographs showing morphological changes of the lava lake. **a.** (Left) 14 Feb 2002, the lava lake occupies nearly half the active southern crater. **b.** (Right) 24 Nov 2003, the lava lake has shrunk to a 20m area near the center of the active southern crater. Photographs by the author.

The Erta 'Ale lava lake has already been the subject of one study (Harris et al. 2005, Jones et al. 2006), in which seismic, thermal, and video data were collected for 5 days in February 2002, to better understand the dynamics of the shallow magma system that feeds the summit lava lake. 3 seismic stations were installed for a period of 5 days in Feb 2002 (Fig. 2.3a). The 2002 campaign found that the lava lake fluctuated between two convective regimes, characterized by low (0.01 – 0.08 m s^{-1}) and high (0.1 – 0.4 m s^{-1}) velocities of cooled crust on the lava lake surface, which corresponded to sluggish and vigorous convection of the lava lake (Harris et al. 2005). Each convective regime lasted tens to hundreds of minutes, and the tremor had unique spectral characteristics for each (Fig. 2.4). A persistent, continuous tremor signal was described by Jones et al. (2006), in which we found distinct spectral characteristics and non-overlapping centroid locations corresponding to each convective regime. Because active lava lakes can be considered the exposed upper surface of a convecting magma column (Harris et al. 1999; Swanson et al. 1979), these changes could be explained by cooling and degassing processes in the shallow part of the exposed conduit (Harris et al. 2005).

We conducted a seismic experiment in Nov-Dec 2003 to study the relationship between Erta 'Ale tremor and conduit convection. During this time the lava lake was considerably smaller than in 2002, confined to a 20m region near the center of the active southern crater (Fig. 2.2b). Seven seismic stations were installed from 22 November 2003 to 6 December 2003: two Guralp CMG-40T broadband

seismometers (f_0 = 0.033 Hz), and six Mark Products L-22 short period sensors (f_0 = 2 Hz). The geometry of this network is shown in Fig. 2.3b. Two of the sites, EA2 and EA5, were reoccupations of the sites occupied in 2002 by CMG and MAR, respectively, while cracks around the former site of station L22 prevented its reoccupation. EA1 and EA3 each had two acoustic microphones colocated to their seismometers. All stations in 2003 sampled continuously at 100 Hz. Data were recorded until the network was removed on 6 Dec 2003, but interruptions occurred often due to power outages and equipment failure.

Figure 2.3. Station maps of temporary seismometers from each Erta ‘Ale experiment, superimposed on aerial photographs. Notable features of the Erta 'Ale summit caldera are indicated. Short-period sensors (L22 and LE3D) are indicated by red triangles. Broadband sensors (CMG-40T) are indicated by blue triangles **a.** Seismometers of the Feb 2002 experiment. Position of lava lake is consistent with that of the photograph, just left of indicative text (see Fig. 2.2a). **b.** Seismometers of the 2003 experiment. The lava lake was smaller than suggested in the underlying aerial photograph, occupying only the center of the deeper pit region, NNE of station EA3 (see Fig. 2.2b). Lava lake label has been omitted to show detail.

Figure 2.4. Representative samples of trace data (left) and corresponding spectrograms (right) from each Erta ‘Ale experiment. Amplitudes of trace data are normalized to illustrate detail. All data have been detrended, downsampled to 50 Hz, preprocessed using a 3s cosine taper, and filtered to the instrument response of a Lennartz MarsLite (f_0 = 0.2 Hz). Data from stations L22 (2002), and EA1 and EA3 (2003) are further highpass filtered using a 4 pole Butterworth filter at f = 0.4 Hz. Spectrogram scaling is in dB computed from ground velocity. **a.** (Top) 17m 35s of raw data beginning 15 Feb 2002, 16:28:46 GMT, during the “low” convective regime. Spectrogram corresponds to the vertical component of station L22 (Fig. 2.3a). **b.** (Middle) 10m 54s of raw data beginning15 Feb. 2002, 19:53:23 GMT, during the “high” convective regime. Spectrogram corresponds to the vertical component of station L22 (Fig. 2.3a). **c.** (Bottom) 30 min. sample of raw data beginning 02 Dec 2003, 16:30:01 GMT. Spectrogram corresponds to the vertical component of station EA3 (Fig. 2.3b).

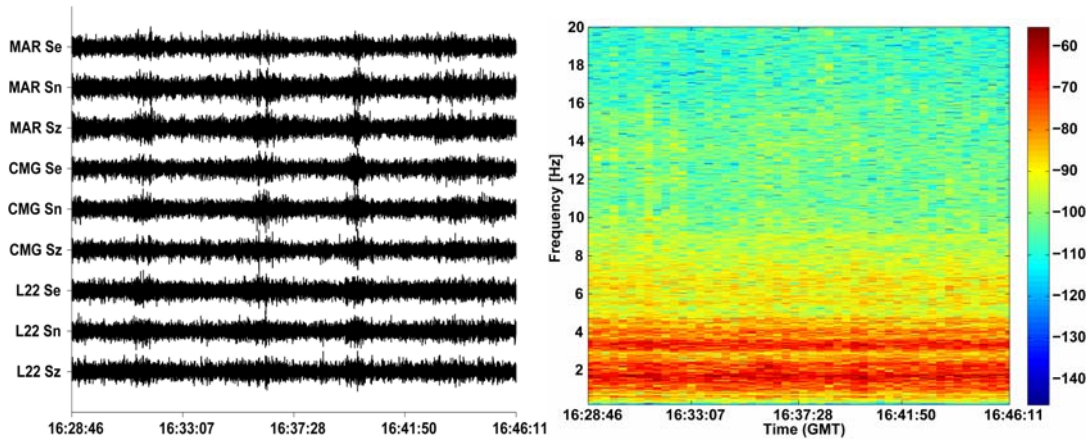
MAR Se
MAR Sn
MAR Sz
CMG Se
CMG Sn
CMG Sz
L22 Se
L22 Sn
L22 Sz
16:28:46
16:33:07
16:37:28
16:41:50
16:46:11
Frequency [Hz]
Time (GMT)

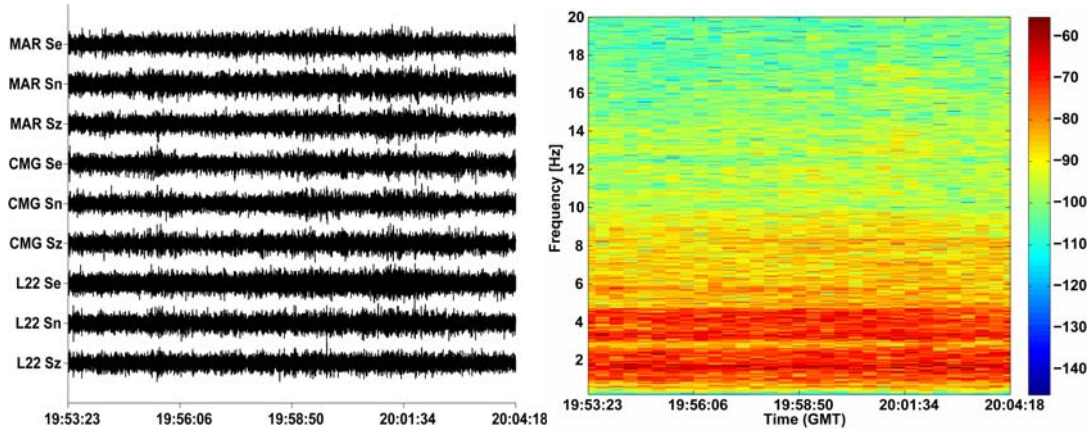
MAR Se
MAR Sn
MAR Sz
CMG Se
CMG Sn
CMG Sz
L22 Se
L22 Sn
L22 Sz
19:53:23
19:56:06
19:58:50
20:01:34
20:04:18
Frequency [Hz]
Time (GMT)

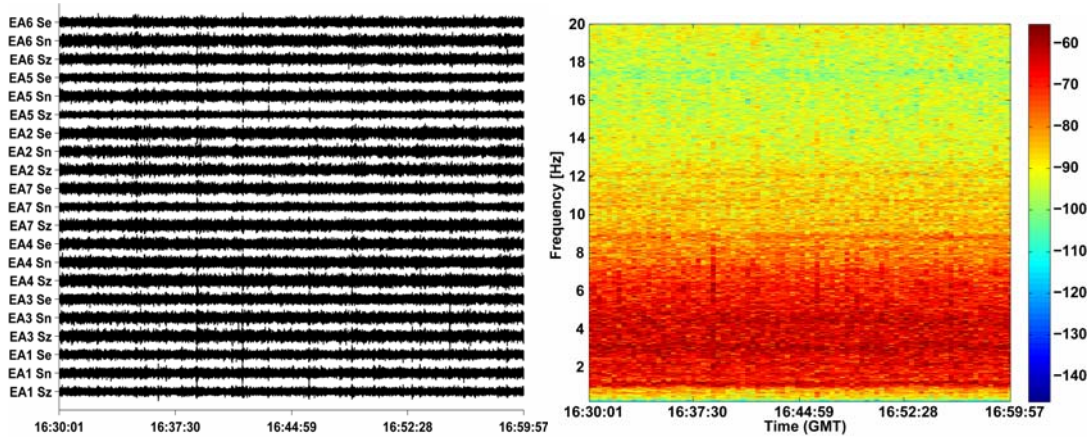
EA6 Se
EA6 Sn
EA6 Sz
EA5 Se
EA5 Sn
EA5 Sz
EA2 Se
EA2 Sn
EA2 Sz
EA7 Se
EA7 Sn
EA7 Sz
EA4 Se
EA4 Sn
EA4 Sz
EA3 Se
EA3 Sn
EA3 Sz
EA1 Se
EA1 Sn
EA1 Sz
16:30:01
16:37:30
16:44:59
16:52:28
16:59:57
Frequency [Hz]
Time (GMT)

Whereas the convection of the lava lake observed in 2002 clearly showed alternating slow and fast convective regimes (Harris et al. 2005), the lava lake was quiescent and stable in 2003. The 2003 seismic data show no obvious spectral transitions (Fig. 2.4c). Seismic records can be described qualitatively as a continuous tremor signal with dominant energy in the range 1 to 5 Hz. Much like the tremor recorded in 2002, the spectrum is too broad to be monochromatic, and there is little evidence for the higher-order harmonics that might indicate a resonating crack (Jones et al. 2006). However, there are no variable convective regimes that would suggest either regular pulses of gas-rich magma reaching the lava lake, or convective overturn triggering in a cooling layer at the lava lake surface (cf. Harris et al. 2005).

Tremor amplitude in 2003 remained relatively constant, averaging around $5x10^{-6}$ m s^{-1} at the stations closest to the lava lake (Fig. 2.4b). However, in contrast to the 2002 experiment, small, low-frequency "B-type" earthquakes were sometimes seen. Unfortunately, due to equipment problems, no low-frequency events were recorded by more than 3 stations, making location and detailed analysis impossible. It should be noted that these low-frequency earthquakes have no immediate, obvious relation to the background tremor, and are neither preceded nor followed by changes in its amplitude or frequency content.

The tremor recorded at Erta 'Ale is a daunting challenge. The signal is continuous, unrelated to other types of seismicity, and undergoes dramatic changes from the early 2002 samples to those from late 2003. We wish to understand

principally what causes this tremor; but it differs so significantly from tremor elsewhere that we must first address several fundamental questions about it, namely:

(1) Is the tremor recorded during each experiment a single signal, or rather a composite of many?

(2) With regards to the 2002 data, are the spectral transitions of Jones et al. (2006) the result of a changing tremor source mechanism, or rather the result of additional signals superimposed on a background signal?

(3) With regards to the 2003 data, what are the time-frequency characteristics of the signal(s) that comprise(s) the tremor? Do they change? Put another way, are the 2003 signals truly static, or do simply change in ways too subtle to detect by spectral analysis?

(4) Can we determine a source location (or locations) for the tremor? If there are several signals, then are there different locations corresponding to different parts of the frequency spectrum where different signals dominate the seismic energy?

(5) What do these locations tell us about the possible tremor source(s)?

Data Selection and Preprocessing

We begin by examining representative samples from the 2002 study that correspond to the "low" and "high" convective regimes of Harris et al. (2005). We complement this data with representative data from 2003 when all 7 stations in Fig. 2.3b were operating. Prior to analysis, all data were downsampled to 50 Hz for

computational efficiency, and a 3s cosine taper was applied to all trace data. The instrument response of all stations from both experiments was then corrected to match that of an LE3D sensor (f_0 = 0.2 Hz). Finally, to prevent low-frequency artifacts that might result this convolution, all data recorded by L22 geophones were high pass filtered using a 4 pole Butterworth filter with corner frequency 0.4 Hz.

In Chapter I, I introduced an algorithm for adaptive subband decomposition and reconstruction (*SDR*) that divides data using the stationary or "maximal overlap" Discrete Wavelet Packet Transform (MODWPT) of Walden and Cristan (1998). Here we use the *SDR* algorithm to analyze and interpret the Erta 'Ale tremor by treating it as a composite signal.

For this paper we will adopt the following convention for discussion of output signals produced by the *SDR* method. Signals are named and numbered by the lowest corner frequency of the lowest frequency passband that comprises part of the recovered signal. Where applicable, the recovered signal whose principal eigenvectors clusters most closely to that of the input data $\mathbf{X}_t$ will be designated with a parenthetical superscript $^{(1)}$. These numbers are a shorthand way of referencing each recovered signal, and do not correspond to any measure of e.g. principal eigenvector distance for subband clustering. We further refer to recovered signals from the low convective regime of 2002 as $\mathbf{L}^{(\cdot)}$, for "low", recovered signals from the high convective regime of 2002 as $\mathbf{H}^{(\cdot)}$, for "high" and recovered signals from a representative 2003 sample as $\mathbf{B}^{(\cdot)}$.

2002 Tremor Recorded During Slow Convection

Because the 2002 experiment had only 3 seismic stations, a thorough analysis using PCA is somewhat difficult, as each subband has a maximum of 3 principal components. It has been shown using synthetics (Chapter I) that recovered signals from 3 stations are about a factor of 2 lower in quality than recovered signals from 5 or more stations. Thus examination of the 2002 data must be treated as somewhat illustrative.

We begin with the quiescent, "low" convective regime described in Harris et al. (2005), i.e. those periods characterized by lava lake convection of 0.01-0.08 ms^{-1}. Fig. 2.4a shows a raw data sample and spectrogram from station L22. Observe that the signal's spectral energy contains few transients and is concentrated mostly below 5 Hz. Fig. 2.5a shows a dendrogram of the chosen wavelet decomposition, with the frequencies of each subband placed in the appropriate nodes. Fig. 2.5b shows the wavelet basis that best represents this decomposition, with wavelet packets $\mathbf{W}_{j,n}$ positioned according to wavelet level j and band n. Each wavelet packet is arranged exactly fill its nominal passband, and shaded so that all wavelet packets with the same shade belong to the same cluster. Fig. 2.5c shows the logarithmic spectral leakage of each subband. From Fig. 2.5a, we see that our algorithm returns 10 recovered signals $\mathbf{L}^{(\cdot)}$. From Fig. 2.5b, we see that most of these are narrowband signals whose energy is concentrated below 3.13 Hz, i.e. in the regions of the spectrum where seismic energy is highest.

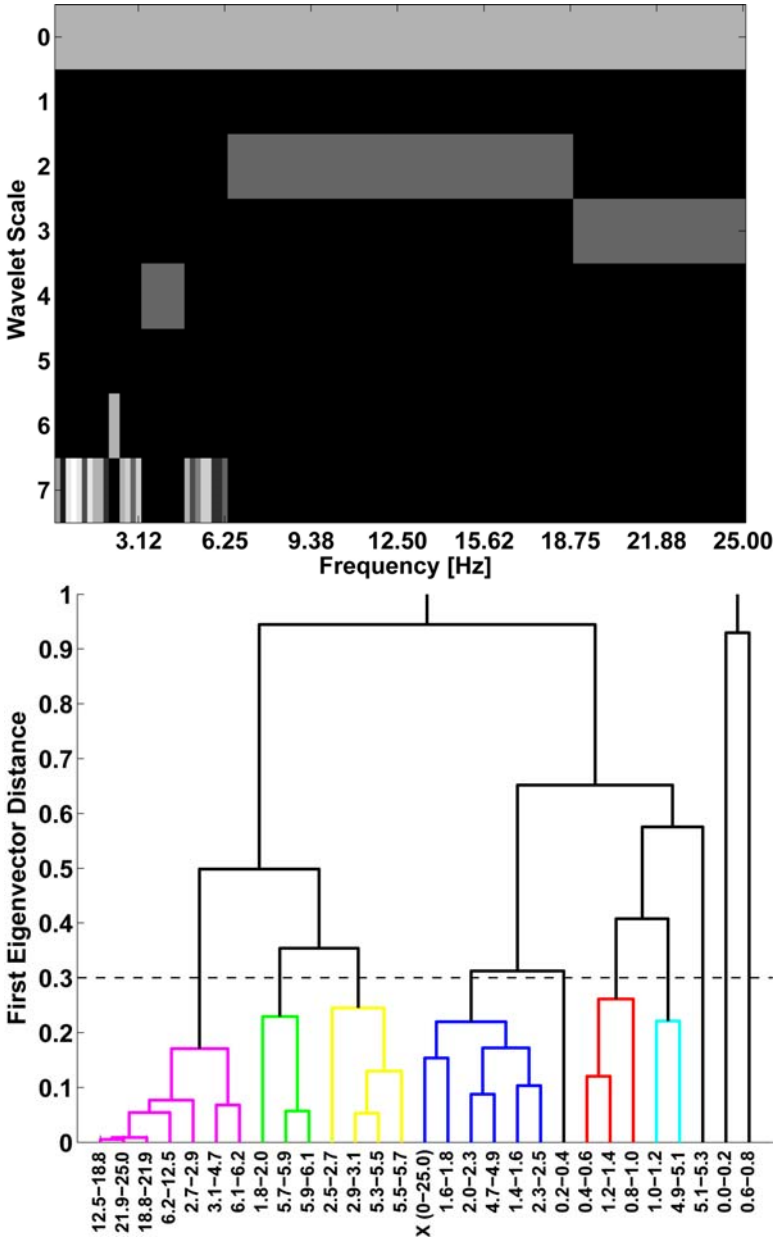

Figure 2.5. Decomposition of the low convective regime using the *SDR* algorithm. **a.** (Top) Wavelet basis selected by subband clustering. Selected wavelet packets are shaded in grayscale to show clustering. *Y*-axis shows wavelet scale *j*, with *j*=0 corresponding to the wideband (input) signal. *X*-axis shows the position and nominal passband for each wavelet packet in the interval [0 f_n]. **b.** (Bottom) Dendrogram of subband clustering. Node denoted with "X (0-25.0)" denotes the input data. Horizontal dashed line indicates distance threshold distance δ=0.3 for clustering of principal components eigenvectors.

The frequency content, subband polarization, subband energy, cost $M(\mathbf{W}_{j,n})$, spectral leakage, and principal eigenvectors for each recovered signal are all given in Table 1. We wish now to discuss this decomposition in detail, and focus in particular on its implications for the tremor sources. Thus we begin with the signal whose principal components cluster most closely to those of the input data $\mathbf{X}_t$, then discuss other notable signals.

The signal $\mathbf{L}^{(1)}$ (Fig. 2.6a) is formed from 5 subbands: $\mathbf{W}_{6,5}$ (nominal passband 1.94-2.34 Hz), $\mathbf{W}_{7,7}$ (1.36-1.56 Hz), $\mathbf{W}_{7,8}$ (1.56-1.76 Hz), $\mathbf{W}_{7,12}$ (2.34-2.53 Hz), and $\mathbf{W}_{7,24}$ (4.69-4.88 Hz). It contains the most energetic spectral peak of the input data at stations L22 and CMG (Fig. 2.4a). A spectrogram of the *Z'* component of the reconstructed signal is shown in Fig. 2.6b for station L22, with a spectrogram of the *Z*-component input data presented for comparison purposes. The recovered signal's subbands are generally rectilinear at station L22, the station nearest the lava lake, with a computed rectilinearity (cf. Jurkevics 1988) of 0.90-0.98 ($\mathbf{W}_{7,24}$ is an obvious outlier, with $r = 0.7$). Its polarizations at MAR and CMG are also rectilinear for some subbands, and from Table 1 we see that the recovered *Z'* components contain an order of magnitude more energy than *R* or *T*. Fig. 2.6c shows a plot of the azimuths of the subbands that form this recovered signal, in which azimuth vectors are rescaled to the relative energy of that subband at that station. Thus the largest azimuth vector in Fig. 2.6c corresponds to $\mathbf{W}_{7,8}$, whose nominal passband is 1.56-1.76 Hz. Notably this subband is also the most rectilinear.

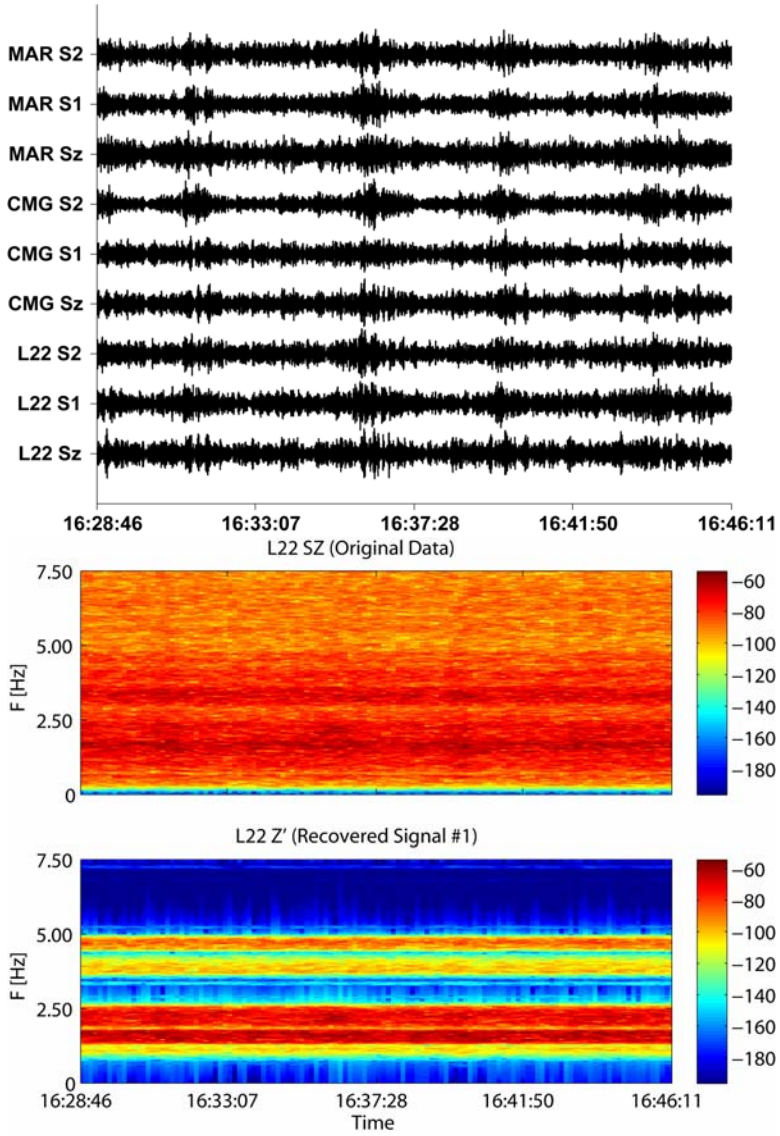

Figure 2.6. Trace data and spectrograms for recovered signal $\mathbf{L}^{(1)}$ from the low convective regime. **a.** (Top) The recovered signal $\mathbf{L}^{(1)}$. Amplitudes of each trace are normalized to illustrate detail. **b.** (Bottom) Spectrograms of the input *Z* data at station L22 (top) and the *Z′* component of recovered signal $\mathbf{L}^{(1)}$ at L22 (bottom). Color scaling is in dB. Color scaling of input data is computed from true ground velocity. c. Azimuths of subbands $\mathbf{W}_{j,n}$ that form recovered signal $\mathbf{L}^{(1)}$ are superimposed on an aerial photograph showing station locations and relevant physical features in the Erta 'Ale summit caldera. Azimuths are scaled according to relative energy of each $\mathbf{W}_{j,n}$ at each station. The largest azimuth vector corresponds to $\mathbf{W}_{7,8}$ at L22, whose nominal passband is 1.56-1.76 Hz.

The computed incidence angles of these subbands are 24-33° from vertical at L22. If we assume that the source underlies this part of the crater, and that the azimuth points toward the source, then simple trigonometry (from Fig. 2.3a) constrains the maximum depth to about 100m a.s.l., or about 420m below the crater floor. If we further assume that the source of this tremor is related to fresh, hot magma upwelling roughly in the center of the lava lake (Harris et al. 2005), then the source is probably 40-100m below the lava lake surface. This range of depths corresponds to estimates of the lava lake depth in Harris et al. (2005) and Oppenheimer and Francis (1999).

Unfortunately, such a source depth contraindicates location. 3 stations cannot adequately constrain a tremor centroid in 3 dimensions, and neglecting depths comparable to (or greater than) the farthest epicentral distance introduces grievous errors to the calculation. However, we can obtain some additional clues about this recovered signal's source by examining its spectrogram. From Fig. 2.6b, observe that the peaks of this signal correspond roughly to two sets of harmonics: One set of spectral peaks (i.e. fundamental and first overtone) at 1.8 and 3.6 Hz, one at 2.4 and 4.8 Hz. We note that the narrowband energy centered at 3.6 Hz is not an aliasing phenomenon, but a result of wavelet filters not being ideal bandpass filters (see e.g. Percival and Walden 2000). It could be that these are real harmonics, and that their spectra lack very sharp peaks merely because many other signals are superimposed on them at similar frequencies (cf. Fig. 2.6b).

It is not the case that all recovered signals appear to originate in the lava lake. An excellent counter-example of this is shown in Fig. 2.7 for signal $\mathbf{L}^{(4)}$, formed from subbands $\mathbf{W}_{7,2}$ (0.39-0.59 Hz), $\mathbf{W}_{7,4}$ (0.79-0.98 Hz), and $\mathbf{W}_{7,6}$ (1.17-1.37 Hz). A spectrogram of this recovered signal is shown in Fig. 2.7c and Fig. 2.7d, showing what might be a first and second harmonic for a fundamental overtone f = 0.45 Hz. As with $\mathbf{L}^{(1)}$, it may be that these are true harmonics mixed with other signals that comprise the observed tremor. Observe from Fig. 2.7b that the energy of this recovered signal's subbands is greatest at station CMG, which is also where the subbands are most rectilinearly polarized, and that the azimuths of this signal's constituent subbands do not point toward the lava lake. Incidence angles at station CMG range from 77-87°, suggesting that its source is shallow. At station L22, azimuths and incidence angles of the recovered signal Z' component point to the lava lake. However, from Fig. 2.7c, this appears to be because the signal at L22 is contaminated by spectral leakage from $\mathbf{L}^{(1)}$. Notably, recovered signals $\mathbf{L}^{(5)}$ (and to a lesser degree $\mathbf{L}^{(6)}$) have similar features, though obviously both lack the apparent harmonic structure of $\mathbf{L}^{(4)}$. In all cases, the azimuths at CMG -- where the signal energy is strongest and least contaminated by the intense spectral energy of $\mathbf{L}^{(1)}$ -- point toward the north crater, which was a source of fumarolic degassing in 2002 (Harris et al. 2005).

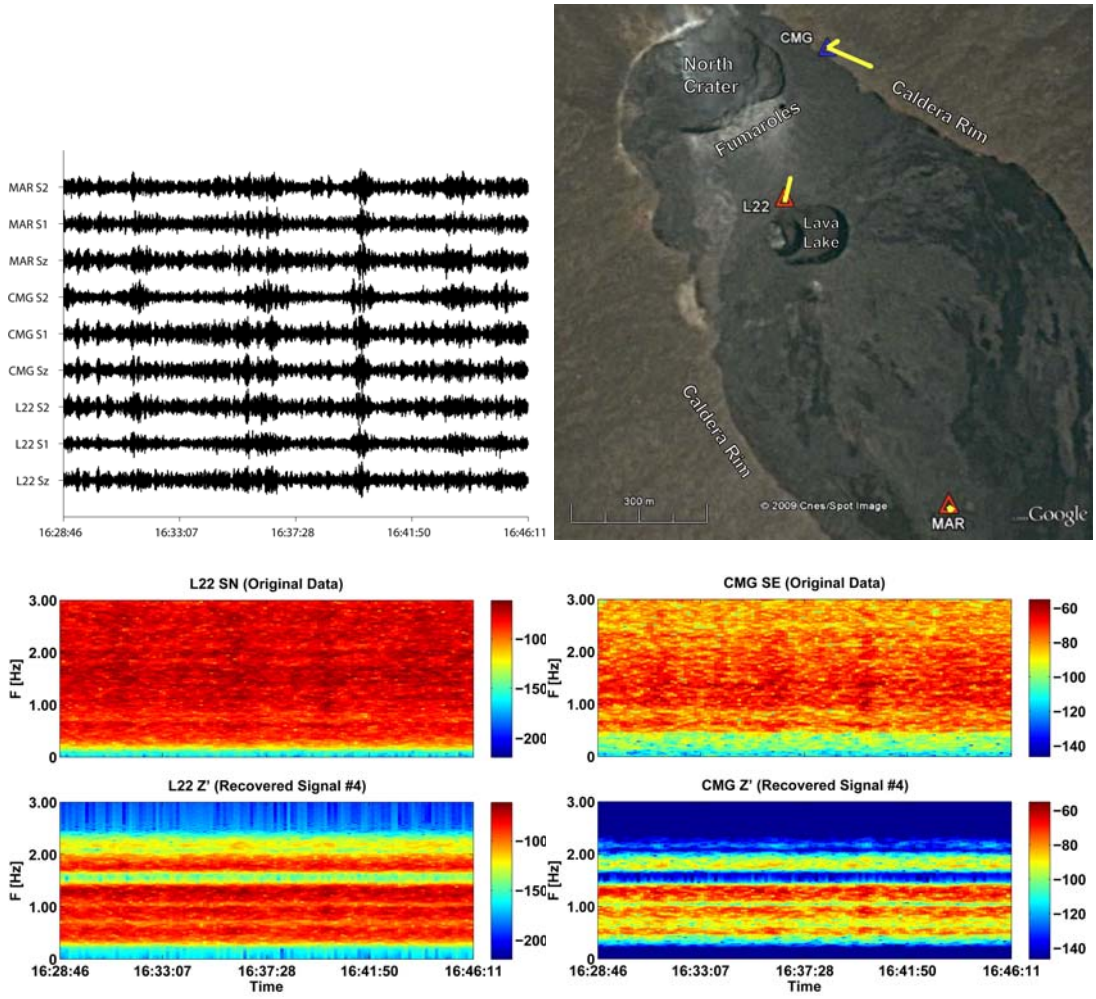

Figure 2.7. Data and spectrograms of recovered signal $\mathbf{L}^{(4)}$ from the low convective regime. **a.** (Upper Left) Trace data for recovered signal $\mathbf{L}^{(4)}$. Amplitudes are normalized to illustrate detail.). **b.** (Upper Right) Azimuths of subbands $\mathbf{W}_{j,n}$ that form recovered signal $\mathbf{L}^{(4)}$ are superimposed on an aerial photograph showing station locations and relevant physical features in the Erta 'Ale summit caldera. Azimuths are scaled according to relative energy of each $\mathbf{W}_{j,n}$ at each station **c.** (Lower Left) Spectrograms of the input *N* data at station L22 (top) and the *Z*′ component of recovered signal $\mathbf{L}^{(4)}$ (bottom. **d.** (Lower Right) Spectrograms of the input *E* data at station CMG (top) and the *Z*′ component of recovered signal $\mathbf{L}^{(4)}$ (bottom). Color scaling is in dB computed from true ground velocity.

It is not necessarily true that every recovered signal has an obvious physical association. For example, the principal eigenvectors of the subbands that form recovered signal $\mathbf{L}^{(9)}$ (Fig. 2.8) all fall within the clustering distance $\delta = 0.3$ of the L22 "axis" in the K-dimensional space defined by each of the K=3 stations' Z' components. Thus the recovered signal $\mathbf{L}^{(9)}$ is literally formed from subbands whose energy is only coherent at the station closest to the lava lake. Comparison of sample spectrograms from L22 (Fig. 2.8a) and MAR (Fig. 2.8b) confirms that this is true; the spectrograms of MAR contain 1-2 orders of magnitude less energy, and are unable to capture the high-frequency transients seen at L22. All of the subbands that form $\mathbf{L}^{(9)}$ are rectilinearly polarized at L22, with incidence angles of 8-40°, suggesting that these may also originate in or near the lava lake. The most energetic subband of $\mathbf{L}^{(9)}$ is $\mathbf{W}_{4,2}$, whose nominal passband is 3.13-4.68 Hz, accounting for 82% of the total energy of $\mathbf{L}^{(9)}$ at L22. The polarization of this subband is highly rectilinear at L22. Its azimuth is 31° from vertical at this station, suggesting that its source could be similar to $\mathbf{L}^{(1)}$, with the signal energy merely becoming scattered above 3.13 Hz.

Now, a station whose distance from the source is less than λ sees no scattering. Thus, for this recovered signal to contain a source similar to $\mathbf{L}^{(1)}$, scattered at CMG and MAR (but not L22), the maximum phase velocity for these frequencies would be 1.6 km s^{-1}. Following the models of Dawson et al. (1999) for the shallow velocity structure of Kilauea, whose geologic similarities to Erta 'Ale have already been noted in e.g. Harris et al (2005), this velocity is too low for a *P*-

wave in basalt, but could be consistent with an *S*-wave in a material whose Poisson's ratio is high, i.e. a densely-cracked, hot volume which contains some partial melt. The existence of such a region at shallow depths below the caldera floor is consistent with the "endogenous growth" model for persistently active volcanoes (Francis et al. 1993) and the suggestion of a shallow magmatic system that connects the northern and southern craters of the summit caldera (Oppenheimer and Francis 1998, Tazieff 1994). Thus the scattering of this signal at CMG and MAR could potentially arise from phase conversions in the heterogeneous, cracked region below the summit caldera, even at relatively low frequencies.

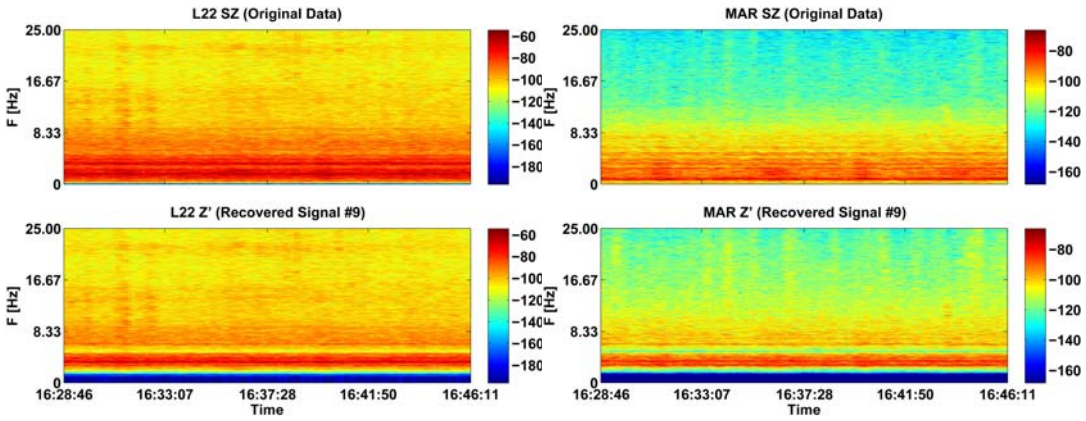

Figure 2.8. Spectrograms of recovered signal $\mathbf{L}^{(9)}$ from the low convective regime. **a.** (Left) Spectrograms of the input *Z* data at station L22 (top) and the *Z*′ component of recovered signal $\mathbf{L}^{(9)}$ (bottom). Color scaling is in dB computed from velocity. **b.** (Right) Raw *Z* component data (top) and *Z*′ component of the same recovered signal (bottom) seen at station CMG. The high-frequency energy is two orders of magnitude lower than at L22, and transients generally cannot be seen.

What we can infer from this analysis is the following. First, during the "slow" lava lake convection of Harris et al. (2005), there is no clear evidence of multiple signals whose sources are in or near the lava lake. The signals $\mathbf{L}^{(1)}$ and $\mathbf{L}^{(9)}$, each of which appear to originate near station L22, cannot be unambiguously associated with unique sources. It may be that these signals all originate from a single tremor source, and -- following the surface morphology described in e.g. Oppenheimer and Francis (1998) -- undergo phase conversions in the complex structure that underlies the Erta 'Ale summit caldera. There is, however, good evidence that at least three signals ($\mathbf{L}^{(4)}$ through $\mathbf{L}^{(6)}$) contain energy at CMG (and possibly L22) that originates elsewhere.

2002 Tremor During Rapid Convection

We now turn to tremor related to more rapid convection of the lava lake in 2002. This convective regime was characterized by Harris et al. (2005) by more rapid surface velocities of the lava lake, ranging from 0.1-0.4 ms^{-1}, corresponding to vigorous overturn of cooled crust on the lava lake surface, with frequent episodes of very small lava fountains. Fig. 2.4b shows sample data and a spectrogram for the "high" convective regime at station L22. Note that there is far more energy seen at high frequencies (f >6 Hz) during the "high" convective regime.

For this sample, recorded during a period of rapid convection, *SDR* forms 15 recovered signals $\mathbf{H}^{(.)}$, suggesting more seismic sources are present in the "high" convective regime. Fig. 2.9 shows a dendrogram of the chosen wavelet

decomposition, with the frequencies of each subband placed in the appropriate nodes. In this case, however, careful examination of the principal eigenvectors $\boldsymbol{v}_{j,n,1}$ reveals that some of these new signals (namely $\mathbf{H}^{(12)}$- $\mathbf{H}^{(15)}$) are most coherent at station MAR, the station farthest from the lava lake. It is difficult to conceive of any physical way that rapid lava lake convection can generate local transients at the station furthest from the lava lake; thus, not all these new signals should be interpreted as meaningful.

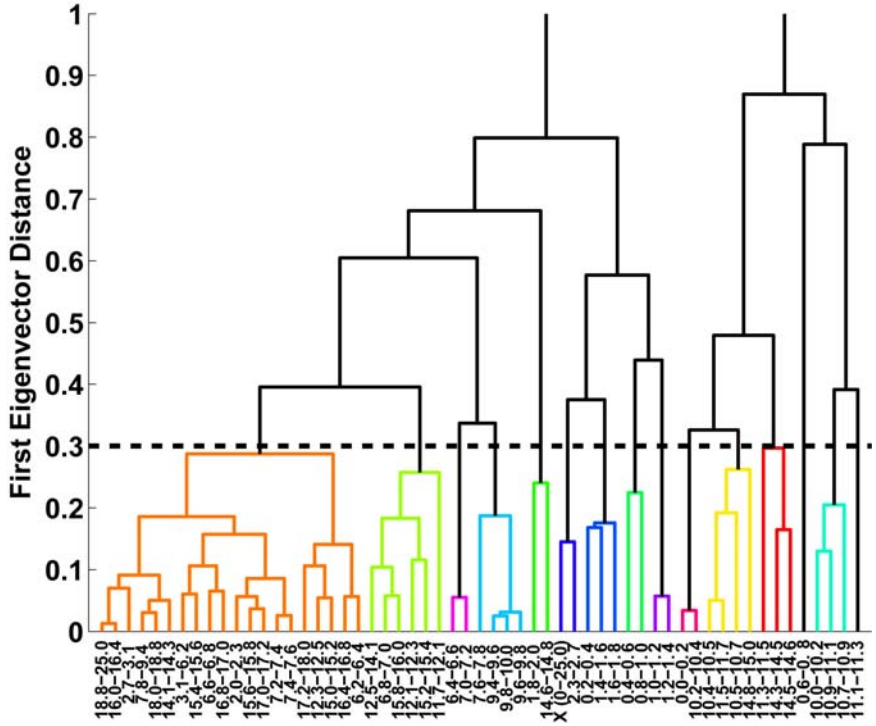

Figure 2.9. Dendrogram showing decomposition of sample seismic data from the "high" convective regime at Erta 'Ale, using the *SDR* algorithm. Node denoted with "X (0-25.0)" denotes the input data. Horizontal dashed line indicates distance threshold δ (Chapter I) for clustering of principal components eigenvectors.

We begin by discussing which signals have changed, and which signals remain consistent, between the two convective regimes. As noted in Chapter I, we can track signals that persist between these two periods by finding principal eigenvectors $v_{j,n,1}$ from subbands $\mathbf{W}_{j,n}$ of recovered signals in the "low" convective regime that cluster to principal eigenvectors $v_{j,n,1}$ from subbands of recovered signals in the "high" convective regime. Comparing Table 2.1 with Table 2.2 shows that several such signals persist: $\mathbf{L}^{(1)}$, $\mathbf{L}^{(4)}$- $\mathbf{L}^{(6)}$, and $\mathbf{L}^{(9)}$, which are recovered as $\mathbf{H}^{(1)}$ and $\mathbf{H}^{(3)}$, $\mathbf{H}^{(4)}$- $\mathbf{H}^{(6)}$, and $\mathbf{H}^{(8)}$, respectively. The polarization of each recovered signal also remains constant between the two regimes, at those stations where its energy is largest. The signals $\mathbf{H}^{(1)}$ and $\mathbf{H}^{(3)}$ have similar principal eigenvectors, and each clusters to signal $\mathbf{L}^{(1)}$. That they do not cluster to one another is simply a consequence of there being no intermediary subbands to cluster their principal eigenvectors. Signals $\mathbf{H}^{(4)}$-$\mathbf{H}^{(6)}$ are very similar to signals $\mathbf{L}^{(4)}$-$\mathbf{L}^{(6)}$, which suggests that the source of these signals may not change between convective regimes. Their persistence and polarization are most consistent with sources *not* related to the lava lake at all, such as degassing at fumaroles. The slight change in the frequency content of $\mathbf{L}^{(4)}$-$\mathbf{L}^{(6)}$ could be related to the masking of the recovered signals in different frequency bands, by new seismic sources related to the changing lava lake convection.

We have now answered the question of what causes the changes in spectral content between the "low" and "high" convective regimes. Because we observe that (part of) the recovered signal $\mathbf{L}^{(1)}$ is unchanged, and that this signal is persistent, it

follows that the source mechanism for (part of) the tremor remains unchanged, and instead there are secondary sources superimposed. It remains, however, to constrain what these new sources might be, as well as to understand what this invariant tremor signal means for the process that triggered convective overturn in the lava lake.

We first discuss some of the new recovered signals during the "high" convective regime. Recovered signals $\mathbf{H}^{(12)}$- $\mathbf{H}^{(15)}$ appear to be transients at station MAR, as was already discussed. The signal $\mathbf{H}^{(7)}$ differs from signal $\mathbf{L}^{(7)}$ primarily by a sign swap along the CMG "axis" in the 3-dimensional space defined by each station's Z' components; it is therefore difficult to interpret this signal as new. However, signals $\mathbf{H}^{(9)}$-$\mathbf{H}^{(11)}$ have different principal eigenvectors from any signal seen during the "low" convection, and are narrowband signals at high frequencies, where little energy exists during "low" convection. From the example of $\mathbf{H}^{(9)}$ (Fig. 2.10), each recovered signal seemingly corresponds to narrow bands of high-frequency energy (Fig. 2.10b). Each shows primarily planar polarization (Fig. 2.10a), though Z' azimuths at L22 still point toward a source beneath the active lava lake. These recovered signals could therefore correspond to different spectral peaks of repeating "brittle failure" type events in or below the lava lake surface, that occur as cooled, sinking, brittle crust scrapes against the lava lake sides.

Finally, we observe one remarkable difference between signals $\mathbf{L}^{(9)}$ and $\mathbf{H}^{(8)}$, i.e. those subbands that contain local transients to station L22. Signal $\mathbf{H}^{(8)}$ is dominated by the subband $\boldsymbol{W_{3,1}}$, whose nominal passband is 3.13-6.3 Hz, and which accounts for 74% of the energy in this signal. This subband contains the nominal

passband of subband $\mathbf{W}_{4,2}$, i.e. the subband that contained the most energy during the "low" convection. However, during the "high" regime, its incidence angle is noticeably shallower (45° vs. 31°), and its azimuth (139°) points to the East edge of the active lava lake (Fig. 2.11). This suggests that its source is very shallow in the lava lake, rather than toward the bottom. Time-lapse photography (Alean 2002) suggests that its physical source process may be cooled, hardened crust subducting at the edges of the lava lake. The high energy of this signal during the "high" convective phase is consistent with this interpretation, as the rate of subduction during the "low" convective phase is an order of magnitude slower, and may not be enough to generate an energetic seismic signal.

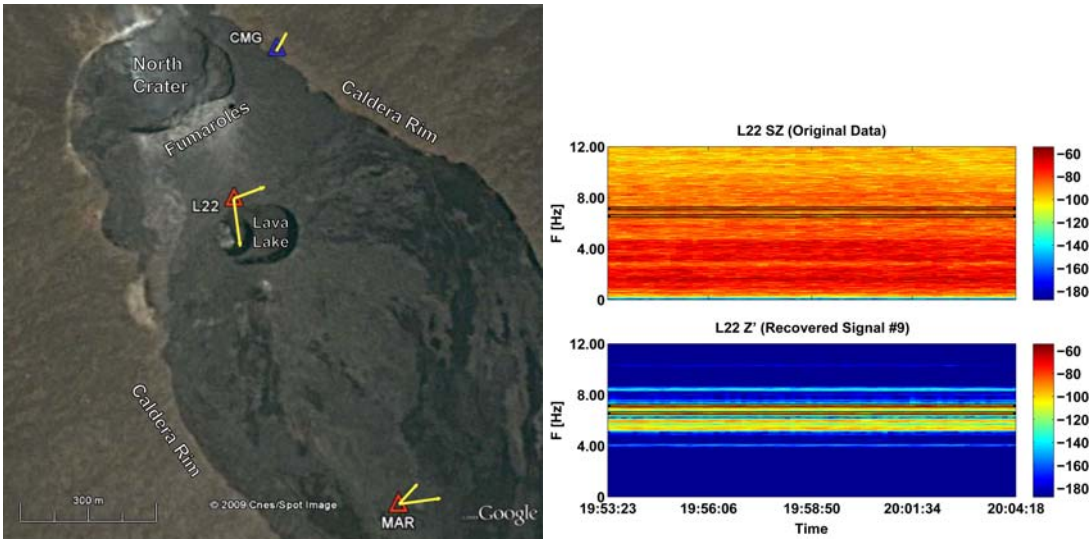

Figure 2.10. Spectrograms and azimuths of recovered signal $\mathbf{H}^{(9)}$, seen only during the "high" convective phase. **a.** (Left) Azimuths of subbands $\mathbf{W}_{j,n}$ that form recovered signal $\mathbf{H}^{(9)}$ are superimposed on an aerial photograph showing station locations and relevant physical features in the Erta 'Ale summit caldera. Azimuths are scaled according to relative energy of each $\mathbf{W}_{j,n}$ at each station. **b.** (Right) Spectrograms of the input Z data at station L22 (top) and the Z' component of recovered signal $\mathbf{H}^{(9)}$ (bottom). Color scaling is in dB computed from true ground velocity.

Figure 2.11. Azimuths of subbands $\mathbf{W}_{j,n}$ that form recovered signal $\mathbf{H}^{(8)}$ are superimposed on an aerial photograph showing station locations and relevant physical features in the Erta 'Ale summit caldera. Azimuths are scaled according to relative energy of each $\mathbf{W}_{j,n}$ at each station. The most energetic subband of $\mathbf{H}^{(8)}$ "points" toward the edge of the active lava lake.

2002 Interpretations

We now have sufficient information to describe the majority of the seismic signals recorded at Erta ‘Ale in 2002. A plot of seismic power spectrum is given for each convective regime in Fig. 2.12, labeled according to our conceptual model. We interpret the signals $\mathbf{L}^{(1)}$, $\mathbf{H}^{(1)}$, and $\mathbf{H}^{(3)}$ as the response of a conduit beneath the lava lake to the flow of fresh, hot, gas-rich magma from a deeper reservoir. We interpret

signals $\mathbf{L^{(4)}}$- $\mathbf{L^{(6)}}$ as passive degassing in the fumaroles and the north crater, which is unaffected by shallow processes in the lava lake. The signals $\mathbf{L^{(9)}}$ and $\mathbf{H^{(8)}}$ are dominated by shallow processes close to station L22. During the "high" convection, these include an energetic signal related to the subduction of cooled, brittle lava lake crust.

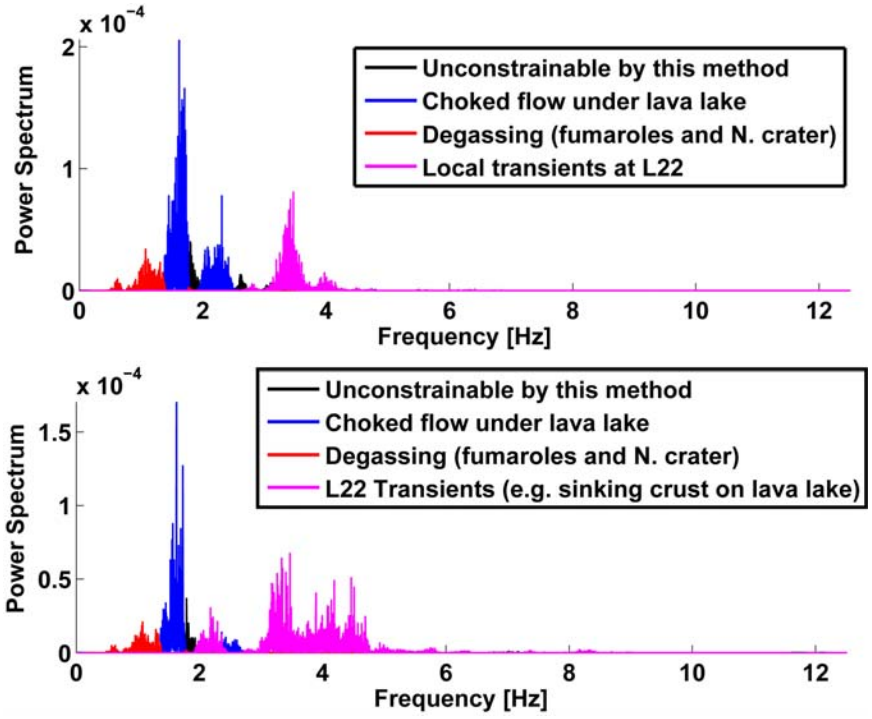

Figure 2.12. Conceptual model of tremor for each convective regime, illustrated using power spectra for Z' component of recovered signals at station L22.

Because we have determined that the main signal from the lava lake is largely unaffected by changing convective regimes, we can constrain conceptual models of the processes that might trigger rapid lava lake convection. A review of two competing conceptual models is given in Harris (2008). Following the modeling

of Harris (2008), the changing rates of lava lake convection would require that magma feeding the lava lake decrease in viscosity from $\eta = 10^3$ Pa s to $\eta = 10^2$ Pa s to completely explain the differences in rates of lava lake convection. However, following the model of Chouet (1988, 1986), this changing viscosity affects crack stiffness, which in turn causes the resonance frequency of the conduit to change. Thus, in our interpretation, the magma must feed the convecting lava lake at a relatively steady supply rate and constant viscosity, which favors the second model of Harris (2008), i.e. that the changing rate of convection is driven entirely by shallow processes within the lava lake.

Changes from 2002 to 2003

We have already discussed the morphological changes of the lava lake system from Feb 2002 to Nov 2003 (Fig. 2.2), and changes to the amplitude and spectrograms of seismic data (Fig. 2.4). Now we wish to investigate how the seismic sources that form the composite tremor signal changed between the two experiments. Because the 2003 experiment featured 7 seismic stations, we caution that decomposing the 2003 data will recover many more input signals than for the 3 station array of 2002. Additionally, the cost functional will now attain a maximum normalized value of $M(\mathbf{W}_{j,n}) = 6$, rather than 2. Because 2003 tremor showed no obvious spectral transitions or even large amplitude variations, we first analyze a representative sample of the tremor, then discuss the persistence of the recovered signals.

Fig. 2.4c shows a spectrogram of the selected data sample. Almost all seismic energy is concentrated below 6 Hz, with few transients and no bands of high-frequency energy. Fig. 2.13a shows the wavelet basis that best represents this decomposition. Fig. 2.13b shows a dendrogram of this sample's best wavelet decomposition. From Fig. 2.13b, *SDR* finds 30 recovered signals $\mathbf{B}^{(\cdot)}$. From Fig. 2.13b, we see that most of these are narrowband signals with passbands of 0.2-0.4 Hz. Analysis of such a data set seems impossibly daunting, but note from the dendrogram (Fig. 2.13b) that half of this sample's recovered signals $\mathbf{B}^{(\cdot)}$ have a lowest lower corner frequency $f_L \geq 9.38$ Hz. This simplifies the problem considerably, as there is very little signal energy at these frequencies (Fig. 2.4c), and from Fig. 2.3b we see that, regardless of a high-frequency signal's true source, most stations will record scattered, incoherent energy that can neither be located reliably nor constrained by polarization analysis. We therefore focus primarily on lower frequency signals recovered from subband decomposition, i.e. $\mathbf{B}^{(1)}$ through $\mathbf{B}^{(15)}$.

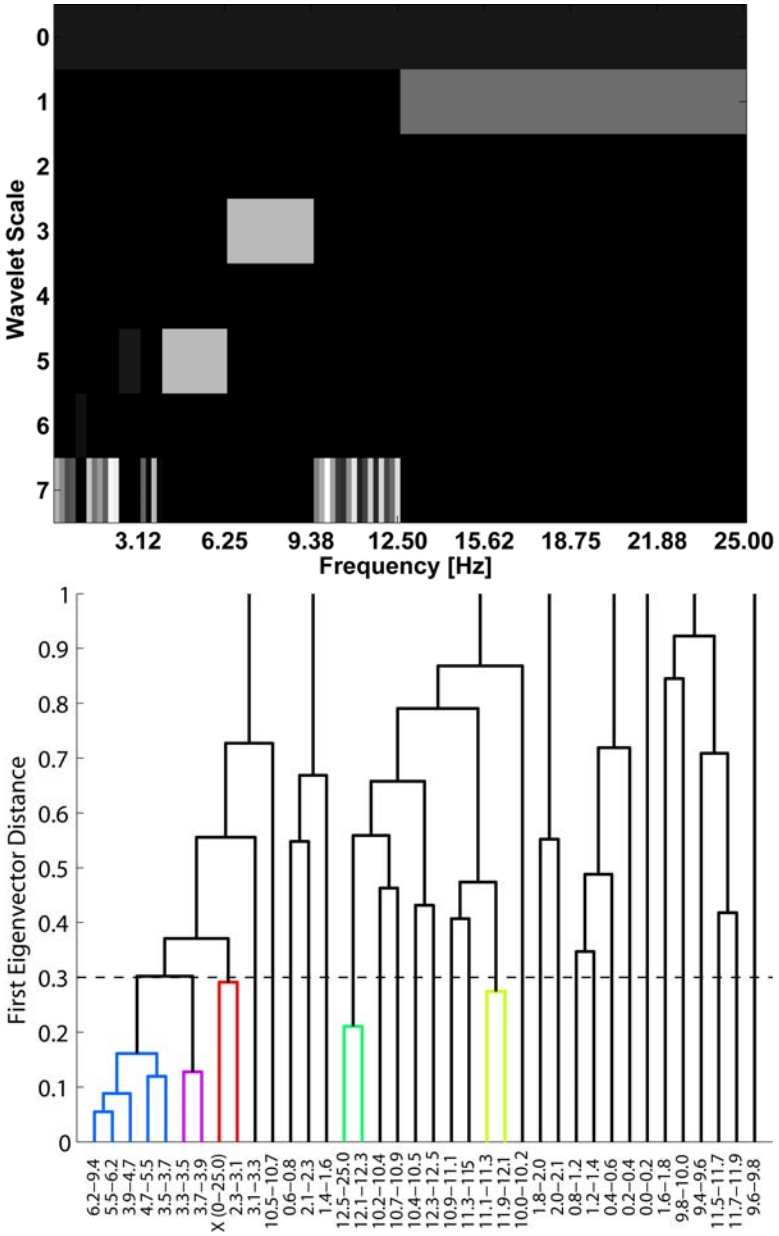

Figure 2.13. Decomposition of the 2003 Erta 'Ale seismic data sample of Fig. 2.4c, using the *SDR* algorithm (Chapter I). **a.** (Top) Wavelet basis selected by subband clustering. Selected wavelet packets are shaded in grayscale according to their clustering in a. *Y*-axis shows wavelet scale *j*, with *j*=0 corresponding to the wideband (input) signal. *X*-axis shows the position and nominal passband for each wavelet packet in the interval [0 f_n]. **b.** (Bottom) Dendrogram, showing subband clustering. Node denoted with "X (0-25.0)" denotes the input data. Horizontal dashed line indicates distance threshold δ for clustering of principal components eigenvectors.

Tremor Location

Because the 2003 campaign featured 7 temporary stations, we can locate the recovered signals $\mathbf{B}^{(\cdot)}$ from this time. We choose the energy-based grid search location routine of Gottschämmer and Surono (2000) due to the energy-preserving properties of wavelet transforms (Percival and Walden 2000). This method also formed the basis for the least-squares inversion of Jones et al. (2006). Although the grid-search routine is slower, it is more appropriate for tremor sources which are *not* point sources, and the misfit associated with the tremor centroid can sometimes associate the shape of a distributed source with meaningful geologic surface features (e.g. Furumoto et al. 1992).

As noted by Konstantinou and Schlindwein (2002), the method of Gottschämmer and Surono (2000) is almost identical to amplitude and semblance-based techniques, but makes the assumption that tremor amplitude decays as a body wave, and accounts only for intrinsic absorption. To review, this technique involves searching a 3-dimensional grid for the isotropic source power, given by

$$P = 4\pi R^2 \rho v e^{kR} \int_{t_1}^{t_2} y(t)^2 dt \qquad (1)$$

where R is source-receiver distance, ρ is density, v is phase velocity, and the integral represents seismic source energy, i.e. the directly measured quantity. The point whose source-receiver distances R yield the most nearly isotropic source is called the tremor hypocentroid. With the misfit for each station k defined (as in Jones et al. 2006) by $r_k \equiv P_k - \overline{P}$, it is easy to estimate χ^2 contours from the grid

search. Thus we include in all location plots the χ^2 contours corresponding to a 90% error ellipse for each point.

Because reconstructed signals are formed by summation of many subbands, their azimuth and incidence angle are not preserved with regard to true North. However, their rectilinearity and planarity (Jurkevics 1988) are. Thus we can construct a weighted grid search for the minimum residual at each station (Bevington et al. 2002), using the rectilinearity of the reconstructed signal $\boldsymbol{B_k}^{(.)}$ at station *k* as the weighting parameter. Since we assume a rectilinearly polarized body wave, we compute the signal energy in (1) by summing the seismic energy over all 3 components, i.e. substituting $\sum_{m=1}^{3}\int_{t_1}^{t_2} {y_m}^2(t)dt$ for $\int_{t_1}^{t_2} y(t)^2 dt$. In this way the weight of the observed parameter (the signal energy) is a truly independent quantity. All locations are computed using a grid with 10m spacing, between 0 and 600m a.s.l., whose geographic boundaries are 13.600-13.608° N and 40.660-40.668° E.

Location Results

Fig. 2.14 shows illustrative locations of some recovered signals from the 2003 experiment. We find that locations of recovered signals generally fall into one of 4 non-overlapping geographic regions. Each region is associated with a non-overlapping part of the frequency spectrum. The 2002 data already suggested that tremor sources could occupy non-overlapping regions of the frequency spectrum, which means that some seismic sources may even have persisted from 2002 to 2003.

We now wish to discuss these recovered signals $\mathbf{B}^{(\cdot)}$ in the context of their locations and relations to geologic features within and under the Erta 'Ale summit caldera.

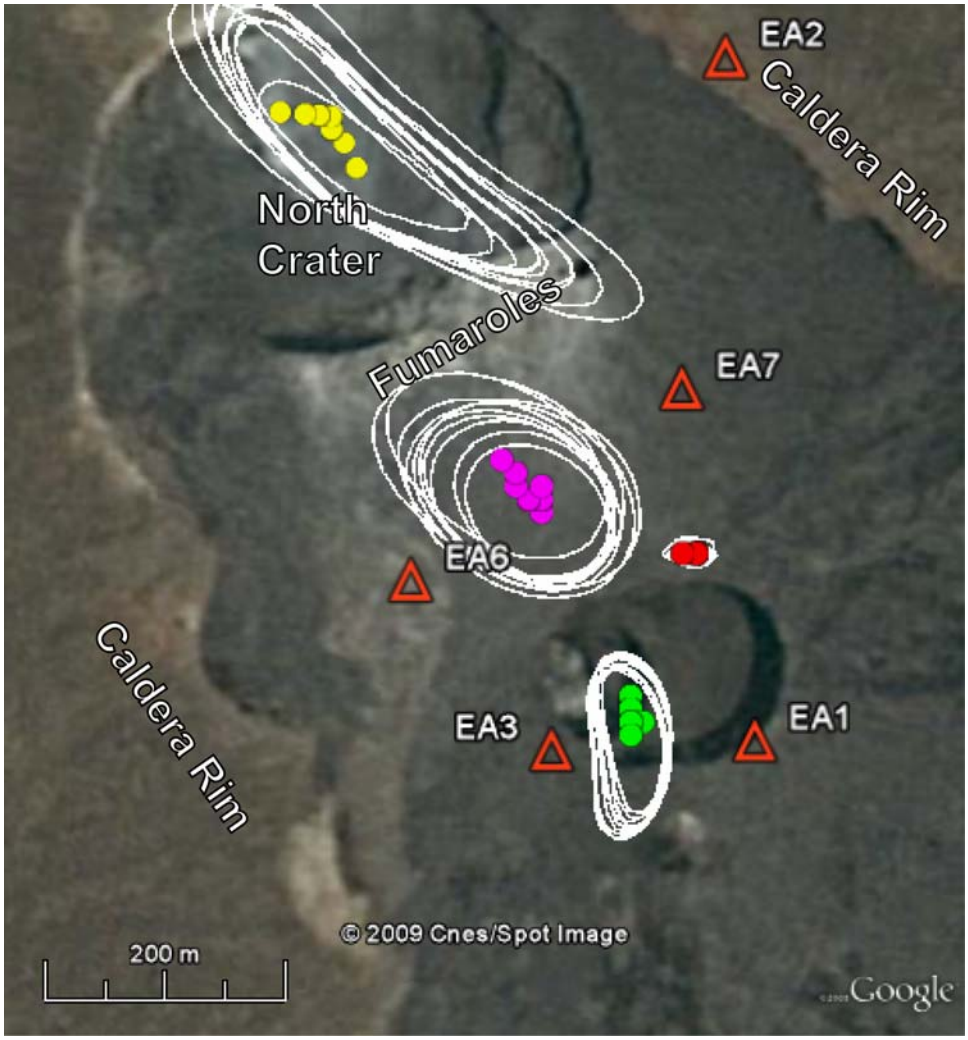

Figure 2.14. Locations of sample recovered signals from 2003. Locations generally fall into one of four geographic regions: The lava lake (green circles); the north crater (yellow circles); the region between the two craters (magenta circles); or the region near the northern rim of the crater that held the active lava lake (red circles). Solid white lines denote χ^2 contours for each point corresponding to a confidence interval of 0.9.

Signals in the Northern Crater

Some recovered signals locate to the northern crater, which held a lava lake during the 1960s (Barberi and Varet 1970), and many fumaroles during the 2002 and 2003 campaigns. These recovered signals are always low frequency ($0.4 \leq f \leq 1.4$ Hz) and are typically narrowband, with passbands ~0.2 Hz wide. The example shown in Fig. 2.15a corresponds to a narrowband signal formed from the single subband $\mathbf{W}_{7,5}$, whose nominal passband is 0.97-1.17 Hz. Locations of "north crater" signals are uniformly shallow (550-580m a.s.l., i.e. just below the surface). They are most energetic and most rectilinearly polarized at EA2 and EA7, i.e. the stations closest to the north crater (Fig. 2.15b). However, azimuths of their constituent subbands at EA3 always point toward the lava lake, and the recovered signal is disproportionately energetic at this station (Table 2.3). For this reason, we exclude EA3 from location of these recovered signals.

Observe from Fig. 2.15b that typical χ^2 contours for these signals lie almost completely within the north crater. Presumably the large uncertainty in their location is because of the influence of sources from the lava lake at e.g. EA6, combined with a "true" location that lies outside the array. Because these signals are shallow, rectilinearly polarized, and narrowband, we interpret them as the seismic signature of degassing at the fumaroles. Conceptually, the generation of such signals could be no different than the generation of harmonic tremor (e.g. Chouet 1988, 1986), but in this case the "fluid" would be gas and the "conduits" would be the system of cracks that feeds the fumaroles.

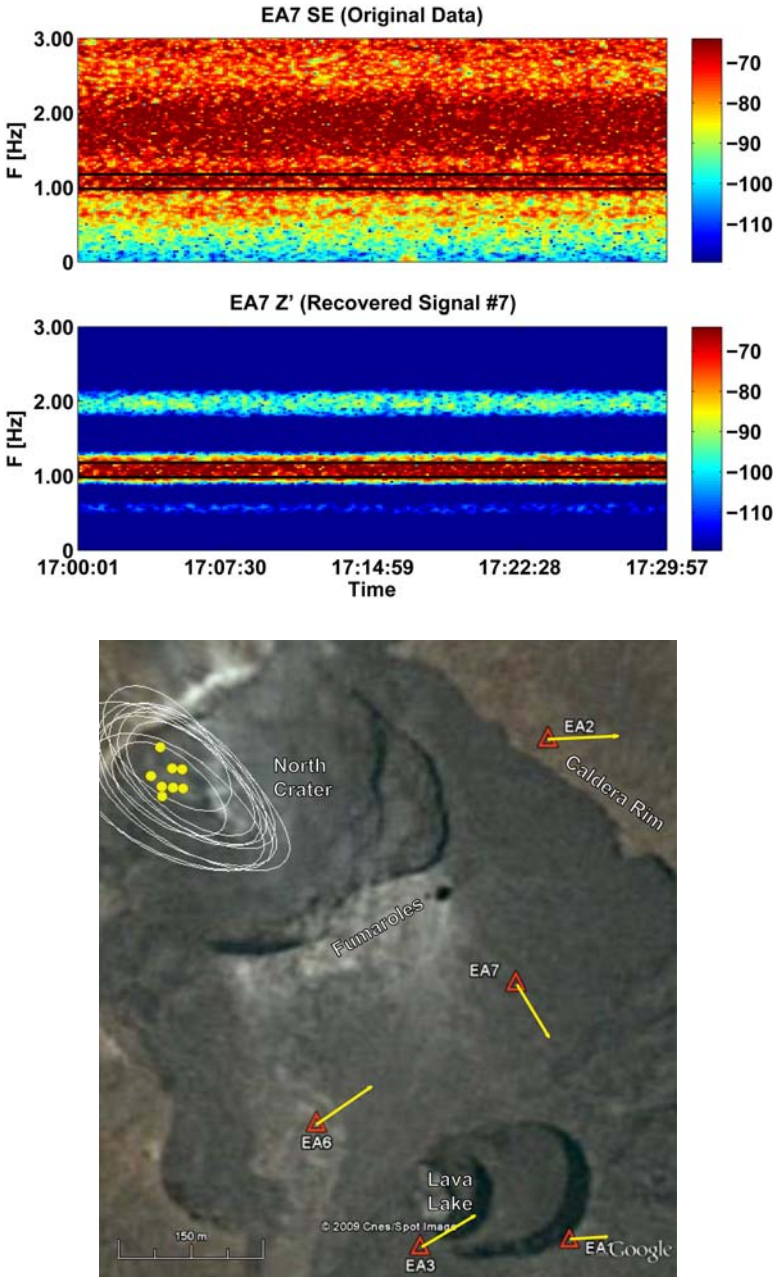

Figure 2.15. Spectrogram and locations of a representative signal from the north crater. **a.** (Top) Spectrogram of recovered signal $\mathbf{B}^{(7)}$, formed from $\mathbf{W}_{7,5}$ (nominal passband 0.97-1.17 Hz), from a half-hour data sample beginning 17:00 GMT, 2 Dec 2003. Top: Input *E* component data at EA7. Bottom: Recovered *Z′* data. Color scaling is in dB computed from true ground velocity. **b.** (Bottom) Locations and azimuths for the signal in a. Azimuths are scaled relative to the station whose recovered signal energy is highest, in this case EA2.

Signals Between Craters

In the range $1.4 \leq f \leq 2.2$ Hz, *SDR* typically recovers narrowband signals that locate between the north and south craters (Fig. 2.16). Analysis and interpretation of these signals is somewhat difficult, because their locations are well below the surface (300-400m a.s.l.), and they do not correspond to an obvious geologic feature in the summit caldera. It could also be true that these signals are a mixture of low frequency energy from seismic sources in the north crater (at EA2 and EA7), and high frequency energy from signals in the lava lake (at EA3 and EA1). This seems unlikely, however, as the recovered signal energy (Table 2.3) is low stations near the lava lake, and removing these stations from the location routine does not change the locations. Additionally, these recovered signals do not meet the criteria for signal persistence discussed in Chapter I. Thus it is unlikely that they result from combinations of other signals.

Instead, we suggest the following. If the locations are correct in an absolute sense, then, from the geometry of Fig. 2.16, these signals are polarized like *P*-waves (i.e. azimuths point toward centroid locations) at EA7, EA6, and EA4, and *S*-waves (i.e. azimuths rotated 90° to centroid locations) at EA2. Additionally the incidence angle of the located sample is 75° at EA7, the nearest station. This is consistent with the location depths of the recovered signal. Thus there are two possible explanations for tremor in this frequency range: either a series of repeating double couples, with recovered signals that correspond to spectral peaks of repeating events; or persistent signals related to a magma body that underlies the area between the two craters. The

latter has been proposed before, at comparable depths, based on the similar lavas erupted.

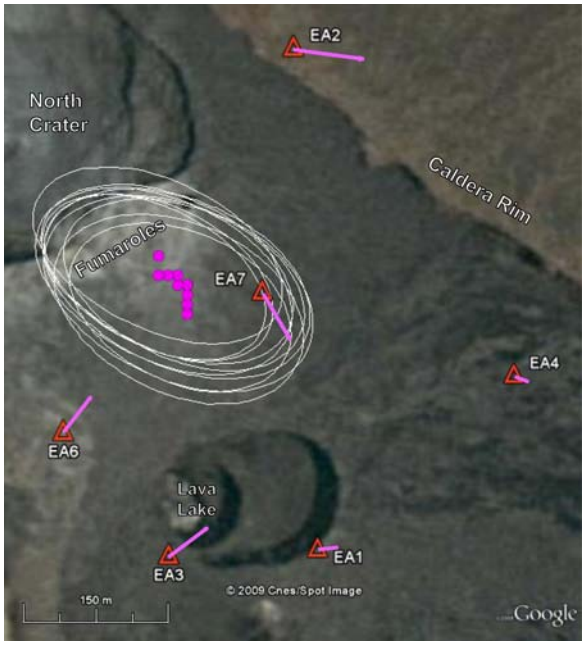

Figure 2.16. Locations and azimuths of a representative signal from between the two craters. Azimuths are scaled relative to the station whose recovered signal energy is highest, in this case EA7. Relevant geographic features are labeled.

Lava Lake Signals

In general, recovered signals that locate to the lava lake have nominal passbands between 2.15 and 9.37 Hz. Locations of three recovered lava lake signals from the time sample of Fig. 2.4c are shown in Fig. 2.17. In this sample, signal $\mathbf{B}^{(1)}$, whose nominal passband is 2.34-3.13 Hz (Fig. 2.13b), locates to depths of 450-490m a.s.l., or 30-70m below the lava lake surface. These depths are consistent with the bottom of lava lake, or a region slightly underlying it, as inferred by

Oppenheimer and Francis (1998). Thus $\mathbf{B}^{(1)}$ could be generated by flow of fresh magma into the lava lake from below, similar to the recovered signals $\mathbf{L}^{(1)}$ and $\mathbf{H}^{(1)}$ from 2002. Following this interpretation, the change in frequency content of this signal from 2002 to 2003 suggests that either the conduit geometry or the properties of the ascending magma also changed. Either change could be supported by the change in lava lake morphology seen in Fig. 2.2.

Signal $\mathbf{B}^{(14)}$, whose passbands are 3.32-3.51 Hz and 3.71-3.91 Hz, locates to depths shallower than 520m a.s.l., at (or even above) the lava lake surface. Signal $\mathbf{B}^{(15)}$, whose passbands are 3.51-3.71 Hz and 3.91-9.37 Hz, locates to depths of 500-520m a.s.l., at or slightly below the lava lake surface. Each signal cross-correlates to the others weakly ($0.06 < \rho < 0.33$) but significantly ($p < 10^{-10}$) with no lag, suggesting that they may be related. Clearly, because the χ^2 contours of each location overlap, all 3 signals correlate, and (from Table 2.3) signals $\mathbf{B}^{(14)}$ and $\mathbf{B}^{(15)}$ each fall within the threshold distance $\delta = 0.3$ of the EA3 "axis" in the 7-dimensional space defined by each station's Z' wavelet coefficients, it is necessary to ask whether these signals truly represent 3 sources, or some combination of fewer seismic sources plus local transients coherent only at EA3.

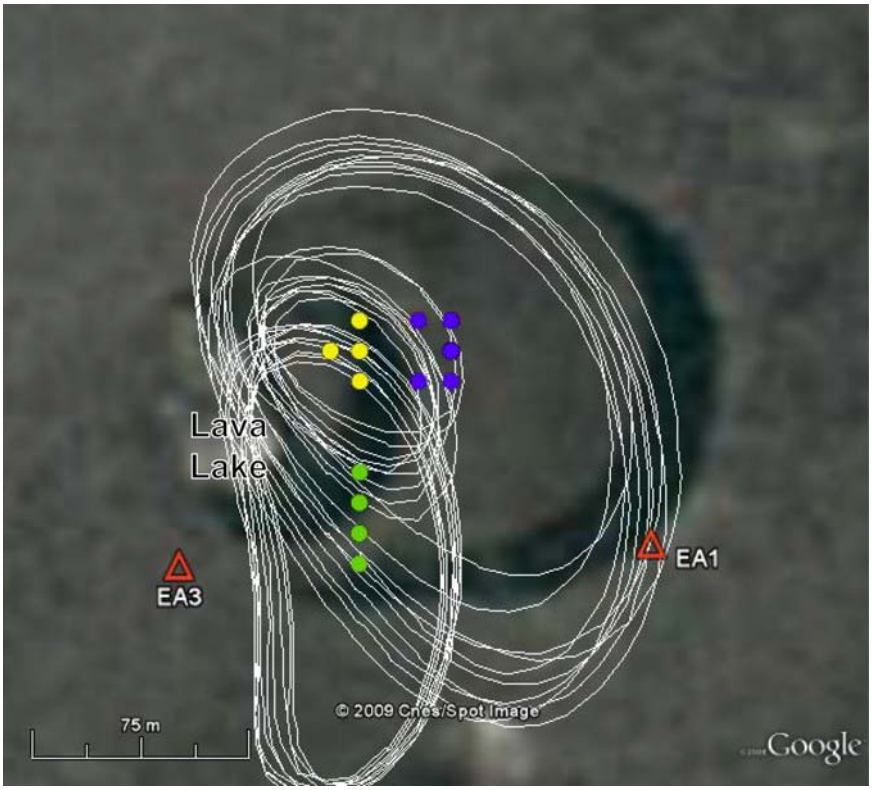

Figure 2.17. Locations of three recovered signals from a half hour data sample beginning 16:30 GMT, 02 Dec 2003. Blue dots correspond to the recovered signal $\mathbf{B}^{(1)}$, with nominal passband 2.34-3.13 Hz. Yellow dots correspond to recovered signal $\mathbf{B}^{(14)}$, with nominal passband 3.3-3.5 and 3.7-3.9 Hz. Green dots correspond to recovered signal $\mathbf{B}^{(15)}$, with nominal passband 3.5-3.7 and 3.9-9.4 Hz. Solid white lines denote χ^2 contours for each point corresponding to a confidence interval of 0.9. Approximate location of lava lake is labeled.

Correlation of Lava Lake Signals with Acoustic Signals

We proceed by first noting that the signal of Fig. 2.4c was recorded during a period of calm wind. Thus, the acoustic data can be compared directly to the seismic data. Fig. 2.18a shows a comparison between recovered signal $\mathbf{B}^{(15)}$ and the raw acoustic data from this time period. Clearly there is some similarity between the signals, as the sharp transients of the acoustic data are present in the recovered

signal. This is not the case for signal $\mathbf{B}^{(1)}$ (Fig. 2.18b). It is instructive to see whether or not acoustic signals can be recovered in a similar way to seismic signals using the *SDR* algorithm, and which of these recovered acoustic signals (if any) correlate to the recovered seismic signals whose locations correspond to regions near the lava lake. Because the data set includes 4 acoustic microphones, and synthetic tests suggest that RMS of recovered signals is slightly higher for 4 channels than for 5+, we caution that the number of elements in this seismo-acoustic array is adequate for *SDR*, but not ideal. Recovered acoustic signals will be designated $\mathbf{A}^{(\cdot)}$ for this analysis. Only the frequency content of recovered acoustic signals will be discussed

Fig. 2.19 shows a dendrogram for the subbands of acoustic signals recorded during this period. 17 acoustic signals are recovered. We wish now to examine which recovered acoustic signals correlate to which recovered seismic signals. Thus we correlate each recovered acoustic signal with each recovered seismic signal, matching each channel of acoustic data to data from its colocated seismometer. We search for significant correlations between any channel j of a recovered acoustic signal $\mathbf{A}^{(\cdot)}$ and any Z' channel k of a recovered seismic signal $\mathbf{B}^{(\cdot)}$. Using this approach, 5 sets of cross-correlations are found whose maximum values anywhere are $\rho_{j,k} \geq 0.1$. Each of these correlations includes exactly one recovered seismic signal that locates in the shallow lava lake ($\mathbf{B}^{(14)}$ and $\mathbf{B}^{(15)}$), which correlates to exactly one acoustic signal ($\mathbf{A}^{(8)}$ and $\mathbf{A}^{(11)}$, respectively).

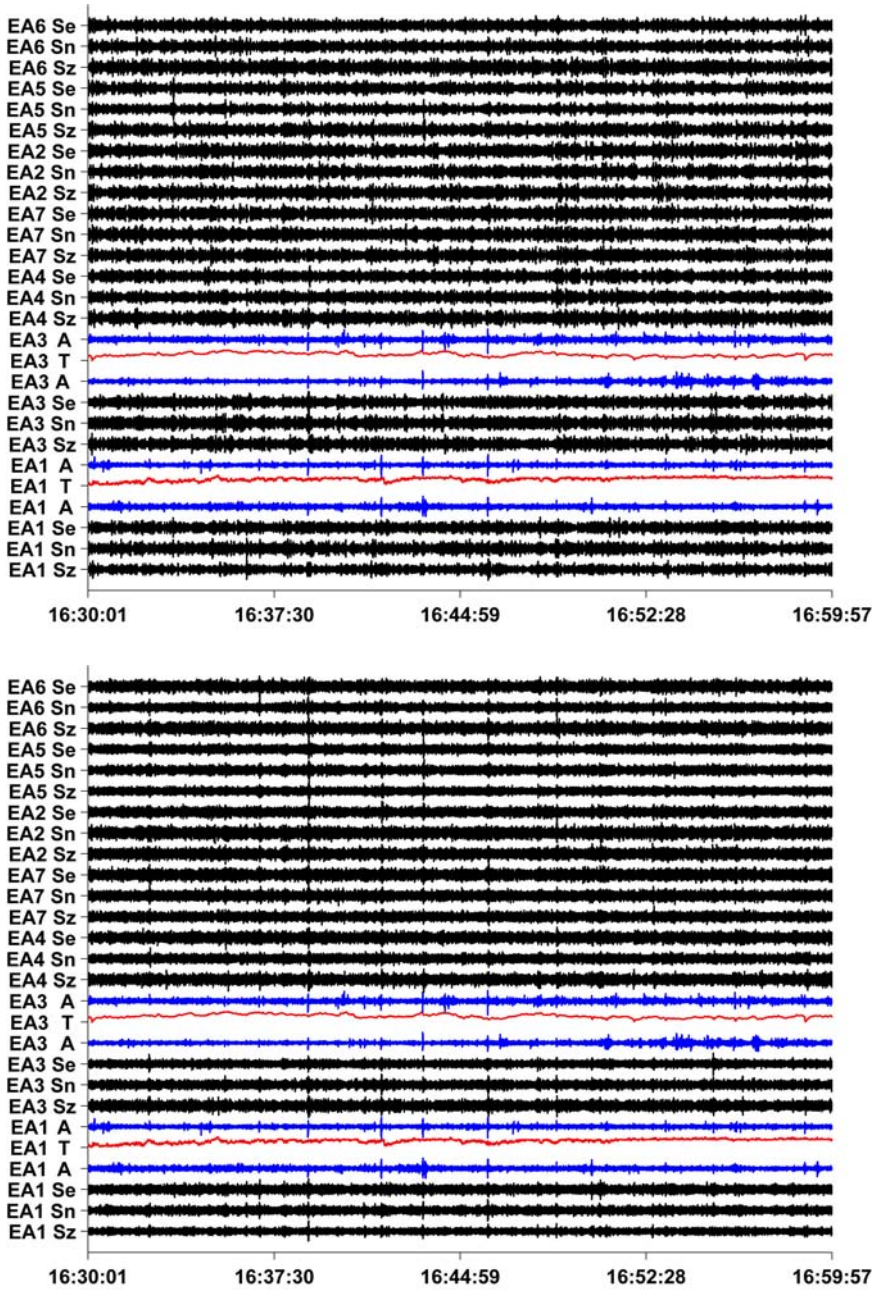

Figure 2.18. Seismic data for two recovered signals are compared visually to raw thermal and raw seismo-acoustic trace data from the same time period, beginning 16:30 GMT, 02 Dec 2003. Amplitudes of trace data are normalized. a. Recovered signal $\mathbf{B}^{(1)}$, with nominal passband 2.34-3.13 Hz. b. Recovered signal $\mathbf{B}^{(15)}$, with nominal passband 3.5-3.7 and 3.9-9.4 Hz.

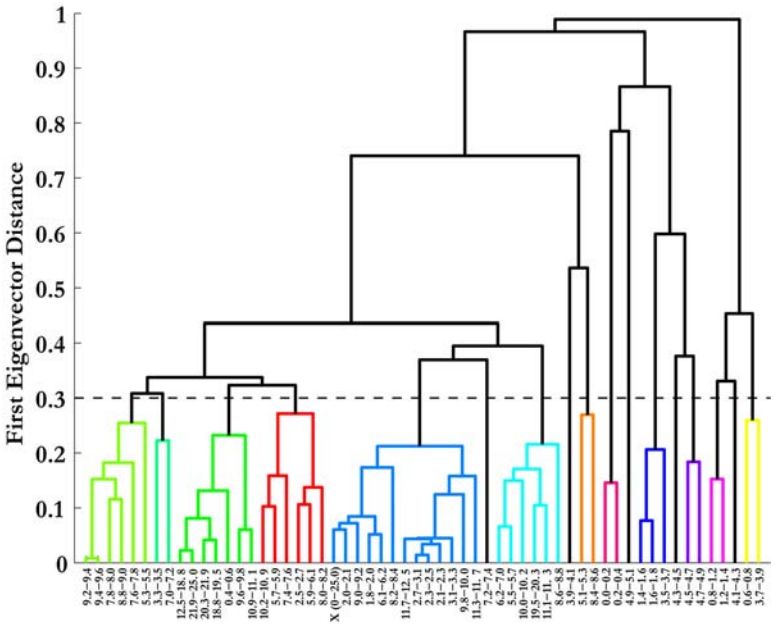

Figure 2.19. Dendrogram showing the decomposition of the 4 channels of acoustic data using the *SDR* algorithm (Chapter I). 17 signals are recovered. Node denoted with "X (0-25.0)" denotes the input data. Horizontal dashed line indicates distance threshold δ (Chapter I) for clustering of principal components eigenvectors.

We wish to explore this result in detail. Recovered "lava lake" signal $\mathbf{B}^{(14)}$ correlates to recovered acoustic signal $\mathbf{A}^{(8)}$ at $\rho = 0.12$ at EA3, and $\mathbf{B}^{(15)}$ correlates to recovered acoustic signal $\mathbf{A}^{(11)}$ at $\rho = 0.11$ at EA3. The p-values associated with these cross-correlations are $\sim 10^{-11}$, indicating that each correlation is statistically significant. Recovered acoustic signals $\mathbf{A}^{(8)}$ and $\mathbf{A}^{(11)}$ do not correlate significantly to one another ($\rho_{\max} < .0004$, $p = 0.91$), $\mathbf{B}^{(15)}$ correlates weakly to $\mathbf{A}^{(8)}$ ($\rho_{\max} = .02$, $p < 10^{-8}$), and $\mathbf{B}^{(14)}$ correlates weakly to $\mathbf{A}^{(11)}$ ($\rho_{\max} = .02$, $p < 10^{-9}$). Recovered signals $\mathbf{B}^{(14)}$ and $\mathbf{A}^{(8)}$ each include energy between frequencies 3.3-3.5 Hz, while $\mathbf{B}^{(15)}$ and $\mathbf{A}^{(11)}$ each include energy at 4.3-4.5 Hz. Thus, each of the two recovered seismic signals from the shallow lava lake correlates significantly at $\rho > 0.1$ only to a single

recovered acoustic signal with energy at similar frequencies. Meanwhile, recovered seismic signal $\mathbf{B}^{(1)}$ does not correlate significantly to *any* recovered acoustic signal, confirming its relatively deep location. We conclude from this analysis that the 3 recovered seismic signals (and their two acoustic counterparts) are likely 3 real signals, and each shallow signal is correctly located to the very shallow lava lake.

We can further place constraints on the source of shallow lava lake signals by examining the lag times between the maximum cross-correlations of the seismic and acoustic data at each channel. In all cases with $\rho > .07$, lag times between colocated seismic and acoustic traces are consistently 66-92 samples, or 1.32-1.84s. The distance to the lava lake is ~80m at EA3 and ~160m at EA1. A much lower lag time is expected if these signals originate directly at the lava lake surface. This suggests, instead, that the seismic signals are triggered by processes slightly below the surface, such as gas bubble coalescence (Ripepe and Gordeev 1998), which generate (weakly correlated) acoustic signals as bubbles burst at the lava lake surface.

Persistence of Recovered Signals

We now discuss which recovered signals persist through time. To investigate the invariance of recovered signals as a function of their frequency, we analyze 20 consecutive 30 min samples of data, including the sample in Fig. 2.4c. For purposes of this discussion, we define a persistent signal, as in Chapter I, as any recovered signal with subbands whose principal eigenvectors *each* cluster to *each* principal

eigenvector of some earlier signal, using a distance threshold of $\delta = 0.3$ and a median clustering rule. Thus, a unique signal is defined as *any* recovered signal for which *at least one* constituent subband has a principal eigenvector that *does not* cluster to the principal eigenvectors of the subbands that form an existing signal (using the same threshold and clustering). Fig. 2.20a shows the number of unique signals (out of 20 possible) recovered in this way, as a function of frequency. A subband that contains 10 unique signals in this time period therefore contains a single signal for no greater than 5 hours. To compliment this data, Fig. 2.20b shows the maximum number of half-hour samples in which a single recovered signal persists. From these figures, observe that the signal content of the tremor is relatively stable -- that is, a single recovered signal persists in each subband for at least half the observed time period -- from 2.73-9.57 Hz. It is entirely unsurprising that signals from 9.57-15.63 Hz are shown from Fig. 2.20b to be high-frequency transients. The recovered signals above 15.63 Hz always fall within the threshold distance $\delta = 0.3$ of one station's "axis" in the 7-dimensional space defined by each station's Z' wavelet coefficients. Thus, are effectively always dominated by transients recorded at a single station. Most commonly, this is EA3, which unsurprisingly suggests that these frequencies sometimes contain recovered signals from shallow lava lake processes.

The most persistent signals over this time period are 3 recovered signals, each formed from a single subband: their nominal passbands are 1.36-1.56 Hz, 1.76-1.95 Hz, and 1.95-2.15 Hz, respectively. Each signal persists through the entire

period. Recall that one possible interpretation of these recovered signals was oscillation of a fluid-filled cavity or conduit system that connects the two craters, the existence of which was deduced by Oppenheimer and Francis (1998) and Tazieff (1994). Such an interpretation is consistent with these signals' invariance if magma propagated from this deeper reservoir at a relatively constant rate in 2003, which is also a necessary condition to explain the constant rate of lava lake convection. Thus the persistence of these three recovered signals strongly favors this model for the source of seismic energy at these frequencies.

The frequencies whose energy most commonly locates to in or below the lava lake are each associated with recovered signals that persist 50-75% of the time. Note that 4-9 recovered signals are seen in each subband of the frequency range 2.73-9.57 Hz. This suggests that there are *always* multiple signals at these frequencies, and agrees with our interpretation of the correlations between seismic and seismo-acoustic data. Following the conceptual model for tremor at Stromboli (Ripepe and Gordeev 1998), there could be several locations where forced bubble coalescence occurs simultaneously. Furthermore, those recovered signals that locate below the lava lake could correspond to multiple resonating cracks, or a single crack whose resonance is sometimes buried in signals from gas bubble coalescence and bursting in the shallow lava lake. It is nonetheless noteworthy that a steady rate of lava lake convection does not necessarily indicate that its associated seismic signals are static.

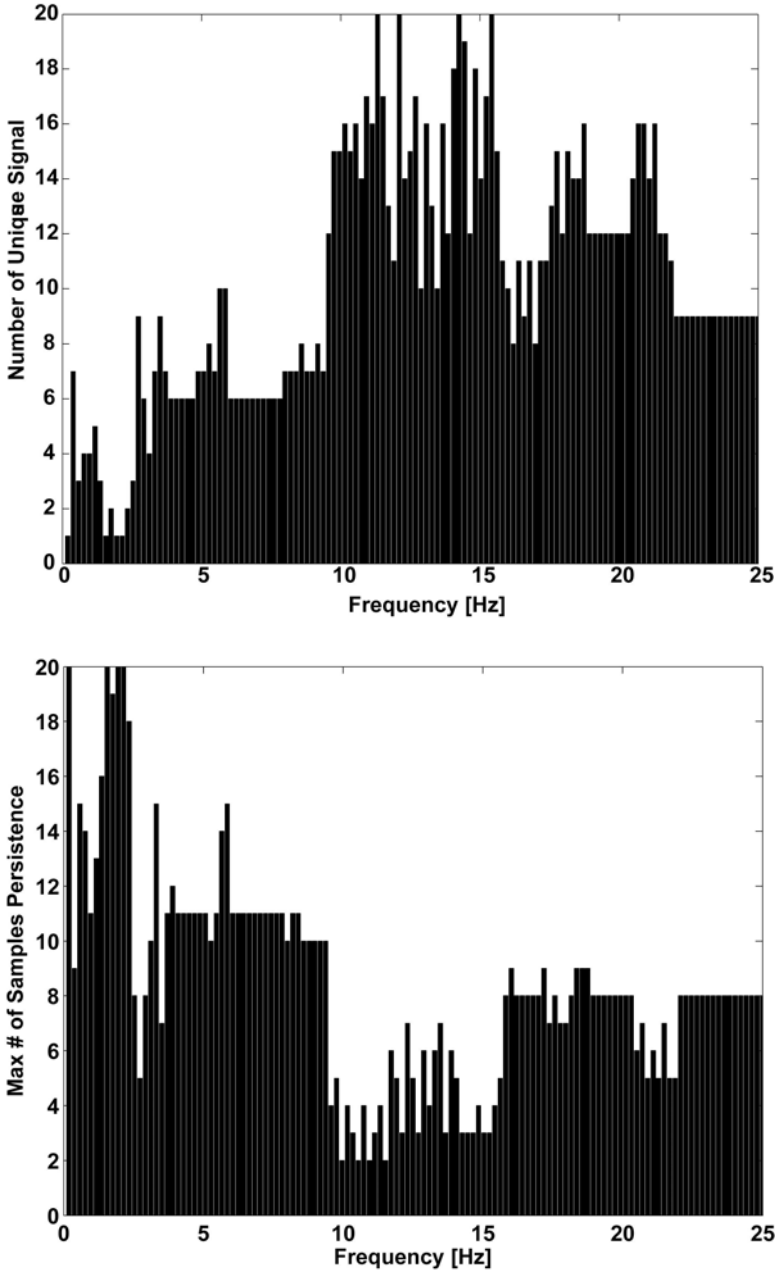

Figure 2.20. Persistence of signals over a 10h period beginning 15:30:00 GMT, 02 Dec 2003, divided into 20 samples of 30 min length. **a.** (Top) Number of unique signals recovered in each frequency band. **b.** (Bottom) The longest duration (in number of 30 min samples) of a signal in each frequency band.

2003 Interpretations

We can make the following interpretations based on our analysis of the 2003 Erta 'Ale tremor data. In the low frequency seismic energy (0.59-1.36 Hz), several recovered signals are seen as a result of shallow degassing processes in and around the northern crater. These correspond physically to both the northern crater and the system of fumaroles near its southern edge. At frequencies of 1.36-2.53 Hz, several narrowband signals are recovered, corresponding to the resonance of cracks and magma bodies below and between the two craters. We interpret these signals as a result of fresh, hot, gas-rich magma propagating upward from depth, and propagating outward in turn to feed the active lava lake. These correspond to an inferred system of conduits and reservoirs that connects the two lava lakes (Oppenheimer and Francis 1998). The relatively constant supply rate of magma gives rise to the persistence of the signals.

At frequencies of 2.53-9.57 Hz, several signals are generated by a combination of gas bubble coalescence in the active lava lake (Ripepe and Gordeev 1998), gas bubble bursting at the lava lake surface, and choked flow of fresh, hot magma through a conduit (Chouet 1986, 1988), which feeds the lava lake from below. The first two processes are shallow, giving rise to a significant correlation between seismic and seismo-acoustic data during periods of little or no wind.

Above 9.57 Hz, no coherent, persistent signals exist. However, some evidence suggests that persistent signals of processes from the shallow lava lake can be seen at EA3 up to 25 Hz.

Summary and Conclusions

The *SDR* algorithm is useful because it provides a quantitative, semi-automated means of decomposing seismic data into subbands, while preserving many properties that are classically used to analyze volcanic tremor. Here, applied to data recorded during two seismic experiments at Erta 'Ale, Ethiopia, we are able to identify several signals from each time period that correspond to both the lava lake and other geophysical features (observable and implied). The data from the 2002 experiment are dominated by a persistent signal that might correspond to choked flow of fresh, hot magma to the lava lake. The persistence of this signal implies a relatively constant magma viscosity, limiting the possible causes of variable lava lake convection in 2002. The data from the 2003 experiment suggest multiple tremor source processes active in the lava lake at all times, and imply that several types of tremor sources (e.g. Chouet 1996, Ripepe and Gordeev 1998) can exist at the same time at the same volcano. In reality, the tremor at Erta 'Ale, and indeed persistent tremor everywhere, may be formed from several seismic sources, each physically meaningful, and each contributing part of the energy.

Table 2.1. Recovered signals from a data sample recorded during the "low" convective regime in 2002, beginning 15 Feb 2002, 16:28:46 GMT. Signal names use the convention $\mathbf{L}^{(n)}$, described in the text. Values for eigenvectors $v_{j,n}$ correspond to the largest eigenvalue $\lambda_{j,n,1}$ of the principal components of each wavelet packet $\boldsymbol{W_{j,n}}$. $v_{j,n}$, energy (En), azimuth (Az), incidence angle (In), rectilinearity (Rc), and planarity (Pl) are arranged in columns by station. Az and In are in degrees. Wavelet packets are designated $\boldsymbol{W_{j,n}}$ and nominal passbands f_{min} - f_{max} for each $\boldsymbol{W_{j,n}}$ are given in Hz. Cost functional M($\boldsymbol{W}$) is renormalized (multiplied by normalized bandwidth 2^{j+1}) so that $0 \le M(\boldsymbol{W}) < 3$. Spectral leakage for each subband is tabulated in the form $\log_{10}(E_{out}/E_{in})$, the base 10 logarithm of spectral energy outside the passband to spectral energy inside the passband. Relative lags of each subband are given in seconds for subbands whose wavelet cross-correlations are well constrained.

Signal		Sta	L22	CMG	MAR
$L^{(1)}$					
$W_{7,7}$		$v_{7,7}$	-0.76	0.64	-0.02
f_{min}-f_{max} (Hz)	1.37-1.56	En	1.9e-07	1.5e-07	5.1e-08
M($W_{7,7}$)	0.123	Lag	-0.10	-0.12	0.22
$\log_{10}(E_{out}/E_{in})$	-0.081	Az	-166.97	-53.89	116.45
		In	28.01	71.45	87.99
		Rc	0.97	0.79	0.86
		Pl	0.96	0.83	0.97
$W_{7,8}$		$v_{7,8}$	0.80	-0.53	0.27
f_{min}-f_{max} (Hz)	1.56-1.76	En	2.5e-07	1.2e-07	5.4e-08
M(W7,8)	0.303	Lag	-0.02	-0.02	0.04
$\log_{10}(E_{out}/E_{in})$	-0.000	Az	-173.10	-44.29	-73.91
		In	24.75	69.19	89.27
		Rc	0.98	0.74	0.86
		Pl	0.98	0.81	0.97
$W_{6,5}$		$v_{6,5}$	-0.90	0.44	0.02
f_{min}-f_{max} (Hz)	1.95-2.34	En	1.4e-07	5.9e-08	1.7e-08
M($W_{6,5}$)	0.313	Lag	-0.22	-0.12	0.34
$\log_{10}(E_{out}/E_{in})$	-0.193	Az	160.32	-45.96	56.54
		In	30.37	74.04	84.95
		Rc	0.91	0.57	0.66
		Pl	0.97	0.90	0.85
$W_{7,12}$		$v_{7,12}$	-0.82	0.57	-0.07
f_{min}-f_{max} (Hz)	2.34-2.54	En	4.4e-08	2.9e-08	7e-09
M($W_{7,12}$)	0.375	Lag	-0.04	-0.12	0.16
$\log_{10}(E_{out}/E_{in})$	-0.139	Az	160.74	163.14	69.21
		In	33.73	87.01	71.88
		Rc	0.90	0.78	0.79
		Pl	0.97	0.90	0.85
$W_{7,24}$		$v_{7,24}$	-0.86	0.52	0.01
f_{min}-f_{max} (Hz)	4.69-4.88	En	3.8e-09	2.8e-09	5.4e-10
M($W_{7,24}$)	0.615	Lag	-0.18	-0.10	0.28
$\log_{10}(E_{out}/E_{in})$	-0.040	Az	-179.80	8.05	55.94
		In	45.67	80.52	77.74
		Rc	0.70	0.77	0.48
		Pl	0.90	0.89	0.55

Table 2.1 continued.

Signal		Sta	L22	CMG	MAR
$L^{(2)}$					
$W_{7,0}$		$v_{7,0}$	-0.00	-0.01	1.00
f_{min}-f_{max} (Hz)	0.00-0.20	En	1.9e-12	4.1e-11	8.2e-11
M($W_{7,0}$)	0.530	Az	-174.05	34.52	130.47
$\log_{10}(E_{out}/E_{in})$	0.977	In	49.00	47.28	85.64
		Rc	0.74	0.22	0.27
		Pl	0.63	0.16	0.40
$L^{(3)}$					
$W_{7,1}$		$v_{7,1}$	-0.84	0.50	0.22
f_{min}-f_{max} (Hz)	0.20-0.39	En	4.2e-10	3e-10	1.5e-10
M($W_{7,1}$)	0.904	Az	-157.55	66.88	60.48
$\log_{10}(E_{out}/E_{in})$	-0.211	In	79.85	86.77	77.45
		Rc	0.34	0.68	0.24
		Pl	0.35	0.57	0.31
$L^{(4)}$					
$W_{7,2}$		$v_{7,2}$	0.48	-0.81	0.32
f_{min}-f_{max} (Hz)	0.39-0.59	En	4.4e-09	8.5e-09	2.2e-09
M($W_{7,2}$)	0.248	Az	-172.57	79.89	-53.33
$\log_{10}(E_{out}/E_{in})$	-0.117	In	50.11	87.45	65.77
		Rc	0.74	0.95	0.87
		Pl	0.63	0.94	0.84
$W_{7,4}$		$v_{7,4}$	0.28	-0.86	0.42
f_{min}-f_{max} (Hz)	0.78-0.98	En	1.3e-08	3.1e-08	1.7e-08
M($W_{7,4}$)	0.566	Lag	-0.14	0.18	-0.04
$\log_{10}(E_{out}/E_{in})$	-0.438	Az	-173.39	-121.89	-52.51
		In	29.00	80.35	49.56
		Rc	0.89	0.85	0.88
		Pl	0.95	0.93	0.96
$W_{7,6}$		$v_{7,6}$	0.47	-0.86	0.21
f_{min}-f_{max} (Hz)	1.17-1.37	En	6.2e-08	1.2e-07	1.1e-08
M($W_{7,6}$)	0.288	Lag	-0.20	0.02	0.18
$\log_{10}(E_{out}/E_{in})$	-0.170	Az	-167.14	-67.01	-22.29
		In	30.11	77.43	87.98
		Rc	0.92	0.88	0.54
		Pl	0.94	0.89	0.93
$L^{(5)}$					
$W_{7,3}$		$v_{7,3}$	-0.42	-0.72	0.56
f_{min}-f_{max} (Hz)	0.59-0.78	En	8.7e-09	2.4e-08	1.8e-08
M($W_{7,3}$)	0.369	Lag	-0.12	-0.10	0.22
$\log_{10}(E_{out}/E_{in})$	0.169	Az	-179.57	-97.64	-53.46
		In	43.61	87.27	53.25
		Rc	0.89	0.88	0.94
		Pl	0.87	0.97	0.91

Table 2.1 continued.

Signal		Sta	L22	CMG	MAR
$L^{(6)}$					
$W_{7,5}$		$v_{7,5}$	-0.54	0.84	-0.00
f_{min}-f_{max} (Hz)	0.98-1.17	En	4.3e-08	9.4e-08	7.2e-09
M($W_{7,5}$)	0.107	Lag	-0.12	0.10	0.00
$\log_{10}(E_{out}/E_{in})$	-0.655	Az	-176.24	-93.68	-92.81
		In	36.12	87.88	59.06
		Rc	0.92	0.83	0.56
		Pl	0.94	0.94	0.85
$W_{7,25}$		$v_{7,25}$	0.38	-0.91	-0.13
f_{min}-f_{max} (Hz)	4.88-5.08	En	1.2e-09	2.4e-09	5.1e-10
M($W_{7,25}$)	0.564	Lag	-0.10	-0.20	0.30
$\log_{10}(E_{out}/E_{in})$	-0.040	Az	-36.48	3.92	58.76
		In	30.55	87.48	64.04
		Rc	0.53	0.83	0.61
		Pl	0.68	0.86	0.69
$L^{(7)}$					
$W_{7,9}$		$v_{7,9}$	-0.82	-0.50	0.28
f_{min}-f_{max} (Hz)	1.76-1.95	En	9.5e-08	5.7e-08	2.9e-08
M($W_{7,9}$)	0.473	Lag	-0.14	0.22	-0.08
$\log_{10}(E_{out}/E_{in})$	-0.228	Az	179.88	-97.73	73.19
		In	16.42	69.55	88.19
		Rc	0.89	0.58	0.85
		Pl	0.97	0.85	0.96
$W_{7,29}$		$v_{7,29}$	0.82	0.57	-0.08
f_{min}-f_{max} (Hz)	5.66-5.86	En	1.1e-09	9.3e-10	2.1e-10
M($W_{7,29}$)	0.814	Lag	0.02	-0.06	0.04
$\log_{10}(E_{out}/E_{in})$	-0.155	Az	-65.96	-162.16	-121.90
		In	25.66	89.20	87.91
		Rc	0.65	0.82	0.62
		Pl	0.68	0.95	0.65
$W_{7,30}$		$v_{7,30}$	-0.79	-0.61	0.06
f_{min}-f_{max} (Hz)	5.86-6.05	En	1e-09	9.2e-10	2e-10
M($W_{7,30}$)	0.779	Lag	0.16	0.00	-0.16
$\log_{10}(E_{out}/E_{in})$	-0.056	Az	-64.56	15.21	-135.41
		In	12.07	87.69	68.38
		Rc	0.69	0.87	0.63
		Pl	0.63	0.94	0.62
$L^{(8)}$					
$W_{7,13}$		$v_{7,13}$	-0.89	-0.44	-0.13
f_{min}-f_{max} (Hz)	2.54-2.73	En	3e-08	1.3e-08	6.4e-09
M($W_{7,13}$)	0.356	Lag	-0.14	-0.14	0.26
$\log_{10}(E_{out}/E_{in})$	-0.236	Az	176.35	169.59	70.10
		In	60.36	80.20	79.14
		Rc	0.87	0.54	0.83
		Pl	0.97	0.49	0.81

Table 2.1 continued.

Signal		Sta	L22	CMG	MAR
$W_{7,15}$		$v_{7,15}$	-0.96	-0.27	0.00
f_{min}-f_{max} (Hz)	2.93-3.12	En	5.8e-08	1.4e-08	6.1e-09
M($W_{7,15}$)	0.253	Lag	-0.12	-0.14	0.26
$\log_{10}(E_{out}/E_{in})$	0.204	Az	155.27	30.83	-140.20
		In	31.85	83.79	84.67
		Rc	0.94	0.63	0.83
		Pl	0.98	0.83	0.84
$W_{7,27}$		$v_{7,27}$	-0.95	-0.32	0.01
f_{min}-f_{max} (Hz)	5.27-5.47	En	1e-09	6.1e-10	2e-10
M($W_{7,27}$)	0.715	Lag	-0.14	0.06	0.08
$\log_{10}(E_{out}/E_{in})$	-0.140	Az	-30.67	21.86	-104.19
		In	34.67	84.17	81.52
		Rc	0.67	0.77	0.52
		Pl	0.77	0.85	0.75
$W_{7,28}$		$v_{7,28}$	-0.97	-0.21	0.10
f_{min}-f_{max} (Hz)	5.47-5.66	En	1.3e-09	8.7e-10	2.5e-10
M($W_{7,28}$)	0.816	Lag	-0.06	-0.06	0.12
$\log_{10}(E_{out}/E_{in})$	-0.163	Az	-50.21	22.70	-128.22
		In	26.45	87.82	81.33
		Rc	0.74	0.84	0.60
		Pl	0.78	0.92	0.75
$L^{(9)}$					
$W_{7,14}$		$v_{7,14}$	-1.00	0.06	-0.00
f_{min}-f_{max} (Hz)	2.73-2.93	En	4.2e-08	9.4e-09	6.1e-09
M($W_{7,14}$)	0.258	Lag	-0.04	-0.26	0.30
$\log_{10}(E_{out}/E_{in})$	-0.000	Az	164.27	40.42	54.76
		In	37.15	74.83	85.66
		Rc	0.87	0.70	0.80
		Pl	0.97	0.63	0.89
$W_{4,2}$		$v_{4,2}$	-0.99	0.14	0.01
f_{min}-f_{max} (Hz)	3.12-4.69	En	2.6e-07	3.8e-08	1.9e-08
M($W_{4,2}$)	0.506	Lag	-0.10	-0.18	0.28
$\log_{10}(E_{out}/E_{in})$	-0.000	Az	157.87	-164.44	68.02
		In	31.66	88.38	89.43
		Rc	0.93	0.54	0.67
		Pl	0.96	0.74	0.75
$W_{7,31}$		$v_{7,31}$	-0.98	0.20	0.03
f_{min}-f_{max} (Hz)	6.05-6.25	En	1.1e-09	4.9e-10	2.3e-10
M($W_{7,31}$)	0.120	Lag	-0.06	0.16	-0.10
$\log_{10}(E_{out}/E_{in})$	-0.000	Az	-20.71	14.20	-128.37
		In	10.72	84.66	75.98
		Rc	0.77	0.81	0.73
		Pl	0.74	0.89	0.67
$W_{2,1}$		$v_{2,1}$	-1.00	-0.05	-0.00
f_{min}-f_{max} (Hz)	6.25-12.50	En	1.1e-08	4.9e-09	2.1e-09
M($W_{2,1}$)	0.367	Lag	0.02	-0.16	0.14
$\log_{10}(E_{out}/E_{in})$	0.418	Az	-158.09	20.01	-122.18
		In	8.23	86.36	80.80
		Rc	0.62	0.65	0.63
		Pl	0.59	0.88	0.63

Table 2.1 continued.

Signal		Sta	L22	CMG	MAR
$W_{2,2}$		$v_{2,2}$	-1.00	-0.00	0.00
f_{min}-f_{max} (Hz)	12.50-18.75	En	1.5e-09	5.9e-10	1.8e-10
M($W_{2,2}$)	0.201	Az	149.44	-111.71	-116.15
$\log_{10}(E_{out}/E_{in})$	-0.000	In	28.95	85.83	83.82
		Rc	0.54	0.75	0.68
		Pl	0.44	0.79	0.78
$W_{3,6}$		$v_{3,6}$	-1.00	0.00	-0.00
f_{min}-f_{max} (Hz)	18.75-21.88	En	4.6e-10	8.4e-11	3.4e-11
M($W_{3,6}$)	0.614	Az	161.15	65.41	-103.52
$\log_{10}(E_{out}/E_{in})$	0.045	In	39.93	88.80	82.91
		Rc	0.54	0.76	0.60
		Pl	0.55	0.70	0.88
$W_{3,7}$		$v_{3,7}$	-1.00	-0.00	-0.00
f_{min}-f_{max} (Hz)	21.88-25.00	En	4.3e-10	3.3e-11	1.8e-11
M($W_{3,7}$)	0.641	Az	166.25	69.87	-91.47
$\log_{10}(E_{out}/E_{in})$	-0.000	In	34.78	85.75	83.46
		Rc	0.66	0.80	0.56
		Pl	0.67	0.82	0.90
$L^{(10)}$					
$W_{7,26}$		$v_{7,26}$	0.02	-0.99	-0.16
f_{min}-f_{max} (Hz)	5.08-5.27	En	9.6e-10	1.5e-09	2.3e-10
M($W_{7,26}$)	0.769	Lag	-0.08	-0.20	0.28
$\log_{10}(E_{out}/E_{in})$	-0.223	Az	-27.81	179.59	92.89
		In	51.56	89.04	69.32
		Rc	0.57	0.87	0.42
		Pl	0.68	0.90	0.56

Table 2.2. Recovered signals from a data sample recorded during the "high" convective regime in 2002, beginning 02/15 2002 19:53:23 GMT. Signal names use the convention $\mathbf{H}^{(n)}$, described in the text. Values for principal eigenvectors ($v_{j,n,1}$), energy (En), azimuth (Az), incidence angle (In), rectilinearity (Rc), and planarity (Pl) are sorted in columns according to station. Az and In are in degrees. Wavelet packets are designated $\boldsymbol{W_{j,n}}$ and nominal passbands f_{min}-f_{max} for each $\boldsymbol{W_{j,n}}$ are given in Hz. Cost functional M($\boldsymbol{W}$) is renormalized (multiplied by normalized bandwidth) so that $0 \le M(\boldsymbol{W}) < 3$. Spectral leakage for each subband is tabulated in the form $\log_{10}(E_{out}/E_{in})$, the base 10 logarithm of spectral energy outside the passband to spectral energy inside the passband. Relative lags of each subband at each station are given in seconds for subbands whose wavelet cross-correlations are well constrained.

Signal		*Station*	*L22*	*CMG*	*MAR*
$H^{(1)}$					
$W_{6,6}$		$v_{6,6}$	-0.94	0.33	0.02
f_{min} - f_{max}	2.34-2.73	En	6.7e-08	2.4e-08	1.1e-08
$M(W_{6,6})$	0.398	Lag	-0.02	-0.12	0.14
$\log_{10}(E_{out}/E_{in})$	-0.307	Az	166.31	169.90	60.62
		In	35.59	83.39	79.27
		Rc	0.88	0.64	0.73
		Pl	0.96	0.76	0.65
$H^{(2)}$					
$W_{7,0}$		$v_{7,0}$	-0.01	0.37	0.93
f_{min} - f_{max}	0.00-0.20	En	1.3e-12	2.5e-11	4.8e-11
$M(W_{7,0})$	0.424	Az	-176.71	81.25	87.74
$\log_{10}(E_{out}/E_{in})$	1.062	In	47.70	82.13	83.89
		Rc	0.74	0.31	0.33
		Pl	0.60	0.29	0.51
$W_{7,52}$		$v_{7,52}$	-0.02	0.34	0.94
f_{min} - f_{max}	10.16-10.35	En	1.9e-10	1.7e-10	4.2e-10
$M(W_{7,52})$	0.719	Lag	-0.12	-0.16	0.28
$\log_{10}(E_{out}/E_{in})$	-0.091	Az	12.19	-83.45	75.65
		In	88.25	89.67	78.24
		Rc	0.32	0.79	0.81
		Pl	0.53	0.90	0.81
$H^{(3)}$					
$W_{7,1}$		$v_{7,1}$	-0.70	0.66	-0.29
f_{min} - f_{max}	0.20-0.39	En	2.4e-10	2.1e-10	1.2e-10
$M(W_{7,1})$	0.878	Az	-141.99	68.13	-71.34
$\log_{10}(E_{out}/E_{in})$	-0.178	In	86.04	84.16	82.61
		Rc	0.25	0.67	0.32
		Pl	0.38	0.58	0.45
$W_{7,7}$		$v_{7,7}$	0.77	-0.62	0.14
f_{min} - f_{max}	1.37-1.56	En	1.3e-07	9e-08	4.2e-08
$M(W_{7,7})$	0.270	Lag	-0.02	0.00	0.02
$\log_{10}(E_{out}/E_{in})$	-0.122	Az	-167.75	-54.15	-80.08
		In	28.01	71.87	87.75
		Rc	0.96	0.77	0.80
		Pl	0.96	0.74	0.93

Table 2.2 continued.

Signal		*Station*	*L22*	*CMG*	*MAR*
$W_{7,8}$		$v_{7,8}$	0.80	-0.52	0.29
f_{min} - f_{max}	1.56-1.76	En	1.7e-07	7.6e-08	4.8e-08
M($W_{7,8}$)	0.160	Lag	-0.04	0.00	0.04
$\log_{10}(E_{out}/E_{in})$	-0.197	Az	-173.58	-44.62	-87.67
		In	25.25	70.31	86.48
		Rc	0.97	0.72	0.84
		Pl	0.97	0.73	0.95
$H^{(4)}$					
$W_{7,2}$		$v_{7,2}$	0.48	-0.81	0.33
f_{min} - f_{max}	0.39-0.59	En	3.1e-09	6.3e-09	1.7e-09
M($W_{7,2}$)	0.226	Az	-178.39	78.63	-53.95
$\log_{10}(E_{out}/E_{in})$	-0.022	In	48.48	87.16	65.11
		Rc	0.74	0.93	0.86
		Pl	0.63	0.93	0.83
$W_{7,4}$		$v_{7,4}$	-0.28	0.90	-0.32
f_{min} - f_{max}	0.78-0.98	En	1.2e-08	2.4e-08	1.5e-08
M($W_{7,4}$)	0.808	Lag	-0.16	0.16	0.00
$\log_{10}(E_{out}/E_{in})$	-0.586	Az	168.34	-127.51	-52.40
		In	25.31	82.38	46.80
		Rc	0.77	0.77	0.82
		Pl	0.67	0.85	0.74
$H^{(5)}$					
$W_{7,3}$		$v_{7,3}$	-0.45	-0.66	0.60
f_{min} - f_{max}	0.59-0.78	En	6.8e-09	1.4e-08	1.3e-08
M($W_{7,3}$)	0.434	Lag	-0.12	-0.08	0.22
$\log_{10}(E_{out}/E_{in})$	0.117	Az	167.48	-95.96	-52.38
		In	38.85	87.27	53.20
		Rc	0.82	0.83	0.92
		Pl	0.75	0.94	0.90
$H^{(6)}$					
$W_{7,5}$		$v_{7,5}$	-0.54	0.84	0.05
f_{min} - f_{max}	0.98-1.17	En	3.2e-08	6.4e-08	8.9e-09
M($W_{7,5}$)	0.201	Lag	-0.10	0.10	0.02
$\log_{10}(E_{out}/E_{in})$	-0.597	Az	-176.87	-99.79	-86.55
		In	33.71	88.97	55.52
		Rc	0.86	0.74	0.61
		Pl	0.77	0.89	0.62
$W_{7,6}$		$v_{7,6}$	-0.51	0.86	0.09
f_{min} - f_{max}	1.17-1.37	En	4e-08	6.8e-08	1.4e-08
M($W_{7,6}$)	0.452	Lag	-0.16	0.06	0.10
$\log_{10}(E_{out}/E_{in})$	-0.183	Az	-164.67	-67.25	-101.22
		In	27.82	77.09	84.97
		Rc	0.88	0.79	0.70
		Pl	0.89	0.86	0.83

Table 2.2 continued.

Signal		*Station*	*L22*	*CMG*	*MAR*
$H^{(7)}$					
$W_{7,9}$		$v_{7,9}$	-0.78	0.53	0.33
f_{min} - f_{max}	1.76-1.95	En	6.4e-08	4.3e-08	4.1e-08
M($W_{7,9}$)	0.755	Lag	-0.12	-0.06	0.18
$\log_{10}(E_{out}/E_{in})$	-0.380	Az	-176.34	-111.31	-112.15
		In	13.20	71.37	86.27
		Rc	0.85	0.59	0.88
		Pl	0.95	0.83	0.91
$W_{7,75}$		$v_{7,75}$	0.80	-0.35	-0.49
f_{min} - f_{max}	14.65-14.84	En	9.5e-11	7.7e-11	1e-10
M($W_{7,75}$)	1.638	Lag	-0.16	-0.12	0.26
$\log_{10}(E_{out}/E_{in})$	0.264	Az	-178.47	-100.60	75.71
		In	41.67	82.51	82.02
		Rc	0.58	0.79	0.86
		Pl	0.54	0.85	0.81
$H^{(8)}$					
$W_{6,5}$		v6,5	-0.99	0.15	-0.06
f_{min} - f_{max}	1.95-2.34	En	9.7e-08	3.8e-08	2.4e-08
M(W6,5)	0.840	Lag	-0.10	0.08	0.04
$\log_{10}(E_{out}/E_{in})$	-0.003	Az	163.76	-71.23	-127.05
		In	31.34	67.27	85.79
		Rc	0.90	0.53	0.79
		Pl	0.96	0.89	0.82
$W_{6,7}$		v6,7	-1.00	-0.07	-0.02
f_{min} - f_{max}	2.73-3.12	En	7.7e-08	1.7e-08	1.1e-08
M($W_{6,7}$)	0.618	Lag	-0.12	-0.08	0.20
$\log_{10}(E_{out}/E_{in})$	0.232	Az	158.35	39.39	45.30
		In	33.44	82.76	87.99
		Rc	0.90	0.65	0.78
		Pl	0.96	0.74	0.82
$W_{3,1}$		v3,1	-0.99	0.13	0.02
f_{min} - f_{max}	3.12-6.25	En	4.4e-07	6.1e-08	7.1e-08
M($W_{3,1}$)	0.352	Lag	-0.16	-0.14	0.28
$\log_{10}(E_{out}/E_{in})$	-0.000	Az	139.03	107.15	165.42
		In	44.01	46.85	27.21
		Rc	0.54	0.58	0.61
		Pl	0.58	0.59	0.65
$W_{7,32}$		v7,32	-0.96	-0.26	0.02
f_{min} - f_{max}	6.25-6.45	En	2e-09	1.1e-09	1.1e-09
M($W_{7,32}$)	1.198	Lag	0.08	0.20	-0.28
$\log_{10}(E_{out}/E_{in})$	0.546	Az	74.99	29.96	-151.35
		In	23.90	76.28	45.53
		Rc	0.68	0.77	0.78
		Pl	0.68	0.91	0.87

Table 2.2 continued.

Signal		*Station*	*L22*	*CMG*	*MAR*
$W_{7,34}$		v7,34	-0.99	0.08	0.07
f_{min} - f_{max}	6.64-6.84	En	2.7e-09	1e-09	1.2e-09
M($W_{7,34}$)	1.164	Lag	0.14	-0.12	-0.02
$\log_{10}(E_{out}/E_{in})$	0.215	Az	-166.52	38.99	-151.05
		In	19.17	85.87	45.07
		Rc	0.59	0.69	0.62
		Pl	0.70	0.92	0.79
$W_{7,37}$		$v_{7,37}$	1.00	-0.07	0.05
f_{min} - f_{max}	7.23-7.42	En	2.1e-09	6.4e-10	1.1e-09
M($W_{7,37}$)	0.813	Lag	0.06	-0.02	-0.04
$\log_{10}(E_{out}/E_{in})$	0.277	Az	159.50	21.30	72.85
		In	38.32	88.93	88.67
		Rc	0.55	0.70	0.66
		Pl	0.67	0.91	0.65
$W_{7,38}$		$v_{7,38}$	-0.99	0.08	-0.07
f_{min} - f_{max}	7.42-7.62	En	2e-09	4.3e-10	8.5e-10
M($W_{7,38}$)	0.817	Lag	0.02	-0.14	0.12
$\log_{10}(E_{out}/E_{in})$	0.404	Az	-174.55	17.01	-131.72
		In	43.90	85.34	64.28
		Rc	0.65	0.67	0.58
		Pl	0.63	0.91	0.58
$W_{4,5}$		$v_{4,5}$	-0.99	-0.04	0.11
f_{min} - f_{max}	7.81-9.38	En	1.5e-08	2.3e-09	5.3e-09
M($W_{4,5}$)	0.281	Lag	-0.12	0.06	0.08
$\log_{10}(E_{out}/E_{in})$	-0.000	Az	148.24	37.29	-115.99
		In	25.49	87.96	75.82
		Rc	0.81	0.53	0.59
		Pl	0.71	0.89	0.67
$W_{7,63}$		$v_{7,63}$	-0.98	-0.19	0.03
f_{min} - f_{max}	12.30-12.50	En	9.1e-11	6.8e-11	3.8e-11
M($W_{7,63}$)	0.813	Az	138.24	81.63	71.97
$\log_{10}(E_{out}/E_{in})$	0.000	In	42.48	89.59	84.30
		Rc	0.39	0.80	0.34
		Pl	0.27	0.84	0.53
$W_{7,72}$		$v_{7,72}$	-1.00	-0.01	0.06
f_{min} - f_{max}	14.06-14.26	En	2.1e-10	7.6e-11	1.8e-10
M($W_{7,72}$)	0.809	Lag	0.00	0.18	-0.16
$\log_{10}(E_{out}/E_{in})$	-0.000	Az	128.80	-108.13	-114.80
		In	33.38	84.57	80.31
		Rc	0.72	0.75	0.87
		Pl	0.69	0.83	0.83
$W_{7,77}$		$v_{7,77}$	0.99	0.16	0.02
f_{min} - f_{max}	15.04-15.23	En	9.4e-11	4.5e-11	6.6e-11
M($W_{7,77}$)	0.681	Lag	-0.10	0.06	0.06
$\log_{10}(E_{out}/E_{in})$	-0.039	Az	157.87	70.59	74.32
		In	23.63	88.03	87.67
		Rc	0.70	0.72	0.81
		Pl	0.61	0.76	0.82

Table 2.2 continued.

Signal		*Station*	*L22*	*CMG*	*MAR*
$W_{7,79}$		$v_{7,79}$	-0.98	0.19	0.03
f_{min} - f_{max}	15.43-15.62	En	1.1e-10	4.8e-11	4.8e-11
M($W_{7,79}$)	0.585	Lag	-0.10	0.08	0.00
$\log_{10}(E_{out}/E_{in})$	0.084	Az	147.84	56.41	-113.83
		In	29.20	88.77	79.42
		Rc	0.73	0.77	0.75
		Pl	0.59	0.81	0.69
$W_{7,80}$		$v_{7,80}$	-0.99	0.14	-0.10
f_{min} - f_{max}	15.62-15.82	En	1.1e-10	4.6e-11	4.8e-11
M($W_{7,80}$)	0.738	Lag	-0.14	0.20	-0.06
$\log_{10}(E_{out}/E_{in})$	-0.000	Az	145.01	-121.83	-112.37
		In	28.48	89.92	77.28
		Rc	0.73	0.75	0.76
		Pl	0.58	0.79	0.68
$W_{6,41}$		$v_{6,41}$	-1.00	-0.00	0.00
f_{min} - f_{max}	16.02-16.41	En	1.9e-10	7.9e-11	7.9e-11
M($W_{6,41}$)	0.510	Lag	-0.14	-0.06	0.18
$\log_{10}(E_{out}/E_{in})$	-0.000	Az	142.85	-115.02	73.15
		In	29.99	83.29	87.42
		Rc	0.71	0.74	0.69
		Pl	0.56	0.74	0.67
$W_{6,42}$		$v_{6,42}$	-0.95	-0.32	0.03
f_{min} - f_{max}	16.41-16.80	En	1.7e-10	9e-11	6.7e-11
M($W_{6,42}$)	1.142	Lag	0.04	-0.18	0.14
$\log_{10}(E_{out}/E_{in})$	0.048	Az	138.14	-122.75	58.16
		In	26.16	82.09	87.94
		Rc	0.66	0.84	0.66
		Pl	0.58	0.82	0.70
$W_{7,86}$		$v_{7,86}$	-0.98	0.11	0.13
f_{min} - f_{max}	16.80-16.99	En	8.2e-11	3.3e-11	2.6e-11
M($W_{7,86}$)	0.821	Az	-157.10	-128.56	-115.84
$\log_{10}(E_{out}/E_{in})$	-0.000	In	12.87	86.24	81.83
		Rc	0.58	0.80	0.79
		Pl	0.63	0.84	0.77
$W_{7,87}$		$v_{7,87}$	-0.98	0.13	-0.13
f_{min} - f_{max}	16.99-17.19	En	8.2e-11	2.8e-11	2.3e-11
M($W_{7,87}$)	0.240	Lag	0.16	0.12	-0.28
$\log_{10}(E_{out}/E_{in})$	-0.000	Az	-155.88	-111.01	-112.80
		In	11.51	84.38	80.03
		Rc	0.65	0.84	0.67
		Pl	0.61	0.85	0.71
$W_{5,22}$		$v_{5,22}$	-0.99	-0.13	0.10
f_{min} - f_{max}	17.19-17.97	En	1.9e-10	7.7e-11	7.1e-11
M($W_{5,22}$)	1.032	Lag	0.02	0.06	-0.08
$\log_{10}(E_{out}/E_{in})$	0.028	Az	166.09	-114.96	73.58
		In	5.98	85.42	85.92
		Rc	0.45	0.78	0.65
		Pl	0.41	0.74	0.71

Table 2.2 continued.

Signal		*Station*	*L22*	*CMG*	*MAR*
$W_{5,23}$		$v_{5,23}$	-1.00	-0.05	0.08
f_{min} - f_{max}	17.97-18.75	En	1.4e-10	4.7e-11	6.8e-11
M($W_{5,23}$)	0.799	Az	163.38	-116.12	75.19
$\log_{10}(E_{out}/E_{in})$	0.168	In	27.82	87.38	80.09
		Rc	0.44	0.70	0.78
		Pl	0.46	0.61	0.83
$W_{2,3}$		$v_{2,3}$	-1.00	-0.01	0.01
f_{min} - f_{max}	18.75-25.00	En	1.4e-09	1.7e-10	1.8e-10
M($W_{2,3}$)	0.240	Az	160.14	-112.65	61.93
$\log_{10}(E_{out}/E_{in})$	-0.709	In	25.71	88.93	89.25
		Rc	0.68	0.74	0.60
		Pl	0.57	0.69	0.76
H[9]					
$W_{7,33}$		$v_{7,33}$	0.79	0.12	0.61
f_{min} - f_{max}	6.45-6.64	En	1.5e-09	9.6e-10	1.2e-09
M($W_{7,33}$)	0.862	Lag	0.04	-0.14	0.10
$\log_{10}(E_{out}/E_{in})$	0.073	Az	69.28	29.16	-136.95
		In	31.72	82.59	58.61
		Rc	0.37	0.74	0.72
		Pl	0.62	0.89	0.72
$W_{7,36}$		$v_{7,36}$	0.76	0.16	0.63
f_{min} - f_{max}	7.03-7.23	En	2.3e-09	5.9e-10	1.9e-09
M($W_{7,36}$)	0.702	Lag	0.06	0.04	-0.08
$\log_{10}(E_{out}/E_{in})$	0.112	Az	172.08	30.25	82.60
		In	32.55	84.86	85.66
		Rc	0.64	0.67	0.79
		Pl	0.57	0.84	0.77
H[10]					
$W_{7,35}$		$v_{7,35}$	-0.91	0.16	0.38
f_{min} - f_{max}	6.84-7.03	En	2.2e-09	6.4e-10	1.7e-09
M($W_{7,35}$)	0.757	Lag	-0.12	0.06	0.06
$\log_{10}(E_{out}/E_{in})$	0.032	Az	-147.50	14.41	79.82
		In	32.54	79.45	89.84
		Rc	0.65	0.65	0.73
		Pl	0.57	0.86	0.83
$W_{6,30}$		$v_{6,30}$	-0.95	-0.13	0.27
f_{min} - f_{max}	11.72-12.11	En	4.3e-10	1.3e-10	2.4e-10
M($W_{6,30}$)	0.776	Lag	-0.06	-0.02	0.08
$\log_{10}(E_{out}/E_{in})$	0.000	Az	127.93	-108.23	-111.72
		In	22.62	88.71	89.17
		Rc	0.72	0.71	0.79
		Pl	0.70	0.84	0.74
$W_{7,62}$		$v_{7,62}$	-0.90	-0.06	0.42
f_{min} - f_{max}	12.11-12.30	En	1.6e-10	5.2e-11	1e-10
M($W_{7,62}$)	1.073	Az	131.01	69.81	71.44
$\log_{10}(E_{out}/E_{in})$	-0.000	In	13.84	88.57	88.72
		Rc	0.68	0.74	0.78
		Pl	0.58	0.85	0.68

Table 2.2 continued.

Signal		*Station*	*L22*	*CMG*	*MAR*
$W_{4,8}$		$v_{4,8}$	-0.95	0.14	0.27
f_{min} - f_{max}	12.50-14.06	En	1.4e-09	5.8e-10	9.9e-10
M($W_{4,8}$)	0.959	Lag	0.00	0.16	-0.18
$\log_{10}(E_{out}/E_{in})$	0.207	Az	136.24	-105.89	-115.65
		In	26.97	87.16	84.17
		Rc	0.65	0.75	0.81
		Pl	0.60	0.84	0.73
$W_{7,78}$		$v_{7,78}$	-0.90	0.06	0.43
f_{min} - f_{max}	15.23-15.43	En	1.2e-10	4.2e-11	8.4e-11
M($W_{7,78}$)	0.878	Lag	-0.08	0.08	0.00
$\log_{10}(E_{out}/E_{in})$	0.219	Az	157.75	-114.74	71.14
		In	28.36	89.72	82.29
		Rc	0.73	0.72	0.83
		Pl	0.62	0.76	0.73
$W_{7,81}$		$v_{7,81}$	-0.93	0.12	0.35
f_{min} - f_{max}	15.82-16.02	En	1.4e-10	4.8e-11	7.5e-11
M($W_{7,81}$)	0.755	Lag	-0.06	0.02	0.02
$\log_{10}(E_{out}/E_{in})$	0.353	Az	154.02	-120.32	75.16
		In	31.01	88.94	87.37
		Rc	0.78	0.73	0.84
		Pl	0.65	0.78	0.78
$H^{(11)}$					
$W_{7,39}$		$v_{7,39}$	0.96	-0.03	0.27
f_{min} - f_{max}	7.62-7.81	En	2.4e-09	5.2e-10	1.2e-09
M($W_{7,39}$)	0.643	Lag	0.02	-0.06	0.04
$\log_{10}(E_{out}/E_{in})$	0.243	Az	-173.29	-151.61	-117.92
		In	27.75	89.68	74.10
		Rc	0.77	0.70	0.64
		Pl	0.75	0.90	0.79
$W_{7,48}$		$v_{7,48}$	0.90	-0.08	0.43
f_{min} - f_{max}	9.38-9.57	En	6.4e-10	1.7e-10	3.8e-10
M($W_{7,48}$)	0.684	Lag	-0.08	0.06	0.02
$\log_{10}(E_{out}/E_{in})$	0.015	Az	147.96	2.63	-114.06
		In	31.11	77.97	63.85
		Rc	0.75	0.55	0.81
		Pl	0.66	0.90	0.79
$W_{7,49}$		$v_{7,49}$	0.89	-0.08	0.46
f_{min} - f_{max}	9.57-9.77	En	6.3e-10	2e-10	4.9e-10
M($W_{7,49}$)	0.914	Lag	-0.12	0.08	0.04
$\log_{10}(E_{out}/E_{in})$	0.043	Az	170.10	-86.57	-109.67
		In	33.35	87.48	86.00
		Rc	0.76	0.69	0.80
		Pl	0.63	0.84	0.79
$W_{7,50}$		$v_{7,50}$	0.90	-0.06	0.44
f_{min} - f_{max}	9.77-9.96	En	3.8e-10	1.6e-10	3e-10
M($W_{7,50}$)	1.050	Lag	-0.08	0.14	-0.04
$\log_{10}(E_{out}/E_{in})$	0.051	Az	178.05	-90.32	-114.37
		In	29.33	88.88	82.30
		Rc	0.65	0.72	0.71
		Pl	0.57	0.86	0.75

Table 2.2 continued.

Signal		*Station*	*L22*	*CMG*	*MAR*
$H^{(12)}$					
$W_{7,51}$		$v_{7,51}$	-0.54	0.18	0.82
f_{min} - f_{max}	9.96-10.16	En	2.5e-10	1.4e-10	3.1e-10
$M(W_{7,51})$	1.018	Lag	0.08	0.02	-0.10
$\log_{10}(E_{out}/E_{in})$	0.022	Az	-179.56	-83.18	72.38
		In	82.28	86.72	89.35
		Rc	0.53	0.77	0.73
		Pl	0.72	0.88	0.77
$W_{7,55}$		$v_{7,55}$	-0.57	0.02	0.82
f_{min} - f_{max}	10.74-10.94	En	3.5e-10	1.4e-10	5e-10
$M(W_{7,55})$	0.569	Lag	-0.08	0.10	-0.02
$\log_{10}(E_{out}/E_{in})$	-0.206	Az	100.37	-86.44	-114.38
		In	46.93	84.66	75.71
		Rc	0.64	0.75	0.88
		Pl	0.68	0.83	0.88
$W_{7,56}$		$v_{7,56}$	-0.43	0.23	0.87
f_{min} - f_{max}	10.94-11.13	En	2.9e-10	1.3e-10	4.8e-10
$M(W_{7,56})$	0.640	Lag	-0.02	0.08	-0.08
$\log_{10}(E_{out}/E_{in})$	0.019	Az	105.61	-85.51	-112.14
		In	53.23	81.84	75.28
		Rc	0.57	0.76	0.88
		Pl	0.64	0.83	0.85
$H^{(13)}$					
$W_{7,53}$		$v_{7,53}$	0.15	0.19	0.97
f_{min} - f_{max}	10.35-10.55	En	2.5e-10	1.5e-10	5.3e-10
$M(W_{7,53})$	0.689	Lag	-0.04	-0.06	0.10
$\log_{10}(E_{out}/E_{in})$	-0.345	Az	139.03	64.49	72.55
		In	44.01	80.20	79.31
		Rc	0.54	0.74	0.83
		Pl	0.58	0.88	0.84
$W_{7,54}$		$v_{7,54}$	0.31	0.11	0.94
f_{min} - f_{max}	10.55-10.74	En	2.6e-10	1.3e-10	5.5e-10
$M(W_{7,54})$	0.593	Lag	-0.10	-0.18	0.26
$\log_{10}(E_{out}/E_{in})$	-0.378	Az	107.15	-98.68	-113.46
		In	46.85	89.29	82.61
		Rc	0.58	0.72	0.86
		Pl	0.59	0.83	0.88
$W_{7,59}$		$v_{7,59}$	0.15	0.24	0.96
f_{min} - f_{max}	11.52-11.72	En	1.9e-10	5.4e-11	2.1e-10
$M(W_{7,59})$	1.048	Lag	-0.04	0.06	0.00
$\log_{10}(E_{out}/E_{in})$	-0.070	Az	165.42	14.32	-110.45
		In	27.21	78.00	85.58
		Rc	0.61	0.47	0.81
		Pl	0.65	0.86	0.83

Table 2.2 continued.

Signal		*Station*	*L22*	*CMG*	*MAR*
$W_{7,76}$		$v_{7,76}$	0.43	0.25	0.87
f_{min} - f_{max}	14.84-15.04	En	7.4e-11	7.5e-11	8e-11
M($W_{7,76}$)	1.696	Lag	-0.10	-0.18	0.26
$\log_{10}(E_{out}/E_{in})$	0.308	Az	173.16	-98.58	75.06
		In	40.52	82.11	85.58
		Rc	0.54	0.82	0.84
		Pl	0.60	0.87	0.79
$H^{(14)}$					
$W_{7,57}$		$v_{7,57}$	-0.32	-0.17	0.93
f_{min} - f_{max}	11.13-11.33	En	1.7e-10	1.1e-10	2.8e-10
M($W_{7,57}$)	0.867	Lag	-0.04	0.22	-0.18
$\log_{10}(E_{out}/E_{in})$	-0.098	Az	134.06	-100.11	-119.46
		In	47.33	85.49	66.55
		Rc	0.30	0.79	0.83
		Pl	0.55	0.83	0.81
$H^{(15)}$					
$W_{7,58}$		$v_{7,58}$	0.33	-0.12	0.94
f_{min} - f_{max}	11.33-11.52	En	1.7e-10	1e-10	2.7e-10
M($W_{7,58}$)	0.894	Lag	0.10	0.14	-0.24
$\log_{10}(E_{out}/E_{in})$	-0.177	Az	-153.83	-93.86	-116.89
		In	32.16	88.33	79.07
		Rc	0.39	0.74	0.89
		Pl	0.55	0.83	0.90
$W_{7,73}$		$v_{7,73}$	0.63	0.04	0.78
f_{min} - f_{max}	14.26-14.45	En	1.5e-10	8e-11	1.6e-10
M($W_{7,73}$)	0.993	Lag	0.08	0.14	-0.20
$\log_{10}(E_{out}/E_{in})$	0.514	Az	128.97	-108.63	-112.01
		In	32.81	85.73	86.19
		Rc	0.69	0.79	0.86
		Pl	0.64	0.84	0.83
$W_{7,74}$		$v_{7,74}$	0.51	-0.05	0.86
f_{min} - f_{max}	14.45-14.65	En	1.2e-10	5.9e-11	1.4e-10
M($W_{7,74}$)	1.154	Lag	0.14	-0.04	-0.10
$\log_{10}(E_{out}/E_{in})$	0.380	Az	161.92	66.56	72.18
		In	33.46	89.01	81.81
		Rc	0.66	0.75	0.85
		Pl	0.57	0.81	0.82

Table 2.3. Recovered signals from a data sample recorded during 2003, beginning 12/02 2003 16:30:01 GMT. Signal names use the convention $\mathbf{B^{(n)}}$, as described in the text. Values for principal eigenvectors ($v_{j,n}$), energy (En), azimuth (Az), incidence angle (In), rectilinearity (Rc), and planarity (Pl) are sorted in columns according to station. Az and In are in degrees. Wavelet packets are designated $\boldsymbol{W_{j,n}}$ and nominal passbands f_{min}-f_{max} for each $\boldsymbol{W_{j,n}}$ are given in Hz. Cost functional M($\boldsymbol{W}$) is renormalized (multiplied by normalized bandwidth) so that $0 \leq M(\boldsymbol{W}) < 7$. Spectral leakage for each subband is tabulated in the form $\log_{10}(E_{out}/E_{in})$, the base 10 logarithm of spectral energy outside the passband to spectral energy inside the passband. Relative lags of each subband at each station are given in seconds for subbands whose wavelet cross-correlations are well constrained.

Signal		*Sta*	*EA1*	*EA3*	*EA4*	*EA7*	*EA2*	*EA5*	*EA6*
$B^{(1)}$									
$W_{5,3}$		$v_{5,3}$	-0.38	-0.91	-0.13	0.02	-0.00	0.02	0.05
f_{min} - f_{max} (Hz)	2.34-3.12	En	2.6e-06	3.6e-06	6.1e-07	7.6e-07	2.8e-07	9.4e-08	3.9e-07
M($W_{5,3}$)	1.159	Az	-104.85	53.77	128.56	161.17	-139.68	-99.72	13.61
$\log_{10}(E_{out}/E_{in})$	-0.359	In	43.04	33.74	77.80	89.07	78.91	84.25	82.26
		Rc	0.94	0.95	0.81	0.83	0.69	0.62	0.76
		Pl	0.97	0.98	0.83	0.88	0.88	0.81	0.86
$B^{(2)}$									
$W_{7,0}$		$v_{7,0}$	0.00	0.00	1.00	-0.09	-0.03	0.03	0.02
f_{min} - f_{max} (Hz)	0.00-0.20	En	1.9e-12	3.1e-12	1.5e-09	2.8e-10	9e-11	1.9e-10	2e-10
M($W_{7,0}$)	0.504	Az	12.15	141.35	141.77	-130.32	93.76	86.15	-110.27
$\log_{10}(E_{out}/E_{in})$	1.575	In	66.81	59.69	87.77	83.81	88.07	82.66	53.94
		Rc	0.51	0.81	0.83	0.77	0.78	0.84	0.53
		Pl	0.70	0.71	0.78	0.74	0.88	0.78	0.81
$B^{(3)}$									
$W_{7,1}$		$v_{7,1}$	-0.14	-0.13	0.38	-0.34	0.60	0.13	0.57
f_{min} - f_{max} (Hz)	0.20-0.39	En	2.8e-10	9.3e-10	8.2e-10	1.4e-09	1.8e-09	6.1e-10	1.7e-09
M($W_{7,1}$)	0.825	Az	-101.17	59.34	-64.35	142.63	16.15	-23.20	175.74
$\log_{10}(E_{out}/E_{in})$	0.102	In	44.76	47.74	87.66	73.27	80.95	86.59	77.77
		Rc	0.91	0.95	0.94	0.93	0.75	0.76	0.92
		Pl	0.97	0.94	0.90	0.93	0.90	0.91	0.92
$B^{(4)}$									
$W_{7,2}$		$v_{7,2}$	-0.28	-0.03	-0.33	-0.51	0.55	-0.15	0.48
f_{min} - f_{max} (Hz)	0.39-0.59	En	5.6e-09	8.3e-09	4.8e-09	1.3e-08	1.6e-08	1.7e-09	1.1e-08
M($W_{7,2}$)	0.477	Az	-89.78	71.64	108.12	144.19	-98.55	161.10	-70.95
$\log_{10}(E_{out}/E_{in})$	0.120	In	69.45	34.18	82.38	85.20	85.85	65.56	87.06
		Rc	0.76	0.62	0.83	0.89	0.93	0.58	0.49
		Pl	0.88	0.84	0.86	0.92	0.93	0.75	0.91
$B^{(5)}$									
$W_{7,3}$		$v_{7,3}$	-0.49	-0.48	-0.33	0.34	0.27	-0.20	0.44
f_{min} - f_{max} (Hz)	0.59-0.78	En	3.1e-08	2.7e-08	1.3e-08	1.8e-08	3.1e-08	1.9e-08	2.5e-08
M($W_{7,3}$)	0.527	Az	-82.90	-86.64	131.19	-51.49	-98.48	144.13	-13.74
$\log_{10}(E_{out}/E_{in})$	-0.059	In	69.53	76.61	70.45	88.15	82.23	45.46	88.85
		Rc	0.87	0.67	0.76	0.61	0.84	0.92	0.54
		Pl	0.84	0.68	0.86	0.86	0.95	0.89	0.86

Table 2.3. continued

Signal		*Sta*	*EA1*	*EA3*	*EA4*	*EA7*	*EA2*	*EA5*	*EA6*
$B^{(6)}$									
$W_{6,2}$		$v_{6,2}$	0.06	-0.37	-0.23	-0.21	0.62	-0.16	0.59
f_{min} - f_{max} (Hz)	0.78-1.17	En	3.1e-07	7.1e-07	1.6e-07	6.8e-07	9.4e-07	1e-07	8.4e-07
M($W_{6,2}$)	0.640	Az	86.27	61.32	112.37	147.97	-95.09	-135.88	-128.47
$\log_{10}(E_{out}/E_{in})$	-0.642	In	88.30	35.13	80.59	85.89	80.11	84.59	76.63
		Rc	0.82	0.91	0.72	0.89	0.92	0.81	0.88
		Pl	0.94	0.95	0.90	0.91	0.96	0.85	0.95
$B^{(7)}$									
$W_{7,6}$		$v_{7,6}$	-0.19	-0.28	-0.16	-0.36	0.68	-0.03	0.52
f_{min} - f_{max} (Hz)	1.17-1.37	En	2.2e-07	5.7e-07	1.6e-07	6.2e-07	8.3e-07	7.5e-08	5.1e-07
M($W_{7,6}$)	0.842	Lag	0.08	-0.06	0.10	0.00	-0.06	0.02	-0.10
$\log_{10}(E_{out}/E_{in})$	-0.205	Az	-96.42	52.74	110.40	149.35	-82.27	29.61	-142.54
		In	51.68	37.87	84.79	79.52	75.61	89.06	69.21
		Rc	0.75	0.93	0.80	0.89	0.89	0.74	0.77
		Pl	0.93	0.97	0.73	0.82	0.97	0.90	0.90
$B^{(8)}$									
$W_{7,7}$		$v_{7,7}$	0.07	-0.45	-0.03	0.63	0.40	0.10	0.48
f_{min} - f_{max} (Hz)	1.37-1.56	En	6.3e-07	5e-07	3.8e-07	1e-06	4.8e-07	8.9e-08	8.2e-07
M($W_{7,7}$)	0.679	Az	-101.17	59.34	-64.35	142.63	16.15	-23.20	175.74
$\log_{10}(E_{out}/E_{in})$	-0.022	In	44.76	47.74	87.66	73.27	80.95	86.59	77.77
		Rc	0.91	0.95	0.94	0.93	0.75	0.76	0.92
		Pl	0.97	0.94	0.90	0.93	0.90	0.91	0.92
$B^{(9)}$									
$W_{7,8}$		$v_{7,8}$	-0.48	0.39	-0.35	0.43	0.43	-0.06	0.35
f_{min} - f_{max} (Hz)	1.56-1.76	En	8.4e-07	5.7e-07	4.3e-07	1.3e-06	6.9e-07	8e-08	1.1e-06
M($W_{7,8}$)	0.560	Lag	0.06	0.18	0.06	-0.06	-0.10	0.00	-0.14
$\log_{10}(E_{out}/E_{in})$	-0.224	Az	-98.61	61.82	120.11	139.32	22.33	-35.59	174.29
		In	38.54	47.03	88.65	75.98	83.97	87.32	82.50
		Rc	0.92	0.94	0.94	0.93	0.85	0.70	0.94
		Pl	0.98	0.96	0.91	0.95	0.94	0.90	0.94
$B^{(10)}$									
$W_{7,9}$		$v_{7,9}$	0.37	0.32	0.18	-0.52	0.16	0.07	0.66
f_{min} - f_{max} (Hz)	1.76-1.95	En	6.1e-07	5.6e-07	1.9e-07	7.8e-07	3.5e-07	5.7e-08	1.1e-06
M($W_{7,9}$)	0.668	Lag	-0.02	0.04	0.04	-0.10	0.04	0.02	-0.04
$\log_{10}(E_{out}/E_{in})$	-0.322	Az	-93.14	70.45	160.26	126.61	-123.23	-59.08	-0.18
		In	41.35	57.39	74.73	87.48	82.31	79.31	89.33
		Rc	0.90	0.86	0.82	0.89	0.76	0.65	0.91
		Pl	0.96	0.97	0.84	0.91	0.94	0.89	0.94
$B^{(11)}$									
$W_{7,10}$		$v_{7,10}$	0.27	0.50	-0.10	-0.43	-0.25	0.02	0.65
f_{min} - f_{max} (Hz)	1.95-2.15	En	4.1e-07	7.5e-07	1.7e-07	6e-07	4.1e-07	2.8e-08	1.2e-06
M($W_{7,10}$)	0.594	Lag	0.02	0.04	0.10	0.16	-0.10	-0.22	0.00
$\log_{10}(E_{out}/E_{in})$	-0.482	Az	-95.47	75.58	150.52	-62.33	-110.69	76.75	-3.20
		In	48.55	55.11	77.92	88.33	68.24	87.07	85.25
		Rc	0.87	0.86	0.62	0.93	0.80	0.48	0.92
		Pl	0.96	0.97	0.88	0.95	0.97	0.71	0.97

Table 2.3. continued

Signal		*Sta*	*EA1*	*EA3*	*EA4*	*EA7*	*EA2*	*EA5*	*EA6*
$B^{(12)}$									
$W_{7,11}$		$v_{7,11}$	-0.13	-0.51	-0.48	0.52	0.40	0.03	0.25
f_{min} - f_{max} (Hz)	2.15-2.34	En	2.5e-07	7.2e-07	3.6e-07	3.9e-07	2.9e-07	3.3e-08	4.6e-07
M($W_{7,11}$)	1.094	Az	-100.52	64.19	103.16	154.28	-138.80	82.63	8.04
$\log_{10}(E_{out}/E_{in})$	-0.365	In	34.57	36.53	87.21	89.86	72.39	87.44	82.53
		Rc	0.88	0.95	0.86	0.85	0.69	0.66	0.84
		Pl	0.93	0.97	0.95	0.92	0.97	0.76	0.94
$B^{(13)}$									
$W_{7,16}$		$v_{7,16}$	-0.60	-0.79	-0.02	0.10	-0.01	-0.02	0.06
f_{min} - f_{max} (Hz)	3.12-3.32	En	1.1e-06	1.2e-06	6.1e-08	1.4e-07	2.7e-08	1.6e-08	6.6e-08
M($W_{7,16}$)	0.742	Az	-104.22	52.70	138.96	151.93	-139.39	-112.66	15.13
$\log_{10}(E_{out}/E_{in})$	0.050	In	47.24	31.11	83.22	87.14	81.69	75.54	86.15
		Rc	0.96	0.97	0.73	0.78	0.66	0.67	0.72
		Pl	0.98	0.98	0.70	0.85	0.86	0.81	0.90
$B^{(14)}$									
$W_{7,17}$		$v_{7,17}$	0.21	-0.97	0.00	0.08	-0.01	0.01	0.03
f_{min} - f_{max} (Hz)	3.32-3.52	En	5.4e-07	8.3e-07	7.5e-08	1.5e-07	1.7e-08	1.9e-08	5.2e-08
M($W_{7,17}$)	0.965	Lag	0.02	0.06	0.04	0.06	-0.08	-0.04	-0.06
$\log_{10}(E_{out}/E_{in})$	0.098	Az	-104.71	48.14	135.67	145.79	-128.16	83.41	37.50
		In	44.63	32.79	71.95	82.98	83.11	86.03	85.50
		Rc	0.94	0.96	0.75	0.78	0.56	0.76	0.70
		Pl	0.95	0.96	0.72	0.81	0.82	0.82	0.86
$W_{7,19}$		$v_{7,19}$	0.11	-0.99	0.05	0.02	-0.01	0.00	0.06
f_{min} - f_{max} (Hz)	3.71-3.91	En	3.5e-07	8.9e-07	5e-08	1.1e-07	1.7e-08	6.7e-09	2.9e-08
M($W_{7,19}$)	0.607	Lag	-0.04	0.08	-0.08	0.00	-0.06	0.12	-0.02
$\log_{10}(E_{out}/E_{in})$	0.048	Az	-109.73	47.63	144.57	172.01	-156.25	-115.60	42.08
		In	47.44	37.43	77.63	84.69	85.58	89.73	85.13
		Rc	0.93	0.98	0.70	0.77	0.59	0.48	0.44
		Pl	0.90	0.98	0.79	0.86	0.81	0.50	0.85
$B^{(15)}$									
$W_{7,18}$		$v_{7,18}$	0.22	0.97	0.04	0.01	0.01	-0.02	0.06
f_{min} - f_{max} (Hz)	3.52-3.71	En	3.7e-07	8.6e-07	5.4e-08	1e-07	2.1e-08	1.1e-08	3.8e-08
M($W_{7,18}$)	0.632	Lag	-0.02	-0.06	0.08	0.02	0.04	0.00	-0.06
$\log_{10}(E_{out}/E_{in})$	-0.000	Az	-104.85	45.87	143.85	160.23	-146.81	93.54	67.69
		In	44.02	36.30	70.84	83.00	87.90	85.92	86.82
		Rc	0.94	0.97	0.66	0.74	0.70	0.62	0.58
		Pl	0.92	0.97	0.55	0.76	0.86	0.77	0.86
$W_{5,5}$		$v_{5,5}$	-0.04	-1.00	0.02	0.01	0.00	-0.01	0.06
f_{min} - f_{max} (Hz)	3.91-4.69	En	1.2e-06	3.6e-06	1.8e-07	2.2e-07	4.6e-08	3.1e-08	1.1e-07
M($W_{5,5}$)	0.486	Az	-110.94	52.31	155.07	-11.71	-153.45	78.47	-157.47
$\log_{10}(E_{out}/E_{in})$	-0.000	In	42.60	35.04	77.92	82.24	85.46	82.95	87.22
		Rc	0.91	0.98	0.72	0.52	0.68	0.66	0.57
		Pl	0.87	0.98	0.57	0.71	0.81	0.61	0.81
$W_{5,6}$		$v_{5,6}$	-0.20	-0.98	0.01	0.03	-0.01	-0.01	0.03
f_{min} - f_{max} (Hz)	4.69-5.47	En	1e-06	2.1e-06	7.9e-08	1.4e-07	1.6e-08	2e-08	6.5e-08
M($W_{5,6}$)	0.579	Az	-109.80	61.44	148.42	7.38	18.04	62.07	-150.23
$\log_{10}(E_{out}/E_{in})$	-0.000	In	42.03	32.20	75.70	89.30	85.15	83.61	87.44
		Rc	0.91	0.98	0.43	0.57	0.76	0.64	0.66
		Pl	0.92	0.98	0.54	0.72	0.81	0.64	0.69

Table 2.3. continued

Signal		*Sta*	*EA1*	*EA3*	*EA4*	*EA7*	*EA2*	*EA5*	*EA6*
$W_{5,7}$		$v_{5,7}$	0.10	0.99	0.01	-0.00	0.01	-0.00	0.01
f_{min} - f_{max} (Hz)	5.47-6.25	En	3.5e-07	1.1e-06	3.3e-08	7.7e-08	1.1e-08	1.1e-08	2.5e-08
M($W_{5,7}$)	0.459	Az	-104.77	79.09	-14.34	-177.54	30.79	65.86	1.38
$\log_{10}(E_{out}/E_{in})$	-0.000	In	35.10	27.92	80.31	88.20	84.09	78.59	82.66
		Rc	0.82	0.97	0.26	0.47	0.82	0.64	0.58
		Pl	0.81	0.97	0.29	0.67	0.90	0.55	0.71
$W_{3,2}$		$v_{3,2}$	-0.07	-1.00	0.03	0.01	-0.01	0.01	0.01
f_{min} - f_{max} (Hz)	6.25-9.38	En	5.8e-07	1.7e-06	1.3e-07	2.2e-07	2.3e-08	4.5e-08	7e-08
M($W_{3,2}$)	0.637	Az	5.12	168.12	144.29	-155.65	-72.20	75.72	-165.76
$\log_{10}(E_{out}/E_{in})$	-0.003	In	50.78	62.30	88.44	79.39	77.05	78.92	83.68
		Rc	0.66	0.81	0.62	0.61	0.70	0.39	0.43
		Pl	0.56	0.75	0.77	0.73	0.79	0.48	0.57
$B^{(16)}$									
$W_{7,48}$		$v_{7,48}$	-0.83	0.28	-0.17	-0.45	-0.02	-0.06	-0.03
f_{min} - f_{max} (Hz)	9.38-9.57	En	1.6e-08	9.2e-09	5.9e-09	8.6e-09	8.8e-10	8.3e-10	1.3e-09
M($W_{7,48}$)	1.149	Lag	-0.08	0.00	-0.02	-0.08	0.04	0.08	0.06
$\log_{10}(E_{out}/E_{in})$	-0.038	Az	-84.74	128.82	-39.71	-18.84	20.28	-105.68	32.84
		In	69.46	40.63	84.30	85.51	74.68	79.20	79.18
		Rc	0.61	0.63	0.59	0.51	0.57	0.73	0.46
		Pl	0.64	0.67	0.74	0.72	0.84	0.69	0.40
$B^{(17)}$									
$W_{7,49}$		$v_{7,49}$	-0.72	0.46	0.50	0.14	-0.03	-0.03	-0.02
f_{min} - f_{max} (Hz)	9.57-9.77	En	1.5e-08	1.2e-08	9.2e-09	1e-08	9.8e-10	1.4e-09	1.8e-09
M(W)	1.847	Az	-134.65	147.55	-53.77	-151.16	52.07	75.74	-14.90
$\log_{10}(E_{out}/E_{in})$	-0.034	In	39.06	42.05	75.42	75.42	76.69	84.94	83.52
		Rc	0.41	0.75	0.77	0.54	0.64	0.79	0.53
		Pl	0.57	0.74	0.82	0.51	0.89	0.79	0.65
$B^{(18)}$									
$W_{7,50}$		$v_{7,50}$	0.51	-0.65	0.54	-0.05	0.06	-0.10	0.09
f_{min} - f_{max} (Hz)	9.77-9.96	En	1.4e-08	1.4e-08	1.1e-08	1.2e-08	7.7e-10	1.9e-09	2.3e-09
M(W)	1.860	Lag	0.02	0.06	-0.02	-0.02	0.04	-0.04	-0.02
$\log_{10}(E_{out}/E_{in})$	-0.111	Az	-48.44	141.56	-45.05	-164.33	87.63	74.12	169.99
		In	23.88	45.76	71.64	78.73	84.00	83.09	84.54
		Rc	0.32	0.82	0.81	0.67	0.70	0.84	0.56
		Pl	0.54	0.86	0.81	0.62	0.89	0.78	0.71
$B^{(19)}$									
$W_{7,51}$		$v_{7,51}$	-0.14	-0.07	-0.58	-0.77	-0.03	-0.04	0.20
f_{min} - f_{max} (Hz)	9.96-10.16	En	1.2e-08	1.4e-08	1.2e-08	1.5e-08	7.7e-10	1.3e-09	2.6e-09
M(W)	2.022	Lag	-0.04	-0.08	-0.04	-0.06	-0.02	0.20	0.06
$\log_{10}(E_{out}/E_{in})$	-0.179	Az	0.32	149.79	143.98	-153.42	-74.43	80.41	-125.60
		In	64.02	60.20	85.78	81.85	87.77	87.63	56.39
		Rc	0.43	0.84	0.77	0.67	0.69	0.82	0.51
		Pl	0.65	0.77	0.72	0.71	0.85	0.76	0.83

Table 2.3. continued

Signal		*Sta*	*EA1*	*EA3*	*EA4*	*EA7*	*EA2*	*EA5*	*EA6*
$B^{(20)}$									
$W_{7,52}$		$v_{7,52}$	-0.02	-0.40	0.33	-0.85	0.04	0.09	0.03
f_{min} - f_{max} (Hz)	10.16-10.35	En	1.2e-08	1.2e-08	1.1e-08	2.2e-08	9.4e-10	1.1e-09	2.1e-09
M(*W*)	1.154	Lag	-0.10	-0.06	0.06	0.02	-0.02	0.20	-0.08
$\log_{10}(E_{out}/E_{in})$	-0.138	Az	12.15	141.35	141.77	-130.32	93.76	86.15	-110.27
		In	66.81	59.69	87.77	83.81	88.07	82.66	53.94
		Rc	0.51	0.81	0.83	0.77	0.78	0.84	0.53
		Pl	0.70	0.71	0.78	0.74	0.88	0.78	0.81
$B^{(21)}$									
$W_{7,53}$		$v_{7,53}$	-0.53	0.13	0.29	-0.77	0.02	-0.06	0.10
f_{min} - f_{max} (Hz)	10.35-10.55	En	1.5e-08	1.2e-08	5.7e-09	2e-08	7.7e-10	8.9e-10	1.4e-09
M(*W*)	0.962	Lag	-0.06	-0.04	-0.08	-0.04	-0.02	0.28	-0.02
$\log_{10}(E_{out}/E_{in})$	-0.318	Az	25.73	139.69	112.80	-136.64	-83.69	78.76	179.09
		In	57.96	58.95	85.55	86.00	87.45	84.38	75.67
		Rc	0.75	0.76	0.71	0.75	0.79	0.68	0.46
		Pl	0.65	0.69	0.77	0.74	0.76	0.84	0.54
$B^{(22)}$									
$W_{7,54}$		$v_{7,54}$	0.40	0.74	-0.13	0.51	0.00	-0.02	0.14
f_{min} - f_{max} (Hz)	10.55-10.74	En	1.1e-08	1.3e-08	4.9e-09	1.1e-08	6.6e-10	4.6e-10	1.5e-09
M(*W*)	1.534	Lag	0.00	-0.02	-0.02	-0.06	0.08	0.12	-0.08
$\log_{10}(E_{out}/E_{in})$	-0.210	Az	5.12	168.12	144.29	-155.65	-72.20	75.72	-165.76
		In	50.78	62.30	88.44	79.39	77.05	78.92	83.68
		Rc	0.66	0.81	0.62	0.61	0.70	0.39	0.43
		Pl	0.56	0.75	0.77	0.73	0.79	0.48	0.57
$B^{(23)}$									
$W_{7,55}$		$v_{7,55}$	-0.34	-0.38	0.02	-0.86	-0.04	-0.01	0.06
f_{min} - f_{max} (Hz)	10.74-10.94	En	7.4e-09	9.2e-09	3.4e-09	1.5e-08	6.8e-10	6.4e-10	1.3e-09
M(*W*)	1.173	Lag	0.00	0.06	-0.06	0.00	-0.08	0.18	-0.08
$\log_{10}(E_{out}/E_{in})$	-0.056	Az	-12.20	155.98	-3.03	-165.47	-80.43	80.67	-33.50
		In	34.88	60.24	84.40	85.08	80.50	83.55	86.13
		Rc	0.36	0.71	0.56	0.77	0.74	0.74	0.46
		Pl	0.44	0.73	0.60	0.83	0.81	0.80	0.57
$B^{(24)}$									
$W_{7,56}$		$v_{7,56}$	0.28	-0.25	0.13	-0.92	0.02	0.00	0.03
f_{min} - f_{max} (Hz)	10.94-11.13	En	8.2e-09	7.9e-09	4.2e-09	1.4e-08	5.5e-10	7.2e-10	1.5e-09
M(*W*)	1.433	Lag	-0.02	0.08	0.00	0.02	-0.08	0.18	-0.16
$\log_{10}(E_{out}/E_{in})$	0.054	Az	-16.66	163.18	1.98	-160.14	-85.11	77.61	-30.48
		In	32.06	65.52	83.94	84.71	82.31	84.47	80.89
		Rc	0.42	0.67	0.66	0.78	0.67	0.80	0.57
		Pl	0.36	0.67	0.73	0.81	0.76	0.83	0.50
$B^{(25)}$									
$W_{7,57}$		$v_{7,57}$	-0.46	-0.17	0.04	0.86	-0.03	0.10	0.05
f_{min} - f_{max} (Hz)	11.13-11.33	En	9.4e-09	9e-09	3.9e-09	1.4e-08	4.8e-10	7.4e-10	1.4e-09
M(*W*)	1.465	Lag	0.08	-0.02	-0.02	-0.08	0.04	0.16	-0.16
$\log_{10}(E_{out}/E_{in})$	-0.105	Az	-4.40	170.93	8.10	-171.93	-102.83	-110.31	-20.47
		In	45.60	70.39	84.14	85.45	82.24	88.06	74.79
		Rc	0.50	0.77	0.60	0.56	0.56	0.79	0.58
		Pl	0.63	0.71	0.71	0.73	0.62	0.82	0.51

Table 2.3. continued

Signal		*Sta*	*EA1*	*EA3*	*EA4*	*EA7*	*EA2*	*EA5*	*EA6*
$W_{7,61}$		$v_{7,61}$	0.57	0.18	0.13	-0.78	0.08	0.04	0.02
f_{min} - f_{max} (Hz)	11.91-12.11	En	1.4e-08	6.5e-09	4e-09	1.4e-08	6.6e-10	7.3e-10	9.7e-10
M(*W*)	1.489	Lag	0.06	-0.02	0.02	-0.06	-0.08	0.12	-0.04
$\log_{10}(E_{out}/E_{in})$	-0.012	Az	-119.99	177.37	177.02	-164.14	-90.93	78.16	-157.43
		In	52.32	62.80	87.83	73.99	77.86	82.85	68.73
		Rc	0.67	0.64	0.58	0.61	0.77	0.87	0.46
		Pl	0.78	0.67	0.67	0.82	0.78	0.80	0.53
B$^{(26)}$									
$W_{7,58}$		$v_{7,58}$	0.61	-0.17	0.07	-0.75	0.05	-0.10	0.12
f_{min} - f_{max} (Hz)	11.33-11.52	En	1.1e-08	9e-09	3.6e-09	1.2e-08	7.5e-10	5.2e-10	1.5e-09
M(*W*)	1.765	Lag	-0.02	-0.10	0.04	-0.08	0.06	0.14	-0.04
$\log_{10}(E_{out}/E_{in})$	-0.126	Az	10.00	165.66	175.65	-50.43	-116.50	63.88	15.10
		In	87.29	80.69	83.70	66.75	81.67	83.90	83.15
		Rc	0.56	0.75	0.53	0.46	0.74	0.82	0.58
		Pl	0.72	0.79	0.69	0.66	0.72	0.81	0.52
B$^{(27)}$									
$W_{7,59}$		$v_{7,59}$	-0.89	0.07	-0.29	0.33	-0.05	-0.01	-0.08
f_{min} - f_{max} (Hz)	11.52-11.72	En	1.5e-08	8.1e-09	6.8e-09	1.1e-08	7.7e-10	4.9e-10	1.6e-09
M(*W*)	1.676	Az	-142.11	157.19	179.49	-86.49	-105.90	67.41	13.89
$\log_{10}(E_{out}/E_{in})$	0.001	In	53.29	79.79	88.42	70.04	83.81	81.71	75.66
		Rc	0.73	0.74	0.79	0.53	0.81	0.81	0.60
		Pl	0.83	0.76	0.85	0.65	0.82	0.76	0.58
B$^{(28)}$									
$W_{7,60}$		$v_{7,60}$	-0.96	-0.12	-0.25	-0.03	-0.01	-0.04	-0.04
f_{min} - f_{max} (Hz)	11.72-11.91	En	1.7e-08	5.9e-09	7e-09	1e-08	7.5e-10	5.7e-10	1e-09
M(*W*)	1.348	Lag	-0.06	-0.02	-0.12	-0.02	0.08	0.08	0.04
$\log_{10}(E_{out}/E_{in})$	0.102	Az	-147.34	161.19	-177.16	-125.67	-92.34	74.42	9.30
		In	55.89	78.71	87.33	74.08	77.89	85.99	70.64
		Rc	0.71	0.66	0.80	0.51	0.80	0.81	0.35
		Pl	0.76	0.70	0.85	0.68	0.82	0.76	0.37
B$^{(29)}$									
$W_{7,62}$		$v_{7,62}$	0.06	0.08	0.05	0.99	0.02	-0.04	0.01
f_{min} - f_{max} (Hz)	12.11-12.30	En	1.1e-08	7.3e-09	4.1e-09	1.7e-08	7e-10	5.5e-10	1.3e-09
M(*W*)	1.418	Az	-144.18	163.14	-19.39	-166.60	-105.90	79.68	-177.12
$\log_{10}(E_{out}/E_{in})$	0.123	In	70.01	68.64	84.40	76.50	87.07	81.60	75.69
		Rc	0.53	0.68	0.66	0.65	0.87	0.86	0.63
		Pl	0.77	0.63	0.72	0.85	0.89	0.81	0.51
$W_{1,1}$		$v_{1,1}$	0.08	0.07	-0.01	-0.99	-0.00	0.01	0.01
f_{min} - f_{max} (Hz)	12.50-25.00	En	1.6e-07	1.6e-07	8.1e-08	2.7e-07	1.4e-08	7.6e-09	2.3e-08
M(*W*)	1.622	Az	-4.40	-119.99	170.93	177.37	8.10	177.02	-171.93
$\log_{10}(E_{out}/E_{in})$	-0.401	In	45.60	52.32	70.39	62.80	84.14	87.83	85.45
		Rc	0.50	0.67	0.77	0.64	0.60	0.58	0.56
		Pl	0.63	0.78	0.71	0.67	0.71	0.67	0.73

Table 2.3. continued

Signal		*Sta*	*EA1*	*EA3*	*EA4*	*EA7*	*EA2*	*EA5*	*EA6*
$B^{(30)}$									
$W_{7,63}$		$v_{7,63}$	-0.26	0.33	0.08	-0.90	0.04	0.04	0.07
f_{min} - f_{max} (Hz)	12.30-12.50	En	1.2e-08	1.2e-08	3.6e-09	1.5e-08	5.4e-10	4.9e-10	1.4e-09
M(*W*)	1.599	Az	-110.74	165.70	-5.37	-165.74	67.16	71.54	-168.36
$log_{10}(E_{out}/E_{in})$	-0.006	In	55.59	82.65	85.94	73.98	85.68	77.17	64.04
		Rc	0.52	0.83	0.68	0.69	0.80	0.89	0.74
		Pl	0.66	0.77	0.62	0.86	0.89	0.86	0.67

Notes to Chapter II

Amelung, F., Oppenheimer, C., Segall, P., Zebker, H., 2000. Ground deformation near Gada ‘Ale Volcano, Afar, observed by radar interferometry. *Geophys. Res. Lett.* 27, 3093-3096.

Aster, R., McIntosh, W., Kyle, P., Esser, R., Bartel, B., Dunbar, N., Johns, B., Johnson, J., Karstens, R., Curnik, C., McGowan, N., McNamara, S., Meertens, C., Pauly, B., Richmond, M., Ruiz, M., 2004. Real-time data received from Mount Erebus Volcano, Antarctica, *Eos Trans. AGU 85*, 97-100.

Bajope, B., Mahinda, K., Alean, J., Caillet, M., Carniel, R, Fulle, M., Vetsch, P., 2006. Continuous ash plumes and active lava lake, *B. Glob. Volc. Net.* 31:01.

Barberi, F., Varet, J., 1970. The Erta ’Ale volcanic range, *B. Volc.* 34, 848-917.

Bardintzeff, J.-M., Gaudru, H., 2004. On 4-5 December 2004 visitors noted active hornitos but solidified lava lake, *B. Glob. Volc. Net.* 29:11.

Bevington, P., Robinson, D., 2002. Data reduction and error analysis for the physical sciences. New York: McGraw-Hill, 3rd ed.

Carniel, R., Di Cecca, M., Rouland, D. 2003. Ambrym, Vanuatu (July-August 2000): spectral and dynamical transitions on the hours-to-days timescale. *J. Volcanol. Geotherm. Res.* 128, 1-13.

Coifman, R.R., Wickerhauser, M.V., 1992. Entropy-based algorithms for best basis selection. *IEEE Trans. Inf. Theory* 38, 713-718.

Dainelli, G., Marinelli, O., 1907. Vulcani attivi della Dancalia. *Rivista Geografica Italiana* 13, 261-270.

Francis, P., Oppenheimer, C., Stevenson, D., 1993. Endogenous growth of persistently active volcanoes, *Nature* 366, 554 - 557, doi:10.1038/366554a0.

Furumoto, M., Kunitomo, T., Inoue, H., Yamada, I., Yamaoka, K., Ikami, A. Fukao, Y., 1990. Twin sources of high-frequency volcanic tremor of Izu-Oshima Volcano, Japan. *Geophys. Res. Lett.* 17(1): doi: 10.1029/89GL03678. issn: 0094-8276.

Gottschämmer, E., Surono, I., 2000. Locating tremor and shock sources at Bromo Volcano. *J. Volcanol. Geotherm. Res.* 101, 199-209.

Grandjean, V., 2006. Molten lava lake observations as late as 3 January 2006, *Bull. Glob. Volc. Net.* 31:03.

Hamaguchi, H., Nishimura, T., Zana, N., 1992. Process of the 1977 Nyiragongo eruption inferred from the analysis of long-period earthquakes and volcanic tremors. *Tectonophysics* 209, 241-254.

Harris, A.J.L., Carniel, R., Jones, J., 2005. Identification of variable convective regimes at Erta Ale Lava Lake. *J. Volcanol. Geotherm. Res.*, 142, 207-223.

Harris, A.J.L., Flynn, L.P., Rothery, D.A., Oppenheimer, C., Sherman, S.B., 1999. Mass flux measurements at active lava lakes: Implications for magma recycling. *J. Geophys. Res.* 104 (B4), 7117-7136.

Jones, J., Carniel, R., Harris, A.J.L., Malone, S., 2006. Seismic characteristics of variable convection at Erta `Ale lava lake, Ethiopia, *J. Volcanol. Geotherm. Res.* 153, 64-79.

Jurkevics, 1988. Polarization analysis of three-component array data. *B. Seis. Soc. Am.* 78, 1725-1743.

Kaminuma, K., 1994. The seismic activity of Mount Erebus in 1981–1990. *In*: Kyle, P.R. (Ed.), *Volcanological and Environmental Studies of Mount Erebus, Antarctica*. Antarctic Research Series, American Geophysical Union, Washington DC, pp. 35–50.

Konstantinou, K.I., Schlindwein, V., 2002. Nature, wavefield properties and source mechanism of volcanic tremor: a review. *J. Volcanol. Geotherm. Res.* 119, 161-187.

Kyle, P.R., 1994. Volcanological and environmental studies of Mount Erebus, Antarctica. AGU Antarctic Research Series, 66, 162 pp.

Le Guern, F., 1987. Mechanism of energy transfer in the lava lake of Nyiragongo (Zaire), 1959-1977. *J. Volcanol. Geotherm. Res.* 31, 17-31.

Martini, M., 1969. Studio di prodotti fumarolici di alcuni vulcani della catena dell'Erta Ale (Etiopia). *Rend. Soc. Min. Ital.* 25, 79-92.

Oppenheimer, C., Francis, P., 1998. Implications of longeval lava lakes for geomorphological and plutonic processes at Erta 'Ale volcano, north Afar. *J. Volcanol. Geotherm. Res.* 80, 101-111.

Oppenheimer, C., Francis, P, 1997. Remote sensing of heat, lava and fumarole emissions from Erta 'Ale volcano, Ethiopia. *Int. J. Rem. Sensing* 18, 1661-1692.

Patrick, M.P., Smellie, J.L., Harris, A.J.L., Garbeil, H., Pilger, E., 2004. First recorded eruption of Mount Belinda volcano, South Sandwich Islands. *B. Volc.* 67(5), 415-422.

Ripepe, M., Gordeev, E., 1999. Gas bubble dynamics model for shallow volcanic tremor at Stromboli, *J. Geophys. Res.* 104(B5), 10,639–10,654.

Rivallin, P., Mougin, D., 2008. Trip report of Pierrette Rivallin and Dédé Mougin: *LAVE Bulletin* 79, May 2008.

Rymer, H., van Wyk de Vries, B., Stix, J., Williams-Jones, G., 1998. Pit crater structure and processes governing persistent activity at Masaya Volcano, Nicaragua. *B. Volc.* 59, 345-355.

Swanson, D.A., Duffield, W.A., Jackson, D.B., Peterson, D.W., 1979. Chronological narrative of the 1969-71 Mauna Ulu eruption of Kilauea volcano, Hawaii. *USGS Prof. Pap.* 1056, 55 pp.

Tazieff, H., 1994. Permanent lava lakes: observed facts and induced mechanisms, *J. Volcanol. Geotherm. Res.* 63(1-2), pp. 3-11.

Vidale, J., 1986. Complex polarization analysis of particle motion. *B. Seis. Soc. Am.* 76(5), 1393-1405.

Witter, J.B., 2003. Convection of magma in volcanic conduits as a degassing mechanism at active volcanoes, *Ph.D. Thesis, Univ. Washington, Seattle, WA, USA*.

Wright, R., Flynn, L.P., 2004, Space-based estimate of the volcanic heat flux into the atmosphere during 2001 and 2002. *Geology* 32, p. 189-192.

Yirgu, G., Kirkos, W., Philpotts, A., MODIS/MODVOLC Thermal Alerts Team, 2005. Agitated lava lake during time of September 2005 earthquake swarm ~ 100 km S, *Bull. G. Volc. Net.* 30:09.

III. The 23-24 Nov 2006 Paroxysm of Mt. Etna, Italy

Background

Mt. Etna has one of the longest documented records of historical volcanism, dating to at least 1500 BC. Etna experiences explosive summit eruptions, sometimes with minor ash emissions, and rare sub-Plinian to Plinian eruptions (Del Carlo et al., 2004). Less frequently Etna experiences flank eruptions that produce basaltic lava flows extending downward from near the summit. In the early part of the current decade, Mt. Etna experienced two unusually persistent explosive eruptions, followed by quiet summit eruptions in 2004-5 and an eruptive phase at the summit in 2006 (Patanè et al. 2008, Allard et al., 2006). Both eruptive styles are thought to be controlled by processes within the volcanic conduit reflecting changes in volatile content and magma flow rate (Jaupart and Vergniolle 1988, Woods and Cardoso, 1997).

Seismic activity at Mt. Etna consists of persistent background tremor with LP and VLP events superimposed, and a low rate of VT seismicity (Saccorotti et al. 2007, Di Grazia et al. 2006). VLP events have a peak frequency between .06 and 0.1 Hz and can occur as either VLP tremor or a single pulse (Patanè et al. 2008, Saccorotti et al. 2007, Lockmer et al. 2007). LP events, which are generally associated with fluids moving in volcanic conduits (Chouet 1996), sometimes occur more frequently before lava fountaining episodes. Their dominant frequencies are typically between 0.4 and 0.6 Hz (Patanè et al. 2008). Persistent background tremor

is considered a single signal extending from roughly 0.5-5 Hz. Attempts to constrain the tremor centroid associate it with two distinct source regions, whose geometries suggest connected dike-like bodies extending from sea level to the surface (Patanè et al. 2008, Di Grazia et al 2006).

These results are corroborated by important evidence recorded during periods of unrest, which typically consist of vigorous lava fountaining and flows. Di Grazia et al (2006) have found changes in tremor hypocentroids after such periods of unrest. Similarly, tremor hypocentroids sometimes change during and after lava fountaining episodes, including a paroxysmal lava fountaining phase of 23-24 Nov 2006 (S. Falsaperla, pers. comm.). These tremor centroids are effectively an average location of all sources that generate seismic energy between 0.5 and 5 Hz (Patanè et al. 2008).

In this work, we investigate what changes can be seen in the tremor when we treat it as the composite of many signals, and whether these recovered signals change before and during periods of unrest. Having already introduced a method to recover signals from continuous tremor in Chapter I, we now investigate its applicability to detection and tracking of signals associated with unrest.

Data Selection

Our sample data set includes 7 discontinuous hours of data from before, during, and after the paroxysmal lava fountaining of 23-24 Nov 2006. These data include 4 half-hour samples of continuous data from before and during the

paroxysm, and 10 samples following the paroxysm. The stations used in this study (Fig. 3.1) are part of the Mt. Etna permanent broadband seismic network. All stations use CMG40-T sensors (f_0 = 0.033 Hz) sampling at 100 Hz. However, for processing efficiency, all data are detrended and downsampled to 50 Hz prior to analysis. Scaling constants and site amplifications are divided out from the data using the values of Patanè et al (2008). After preprocessing, all data are analyzed using the *SDR* algorithm.

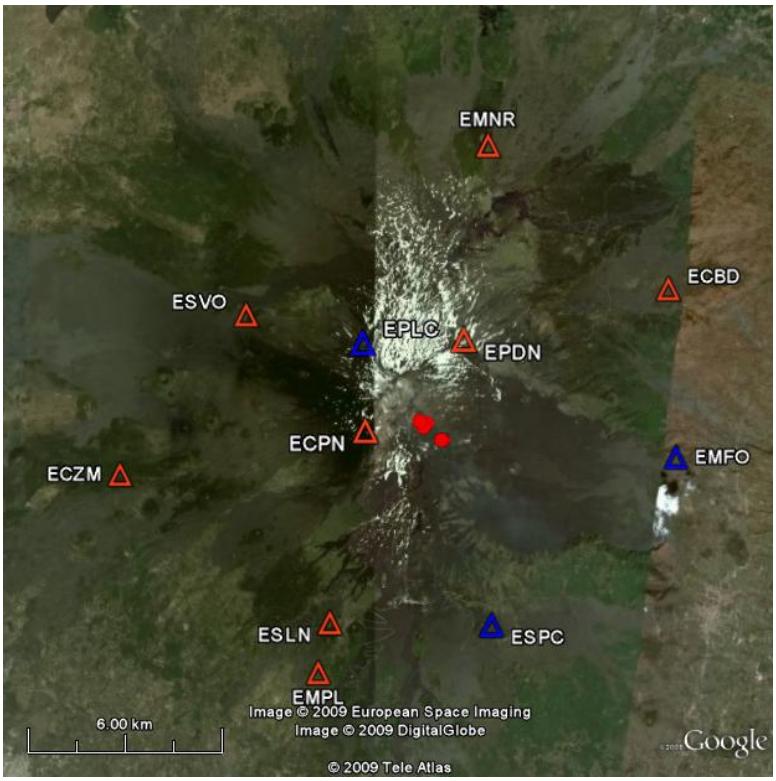

Figure 3.1. Google Earth[tm] Map showing 11 permanent broadband stations at Mt. Etna. Stations used to track signal persistence (as described in text) are in red. Other stations are in blue.

Tracking New and Persistent Signals

As discussed in Chapter I, recovered signals can be tracked through time provided that the seismic network geometry does not change. We say that a signal from some time period t_1 persists at some time period t_2 if the principal eigenvectors $v_{j,n,1}$ of its constituent subbands $\boldsymbol{W}_{j,n}$ cluster to the principal eigenvector of some recovered signal in time period t_2. Conversely, a new signal is defined as any recovered signal in time period t_2 for which the principal eigenvectors of some $\boldsymbol{W}_{j,n}$ do *not* cluster to the principal eigenvectors that form any existing signals. Thus we can track which recovered signals persist through time and which recovered signals are new.

We wish to focus specifically on which recovered signals persist, and which recovered signals change, before and during the paroxysmal lava flows of 23-24 Nov 2006. Because of station outages, such a direct comparison of signal persistence is not possible with the post-paroxysmal tremor data. Thus, we restrict our initial analysis to 4 half-hour samples recorded by the 8 stations that remained active in each time period (red triangles in Fig. 3.1). The first pair of samples represent an hour of continuous data beginning 11:00 GMT, 23 Nov 2006, shortly before the paroxysm. The second pair represents an hour of continuous data beginning 11:00 GMT, 24 Nov 2006, during the paroxysm. Here, we define a persistent signal as one in which over 90% of the principal eigenvectors $v_{j,n,1}$ of the subbands $\boldsymbol{W}_{j,n}$ of a new signal cluster to those of an existing signal, using a distance threshold of $\delta = 0.3$ and a median clustering rule.

By this method, applying *SDR* to each 30 min. sample, a total of only 8 unique signals are recovered from the 4 samples recorded before and during the paroxysm. Fig. 3.2 shows the results of this analysis. Fig. 3.2 shows the number of unique signals (with a maximum of 4 possible) recovered from the 4 data samples in each (0.19 Hz width) frequency bin. Thus, when a frequency bin contains a single signal, the signal content does not change at all over those frequencies. To compliment this data, also shown is the maximum signal persistence, in samples (out of 4 possible), for each frequency bin. If a signal persists in 4 samples for a given frequency bin, then the signal content does not change over those frequencies. Clearly, *SDR* cannot effectively resolve any changes to recovered signal content, before and during the paroxysm, at $f > 1.76$ Hz. While subtle changes may exist, they are below the detection threshold of the *SDR* method. This could be due to the network geometry (specifically too few active stations near the vents); the principal eigenvectors of the subbands that form the high-frequency tremor all lie within $\delta =$ 0.3 of the "axis" of station ECPN, the station nearest the active vents (Fig. 3.1), in the 8-dimensional space defined by each station's *Z'* wavelet coefficients. However, it may also be true that the tremor source is decoupled from whatever physical process drove the paroxysmal lava flows of 23-24 Nov 2006. Such an interpretation is consistent with INGV tremor centroid locations from this time period, which did not change before or during the paroxysm (S. Falsaperla, pers. comm.).

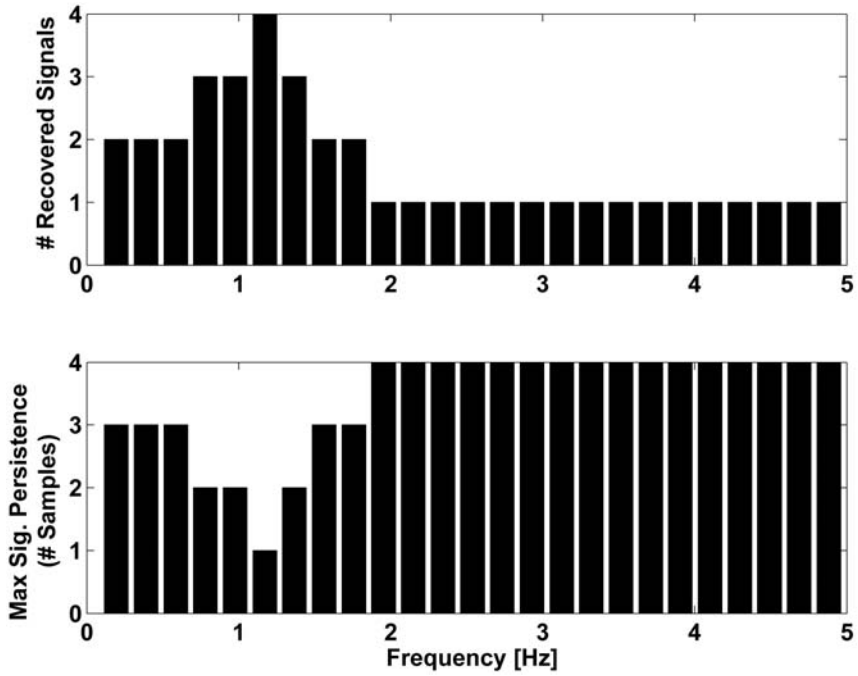

Figure 3.2. Signal persistence for the pre-paroxysmal tremor. The frequency spectrum is sorted into bins of approx 0.19 Hz width. The upper plot shows the number of recovered signals with energy in each frequency bin. A single recovered signal indicates that one signal persists in a frequency bin during all 4 sample time periods. The lower plot shows the maximum number of samples in which a single signal persists in each frequency bin.

Pre-Paroxysmal Signals

The changing signal content of the tremor is interesting. It suggests that some recovered signals, particularly those at $f \leq 1.76$ Hz, could be related to unrest. We wish to explore this possibility. We begin by analyzing two 30 min samples from before the onset of lava fountaining, for a total of 60 min of continuous data beginning at 11:00:00 (GMT), 23 Nov 2006. Trace data from each sample are shown in Fig. 3.3. A total of 9 stations from the Mt. Etna network were active

during this time; these were the stations in red in Fig. 3.1, plus station ESPC. The subband clustering for each time sample is shown in Figs. 3.4a and 3.4b. By the method described above, and with the added resolution from station ESPNC a total of 8 unique recovered signals are found in the pre-paroxysmal data.

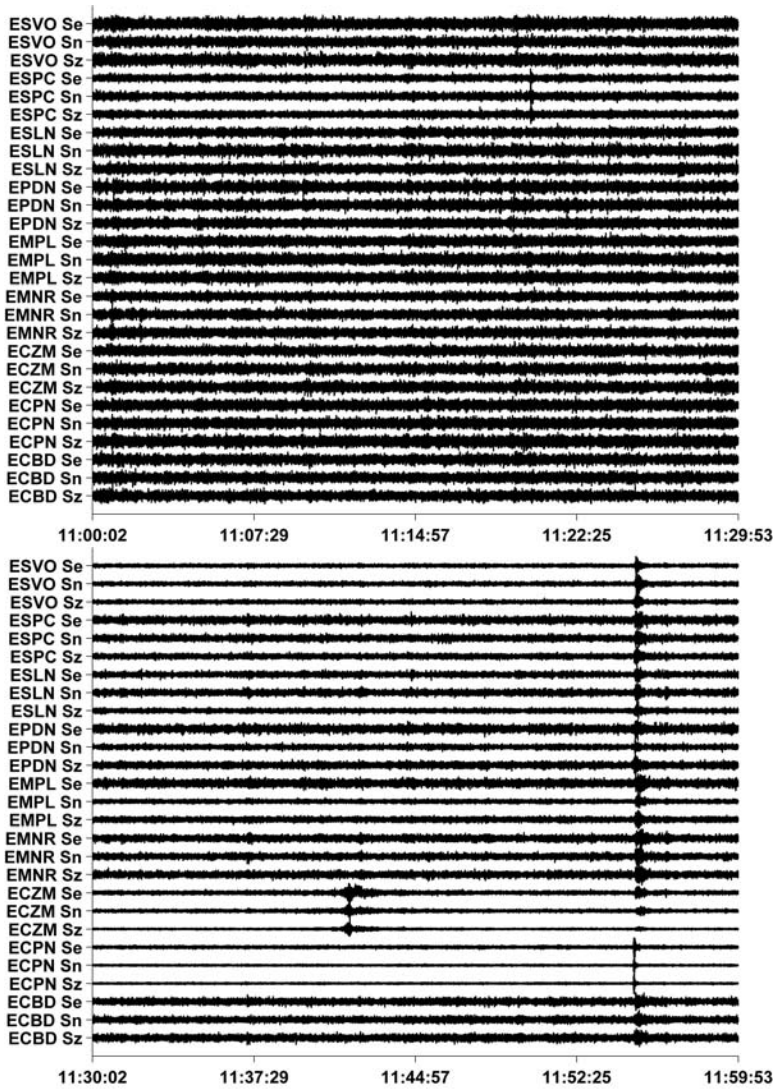

Figure 3.3. Amplitude-normalized seismic trace data for two half-hour data samples preceding the paroxysm. **a.** (Top) Trace data for the half-hour period beginning 23 Nov 2006, 11:00 GMT. **b.** (Bottom) Trace data for the half-hour period beginning 23 Nov 2006, 11:30 GMT.

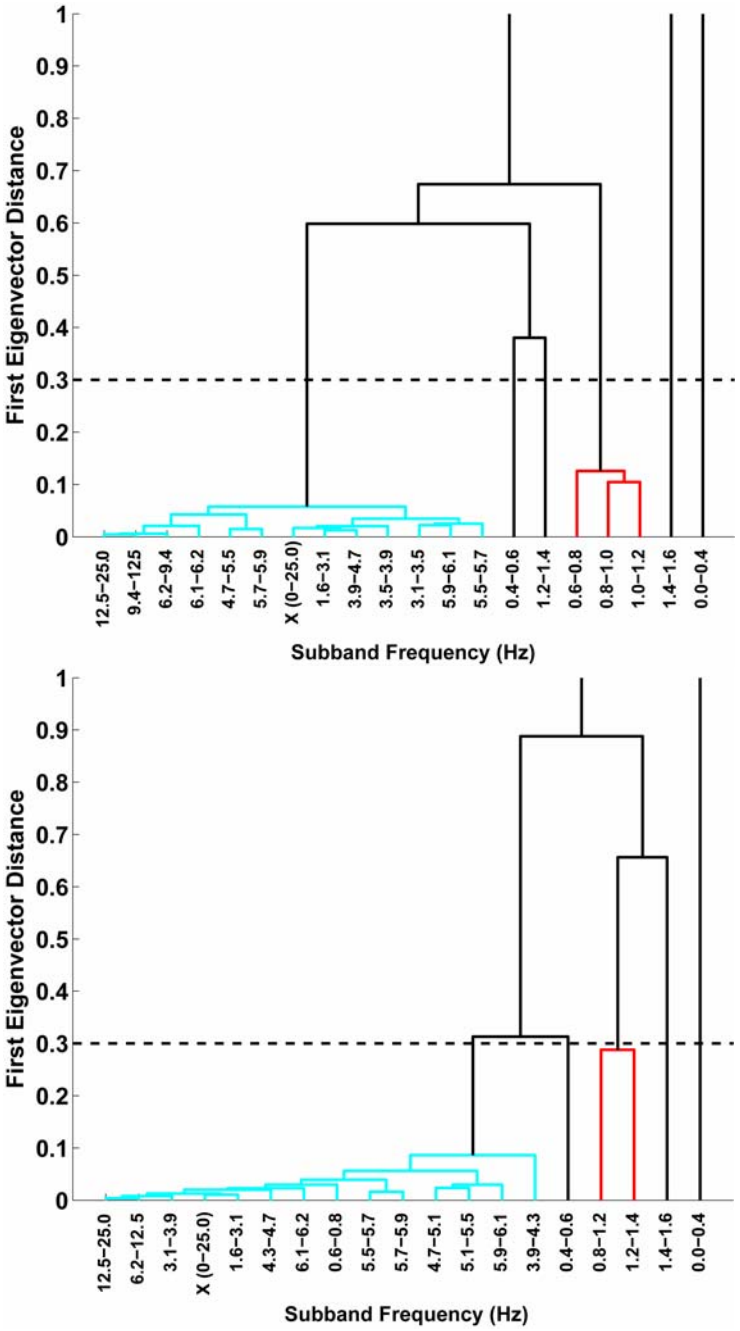

Figure 3.4. Decomposition of the pre-paroxysmal tremor using the *SDR* algorithm. **a.** (Top) Dendrogram for the sample beginning 23 Nov 2006, 11:00 GMT, showing subband clustering. **b.** (Bottom) Dendrogram for the sample beginning 23 Nov 2006, 11:30 GMT. In both figures, node denoted with "X (0-25.0)" denotes the input data. Horizontal dashed lines indicate distance threshold $\delta = 0.3$ for clustering of principal components eigenvectors.

It is a simple, straightforward process to analyze each recovered signal in detail. These recovered signals will be described using the shorthand convention $\mathbf{A}^0$. Details of these recovered signals (energy, polarization, etc.) are given in Table 3.1.

First, we observe that, to within the limitations of the network geometry and the algorithm's resolution, recovered signal $\mathbf{A}^{(1)}$ contains incoherent information that is most energetic at station ECPN, the station nearest to the active vents (Fig. 3.1). This signal is formed from all subbands that lie above f = 1.56 Hz, i.e. it includes most of the frequency content classified as "tremor" by Patanè et al. (2008). Because this signal is quasi-continuous, we can attempt to locate it using energy-based methods (Jones et al. 2006, Gottschämmer and Surono 2000), though Table 3.1 suggests that the complexity of the wavefield will result in a high degree of misfit. Fig. 3.5 shows best fit locations of a grid search over the upper edifice of Mt. Etna, using a 300s sliding window and a 200m grid, with χ^2=90% contours for these locations. INGV locations computed by the method of Patanè et al. (2008) are shown for comparison purposes (S. Falsaperla, pers. comm). We remark that these contours are surprisingly small relative to the aperture of the Etna seismic network (Fig. 3.1) and partly underlie the locations of Patanè et al (2008) for the (composite) tremor in the frequency range 0.5-5 Hz. There is an absolute shift of 2 km W, presumably due to the lack of data from two summit stations used in their study (EPLC and EBEL), which would help constrain the NW-SE extent of the tremor centroid. However, these locations are not inconsistent with the hypothesis of Patanè et al. (2008) that most tremor is generated in a dike-like body underneath the

summit crater. The only unambiguous discrepancy between this result and their work is the inclusion of energy above 5 Hz.

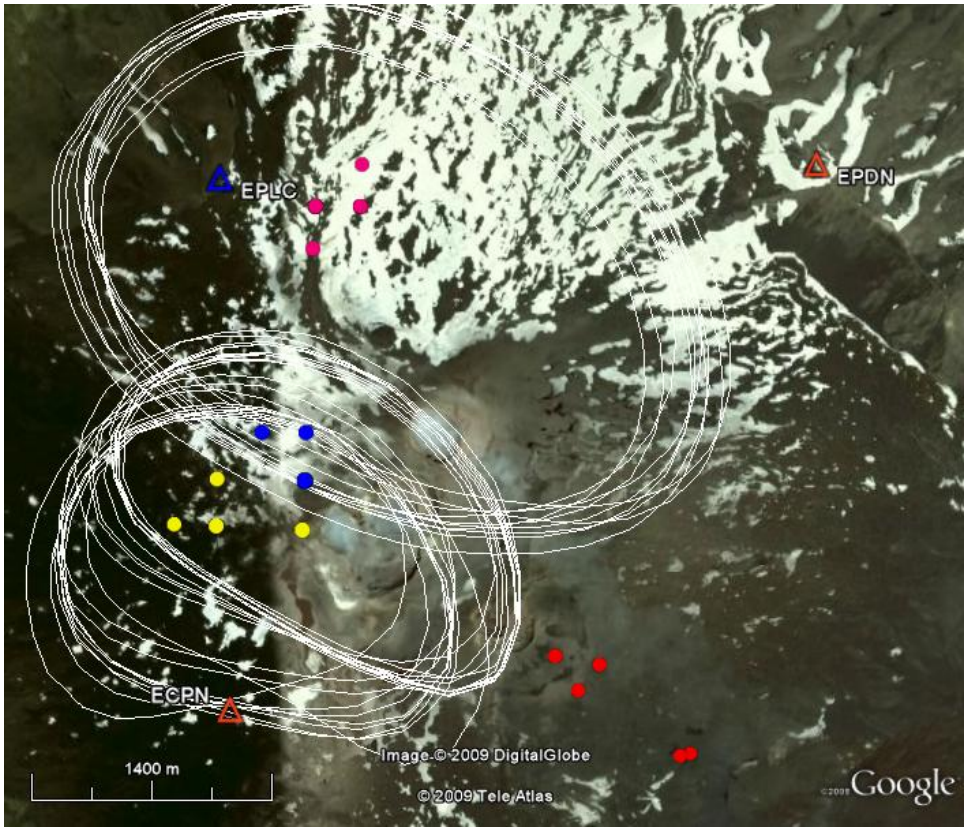

Figure 3.5. Locations of some recovered signals associated with paroxysmal and pre-paroxysmal tremor. Blue and yellow dots indicate locations of recovered signals $\mathbf{A}^{(1)}$ and $\mathbf{P}^{(1)}$, respectively, i.e. the continuous background tremor before and during the paroxysm. Magenta dots indicate locations of recovered signal $\mathbf{A}^{(5)}$, a secondary signal seen in one pre-paroxysmal data sample. Solid lines indicate 90% confidence contours of χ^2 misfit. INGV locations of background tremor during and after the paroxysm, computed by the method of Patanè et al. (2008), are indicated with red circles.

We now discuss some of the low-frequency recovered signals in the pre-paroxysmal tremor. As indicated above, the signal content of these frequencies changes during the paroxysm.

Recovered signal $\mathbf{A}^{(2)}$ is formed from a single subband, $\boldsymbol{W}_{6,0}$ (nominal passband $0 < f < 0.39$ Hz) and persists in both samples. This recovered signal is most energetic at stations ESVO and EMNR, very weak at stations near the Etna summit, and only detectible in the first sample. We conclude that this recovered signal is unrelated to volcanic activity.

Recovered signals $\mathbf{A}^{(3)}$ and $\mathbf{A}^{(4)}$ are interesting. Each signal formed from the single subband $\boldsymbol{W}_{7,2}$ (nominal passband 0.39-0.59 Hz). The first is recovered from the 11:00 GMT sample; the second, from the 11:30 GMT sample. The signal is energetic at all three of the stations high on Mt. Etna (Fig. 3.1). Fig. 3.6 shows amplitude-normalized trace data of recovered signal $\mathbf{A}^{(3)}$, and a spectrogram from station ECPN. Observe that the signal consists of discrete low-frequency pulses that are visible above the background noise at many stations. The nominal passband of 0.39-0.59 Hz is consistent with the frequency content of LF events described in Patanè et al. (2008) and the recovered signal shows discrete pulses that resemble LF events. From Table 3.1, the signals are most energetic at stations ECPN, EPDN, and ESVO, the 3 active stations nearest to the vents (Fig. 3.1). The signal is rectilinear at ECPN. Incidence angles are shallow but inconsistent with scattering at the surface. Interestingly, although its energies change little between the two time samples, its principal eigenvectors (Table 3.1) are separated by a distance of $\delta = 0.68$. Thus, the

suggestion is that either the signal location or signal source process changes, even on timescales as short as 30 minutes.

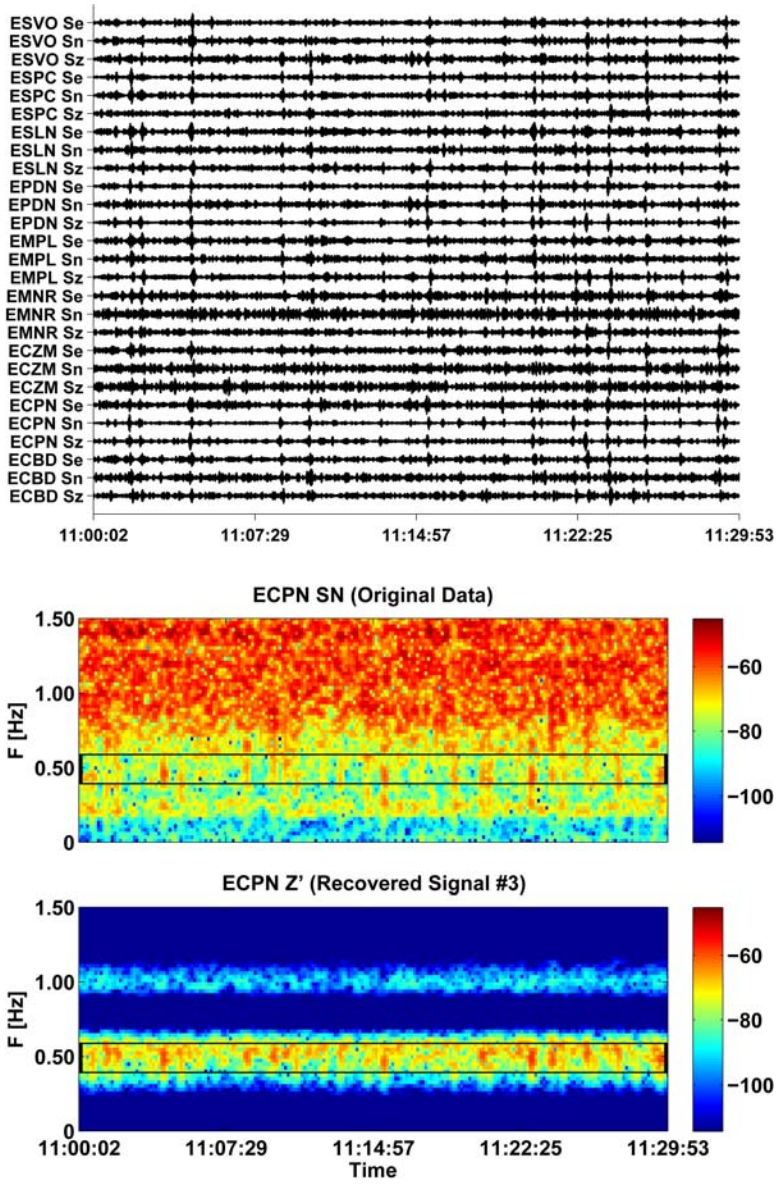

Figure 3.6. Recovered signal $\mathbf{A}^{(3)}$. **a.** (Top) Amplitude-normalized trace data of $\mathbf{A}^{(3)}$. **b.** (Bottom) Spectrogram of the input *N*-component data at station ECPN (top) and the *Z*′ component of recovered signal $\mathbf{A}^{(3)}$ at ECPN (bottom). Color scaling is in dB. Color scaling of input data is computed from ground velocity.

The implications of such a signal are quite interesting. LF event swarms have been known to precede unrest at other volcanoes (Chouet 1996), and have been previously detected at Etna (Patanè et al 2008). However, no obvious change in the background tremor was reported prior to the onset of unrest (S. Falsaperla, pers. comm.), nor detectible by our method (Fig. 3.2 & above). What this suggests, then, is the following: if these signals are interpreted as the response of the Etna conduit system to an injection of fresh, hot, gas-rich magma from depth, i.e. following the interpretation for LP seismic sources of Chouet (1996), then the background tremor is decoupled from these changes to the Etna system. In other words, the source process of the background tremor appears completely unrelated to whatever physical process might drive the unrest.

Recovered signal $\mathbf{A}^{(5)}$ is formed from three subbands, $\boldsymbol{W}_{7,3}$ - $\boldsymbol{W}_{7,5}$ ($0.59 < f <$ 1.17 Hz), and is seen only in the first sample. Recovered signal $\mathbf{A}^{(6)}$ has similar properties to $\mathbf{A}^{(5)}$ (Table 3.1), but persists in both time windows at 1.17-1.37 Hz. Fig. 3.7 shows the amplitude-normalized trace data of $\mathbf{A}^{(5)}$. From Table 3.1, signals $\mathbf{A}^{(5)}$ and $\mathbf{A}^{(6)}$ are most energetic at ECPN, but unlike $\mathbf{A}^{(3)}$ - $\mathbf{A}^{(4)}$ they lack the appearance of discrete pulses. Locations of signal $\mathbf{A}^{(5)}$ (Fig. 3.5) suggest that it is separate from the background tremor. We conclude from *SDR* and location that these signal are different from that of the background tremor, but bears no clear relationship to the unrest. Thus their relationship to volcanic activity cannot be determined.

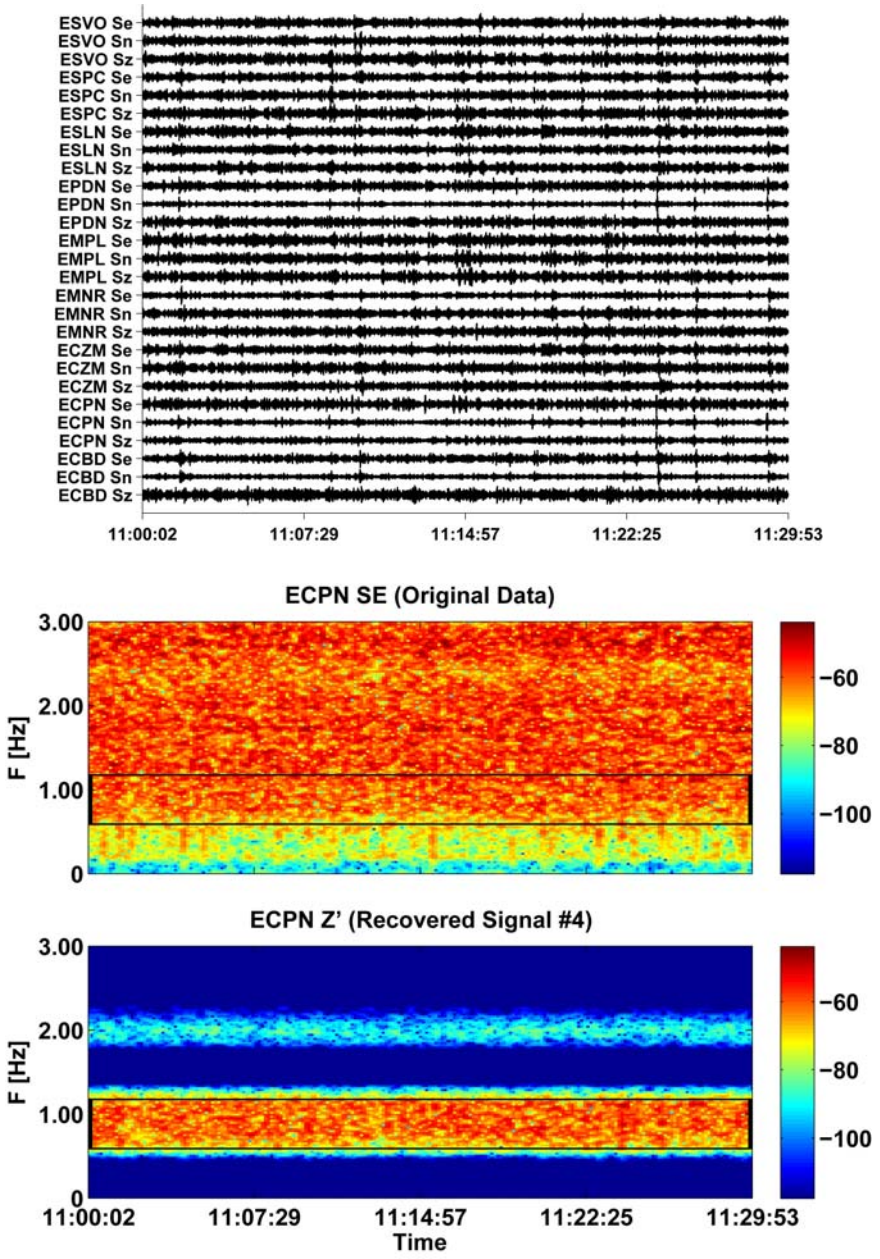

Figure 3.7. Recovered signal $\mathbf{A}^{(5)}$. **a.** (Top) Amplitude-normalized trace data of $\mathbf{A}^{(5)}$. **b.** (Bottom) Spectrogram of the input *E*-component data at station ECPN (top) and the *Z′* component of recovered signal $\mathbf{A}^{(5)}$ at ECPN (bottom). Color scaling is in dB. Color scaling of input data is computed from ground velocity.

Recovered signals $\mathbf{A}^{(7)}$ and $\mathbf{A}^{(8)}$ are each narrowband, and each is detected in one sample at 1.37-1.56 Hz. From Table 3.1, each signals is most rectilinearly polarized (and most energetic) at EPDN, which lies approx. 2 km NE of the active vents (Fig. 3.1). Additionally, $\mathbf{A}^{(8)}$ lies within $\delta = 0.3$ of the "axis" of station EPDN in the 9-dimensional space formed by the *Z'* component of each subband. Thus these two recovered signals appear to consists of transients whose energy is highest at EPDN.

Paroxysmal Signals

We now discuss two 30 min samples recorded during the paroxysmal lava fountaining, for a total of 60 min of continuous data beginning at 11:00:00 (GMT), 23 Nov 2006. Trace data from each sample are shown in Fig. 3.8. A total of 9 stations from the Mt. Etna network were active during this time; these were the stations in red in Fig. 3.1, plus station EPLC. The subband clustering for each time sample is shown in Fig. 3.9a and 3.9b. By the method described above, 6 of the recovered signals from these samples are unique. Thus, it is once again relatively simple to analyze each unique recovered signal in detail. These recovered signals will be named using the convention $\mathbf{P}^{0}$. Details of these recovered signals (energy, polarization, nominal passbands, etc.) are given in Table 3.2.

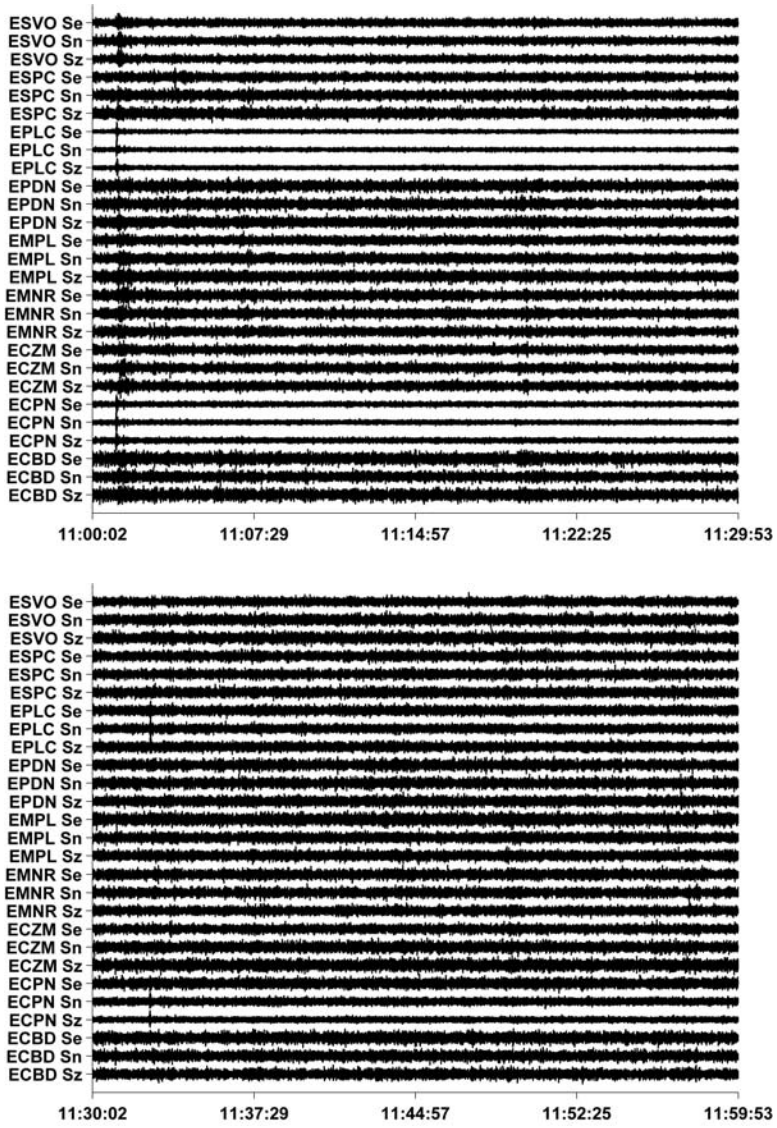

Figure 3.8. Amplitude-normalized seismic trace data for two half-hour data samples recorded during the 23-24 Nov 2006 paroxysmal lava flows. **a.** (Top) Trace data for the half-hour period beginning 24 Nov 2006, 11:00 GMT. **b.** (Bottom) Trace data for the half-hour period beginning 24 Nov 2006, 11:30 GMT.

It is apparent that recovered signal $\mathbf{P}^{(1)}$, similar to $\mathbf{A}^{(1)}$, contains incoherent information that is most energetic at station ECPN, the station nearest to the active vents (Fig. 3.1). This signal is formed from all subbands that lie above f = 1.76 Hz, but now includes frequency content at 0.19-0.39 Hz. The inclusion of these low frequencies is significant, as it suggests a persistent VLP signal with a dominant period of 2.5-5s was present during the paroxysm. From Table 3.1, any such VLP signal must be relatively weak in comparison to the background tremor, as its seismic energy is two orders of magnitude less. However, its presence is nonetheless noteworthy, as it suggests that a weak, shallow VLP signal was elicited in response to the paroxysmal lava flows.

Tremor centroid locations of signal $\mathbf{P}^{(1)}$ are identical to those of signal $\mathbf{A}^{(1)}$ (Fig. 3.5). Thus we conclude that there is no change in the location or properties of the background tremor during the paroxysm. This favors the interpretation, previously supported by INGV locations, that the source of the background tremor is largely decoupled from whatever physical process drove the 23-24 Nov 2006 paroxysm.

Signal $\mathbf{P}^{(2)}$ (Fig. 3.10) includes subbands $\boldsymbol{W}_{7,2}$ (0.39-0.59 Hz) in both samples from the paroxysm. However, from the analysis above, this cannot be the same signal as $\mathbf{A}^{(3)}$ (or $\mathbf{A}^{(4)}$). There are two reasons why we claim this signal is unique. First, while $\mathbf{A}^{(3)}$ is detectible above the background noise, even with only 8 stations included in the *SDR* analysis, signal $\mathbf{P}^{(2)}$ is not. Inspection of Table 3.1

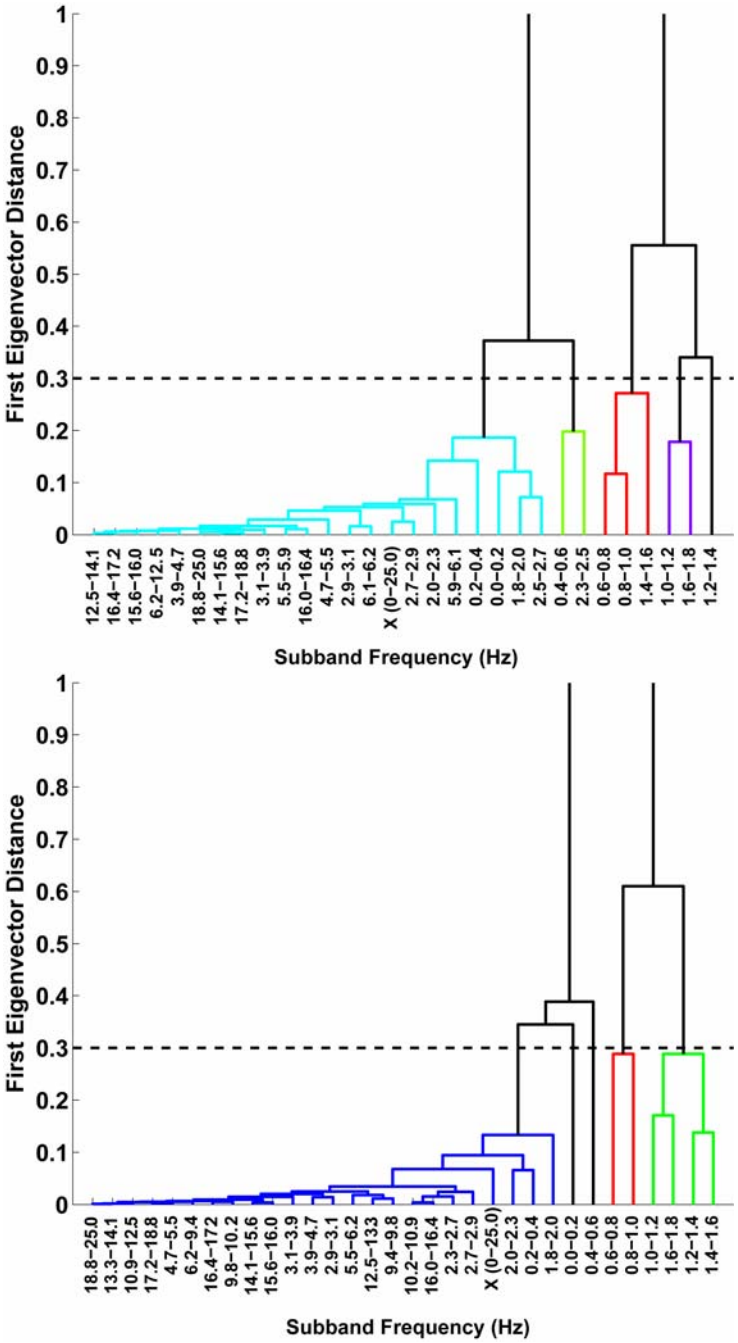

Figure 3.9. Decomposition of the paroxysmal tremor using the *SDR* algorithm. **a.** (Top) Dendrogram for the sample beginning 24 Nov 2006, 11:00 GMT, showing subband clustering. **b.** (Bottom) Dendrogram for the sample beginning 24 Nov 2006, 11:30 GMT. In both figures, node denoted with "X (0-25.0)" denotes the input data. Horizontal dashed lines indicate distance threshold $\delta = 0.3$ for clustering of principal components eigenvectors.

reveals that this is because $\mathbf{P}^{(2)}$ contains an order of magnitude less seismic energy than $\mathbf{A}^{(3)}$. Second, $\mathbf{P}^{(2)}$ is a quasi-continuous signal, rather than a series of discrete pulses (Fig 10a). Thus, if our interpretations of $\mathbf{A}^{(3)}$ and $\mathbf{A}^{(4)}$ are correct, the discrete LF events preceding the paroxysmal phase ceased sometime before the beginning of this data sample, and were replaced with energy generated by a different seismic source.The notion that this signal changes merits further discussion, as it has implications for the source of these LF signals. If we follow the interpretation of Chouet (1996) for the discrete LF events, then we must also conclude that the pulses of fresh magma had effectively shut off by this point in the paroxysm. Because $\mathbf{P}^{(2)}$ is quasi-continuous, the new signal at these frequencies could represent a seismic response to magma injection (or retreat) at a steady flow rate. Thus, $\mathbf{P}^{(2)}$ could represent a persistent LF signal generated by a constant flow of degassed magma, such as convection in a conduit.

The relationship of other low-frequency signals to the paroxysm is less clear. For example, signal $\mathbf{P}^{(3)}$ is formed from subbands $\boldsymbol{W}_{7,3}$, $\boldsymbol{W}_{7,4}$, and $\boldsymbol{W}_{7,6}$, (0.59-0.98 Hz and 1.37-1.56 Hz), and is identical to signal $\mathbf{A}^{(6)}$. Signal $\mathbf{P}^{(5)}$ appears identical to signal $\mathbf{A}^{(7)}$. Inspection of Table 3.2 reveals that $\mathbf{A}^{(6)}$ lies within $\delta = 0.3$ of the "axis" of station EPDN in the 9-dimensional space formed by the *Z'* component of each subband. Thus, while the transients at station EPDN are more energetic during the paroxysm at frequencies 0.59-0.98 Hz, there is no easily discernible relationship between this signal and the paroxysm.

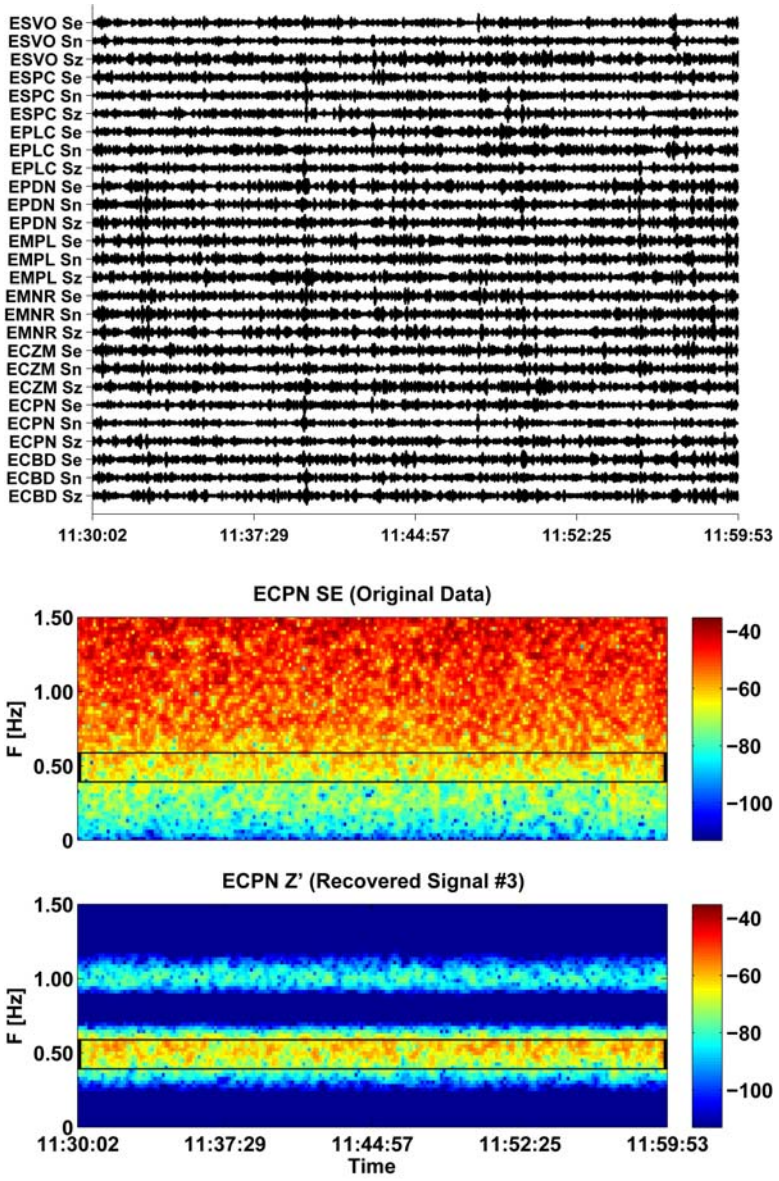

Figure 3.10. Recovered signal $\mathbf{P}^{(2)}$. **a.** (Top) Amplitude-normalized trace data for recovered signal $\mathbf{P}^{(2)}$ beginning at 11:30 GMT, 24 Nov 2006. **b.** (Bottom) Spectrogram of the input *E*-component data at station ECPN (top) and the *Z′* component (bottom) of recovered signal $\mathbf{P}^{(2)}$ at ECPN. Color scaling is in dB. Color scaling of input data is computed from ground velocity.

Signal $\mathbf{P}^{(4)}$, formed from subbands $\boldsymbol{W}_{7,5}$ and $\boldsymbol{W}_{7,8}$, (0.98-1.17 Hz and 1.56-1.76 Hz) is qualitatively similar to $\mathbf{P}^{(3)}$. It colocates to recovered signal $\mathbf{A}^{(5)}$ (Fig. 3.5) and χ^2 contours do not overlap INGV locations of background tremor at the 90% level. We conclude from *SDR* and location that signal $\mathbf{P}^{(4)}$ is different from $\mathbf{A}^{(5)}$ and different from the background tremor. But, much like $\mathbf{A}^{(4)}$, its relationship to volcanic activity cannot be determined by this method. Similarly, $\mathbf{P}^{(6)}$, formed from subbands $\boldsymbol{W}_{7,3}$ and $\boldsymbol{W}_{7,4}$ (0.58-0.98 Hz), is only present in the second paroxysmal sample, and cannot otherwise be constrained.

Post-Paroxysmal Signals

Unfortunately, due to the loss of summit station ECPN, recovery of post-paroxysmal signals is almost impossible. In most post-paroxysmal samples, as exemplified by Fig. 3.11, only two signals can be recovered: low-frequency energy, which is most energetic at station EPDN, and high-frequency energy, which is most energetic at station EPLC. The recovered signals are extremely static throughout the post-paroxysmal period, with the first recovered signal nearly always corresponding to frequencies $f \leq 6.25$ Hz, and the second nearly always corresponding to frequencies $f > 6.25$ Hz. The persistence of these signals is shown in Fig. 3.12; note that only a handful of transients are present in the data, and most of these occur in the sample beginning at 23:00 GMT, 24 Nov 2006. Location of the persistent recovered signal (i.e. the signal that is most energetic at EPDN) is possible, but locations are shifted uniformly 3 km to the NW of the INGV locations and 1-2 km

N of our pre- and paroxysmal locations (Fig. 3.13). Note, however, that χ^2 contours only slightly overlap those of pre-paroxysmal and paroxysmal background tremor, providing the first evidence that the background tremor changed as a result of the unrest of 23-24 Nov 2006. However, details about these changes are beyond the ability of *SDR* to resolve.

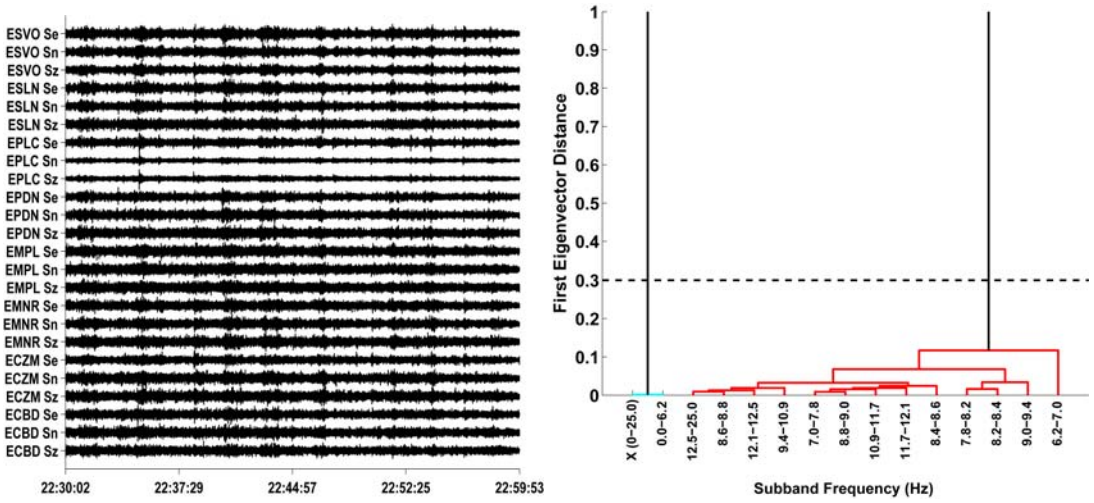

Figure 3.11. Amplitude-normalized seismic trace data and subband decomposition of an example half-hour data sample recorded after the 23-24 Nov 2006 paroxysmal lava flows. Sample shown begins at 22:00 GMT. **a.** (Left) Trace data for the half-hour period beginning 24 Nov 2006, 20:00 GMT. **b.** (Right) Dendrogram for the same sample, showing subband clustering. In both figures, node denoted with "X (0-25.0)" denotes the input data. Horizontal dashed lines indicate distance threshold δ = 0.3 for clustering of principal components eigenvectors.

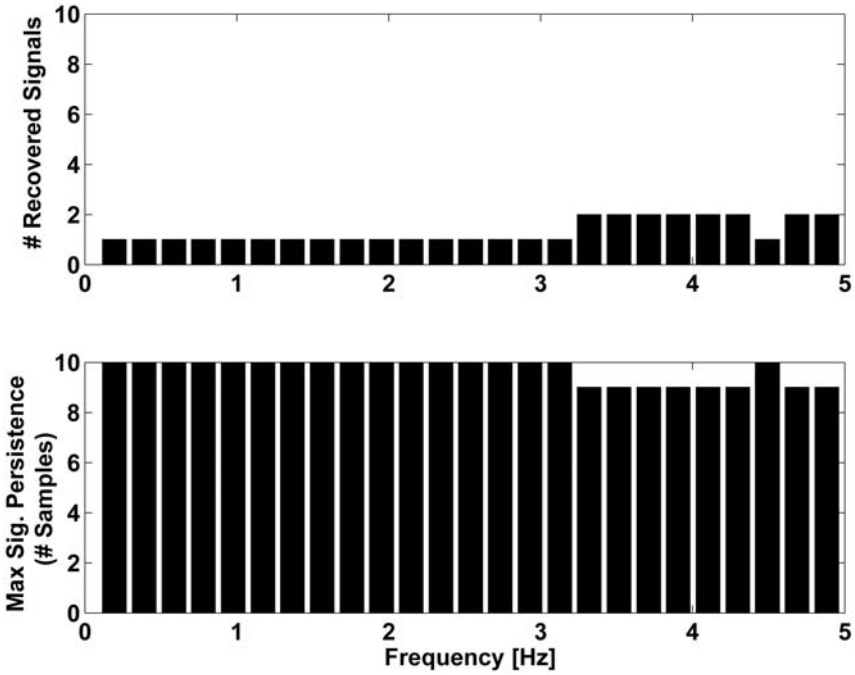

Figure 3.12. Signal persistence of the post-paroxysmal tremor. The frequency spectrum is sorted into bins of approx 0.19 Hz width. The upper plot shows the number of recovered signals with energy in each frequency bin. A single recovered signal indicates that one signal persists in a frequency bin during all 10 sample time periods. The lower plot shows the maximum number of samples in which a single signal persists in each frequency bin.

Interpretations and Conclusions

We can now suggest a rough conceptual model that explains some of the low-frequency signals recorded on 23-24 Nov 2006. First, following the interpretation of Patanè et al. (2008), we interpret the discrete LP events that form signals $\mathbf{A}^{(3)}$ and $\mathbf{A}^{(4)}$ as the result of choked flow in a conduit (cf. Chouet 1996) that feeds the upper magma chamber(s) of Mt. Etna. Thus this signal could result from gas-rich magma propagating into the lower of the two dike-like bodies detected by Patanè et al. (2008). The change in signal content of these frequencies during the

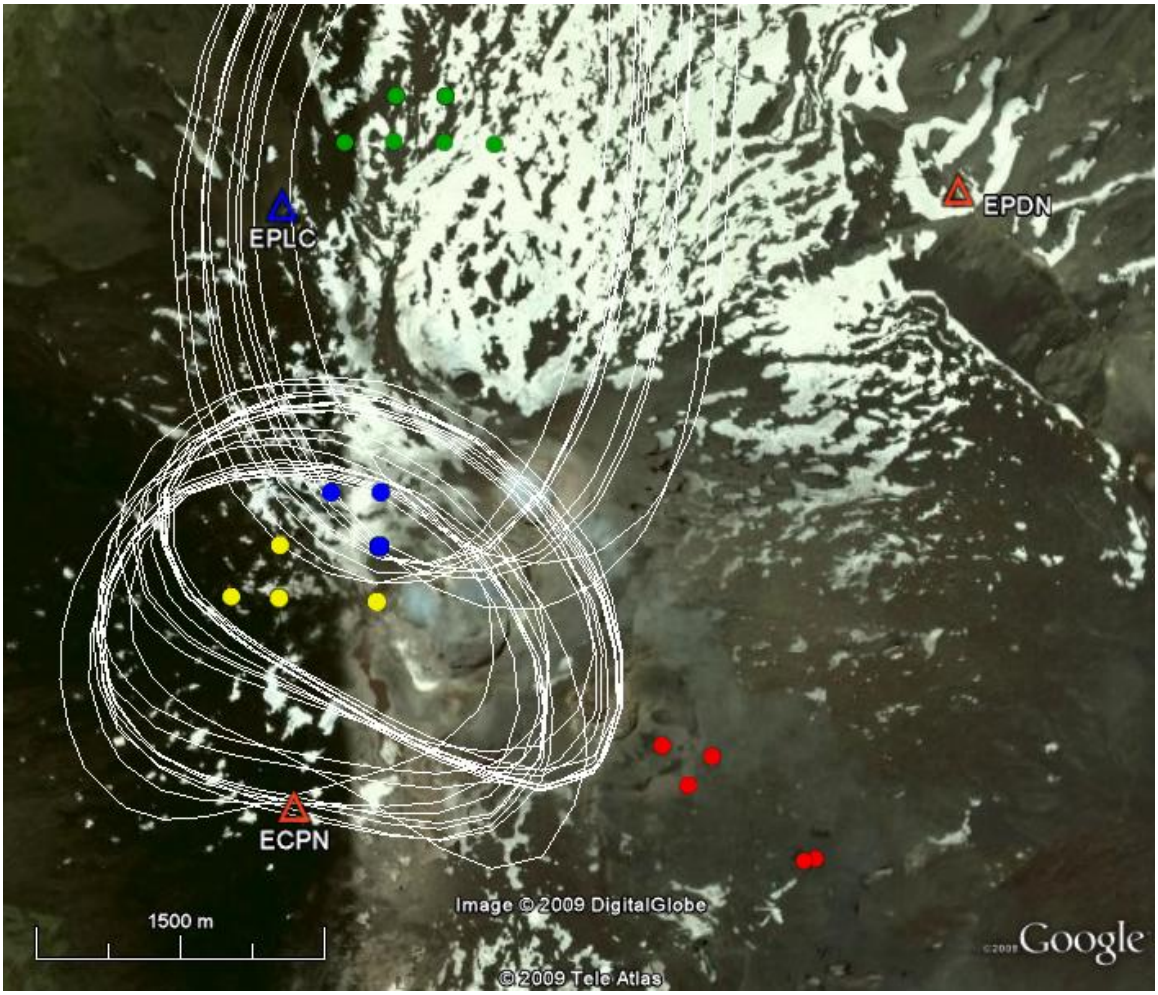

Figure 3.13 Locations of the recovered background tremor signal that postdates the 23-24 Nov 2006 paroxysmal lava flows (green circles) are compared to locations of the background tremor during (yellow circles) and before (blue circles) the paroxysm. Solid lines indicate 90% confidence contours of χ^2 misfit. INGV locations of background tremor during and after the paroxysm, computed by the method of Patanè et al. (2008), are indicated with red circles.

paroxysm supports this hypothesis, as the paroxysmal phase ended shortly after the time window analyzed. Thus, if an injection of gas-rich magma drove the paroxysmal lava flows, it would have stopped by 11:00 GMT on 24 Nov 2006. Furthermore, the signal $\mathbf{A}^{(5)}$ could merely be the response of another part of the

conduit system to the magma injection. The signal $\mathbf{P}^{(2)}$, which shares a nominal passband with signal $\mathbf{A}^{(3)}$, might correspond to resonance of another conduit, elsewhere in the magmatic system of Mt. Etna, in response to magma with similar properties propagating through it; the quasi-continuous appearance of signal $\mathbf{P}^{(2)}$ suggests that it originates in response to a nearly constant flow rate.

Based on our analysis, we can interpret the background tremor signal at Mt. Etna in the following way. First, we note that background tremor is driven by a source process that changes little before or during the paroxysm, and experiences changes only after the paroxysm. The suggestion of Patanè et al (2008) that this tremor is related to propagation of magma through a shallow dike system is one possible explanation, but the lack of change during the paroxysm suggests that this resonance is not closely connected to a central conduit. Instead, we suggest that the shallow dike system at Mt. Etna could extend radially outward from a central conduit, and that tremor might be generated as magma feeds into these outer dikes. This could explain why the tremor centroid did not change until after the paroxysm ended, as there would be a significant lag time in the outward propagation of the gas-rich, hot magma that generated LF signals $\mathbf{A}^{(3)}$ and $\mathbf{A}^{(4)}$.

Such an explanation for the background tremor is consistent with endogenous growth models to explain persistently active volcanic systems (Francis et al. 1993); here the "choke points" where tremor is generated, following the model of Chouet (1996), would be the base of new dikes that open as new magma intrudes. Such an explanation would also be consistent with the rarity of VT seismicity

(Patanè et al. 2008). Such a disconnection of background tremor from changes in eruptive behavior is roughly similar to persistent signals seen elsewhere, notably at Erta 'Ale, Ethiopia (Chapter II). Thus, it may be generally true that not all parts of continuous volcanic tremor respond immediately, or in any diagnostic way, to injection of gas-rich magma that drives volcanic unrest, and that secondary signals recoverable via methods such as *SDR* could provide far more information and warnings about the potential for unrest.

Table 4.1. Recovered signals from two half-hour samples of pre-paroxysmal data. Signal names are designated $\mathbf{A}^{(n)}$. Times are given in formal MM/DD HH:MM. All times are GMT. Values for principal eigenvectors ($v_{j,n,1}$), energy (En), azimuth (Az), incidence angle (In), rectilinearity (Rc), and planarity (Pl) are sorted in columns according to station. Az and In are in degrees. Wavelet packets are designated $\boldsymbol{W_{j,n}}$ and nominal passbands f_{min}-f_{max} for each $\boldsymbol{W_{j,n}}$ are given in Hz. Cost functional M($\boldsymbol{W}$) is renormalized (multiplied by normalized bandwidth) to assume values $0 \le M(\boldsymbol{W}) < 9$. Spectral leakage for each subband is tabulated in the form $\log_{10}(E_{out}/E_{in})$, i.e. the base 10 logarithm of energy outside the passband to energy inside the passband. Relative lags of each subband at each station are given in seconds for subbands whose wavelet cross-correlations are well constrained.

Signal	*Time*	*Sta*	*ECBD*	*ECPN*	*ECZM*	*EMNR*	*EMPL*	*EPDN*	*ESLN*	*ESPC*	*ESVO*
$A^{(1)}$	11/23 11:00										
$W_{4,1}$		$v_{4,1}$	0.00	1.00	0.00	-0.00	-0.01	0.03	0.01	0.00	0.02
f_{min}-f_{max} (Hz)	1.56-3.12	En	2.3e-07	1.8e-05	1.2e-07	7.4e-07	3.2e-07	9.6e-06	3.1e-07	2.8e-07	3.3e-06
M($W_{4,1}$)	0.135	Az	111.37	-113.17	176.92	91.92	-40.67	-79.34	118.60	3.09	-3.41
$\log_{10}(E_{out}/E_{in})$	-0.000	In	87.00	84.33	89.13	89.22	84.48	88.41	86.20	75.71	88.70
		Rc	0.53	0.70	0.58	0.57	0.51	0.65	0.59	0.39	0.62
		Pl	0.68	0.86	0.64	0.76	0.73	0.82	0.53	0.56	0.77
$W_{6,8}$		$v_{6,8}$	-0.00	1.00	0.00	0.01	-0.00	0.05	-0.00	0.00	0.01
f_{min}-f_{max} (Hz)	3.12-3.52	En	2.1e-08	5.3e-06	1.3e-08	8.2e-08	4.1e-08	7.4e-07	2e-08	2.6e-08	3.6e-07
M($W_{6,8}$)	0.111	Lag	-0.50	-3.02	2.62	1.36	0.96	-1.84	1.28	-1.18	0.34
$\log_{10}(E_{out}/E_{in})$	-0.355	Az	94.67	-129.45	169.97	102.46	14.41	89.15	-61.21	172.67	-174.47
		In	88.47	85.88	84.24	88.38	85.77	82.43	82.36	10.79	86.31
		Rc	0.63	0.71	0.58	0.63	0.54	0.70	0.50	0.27	0.65
		Pl	0.65	0.83	0.53	0.79	0.76	0.66	0.50	0.31	0.72
$W_{6,9}$		$v_{6,9}$	-0.00	1.00	0.00	0.01	0.00	0.03	-0.00	-0.00	0.01
f_{min}-f_{max} (Hz)	3.52-3.91	En	9.5e-09	3.8e-06	7e-09	3.9e-08	3.4e-08	5.4e-07	1.6e-08	2e-08	2.2e-07
M($W_{6,9}$)	0.131	Lag	2.44	-1.52	1.92	0.60	-0.30	-0.78	-1.92	-1.74	1.28
$\log_{10}(E_{out}/E_{in})$	-0.336	Az	78.14	-116.21	179.98	101.89	3.77	-102.17	115.16	-19.52	8.42
		In	84.95	89.51	80.13	86.24	87.44	85.51	80.41	8.47	85.15
		Rc	0.43	0.82	0.55	0.60	0.61	0.60	0.56	0.51	0.64
		Pl	0.65	0.87	0.55	0.75	0.71	0.57	0.62	0.39	0.80

Table 4.1. continued

Signal	*Time*	*Sta*	*ECBD*	*ECPN*	*ECZM*	*EMNR*	*EMPL*	*EPDN*	*ESLN*	*ESPC*	*ESVO*
$W_{5,5}$		$v_{5,5}$	0.00	1.00	-0.00	0.00	0.00	0.03	-0.00	-0.00	0.02
f_{min}-f_{max} (Hz)	3.91-4.69	En	7.1e-09	7.6e-06	4.9e-09	4.2e-08	5.5e-08	6.4e-07	1.3e-08	1.2e-08	2.5e-07
M($W_{5,5}$)	0.145	Lag	1.64	-2.62	0.26	2.14	-0.50	-0.90	-0.56	0.98	-0.44
$\log_{10}(E_{out}/E_{in})$	-0.000	Az	101.33	-120.23	167.15	105.65	-15.59	-80.12	-56.43	76.29	9.60
		In	83.37	86.09	78.37	86.15	83.59	89.93	83.38	33.29	83.16
		Rc	0.38	0.82	0.42	0.47	0.66	0.54	0.42	0.19	0.61
		Pl	0.63	0.85	0.37	0.70	0.71	0.50	0.58	0.14	0.83
$W_{6,12}$		$v_{6,12}$	-0.00	-1.00	-0.00	-0.00	0.00	0.00	0.01	-0.00	0.00
f_{min}-f_{max} (Hz)	4.69-5.08	En	2.2e-09	1.8e-06	8.6e-10	1.5e-08	1.2e-08	1.6e-07	4.6e-09	4.7e-09	6.1e-08
M($W_{6,12}$)	0.115	Lag	1.34	-2.74	1.76	0.20	0.60	-1.52	-0.42	-1.32	2.10
$\log_{10}(E_{out}/E_{in})$	-0.128	Az	85.19	-146.61	162.21	85.91	-22.38	99.84	123.96	-75.18	97.82
		In	88.20	84.22	70.36	88.00	79.68	82.76	79.21	83.83	86.19
		Rc	0.48	0.62	0.36	0.56	0.43	0.49	0.46	0.44	0.56
		Pl	0.68	0.75	0.36	0.67	0.52	0.40	0.73	0.43	0.81
$W_{7,26}$		$v_{7,26}$	-0.00	1.00	-0.00	-0.01	-0.00	0.08	-0.01	0.01	0.02
f_{min}-f_{max} (Hz)	5.08-5.27	En	8.6e-10	7.6e-07	2.3e-10	6.7e-09	4.4e-09	5.4e-08	1.2e-09	1.7e-09	2e-08
M($W_{7,26}$)	0.098	Lag	-1.02	-2.46	3.48	-0.86	3.36	-0.70	-1.86	-1.12	1.18
$\log_{10}(E_{out}/E_{in})$	-0.218	Az	144.93	-135.26	-26.11	-97.39	-159.39	114.01	103.64	37.84	108.05
		In	81.92	73.01	62.03	80.22	74.29	80.38	25.93	55.66	86.17
		Rc	0.56	0.69	0.36	0.67	0.44	0.55	0.50	0.36	0.58
		Pl	0.61	0.73	0.46	0.62	0.45	0.49	0.67	0.36	0.80
$W_{7,27}$		$v_{7,27}$	0.00	-1.00	-0.00	0.00	-0.01	0.02	0.00	-0.00	0.03
f_{min}-f_{max} (Hz)	5.27-5.47	En	5.1e-10	5.7e-07	2.2e-10	3.3e-09	2.8e-09	5.3e-08	9.6e-10	1.6e-09	1.3e-08
M($W_{7,27}$)	0.102	Lag	0.78	-1.68	1.92	-1.44	2.62	-2.38	-0.14	-0.86	1.20
$\log_{10}(E_{out}/E_{in})$	-0.127	Az	100.91	-131.39	-22.95	82.93	-137.12	-64.95	118.25	104.24	44.48
		In	85.44	86.90	71.78	75.34	54.48	79.26	87.90	84.39	77.56
		Rc	0.50	0.66	0.61	0.43	0.31	0.65	0.57	0.49	0.53
		Pl	0.59	0.75	0.53	0.52	0.22	0.65	0.69	0.50	0.80

Table 4.1. continued

Signal	*Time*	*Sta*	*ECBD*	*ECPN*	*ECZM*	*EMNR*	*EMPL*	*EPDN*	*ESLN*	*ESPC*	*ESVO*
$W_{7,28}$		$v_{7,28}$	-0.00	1.00	-0.00	0.00	0.01	0.02	-0.00	-0.00	0.00
f_{min}-f_{max} (Hz)	5.47-5.66	En	4.8e-10	4.6e-07	1.4e-10	2.5e-09	3e-09	3.6e-08	8.1e-10	1e-09	8.8e-09
M($W_{7,28}$)	0.077	Lag	0.96	-2.04	0.86	0.52	2.80	-1.64	1.58	-1.74	-1.30
$\log_{10}(E_{out}/E_{in})$	-0.063	Az	74.48	-159.00	-17.63	75.99	-138.13	-65.14	119.85	-49.39	-14.32
		In	88.09	78.05	72.65	76.00	71.01	72.67	75.91	88.71	79.44
		Rc	0.58	0.54	0.49	0.51	0.44	0.58	0.57	0.29	0.53
		Pl	0.69	0.70	0.50	0.58	0.34	0.57	0.69	0.43	0.67
$W_{7,29}$		$v_{7,29}$	0.00	-1.00	-0.00	-0.00	0.00	-0.05	-0.00	-0.00	0.00
f_{min}-f_{max} (Hz)	5.66-5.86	En	3.8e-10	4.5e-07	1.1e-10	1.8e-09	2.8e-09	3.2e-08	5.4e-10	1.1e-09	5.3e-09
M($W_{7,29}$)	0.079	Lag	1.78	-2.46	2.64	-0.56	1.66	-2.26	0.06	-1.32	0.44
$\log_{10}(E_{out}/E_{in})$	-0.000	Az	-103.65	-176.16	-143.76	72.23	-124.96	-67.48	122.50	-167.57	19.26
		In	88.17	81.08	8.75	77.43	74.71	69.43	35.54	66.67	82.48
		Rc	0.59	0.63	0.42	0.50	0.53	0.58	0.47	0.43	0.34
		Pl	0.85	0.64	0.57	0.59	0.47	0.54	0.64	0.57	0.52
$W_{7,30}$		$v_{7,30}$	0.00	-1.00	0.00	-0.00	-0.00	-0.05	-0.00	-0.00	0.01
f_{min}-f_{max} (Hz)	5.86-6.05	En	3.7e-10	4.2e-07	8.4e-11	1.6e-09	2.5e-09	3.2e-08	6.5e-10	1.3e-09	5.5e-09
M($W_{7,30}$)	0.059	Lag	1.78	-2.34	-0.20	3.28	0.22	-1.96	0.70	-2.56	1.08
$\log_{10}(E_{out}/E_{in})$	-0.000	Az	-108.45	-160.60	152.14	45.05	-107.83	-64.34	122.00	157.85	-131.45
		In	88.00	87.88	20.35	77.59	78.43	59.13	55.44	84.57	88.90
		Rc	0.65	0.58	0.40	0.44	0.56	0.67	0.64	0.63	0.44
		Pl	0.84	0.81	0.46	0.65	0.52	0.63	0.81	0.57	0.64
$W_{7,31}$		$v_{7,31}$	-0.00	1.00	-0.00	-0.00	-0.00	-0.02	-0.00	0.00	0.01
f_{min}-f_{max} (Hz)	6.05-6.25	En	3.8e-10	5.7e-07	6.5e-11	2.5e-09	2.1e-09	3.1e-08	5e-10	4.8e-10	6.7e-09
M($W_{7,31}$)	0.129	Lag	0.74	-3.14	0.96	0.84	1.20	0.34	0.62	-0.94	-0.62
$\log_{10}(E_{out}/E_{in})$	-0.000	Az	-134.90	139.41	143.67	77.04	-114.79	-78.60	116.85	167.19	-8.07
		In	80.53	87.59	51.53	89.11	63.23	84.59	59.54	77.55	70.91
		Rc	0.59	0.68	0.23	0.62	0.53	0.62	0.50	0.33	0.57
		Pl	0.85	0.79	0.32	0.62	0.54	0.68	0.84	0.45	0.68

Table 4.1. continued

Signal	*Time*	*Sta*	*ECBD*	*ECPN*	*ECZM*	*EMNR*	*EMPL*	*EPDN*	*ESLN*	*ESPC*	*ESVO*
$W_{3,2}$		$v_{3,2}$	0.00	1.00	-0.00	0.00	-0.00	-0.00	-0.00	-0.00	0.00
f_{min}-f_{max} (Hz)	6.25-9.38	En	3.4e-09	3.4e-06	6.3e-10	2e-08	1.4e-08	1.7e-07	4.7e-09	6.8e-09	4.9e-08
M($W_{3,2}$)	0.246	Az	86.76	175.87	163.36	-106.80	-120.37	-75.85	118.77	-167.47	-12.47
$\log_{10}(E_{out}/E_{in})$	-0.000	In	89.67	83.96	86.33	88.76	58.39	74.58	45.73	79.15	75.62
		Rc	0.50	0.57	0.24	0.45	0.33	0.44	0.52	0.35	0.45
		Pl	0.79	0.74	0.39	0.57	0.35	0.56	0.75	0.40	0.68
$W_{3,3}$		$v_{3,3}$	0.00	-1.00	-0.00	-0.00	-0.00	-0.00	-0.00	0.00	0.00
f_{min}-f_{max} (Hz)	9.38-12.50	En	3.1e-09	4.6e-07	1.1e-10	5.2e-09	2e-09	1.1e-08	4e-10	1.4e-09	4.3e-09
M($W_{3,3}$)	0.230	Az	143.46	170.23	171.62	-86.09	-152.07	-82.36	109.34	161.43	-39.18
$\log_{10}(E_{out}/E_{in})$	-0.000	In	88.71	78.92	78.93	68.26	32.44	87.92	17.45	38.75	78.79
		Rc	0.87	0.58	0.45	0.47	0.40	0.45	0.54	0.25	0.55
		Pl	0.88	0.64	0.34	0.56	0.62	0.62	0.70	0.26	0.69
$W_{1,1}$		$v_{1,1}$	0.00	-1.00	-0.00	0.00	-0.00	-0.00	-0.00	-0.00	0.00
f_{min}-f_{max} (Hz)	12.50-25.00	En	1.2e-08	2.3e-07	5.1e-11	4.7e-09	2.4e-09	3.4e-09	3.8e-10	2.2e-09	3.8e-09
M($W_{1,1}$)	0.805	Az	155.86	175.04	175.80	-80.78	-172.02	-79.34	-13.38	26.26	-25.53
$\log_{10}(E_{out}/E_{in})$	-0.000	In	77.34	84.66	75.12	71.14	66.75	84.01	30.03	64.42	85.58
		Rc	0.71	0.57	0.29	0.35	0.43	0.46	0.46	0.29	0.67
		Pl	0.83	0.60	0.20	0.37	0.70	0.63	0.72	0.23	0.72
$A^{(1)}$	11/23 11:30										
$W_{7,3}$		$v_{7,3}$	0.00	-1.00	0.00	-0.01	-0.00	0.00	0.01	-0.02	0.01
f_{min}-f_{max} (Hz)	0.59-0.78	En	1.4e-08	7.3e-07	2.6e-08	1.5e-07	4.3e-08	5.8e-07	9.4e-08	5.3e-08	3.2e-07
M($W_{7,3}$)	0.074	Lag	2.48	-3.58	1.90	-0.24	2.56	-3.30	1.26	0.82	-1.88
$\log_{10}(E_{out}/E_{in})$	-0.213	Az	-34.96	63.77	170.11	-137.78	118.10	-125.30	-47.10	68.42	0.43
		In	83.43	82.76	88.88	83.95	88.71	87.60	89.13	82.73	85.99
		Rc	0.39	0.74	0.71	0.57	0.75	0.82	0.77	0.81	0.59
		Pl	0.57	0.88	0.78	0.87	0.86	0.90	0.80	0.85	0.72
$W_{4,1}$		$v_{4,1}$	0.00	1.00	0.00	-0.01	-0.01	0.00	0.00	0.00	0.01
f_{min}-f_{max} (Hz)	1.56-3.12	En	2.3e-07	2.4e-05	1.5e-07	8.2e-07	3.3e-07	9.4e-06	3.3e-07	2.9e-07	4.1e-06
M($W_{4,1}$)	0.196	Az	113.91	-123.92	171.82	91.93	-38.27	-77.55	119.16	7.51	-2.95
$\log_{10}(E_{out}/E_{in})$	-0.000	In	87.93	83.68	89.38	89.43	84.58	87.95	86.30	74.14	88.44
		Rc	0.51	0.67	0.54	0.58	0.49	0.64	0.58	0.39	0.63
		Pl	0.67	0.86	0.58	0.75	0.73	0.81	0.53	0.53	0.78

Table 4.1. continued

Signal	*Time*	*Sta*	*ECBD*	*ECPN*	*ECZM*	*EMNR*	*EMPL*	*EPDN*	*ESLN*	*ESPC*	*ESVO*
$W_{5,4}$		$v_{5,4}$	0.00	1.00	0.00	-0.00	0.00	0.01	0.00	-0.00	0.00
f_{min}-f_{max} (Hz)	3.12-3.91	En	3.3e-08	1.2e-05	4e-08	1.3e-07	8.1e-08	1.3e-06	3.8e-08	4.8e-08	7.6e-07
M($W_{5,4}$)	0.132	Lag	-1.82	-2.78	1.04	3.54	0.24	-1.22	-0.24	0.08	1.18
$\log_{10}(E_{out}/E_{in})$	-0.000	Az	91.32	-131.75	171.18	104.74	6.06	86.94	115.81	85.46	-174.52
		In	89.09	86.49	79.02	88.57	85.67	88.22	88.13	10.03	89.88
		Rc	0.54	0.72	0.48	0.61	0.59	0.65	0.52	0.37	0.66
		Pl	0.65	0.83	0.36	0.78	0.74	0.60	0.52	0.29	0.78
$W_{6,10}$		$v_{6,10}$	0.00	-1.00	-0.00	0.00	0.00	-0.08	0.00	-0.00	0.02
f_{min}-f_{max} (Hz)	3.91-4.30	En	4.8e-09	4.6e-06	8.9e-09	2.9e-08	3.3e-08	3.5e-07	8.3e-09	9.1e-09	1.9e-07
M($W_{6,10}$)	0.145	Lag	-0.12	-2.82	2.12	1.60	1.52	-2.96	-0.78	1.96	-0.54
$\log_{10}(E_{out}/E_{in})$	-0.000	Az	109.08	-118.02	163.82	98.96	-13.62	-83.57	123.73	63.93	-0.28
		In	83.47	85.22	70.23	89.19	85.23	83.51	87.51	25.67	83.94
		Rc	0.33	0.78	0.43	0.48	0.69	0.52	0.43	0.38	0.65
		Pl	0.60	0.83	0.42	0.74	0.76	0.56	0.55	0.30	0.82
$W_{6,11}$		$v_{6,11}$	-0.00	-1.00	0.00	0.00	0.00	0.00	-0.00	-0.00	0.02
f_{min}-f_{max} (Hz)	4.30-4.69	En	3e-09	3.3e-06	4.9e-09	1.4e-08	2.4e-08	3e-07	6.5e-09	4.7e-09	1.2e-07
M($W_{6,11}$)	0.119	Az	88.36	-118.33	-7.41	114.44	-12.55	103.11	-52.13	-107.58	22.31
$\log_{10}(E_{out}/E_{in})$	-0.000	In	84.03	83.93	24.62	86.87	80.25	82.11	69.63	76.21	81.93
		Rc	0.44	0.70	0.34	0.38	0.62	0.59	0.50	0.20	0.58
		Pl	0.63	0.77	0.45	0.67	0.67	0.50	0.67	0.29	0.86
$W_{6,12}$		$v_{6,12}$	0.00	1.00	-0.00	0.00	0.00	-0.05	-0.00	0.00	0.00
f_{min}-f_{max} (Hz)	4.69-5.08	En	2.5e-09	2.3e-06	3.8e-09	1.4e-08	1.3e-08	1.6e-07	5e-09	4.6e-09	7.8e-08
M($W_{6,12}$)	0.095	Az	89.12	-166.74	-135.80	77.36	-18.68	108.04	-52.16	-70.64	-35.97
$\log_{10}(E_{out}/E_{in})$	-0.000	In	89.61	75.39	8.20	88.67	80.62	80.06	78.75	77.14	84.08
		Rc	0.51	0.54	0.40	0.56	0.44	0.46	0.45	0.41	0.51
		Pl	0.68	0.72	0.45	0.67	0.55	0.38	0.73	0.44	0.83
$W_{6,13}$		$v_{6,13}$	0.00	1.00	-0.00	0.01	0.00	-0.03	0.00	-0.00	0.01
f_{min}-f_{max} (Hz)	5.08-5.47	En	1.3e-09	1.7e-06	3.5e-09	9.7e-09	8.1e-09	1e-07	2.4e-09	3e-09	3.5e-08
M($W_{6,13}$)	0.078	Az	124.04	-146.74	-51.94	-94.92	-152.07	-66.44	113.74	70.24	99.49
$\log_{10}(E_{out}/E_{in})$	-0.106	In	83.61	80.90	12.80	84.66	65.50	85.92	55.77	77.34	87.71
		Rc	0.50	0.67	0.54	0.60	0.42	0.58	0.47	0.29	0.41
		Pl	0.60	0.75	0.61	0.58	0.37	0.55	0.72	0.30	0.80

Table 4.1. continued

Signal	*Time*	*Sta*	*ECBD*	*ECPN*	*ECZM*	*EMNR*	*EMPL*	*EPDN*	*ESLN*	*ESPC*	*ESVO*
$W_{7,28}$		$v_{7,28}$	0.00	1.00	0.00	-0.00	0.01	0.04	0.00	0.00	0.01
f_{min}-f_{max} (Hz)	5.47-5.66	En	4.7e-10	7.2e-07	1.4e-09	2.4e-09	3.4e-09	3.7e-08	9.3e-10	9.6e-10	1.1e-08
M($W_{7,28}$)	0.084	Az	78.74	-137.46	-35.49	77.07	-145.77	-64.89	118.27	-79.28	-23.50
$\log_{10}(E_{out}/E_{in})$	-0.085	In	89.44	84.72	19.66	79.92	76.68	71.65	83.13	87.18	77.65
		Rc	0.55	0.67	0.53	0.52	0.47	0.58	0.58	0.23	0.50
		Pl	0.69	0.78	0.65	0.58	0.35	0.51	0.69	0.36	0.63
$W_{7,29}$		$v_{7,29}$	0.00	-1.00	0.00	0.00	-0.00	-0.03	-0.00	-0.00	0.01
f_{min}-f_{max} (Hz)	5.66-5.86	En	3.9e-10	6.6e-07	1.2e-09	1.9e-09	2.9e-09	3.4e-08	5.9e-10	1.1e-09	8.4e-09
M($W_{7,29}$)	0.068	Lag	3.12	-2.20	1.14	2.86	-0.54	-1.68	-1.48	-0.90	-0.34
$\log_{10}(E_{out}/E_{in})$	-0.029	Az	-106.55	-156.90	-144.11	71.99	-124.39	-67.24	121.41	170.84	5.45
		In	87.90	86.81	9.45	74.81	76.73	67.50	49.00	69.78	66.29
		Rc	0.58	0.64	0.49	0.53	0.49	0.60	0.41	0.44	0.47
		Pl	0.85	0.72	0.52	0.60	0.45	0.54	0.63	0.51	0.52
$W_{7,30}$		$v_{7,30}$	0.00	-1.00	0.00	0.00	-0.00	0.04	0.00	-0.01	0.02
f_{min}-f_{max} (Hz)	5.86-6.05	En	3.2e-10	5.2e-07	1.5e-09	1.5e-09	2.4e-09	3e-08	7.7e-10	1.1e-09	7.2e-09
M($W_{7,30}$)	0.072	Az	-111.03	32.17	-57.17	50.87	-105.54	-66.04	120.31	155.92	25.87
$\log_{10}(E_{out}/E_{in})$	-0.000	In	86.10	89.67	17.14	78.40	76.78	58.76	56.08	84.27	82.45
		Rc	0.59	0.57	0.58	0.40	0.50	0.64	0.69	0.61	0.44
		Pl	0.84	0.81	0.67	0.63	0.44	0.60	0.81	0.56	0.62
$W_{7,31}$		$v_{7,31}$	0.00	1.00	0.00	-0.01	-0.00	-0.01	0.00	-0.00	0.01
f_{min}-f_{max} (Hz)	6.05-6.25	En	3.8e-10	6.5e-07	1.3e-09	2.1e-09	2.2e-09	2.9e-08	5.5e-10	4.8e-10	8.4e-09
M($W_{7,31}$)	0.361	Az	-142.52	135.39	-68.54	69.03	-112.93	-82.50	94.69	165.15	-0.27
$\log_{10}(E_{out}/E_{in})$	-0.000	In	80.60	86.01	13.95	86.74	64.48	77.67	25.02	80.82	75.37
		Rc	0.64	0.68	0.55	0.59	0.56	0.59	0.47	0.40	0.64
		Pl	0.85	0.82	0.63	0.67	0.55	0.66	0.82	0.49	0.68
$W_{2,1}$		$v_{2,1}$	0.00	1.00	0.00	0.00	-0.00	0.00	-0.00	0.00	0.00
f_{min}-f_{max} (Hz)	6.25-12.50	En	8.7e-09	4.8e-06	3.7e-08	1.9e-08	1.5e-08	1.8e-07	5.8e-09	5.5e-09	6.5e-08
M($W_{2,1}$)	0.659	Az	140.87	177.73	-59.86	-109.33	-117.04	-76.44	117.28	173.84	-12.01
$\log_{10}(E_{out}/E_{in})$	-0.000	In	88.87	83.37	13.63	87.90	58.81	71.62	43.28	72.56	74.67
		Rc	0.73	0.56	0.49	0.43	0.32	0.43	0.50	0.31	0.49
		Pl	0.86	0.73	0.58	0.55	0.36	0.56	0.74	0.34	0.68

Table 4.1. continued

Signal	*Time*	*Sta*	*ECBD*	*ECPN*	*ECZM*	*EMNR*	*EMPL*	*EPDN*	*ESLN*	*ESPC*	*ESVO*
$W_{1,1}$		$v_{1,1}$	0.00	-1.00	0.00	0.00	-0.00	-0.00	-0.00	0.00	0.00
f_{min}-f_{max} (Hz)	12.50-25.00	En	2.8e-08	2.5e-07	4.7e-08	4e-09	9.4e-10	3.4e-09	8.7e-10	1.7e-10	3.8e-09
M($W_{1,1}$)	1.742	Az	164.48	173.98	-179.95	-108.99	-153.16	-79.04	-26.40	-150.66	-19.74
$\log_{10}(E_{out}/E_{in})$	-0.190	In	70.39	84.47	32.54	68.69	55.65	81.31	50.57	67.31	86.99
		Rc	0.70	0.56	0.37	0.26	0.46	0.47	0.52	0.29	0.77
		Pl	0.85	0.60	0.30	0.40	0.64	0.64	0.74	0.30	0.76
$A^{(2)}$	11/23 11:00										
$W_{6,0}$		$v_{6,0}$	-0.01	-0.13	-0.02	0.12	0.05	0.02	0.08	-0.03	0.98
f_{min}-f_{max} (Hz)	0.00-0.39	En	4.2e-08	9.9e-08	4.8e-08	2.3e-07	2.3e-08	7.3e-08	4.4e-08	1.4e-08	4.1e-07
M($W_{6,0}$)	1.326	Az	-31.95	55.07	-21.60	-55.29	121.95	-169.20	132.42	-149.50	8.08
$\log_{10}(E_{out}/E_{in})$	-1.225	In	70.31	77.15	59.83	87.32	67.00	86.85	68.09	85.80	46.54
		Rc	0.48	0.65	0.31	0.46	0.43	0.51	0.62	0.44	0.46
		Pl	0.44	0.75	0.44	0.37	0.52	0.80	0.61	0.76	0.36
$A^{(2)}$	11/23 11:30										
$W_{6,0}$		$v_{6,0}$	-0.02	-0.14	-0.04	-0.02	0.06	0.04	0.05	-0.03	0.98
f_{min}-f_{max} (Hz)	0.00-0.39	En	3.4e-08	8.4e-08	4.4e-08	2.1e-07	2.1e-08	8.6e-08	3.5e-08	1.4e-08	3.7e-07
M($W_{6,0}$)	1.375	Az	-24.97	47.37	-37.38	129.61	104.23	-162.62	137.46	-147.23	-1.71
$\log_{10}(E_{out}/E_{in})$	-1.248	In	77.78	76.83	83.40	89.84	56.23	87.17	68.41	87.38	50.40
		Rc	0.40	0.62	0.14	0.43	0.36	0.58	0.50	0.53	0.46
		Pl	0.44	0.75	0.23	0.37	0.49	0.82	0.59	0.71	0.42
$A^{(3)}$	11/23 11:00										
$W_{7,2}$		$v_{7,2}$	-0.01	-0.90	-0.01	0.03	0.01	-0.42	-0.01	0.00	0.15
f_{min}-f_{max} (Hz)	0.39-0.59	En	8.8e-09	1.9e-07	9.8e-09	5.8e-08	1.3e-08	1.1e-07	2.3e-08	1.6e-08	1.8e-07
M($W_{7,2}$)	1.951	Lag	2.20	-3.16	1.80	-0.34	2.14	-3.46	1.28	0.82	-1.26
$\log_{10}(E_{out}/E_{in})$	-0.391	Az	148.73	63.66	171.43	-142.46	115.22	-155.52	-47.29	-117.44	-163.45
		In	89.47	79.36	75.59	87.18	89.66	87.00	88.59	86.87	88.76
		Rc	0.54	0.78	0.52	0.41	0.79	0.71	0.75	0.72	0.72
		Pl	0.77	0.87	0.40	0.67	0.85	0.92	0.84	0.83	0.69

Table 4.1. continued

Signal	*Time*	*Sta*	*ECBD*	*ECPN*	*ECZM*	*EMNR*	*EMPL*	*EPDN*	*ESLN*	*ESPC*	*ESVO*
$A^{(4)}$	11/23 11:30										
$W_{7,2}$		$v_{7,2}$	-0.02	0.95	0.01	-0.02	0.03	-0.11	-0.05	-0.01	0.28
f_{min}-f_{max} (Hz)	0.39-0.59	En	8.2e-09	1.9e-07	9.2e-09	6.5e-08	1.5e-08	1e-07	2.2e-08	1.6e-08	1.8e-07
$M(W_{7,2})$	2.090	Az	-34.29	69.35	-177.94	40.49	115.23	-145.46	134.96	-116.23	-158.40
$\log_{10}(E_{out}/E_{in})$	-0.410	In	89.64	74.80	76.07	89.45	86.81	87.85	88.25	85.72	89.12
		Rc	0.52	0.78	0.45	0.51	0.79	0.70	0.71	0.71	0.73
		Pl	0.76	0.85	0.38	0.68	0.84	0.92	0.83	0.82	0.70
$A^{(5)}$	11/23 11:00										
$W_{7,3}$		$v_{7,3}$	-0.00	0.78	-0.01	0.01	0.00	-0.62	0.00	0.00	0.06
f_{min}-f_{max} (Hz)	0.59-0.78	En	1.4e-08	6.5e-07	2.4e-08	1.1e-07	3.8e-08	5.4e-07	8e-08	4.7e-08	2.9e-07
$M(W_{7,3})$	1.168	Az	-24.36	65.51	168.82	-20.08	117.37	-125.49	-46.62	65.71	4.25
$\log_{10}(E_{out}/E_{in})$	-0.177	In	88.38	84.38	88.11	87.16	89.64	88.78	89.54	83.50	88.53
		Rc	0.48	0.74	0.74	0.51	0.74	0.82	0.78	0.83	0.58
		Pl	0.65	0.91	0.77	0.87	0.85	0.92	0.79	0.82	0.68
$W_{7,4}$		$v_{7,4}$	-0.00	0.86	-0.00	-0.01	-0.02	-0.51	-0.05	0.02	0.04
f_{min}-f_{max} (Hz)	0.78-0.98	En	1.4e-08	1.2e-06	4.6e-08	1.9e-07	7.1e-08	8.9e-07	1.3e-07	7.2e-08	4.5e-07
$M(W_{7,4})$	1.307	Az	-21.97	57.35	164.40	-41.67	-71.77	-113.65	126.32	67.15	162.82
$\log_{10}(E_{out}/E_{in})$	-0.413	In	87.23	87.54	88.77	86.79	84.93	89.96	86.07	86.99	88.81
		Rc	0.43	0.63	0.84	0.70	0.79	0.85	0.71	0.86	0.65
		Pl	0.68	0.94	0.80	0.88	0.83	0.95	0.83	0.88	0.68
$W_{7,5}$		$v_{7,5}$	0.00	0.82	-0.01	0.06	0.01	-0.56	0.02	0.00	0.06
f_{min}-f_{max} (Hz)	0.98-1.17	En	4.4e-08	1.6e-06	3.6e-08	3e-07	1.4e-07	1.2e-06	2.3e-07	7.8e-08	7.1e-07
$M(W_{7,5})$	1.308	Lag	2.94	-2.74	0.68	4.32	1.64	-3.30	-0.22	-0.34	-2.98
$\log_{10}(E_{out}/E_{in})$	-0.489	Az	-21.00	98.00	-2.45	-100.51	-81.19	-100.38	-57.36	58.72	16.80
		In	86.15	88.15	85.81	88.65	87.96	88.10	86.02	83.64	78.97
		Rc	0.79	0.52	0.73	0.57	0.88	0.79	0.91	0.83	0.73
		Pl	0.78	0.96	0.75	0.81	0.90	0.96	0.87	0.80	0.71

Table 4.1. continued

Signal	*Time*	*Sta*	*ECBD*	*ECPN*	*ECZM*	*EMNR*	*EMPL*	*EPDN*	*ESLN*	*ESPC*	*ESVO*
$A^{(6)}$	11/23 11:00										
$W_{7,6}$		$v_{7,6}$	0.01	0.71	0.00	0.00	-0.00	0.71	-0.02	-0.01	0.01
f_{min}-f_{max} (Hz)	1.17-1.37	En	6.1e-08	2.4e-06	2.9e-08	2.4e-07	7.8e-08	2.4e-06	2e-07	7.4e-08	7.8e-07
M($W_{7,6}$)	1.144	Lag	1.46	-2.70	-1.14	4.30	1.56	-3.66	0.26	2.74	-2.82
$\log_{10}(E_{out}/E_{in})$	-0.386	Az	-16.02	-109.50	-136.20	104.40	114.09	103.19	116.16	48.23	-161.69
		In	87.92	89.57	88.48	78.68	84.73	88.66	86.75	80.11	85.70
		Rc	0.62	0.67	0.50	0.56	0.74	0.80	0.84	0.47	0.69
		Pl	0.73	0.95	0.65	0.79	0.80	0.94	0.77	0.74	0.78
$A^{(6)}$	11/23 11:30										
$W_{6,2}$		$v_{6,2}$	-0.00	0.84	0.00	-0.02	0.00	0.54	0.00	-0.00	0.05
f_{min}-f_{max} (Hz)	0.78-1.17	En	5.9e-08	2.8e-06	7.6e-08	4.3e-07	2e-07	2.1e-06	3.6e-07	1.5e-07	1.3e-06
M($W_{6,2}$)	1.293	Lag	3.40	-2.14	1.90	2.40	1.94	-3.08	-0.48	-0.86	-3.06
$\log_{10}(E_{out}/E_{in})$	-0.000	Az	-22.65	72.06	169.35	-88.64	-78.25	-102.71	-57.36	63.55	6.83
		In	87.78	87.93	89.27	87.82	86.74	89.11	89.59	84.94	85.30
		Rc	0.66	0.56	0.76	0.50	0.83	0.80	0.82	0.83	0.67
		Pl	0.72	0.94	0.77	0.81	0.87	0.95	0.83	0.83	0.70
$W_{7,6}$		$v_{7,6}$	-0.00	-0.66	-0.00	0.02	-0.02	-0.75	0.02	0.01	0.02
f_{min}-f_{max} (Hz)	1.17-1.37	En	7.2e-08	2.7e-06	3.3e-08	2.8e-07	7.8e-08	2.8e-06	2.1e-07	7.9e-08	1e-06
M($W_{7,6}$)	1.218	Lag	1.62	-2.62	0.12	2.52	1.50	-3.18	0.70	1.84	-2.52
$\log_{10}(E_{out}/E_{in})$	-0.416	Az	164.02	75.32	-151.20	104.40	115.88	105.77	115.31	58.89	-161.30
		In	89.95	89.51	88.70	78.09	85.71	88.69	84.89	81.16	85.58
		Rc	0.65	0.67	0.49	0.60	0.71	0.84	0.83	0.49	0.72
		Pl	0.74	0.95	0.67	0.78	0.80	0.95	0.77	0.75	0.79
$A^{(7)}$	11/23 11:00										
$W_{7,7}$		$v_{7,7}$	-0.00	0.11	-0.00	0.03	-0.01	-0.99	-0.00	0.00	0.08
f_{min}-f_{max} (Hz)	1.37-1.56	En	1.2e-07	2.2e-06	4.3e-08	3.3e-07	9.4e-08	4.5e-06	1.1e-07	8.1e-08	1.3e-06
M($W_{7,7}$)	0.903	Lag	1.04	-2.50	0.20	4.40	1.38	-2.76	-0.68	0.44	-1.52
$\log_{10}(E_{out}/E_{in})$	-0.245	Az	109.02	-84.79	178.79	30.40	-67.35	-96.89	131.95	27.33	-14.62
		In	81.56	83.08	84.58	77.81	85.67	87.84	85.42	70.06	85.97
		Rc	0.75	0.53	0.62	0.57	0.68	0.84	0.64	0.44	0.74
		Pl	0.73	0.90	0.73	0.77	0.71	0.87	0.62	0.76	0.76

Table 4.1. continued

Signal	*Time*	*Sta*	*ECBD*	*ECPN*	*ECZM*	*EMNR*	*EMPL*	*EPDN*	*ESLN*	*ESPC*	*ESVO*
$A^{(8)}$	11/23 11:30										
$W_{7,7}$		$v_{7,7}$	-0.01	-0.20	0.00	0.04	0.00	-0.98	-0.02	0.01	0.03
f_{min}-f_{max} (Hz)	1.37-1.56	En	1.1e-07	2.3e-06	3.9e-08	2.9e-07	9.2e-08	4.2e-06	1.1e-07	8e-08	1.2e-06
$M(W_{7,7})$	0.972	Lag	1.68	-2.74	1.00	2.06	2.06	-2.90	-0.28	0.74	-1.62
$\log_{10}(E_{out}/E_{in})$	-0.227	Az	105.86	-59.17	165.42	34.25	-64.40	-94.48	132.83	24.43	-16.01
		In	82.84	81.49	84.97	77.40	86.17	88.85	87.18	71.10	86.53
		Rc	0.73	0.52	0.60	0.52	0.67	0.83	0.61	0.43	0.75
		Pl	0.72	0.91	0.73	0.75	0.69	0.87	0.64	0.73	0.78

Table 4.2. Recovered signals from two half-hour samples of data recorded during the 24 Nov 2006 paroxysm. Signal names are designated $\mathbf{A}^{(n)}$. Times are given in formal MM/DD HH:MM. All times are fGMT. Values for principal eigenvectors ($v_{j,n,1}$), energy (En), azimuth (Az), incidence angle (In), rectilinearity (Rc), and planarity (Pl) are sorted in columns according to station. Az and In are given in degrees. Wavelet packets are designated $\boldsymbol{W_{j,n}}$ and nominal passbands f_{min}-f_{max} for each $\boldsymbol{W_{j,n}}$ are given in Hz. Cost functional M($\boldsymbol{W}$) is renormalized (multiplied by normalized bandwidth) to assume values $0 \le M(\boldsymbol{W}) < 9$. Spectral leakage for each subband is tabulated in the form $\log_{10}(E_{out}/E_{in})$, i.e. the base 10 logarithm of energy outside the passband to energy inside the passband. Relative lags of each subband at each station are given in seconds for subbands whose wavelet cross-correlations are well constrained.

Signal	*Time*	*Sta*	*ECBD*	*ECPN*	*ECZM*	*EMNR*	*EMPL*	*EPDN*	*ESLN*	*ESPC*	*ESVO*
P[1)]	11/24 11:00										
$W_{7,0}$		$v_{7,0}$	0.01	-0.97	0.03	0.01	0.01	-0.23	-0.11	0.00	0.02
f_{min}-f_{max} (Hz)	0.00-0.20	En	9.4e-10	3.7e-08	1.3e-09	7.1e-09	1.2e-09	2.1e-08	2.8e-09	4.9e-10	7.7e-09
M($W_{7,0}$)	0.119	Az	-71.63	54.91	167.01	131.22	88.03	152.78	149.21	63.96	20.71
$\log_{10}(E_{out}/E_{in})$	-0.000	In	59.46	73.28	74.68	79.94	71.32	88.22	82.78	74.30	54.55
		Rc	0.21	0.93	0.23	0.41	0.53	0.52	0.58	0.40	0.40
		Pl	0.26	0.93	0.27	0.37	0.54	0.96	0.68	0.50	0.34
$W_{7,1}$		$v_{7,1}$	0.00	0.99	-0.00	-0.03	0.01	0.11	-0.08	0.01	0.00
f_{min}-f_{max} (Hz)	0.20-0.39	En	7.8e-09	2.7e-07	7.4e-09	6.3e-08	6.8e-09	9.5e-08	5e-08	1.1e-08	7.6e-08
M($W_{7,1}$)	0.123	Az	-157.81	53.55	175.27	80.72	91.90	-143.59	50.10	-129.51	176.75
$\log_{10}(E_{out}/E_{in})$	-0.000	In	83.92	73.08	36.36	79.87	80.99	89.10	77.30	82.53	87.97
		Rc	0.60	0.91	0.45	0.48	0.67	0.80	0.70	0.73	0.50
		Pl	0.50	0.88	0.46	0.44	0.66	0.84	0.84	0.88	0.44
$W_{7,9}$		$v_{7,9}$	-0.00	0.98	-0.00	0.00	0.01	0.18	0.04	0.00	0.03
f_{min}-f_{max} (Hz)	1.76-1.95	En	3.8e-07	3e-05	2.2e-07	2e-06	7.1e-07	1.6e-05	2.8e-06	6.3e-07	6.6e-06
M($W_{7,9}$)	0.106	Az	56.19	-103.15	-8.83	-36.19	140.98	100.83	-168.84	35.30	-174.85
$\log_{10}(E_{out}/E_{in})$	-0.000	In	82.25	85.02	83.07	84.78	85.56	80.71	85.79	74.55	87.38
		Rc	0.46	0.76	0.45	0.61	0.59	0.62	0.48	0.47	0.61
		Pl	0.68	0.92	0.65	0.72	0.70	0.84	0.84	0.69	0.73

Table 4.2. continued

Signal	*Time*	*Sta*	*ECBD*	*ECPN*	*ECZM*	*EMNR*	*EMPL*	*EPDN*	*ESLN*	*ESPC*	*ESVO*
$W_{6,5}$		$v_{6,5}$	-0.00	1.00	0.01	-0.00	0.00	-0.04	-0.01	-0.00	0.03
f_{min}-f_{max} (Hz)	1.95-2.34	En	3.8e-07	4.2e-05	3e-07	1.7e-06	1.1e-06	1.2e-05	5.3e-06	6.1e-07	8.9e-06
M($W_{6,5}$)	0.132	Az	93.79	-94.88	-12.83	95.53	146.84	58.35	-88.95	49.24	-6.55
$\log_{10}(E_{out}/E_{in})$	-0.000	In	86.57	82.49	84.49	87.22	89.90	82.62	86.21	86.59	88.01
		Rc	0.46	0.63	0.58	0.59	0.61	0.37	0.62	0.48	0.66
		Pl	0.74	0.87	0.64	0.71	0.80	0.71	0.73	0.63	0.76
$W_{7,13}$		$v_{7,13}$	-0.00	-0.99	-0.00	0.00	-0.00	-0.12	-0.02	0.00	0.01
f_{min}-f_{max} (Hz)	2.54-2.73	En	8.3e-08	2.3e-05	7.8e-08	3.3e-07	1.8e-07	5.5e-06	2.1e-06	1e-07	2.2e-06
M($W_{7,13}$)	0.131	Az	-69.30	-135.72	4.76	101.86	-3.43	-111.81	-108.24	49.64	-173.81
$\log_{10}(E_{out}/E_{in})$	0.000	In	88.23	85.71	87.81	86.96	88.83	73.79	81.09	73.24	87.41
		Rc	0.35	0.67	0.67	0.67	0.50	0.75	0.68	0.29	0.62
		Pl	0.67	0.88	0.72	0.75	0.81	0.78	0.66	0.40	0.81
$W_{7,14}$		$v_{7,14}$	-0.00	-1.00	-0.00	0.00	0.00	-0.04	0.01	-0.00	0.00
f_{min}-f_{max} (Hz)	2.73-2.93	En	8.8e-08	1.6e-05	6e-08	2.6e-07	1.9e-07	3.3e-06	1.6e-06	8.2e-08	1.3e-06
M($W_{7,14}$)	0.106	Lag	1.18	-2.24	-0.12	-0.22	2.24	-1.62	-0.84	-0.54	2.18
$\log_{10}(E_{out}/E_{in})$	0.000	Az	76.70	-120.12	3.13	-54.61	4.06	-98.71	73.92	69.76	-176.76
		In	89.23	84.48	88.47	88.29	87.52	80.41	89.33	33.72	85.09
		Rc	0.66	0.60	0.63	0.54	0.63	0.71	0.61	0.40	0.52
		Pl	0.71	0.83	0.58	0.78	0.82	0.70	0.74	0.26	0.79
$W_{7,15}$		$v_{7,15}$	-0.00	1.00	-0.00	0.00	-0.00	0.03	0.03	0.01	0.03
f_{min}-f_{max} (Hz)	2.93-3.12	En	5.5e-08	1.6e-05	4.9e-08	2.1e-07	1.3e-07	1.7e-06	1e-06	7.2e-08	1.7e-06
M($W_{7,15}$)	0.089	Lag	-0.44	-2.72	0.12	0.78	2.66	-1.16	-0.64	-0.44	1.84
$\log_{10}(E_{out}/E_{in})$	-0.285	Az	-79.33	-144.78	-16.29	-82.11	-17.87	-103.14	-90.12	100.57	174.02
		In	86.30	86.84	89.96	89.20	84.64	81.57	69.51	8.38	86.19
		Rc	0.62	0.62	0.65	0.55	0.47	0.64	0.50	0.31	0.74
		Pl	0.62	0.84	0.59	0.76	0.67	0.53	0.68	0.36	0.82

Table 4.2. continued

Signal	*Time*	*Sta*	*ECBD*	*ECPN*	*ECZM*	*EMNR*	*EMPL*	*EPDN*	*ESLN*	*ESPC*	*ESVO*
$W_{5,4}$		$v_{5,4}$	-0.00	1.00	0.00	0.00	-0.00	-0.00	0.00	0.00	0.01
f_{min}-f_{max} (Hz)	3.12-3.91	En	1.5e-07	5.5e-05	1.3e-07	6.2e-07	5.8e-07	6.8e-06	4e-06	2.3e-07	4.7e-06
M($W_{5,4}$)	0.424	Az	90.04	-129.60	174.99	103.63	7.44	-101.42	-90.50	45.19	178.32
$\log_{10}(E_{out}/E_{in})$	-0.276	In	89.39	87.04	88.64	88.24	84.34	80.18	77.73	15.83	89.05
		Rc	0.52	0.67	0.58	0.57	0.62	0.61	0.49	0.41	0.68
		Pl	0.68	0.82	0.56	0.77	0.73	0.54	0.71	0.31	0.80
$W_{5,5}$		$v_{5,5}$	0.00	1.00	-0.00	-0.00	-0.00	-0.00	-0.01	-0.00	0.00
f_{min}-f_{max} (Hz)	3.91-4.69	En	4.3e-08	5.1e-05	2.8e-08	2e-07	2.8e-07	2.6e-06	1.8e-06	6.9e-08	1.5e-06
M($W_{5,5}$)	0.306	Az	86.13	-127.52	168.01	90.94	-2.42	-90.55	-103.39	77.43	-1.31
$\log_{10}(E_{out}/E_{in})$	-0.110	In	88.51	86.36	89.46	86.92	89.25	88.17	77.31	18.01	82.45
		Rc	0.52	0.77	0.43	0.45	0.64	0.56	0.46	0.25	0.58
		Pl	0.68	0.78	0.30	0.68	0.69	0.52	0.72	0.21	0.80
$W_{5,6}$		$v_{5,6}$	0.00	1.00	0.00	-0.00	0.00	-0.01	0.03	-0.00	0.00
f_{min}-f_{max} (Hz)	4.69-5.47	En	1.7e-08	2.2e-05	6.3e-09	9.6e-08	8.6e-08	9.3e-07	1.3e-06	2.7e-08	4.9e-07
M($W_{5,6}$)	0.313	Az	98.72	-131.75	160.29	-90.37	-167.50	102.27	-27.76	132.24	109.15
$\log_{10}(E_{out}/E_{in})$	-0.000	In	88.54	84.47	89.20	88.54	81.81	84.88	69.92	79.48	89.37
		Rc	0.53	0.56	0.40	0.59	0.44	0.48	0.40	0.27	0.46
		Pl	0.68	0.73	0.43	0.59	0.51	0.38	0.70	0.18	0.74
$W_{6,14}$		$v_{6,14}$	0.00	-1.00	0.00	0.00	-0.00	0.00	-0.01	0.00	0.00
f_{min}-f_{max} (Hz)	5.47-5.86	En	3.6e-09	6.9e-06	8.4e-10	1.5e-08	2.3e-08	2.2e-07	4.9e-07	7.2e-09	9.4e-08
M($W_{6,14}$)	0.123	Lag	1.26	-2.12	1.90	1.78	1.02	-0.24	-2.58	-1.54	0.54
$\log_{10}(E_{out}/E_{in})$	-0.000	Az	102.50	-164.27	-23.58	50.68	-134.82	-57.85	-42.51	163.55	-44.63
		In	89.62	80.99	37.88	75.73	69.36	71.48	74.00	75.44	76.84
		Rc	0.52	0.57	0.30	0.42	0.46	0.53	0.45	0.29	0.41
		Pl	0.78	0.71	0.50	0.57	0.45	0.53	0.74	0.37	0.51
$W_{7,30}$		$v_{7,30}$	-0.00	-1.00	-0.00	0.00	-0.01	-0.00	0.06	-0.00	0.02
f_{min}-f_{max} (Hz)	5.86-6.05	En	1.4e-09	3.3e-06	3.1e-10	5.6e-09	9.1e-09	8.4e-08	1.9e-07	3.1e-09	4e-08
M($W_{7,30}$)	0.068	Az	-130.68	-172.66	155.86	79.96	-111.68	-69.22	-26.80	-151.98	-12.39
$\log_{10}(E_{out}/E_{in})$	-0.000	In	88.09	81.60	41.26	87.37	84.16	47.03	66.77	68.39	80.88
		Rc	0.49	0.59	0.39	0.40	0.59	0.45	0.57	0.52	0.49
		Pl	0.87	0.76	0.42	0.61	0.56	0.45	0.83	0.54	0.74

Table 4.2. continued

Signal	*Time*	*Sta*	*ECBD*	*ECPN*	*ECZM*	*EMNR*	*EMPL*	*EPDN*	*ESLN*	*ESPC*	*ESVO*
$W_{7,31}$		$v_{7,31}$	-0.00	1.00	-0.00	-0.00	0.00	0.02	0.03	0.00	0.01
f_{min}-f_{max} (Hz)	6.05-6.25	En	1.2e-09	2.6e-06	3.5e-10	6.6e-09	6.2e-09	8.1e-08	2.1e-07	2.1e-09	3.6e-08
M($W_{7,31}$)	0.069	Az	-146.55	129.88	152.26	-106.99	-121.37	-95.72	-36.08	-161.04	-11.27
$\log_{10}(E_{out}/E_{in})$	-0.000	In	84.11	77.06	71.63	89.88	70.72	6.89	66.18	72.62	68.31
		Rc	0.46	0.60	0.51	0.61	0.44	0.48	0.62	0.41	0.53
		Pl	0.80	0.76	0.58	0.64	0.50	0.66	0.82	0.37	0.63
$W_{2,1}$		$v_{2,1}$	0.00	1.00	0.00	0.00	0.00	0.01	-0.01	0.00	0.00
f_{min}-f_{max} (Hz)	6.25-12.50	En	1.3e-08	2.7e-05	3.4e-09	5.4e-08	4.8e-08	5.4e-07	2.3e-06	2e-08	3e-07
M($W_{2,1}$)	1.096	Az	100.38	174.04	-20.01	-103.77	-135.36	-78.57	11.54	-173.37	-32.11
$\log_{10}(E_{out}/E_{in})$	-0.433	In	88.25	79.74	71.72	89.27	66.46	61.01	78.11	69.96	75.41
		Rc	0.49	0.54	0.23	0.42	0.36	0.33	0.58	0.34	0.49
		Pl	0.77	0.69	0.42	0.53	0.38	0.51	0.82	0.31	0.65
$W_{4,8}$		$v_{4,8}$	0.00	1.00	-0.00	-0.00	-0.00	-0.00	-0.01	0.00	0.00
f_{min}-f_{max} (Hz)	12.50-14.06	En	5.5e-10	5.1e-07	3.2e-10	6.6e-10	2.9e-10	2.8e-09	5.6e-08	2.3e-10	2.2e-09
M($W_{4,8}$)	0.946	Az	140.71	164.93	-19.77	-93.39	-99.09	-72.02	6.47	-127.52	-56.46
$\log_{10}(E_{out}/E_{in})$	-0.198	In	88.26	82.30	51.20	55.51	54.48	81.13	86.17	53.69	72.70
		Rc	0.81	0.53	0.18	0.39	0.41	0.58	0.54	0.43	0.60
		Pl	0.79	0.56	0.28	0.48	0.54	0.52	0.69	0.53	0.73
$W_{4,9}$		$v_{4,9}$	-0.00	1.00	0.00	-0.00	-0.00	-0.00	0.00	0.00	0.00
f_{min}-f_{max} (Hz)	14.06-15.62	En	3.7e-10	4.8e-07	3.1e-10	5.3e-10	2.5e-10	2.6e-09	4.5e-08	1.3e-10	1.6e-09
M($W_{4,9}$)	0.716	Az	150.33	155.46	-142.91	-54.05	-122.24	-83.02	12.68	-167.19	-36.48
$\log_{10}(E_{out}/E_{in})$	-0.000	In	87.53	84.38	70.88	43.93	40.84	80.52	86.29	71.17	78.11
		Rc	0.79	0.59	0.32	0.54	0.36	0.51	0.67	0.45	0.51
		Pl	0.81	0.66	0.30	0.54	0.49	0.61	0.78	0.33	0.69
$W_{6,40}$		$v_{6,40}$	-0.00	-1.00	-0.00	-0.00	0.00	-0.00	0.01	0.00	0.00
f_{min}-f_{max} (Hz)	15.62-16.02	En	5.7e-11	8.3e-08	8e-11	8.9e-11	5.5e-11	5.2e-10	9.7e-09	2.7e-11	3.1e-10
M($W_{6,40}$)	0.097	Az	155.26	140.52	-129.09	-73.77	-96.45	110.89	11.88	-154.17	-54.58
$\log_{10}(E_{out}/E_{in})$	-0.144	In	88.73	88.18	74.96	50.52	54.10	18.67	82.22	77.79	76.86
		Rc	0.64	0.55	0.66	0.43	0.30	0.40	0.74	0.40	0.57
		Pl	0.89	0.66	0.63	0.47	0.50	0.71	0.84	0.41	0.66

Table 4.2. continued

Signal	*Time*	*Sta*	*ECBD*	*ECPN*	*ECZM*	*EMNR*	*EMPL*	*EPDN*	*ESLN*	*ESPC*	*ESVO*
$W_{6,41}$		$v_{6,41}$	0.00	1.00	0.00	-0.00	0.00	0.00	0.01	-0.00	0.00
f_{min}-f_{max} (Hz)	16.02-16.41	En	2.7e-11	7.3e-08	1.1e-10	6.6e-11	5.7e-11	6.5e-10	6.6e-09	1.9e-11	2.4e-10
M($W_{6,41}$)	0.129	Az	-58.90	176.33	-132.62	-50.92	-137.35	123.07	24.49	-163.17	-39.78
$\log_{10}(E_{out}/E_{in})$	-0.045	In	87.86	80.94	64.35	51.57	50.35	20.42	85.93	83.33	77.83
		Rc	0.55	0.50	0.78	0.26	0.46	0.62	0.57	0.34	0.53
		Pl	0.78	0.58	0.69	0.46	0.64	0.80	0.86	0.36	0.67
$W_{5,21}$		$v_{5,21}$	-0.00	-1.00	-0.00	-0.00	0.00	0.00	0.01	0.00	0.00
f_{min}-f_{max} (Hz)	16.41-17.19	En	4.2e-11	1.1e-07	1.5e-10	8.8e-11	1.2e-10	7.5e-10	8.2e-09	3.7e-11	4.5e-10
M($W_{5,21}$)	0.130	Az	112.43	-176.52	-140.46	-9.39	-147.55	-163.91	23.41	-175.78	-32.99
$\log_{10}(E_{out}/E_{in})$	-0.000	In	87.44	88.03	65.26	66.92	55.99	3.36	85.66	75.09	73.60
		Rc	0.54	0.51	0.67	0.30	0.55	0.55	0.56	0.42	0.62
		Pl	0.82	0.61	0.56	0.43	0.66	0.68	0.82	0.46	0.67
$W_{4,11}$		$v_{4,11}$	0.00	1.00	-0.00	0.00	-0.00	-0.00	0.00	0.00	0.00
f_{min}-f_{max} (Hz)	17.19-18.75	En	8.7e-11	1.3e-07	2.1e-10	9.6e-11	1.9e-10	6.1e-10	7.4e-09	3.1e-11	4.3e-10
M($W_{4,11}$)	0.440	Az	-61.46	5.07	-147.00	81.03	-132.40	-93.55	-0.82	-152.62	-35.27
$\log_{10}(E_{out}/E_{in})$	-0.465	In	89.08	88.52	75.45	89.82	56.02	23.54	80.26	81.14	74.88
		Rc	0.79	0.68	0.43	0.38	0.59	0.46	0.46	0.35	0.62
		Pl	0.90	0.70	0.40	0.53	0.73	0.62	0.81	0.37	0.68
$W_{2,3}$		$v_{2,3}$	-0.00	1.00	0.00	-0.00	0.00	-0.00	-0.00	-0.00	0.00
f_{min}-f_{max} (Hz)	18.75-25.00	En	1.6e-10	1.1e-07	6.8e-10	1.1e-10	2.9e-10	2.5e-10	5.7e-09	2e-11	3e-10
M($W_{2,3}$)	1.164	Az	123.50	15.00	-134.58	-118.47	-174.24	-80.17	-56.30	26.58	-23.38
$\log_{10}(E_{out}/E_{in})$	-0.210	In	82.72	85.38	75.72	89.34	72.51	34.93	85.49	81.77	84.26
		Rc	0.61	0.60	0.48	0.39	0.51	0.35	0.51	0.20	0.63
		Pl	0.74	0.72	0.57	0.54	0.73	0.56	0.74	0.19	0.68
P[1)]	11/24 11:30										
$W_{7,0}$		$v_{7,0}$	-0.00	-0.94	-0.01	0.02	0.03	-0.31	-0.13	0.02	0.00
f_{min}-f_{max} (Hz)	0.00-0.20	En	1e-09	2.4e-08	1.4e-09	7.8e-09	1.3e-09	1.8e-08	2.3e-09	4.5e-10	8.4e-09
M($W_{7,0}$)	1.552	Az	-41.97	51.75	163.34	129.24	82.41	158.51	128.60	39.11	11.97
$\log_{10}(E_{out}/E_{in})$	-0.423	In	87.72	77.44	75.88	76.90	74.22	87.33	69.65	81.90	45.82
		Rc	0.29	0.91	0.32	0.45	0.53	0.60	0.45	0.35	0.43
		Pl	0.39	0.91	0.20	0.44	0.56	0.95	0.54	0.47	0.40

Table 4.2. continued

Signal	*Time*	*Sta*	*ECBD*	*ECPN*	*ECZM*	*EMNR*	*EMPL*	*EPDN*	*ESLN*	*ESPC*	*ESVO*
$W_{7,1}$		$v_{7,1}$	0.01	-1.00	0.01	0.00	-0.01	0.08	-0.03	-0.00	0.00
f_{min}-f_{max} (Hz)	0.20-0.39	En	6.7e-09	1.7e-07	7.7e-09	5.7e-08	7.3e-09	6.7e-08	4.3e-08	9.8e-09	7.2e-08
M($W_{7,1}$)	0.092	Lag	1.74	-2.98	2.14	2.20	0.98	-1.72	-2.38	0.18	-0.18
$\log_{10}(E_{out}/E_{in})$	0.000	Az	-166.54	49.99	166.67	92.88	97.03	-151.52	69.31	-137.06	-26.07
		In	84.55	74.31	41.14	80.48	80.31	89.57	75.45	80.65	84.70
		Rc	0.58	0.86	0.45	0.49	0.67	0.73	0.58	0.69	0.40
		Pl	0.57	0.83	0.49	0.49	0.69	0.82	0.82	0.87	0.43
$W_{7,9}$		$v_{7,9}$	-0.01	0.99	-0.00	0.01	0.01	0.12	0.04	0.01	0.02
f_{min}-f_{max} (Hz)	1.76-1.95	En	3.3e-07	2.5e-05	2.3e-07	1.7e-06	5.9e-07	1.6e-05	2.6e-06	6e-07	5.7e-06
M($W_{7,9}$)	0.083	Az	55.23	-98.71	-4.31	-39.66	138.71	106.91	-179.45	20.56	-179.52
$\log_{10}(E_{out}/E_{in})$	-0.325	In	84.32	84.16	85.82	83.63	86.26	83.76	85.29	70.96	89.53
		Rc	0.48	0.73	0.54	0.61	0.56	0.67	0.54	0.49	0.63
		Pl	0.67	0.91	0.68	0.74	0.68	0.84	0.83	0.72	0.74
$W_{6,5}$		$v_{6,5}$	-0.00	1.00	0.00	0.01	-0.01	-0.08	-0.02	-0.00	0.03
f_{min}-f_{max} (Hz)	1.95-2.34	En	3.6e-07	4.1e-05	2.8e-07	1.7e-06	1e-06	1.1e-05	4.8e-06	5.7e-07	7.6e-06
M($W_{6,5}$)	0.104	Az	95.10	-82.73	-10.48	93.69	-36.90	0.91	-81.74	44.27	-10.22
$\log_{10}(E_{out}/E_{in})$	-0.000	In	87.19	82.09	86.33	86.64	87.79	79.37	88.38	81.37	88.65
		Rc	0.46	0.67	0.60	0.63	0.63	0.40	0.59	0.50	0.65
		Pl	0.75	0.88	0.66	0.72	0.81	0.75	0.70	0.66	0.75
$W_{6,6}$		$v_{6,6}$	-0.00	-1.00	0.00	-0.00	0.01	0.00	-0.03	0.00	0.01
f_{min}-f_{max} (Hz)	2.34-2.73	En	2.1e-07	4.2e-05	1.7e-07	1e-06	4.7e-07	1.2e-05	4.3e-06	2.5e-07	4.6e-06
M($W_{6,6}$)	0.121	Az	-101.44	-138.30	5.91	100.77	-10.78	-103.41	-104.72	-3.07	173.70
$\log_{10}(E_{out}/E_{in})$	-0.000	In	87.68	86.31	86.64	86.64	89.19	74.69	89.60	67.83	88.02
		Rc	0.42	0.66	0.63	0.69	0.56	0.68	0.69	0.28	0.56
		Pl	0.69	0.89	0.66	0.80	0.80	0.76	0.70	0.38	0.81
$W_{7,14}$		$v_{7,14}$	-0.00	1.00	-0.00	-0.02	-0.01	-0.01	0.02	-0.00	0.01
f_{min}-f_{max} (Hz)	2.73-2.93	En	9e-08	1.7e-05	6.4e-08	3.1e-07	2.1e-07	3.5e-06	1.5e-06	8e-08	1.2e-06
M($W_{7,14}$)	0.066	Lag	-0.44	0.02	-1.02	1.72	0.96	-2.48	-0.98	1.60	0.58
$\log_{10}(E_{out}/E_{in})$	-0.000	Az	-104.37	-113.35	5.94	129.67	5.04	-97.58	69.62	57.22	-172.81
		In	89.12	87.10	87.83	89.34	87.37	80.29	85.32	35.09	87.03
		Rc	0.63	0.60	0.67	0.64	0.68	0.74	0.59	0.37	0.50
		Pl	0.70	0.83	0.63	0.81	0.83	0.71	0.72	0.25	0.81

Table 4.2. continued

Signal	*Time*	*Sta*	*ECBD*	*ECPN*	*ECZM*	*EMNR*	*EMPL*	*EPDN*	*ESLN*	*ESPC*	*ESVO*
$W_{7,15}$		$v_{7,15}$	-0.00	-1.00	-0.00	-0.00	0.01	0.01	0.02	-0.00	0.01
f_{min}-f_{max} (Hz)	2.93-3.12	En	6.5e-08	1.4e-05	4.9e-08	2.3e-07	1.4e-07	1.9e-06	9.1e-07	7.1e-08	1.7e-06
M($W_{7,15}$)	0.062	Az	-84.42	-155.14	-11.16	97.51	-25.90	-101.01	-80.53	59.14	171.08
$\log_{10}(E_{out}/E_{in})$	-0.000	In	83.87	86.64	89.30	88.41	88.10	77.40	66.77	12.62	85.50
		Rc	0.65	0.56	0.65	0.56	0.49	0.63	0.41	0.28	0.72
		Pl	0.63	0.82	0.63	0.73	0.69	0.53	0.63	0.34	0.82
$W_{5,4}$		$v_{5,4}$	-0.00	-1.00	0.00	0.00	0.00	-0.00	0.01	0.00	0.01
f_{min}-f_{max} (Hz)	3.12-3.91	En	1.6e-07	5.4e-05	1.3e-07	6.9e-07	5.9e-07	7.2e-06	3.4e-06	2.4e-07	4.7e-06
M($W_{5,4}$)	0.364	Az	-91.81	-131.15	178.65	103.94	5.51	-101.47	-67.03	35.58	178.70
$\log_{10}(E_{out}/E_{in})$	-0.143	In	89.80	86.24	88.14	86.55	84.03	77.85	68.89	16.64	89.59
		Rc	0.51	0.66	0.59	0.59	0.61	0.61	0.42	0.42	0.67
		Pl	0.67	0.82	0.59	0.77	0.73	0.54	0.68	0.33	0.80
$W_{5,5}$		$v_{5,5}$	0.00	-1.00	-0.00	-0.00	0.00	0.01	0.01	0.00	0.00
f_{min}-f_{max} (Hz)	3.91-4.69	En	4.9e-08	4.9e-05	2.9e-08	2.2e-07	2.9e-07	2.9e-06	1.9e-06	7.8e-08	1.4e-06
M($W_{5,5}$)	0.316	Az	80.37	-128.80	170.10	88.92	-3.61	-89.26	-106.69	73.97	-2.32
$\log_{10}(E_{out}/E_{in})$	-0.000	In	89.60	85.60	84.75	86.81	88.49	88.13	81.63	18.79	82.35
		Rc	0.55	0.78	0.42	0.44	0.65	0.56	0.44	0.34	0.55
		Pl	0.67	0.78	0.32	0.69	0.68	0.53	0.71	0.23	0.80
$W_{5,6}$		$v_{5,6}$	0.00	1.00	0.00	-0.00	-0.00	-0.00	-0.00	0.00	0.00
f_{min}-f_{max} (Hz)	4.69-5.47	En	1.8e-08	1.9e-05	6.2e-09	1.1e-07	9.1e-08	1.1e-06	1.4e-06	2.8e-08	5.2e-07
M($W_{5,6}$)	0.141	Az	98.57	-132.94	-17.02	-89.09	-167.93	105.71	-24.33	127.96	107.04
$\log_{10}(E_{out}/E_{in})$	-0.000	In	85.69	83.88	85.01	87.18	84.13	86.69	71.56	81.85	89.31
		Rc	0.52	0.51	0.39	0.62	0.45	0.47	0.40	0.28	0.49
		Pl	0.70	0.72	0.45	0.62	0.51	0.36	0.69	0.19	0.74
$W_{5,7}$		$v_{5,7}$	0.00	1.00	0.00	-0.00	0.00	0.02	-0.02	-0.00	0.00
f_{min}-f_{max} (Hz)	5.47-6.25	En	6.3e-09	1.2e-05	1.4e-09	2.9e-08	3.9e-08	4.3e-07	8.9e-07	1.3e-08	1.7e-07
M($W_{5,7}$)	0.166	Az	-80.14	-178.01	157.93	64.39	-128.74	-62.46	-34.04	-165.75	-29.47
$\log_{10}(E_{out}/E_{in})$	-0.000	In	89.69	81.35	62.41	82.38	73.63	58.46	70.30	71.58	76.69
		Rc	0.46	0.54	0.33	0.44	0.47	0.45	0.49	0.33	0.43
		Pl	0.80	0.73	0.50	0.60	0.47	0.50	0.76	0.41	0.56

Table 4.2. continued

Signal	*Time*	*Sta*	*ECBD*	*ECPN*	*ECZM*	*EMNR*	*EMPL*	*EPDN*	*ESLN*	*ESPC*	*ESVO*
$W_{3,2}$		$v_{3,2}$	0.00	1.00	0.00	-0.00	0.00	0.00	-0.00	0.00	0.00
f_{min}-f_{max} (Hz)	6.25-9.38	En	1.2e-08	2.4e-05	2.5e-09	5.5e-08	4.9e-08	5.8e-07	1.9e-06	2.1e-08	2.9e-07
M($W_{3,2}$)	1.059	Az	95.24	177.74	161.75	75.59	-137.12	-76.05	7.05	-174.44	-32.91
$\log_{10}(E_{out}/E_{in})$	-0.207	In	88.13	80.07	87.15	89.70	68.76	61.52	75.72	72.00	76.41
		Rc	0.48	0.55	0.32	0.45	0.38	0.34	0.56	0.35	0.47
		Pl	0.78	0.70	0.43	0.58	0.41	0.49	0.82	0.33	0.65
$W_{6,24}$		$v_{6,24}$	0.00	-1.00	0.00	0.00	-0.00	-0.00	0.02	0.00	0.00
f_{min}-f_{max} (Hz)	9.38-9.77	En	3.4e-10	9.8e-07	4.9e-11	1.2e-09	5.1e-10	9e-09	1.1e-07	4e-10	5e-09
M($W_{6,24}$)	0.115	Az	-116.27	130.78	-4.21	-55.25	-32.26	-87.97	13.73	-164.50	-30.14
$\log_{10}(E_{out}/E_{in})$	-0.080	In	85.61	87.30	85.03	47.38	80.17	73.90	80.03	48.17	80.81
		Rc	0.53	0.65	0.47	0.44	0.27	0.36	0.78	0.48	0.55
		Pl	0.78	0.71	0.39	0.55	0.36	0.64	0.88	0.47	0.67
$W_{6,25}$		$v_{6,25}$	-0.00	-1.00	-0.00	0.00	0.00	0.00	0.01	0.00	0.00
f_{min}-f_{max} (Hz)	9.77-10.16	En	2.2e-10	7e-07	3.3e-11	1.1e-09	4.5e-10	7.6e-09	8.4e-08	2.4e-10	3.5e-09
M($W_{6,25}$)	0.110	Az	62.92	147.14	177.55	-25.50	-164.38	-88.01	17.37	-163.32	-39.42
$\log_{10}(E_{out}/E_{in})$	-0.080	In	85.87	77.16	79.21	43.57	66.49	74.13	83.48	73.02	79.06
		Rc	0.46	0.61	0.44	0.52	0.33	0.47	0.77	0.38	0.51
		Pl	0.60	0.68	0.37	0.54	0.44	0.67	0.86	0.47	0.65
$W_{5,13}$		$v_{5,13}$	-0.00	1.00	-0.00	-0.00	-0.00	-0.00	0.02	-0.00	0.00
f_{min}-f_{max} (Hz)	10.16-10.94	En	2.5e-10	9.8e-07	2.3e-11	1.1e-09	5e-10	7.5e-09	8.9e-08	2.5e-10	3.9e-09
M($W_{5,13}$)	0.127	Az	130.96	148.12	176.87	-54.16	-149.07	-80.44	13.30	-174.45	-20.00
$\log_{10}(E_{out}/E_{in})$	-0.000	In	81.04	87.47	81.13	45.75	38.46	75.65	84.66	53.02	77.61
		Rc	0.45	0.57	0.31	0.58	0.41	0.53	0.70	0.37	0.52
		Pl	0.52	0.70	0.37	0.56	0.43	0.54	0.79	0.30	0.70
$W_{4,7}$		$v_{4,7}$	-0.00	1.00	0.00	-0.00	0.00	-0.00	-0.00	-0.00	0.00
f_{min}-f_{max} (Hz)	10.94-12.50	En	5.6e-10	8.5e-07	2.2e-11	1.1e-09	4.9e-10	5.2e-09	9.1e-08	3.3e-10	3.6e-09
M($W_{4,7}$)	0.669	Az	142.90	152.58	2.87	-101.09	-90.97	-70.83	6.74	-146.98	-51.13
$\log_{10}(E_{out}/E_{in})$	-0.000	In	85.99	82.67	57.16	56.16	55.30	80.47	87.23	32.23	74.12
		Rc	0.73	0.60	0.32	0.39	0.40	0.60	0.63	0.42	0.61
		Pl	0.71	0.61	0.48	0.51	0.56	0.54	0.74	0.52	0.75

Table 4.2. continued

Signal	*Time*	*Sta*	*ECBD*	*ECPN*	*ECZM*	*EMNR*	*EMPL*	*EPDN*	*ESLN*	*ESPC*	*ESVO*
$W_{5,16}$		$v_{5,16}$	-0.00	1.00	-0.00	-0.00	0.00	-0.00	-0.03	0.00	0.00
f_{min}-f_{max} (Hz)	12.50-13.28	En	2.5e-10	2.6e-07	9.2e-12	3.8e-10	2.2e-10	1.4e-09	2.6e-08	1.4e-10	9.9e-10
M($W_{5,16}$)	0.124	Az	143.07	176.02	36.10	-112.08	-86.76	-69.68	6.21	-114.96	-69.01
$\log_{10}(E_{out}/E_{in})$	-0.000	In	88.10	76.67	12.53	77.46	63.62	75.03	85.46	66.84	71.83
		Rc	0.78	0.45	0.37	0.32	0.49	0.57	0.42	0.47	0.56
		Pl	0.75	0.51	0.46	0.47	0.57	0.51	0.67	0.55	0.72
$W_{5,17}$		$v_{5,17}$	-0.00	1.00	0.00	-0.00	-0.00	0.00	-0.00	0.00	0.00
f_{min}-f_{max} (Hz)	13.28-14.06	En	1.7e-10	3.1e-07	1.2e-11	3.7e-10	1.9e-10	1.6e-09	3e-08	1.2e-10	1.3e-09
M($W_{5,17}$)	0.124	Az	140.07	159.14	7.64	-97.14	-104.47	-71.78	4.33	-152.82	-48.67
$\log_{10}(E_{out}/E_{in})$	-0.000	In	84.52	83.28	82.65	53.31	53.00	85.82	85.90	45.38	73.14
		Rc	0.69	0.64	0.41	0.46	0.42	0.63	0.65	0.45	0.67
		Pl	0.72	0.60	0.50	0.53	0.55	0.57	0.74	0.53	0.75
$W_{4,9}$		$v_{4,9}$	0.00	-1.00	-0.00	0.00	0.00	-0.00	-0.01	-0.00	0.00
f_{min}-f_{max} (Hz)	14.06-15.62	En	2.1e-10	5.1e-07	2.2e-11	5.2e-10	3.3e-10	2.7e-09	4.5e-08	1.3e-10	1.6e-09
M($W_{4,9}$)	0.538	Az	145.19	154.64	21.03	-56.47	-128.75	-81.85	11.31	-167.90	-36.65
$\log_{10}(E_{out}/E_{in})$	-0.000	In	87.07	84.15	69.89	44.91	44.49	80.56	86.16	70.41	77.65
		Rc	0.67	0.61	0.37	0.52	0.39	0.52	0.66	0.41	0.51
		Pl	0.73	0.67	0.48	0.54	0.48	0.62	0.77	0.31	0.68
$W_{6,40}$		$v_{6,40}$	0.00	-1.00	0.00	0.00	0.00	-0.00	-0.00	-0.00	0.00
f_{min}-f_{max} (Hz)	15.62-16.02	En	3.8e-11	8.6e-08	4.3e-12	9.1e-11	7.2e-11	5.5e-10	9.6e-09	3.1e-11	3e-10
M($W_{6,40}$)	0.099	Az	-60.62	139.26	-144.02	-72.59	-109.66	104.03	11.10	-152.32	-51.99
$\log_{10}(E_{out}/E_{in})$	-0.000	In	88.49	88.19	39.27	51.94	51.76	28.55	82.12	77.02	77.34
		Rc	0.55	0.54	0.30	0.44	0.37	0.40	0.72	0.42	0.57
		Pl	0.85	0.63	0.33	0.46	0.55	0.71	0.83	0.44	0.67

Table 4.2. continued

Signal	*Time*	*Sta*	*ECBD*	*ECPN*	*ECZM*	*EMNR*	*EMPL*	*EPDN*	*ESLN*	*ESPC*	*ESVO*
$W_{6,41}$		$v_{6,41}$	0.00	1.00	-0.00	-0.00	0.00	-0.00	0.02	-0.00	0.00
f_{min}-f_{max} (Hz)	16.02-16.41	En	2.5e-11	7.9e-08	4.2e-12	6.8e-11	7.7e-11	6.4e-10	6.3e-09	2.1e-11	2.3e-10
M($W_{6,41}$)	0.124	Az	-87.94	179.90	-137.21	-22.53	-135.85	124.42	15.99	-157.10	-38.15
$\log_{10}(E_{out}/E_{in})$	0.000	In	86.32	80.64	59.83	60.77	50.58	16.99	82.14	89.31	76.92
		Rc	0.56	0.53	0.37	0.25	0.46	0.58	0.57	0.34	0.52
		Pl	0.76	0.59	0.44	0.44	0.67	0.80	0.85	0.35	0.68
$W_{5,21}$		$v_{5,21}$	-0.00	-1.00	0.00	-0.00	-0.00	0.00	0.01	0.00	0.00
f_{min}-f_{max} (Hz)	16.41-17.19	En	4e-11	1.2e-07	7.8e-12	9.7e-11	1.7e-10	8e-10	8.1e-09	3.9e-11	4.4e-10
M($W_{5,21}$)	0.139	Az	98.34	-170.04	-101.88	5.54	-161.91	-115.43	21.50	-176.25	-34.26
$\log_{10}(E_{out}/E_{in})$	-0.000	In	88.15	86.91	48.26	68.92	63.36	6.84	84.50	74.84	72.81
		Rc	0.52	0.52	0.34	0.30	0.55	0.55	0.56	0.43	0.62
		Pl	0.79	0.63	0.41	0.43	0.72	0.69	0.81	0.46	0.68
$W_{4,11}$		$v_{4,11}$	0.00	1.00	0.00	-0.00	-0.00	0.00	0.00	-0.00	0.00
f_{min}-f_{max} (Hz)	17.19-18.75	En	4.1e-11	1.3e-07	1.9e-11	1.2e-10	3e-10	6.3e-10	7.3e-09	3.2e-11	4e-10
M($W_{4,11}$)	0.403	Az	134.32	6.58	-122.60	-127.71	-129.53	-93.74	-11.46	-152.69	-34.82
$\log_{10}(E_{out}/E_{in})$	-0.269	In	89.66	87.37	46.91	88.31	54.43	24.92	78.35	79.86	74.95
		Rc	0.55	0.69	0.29	0.40	0.67	0.45	0.45	0.36	0.60
		Pl	0.84	0.71	0.33	0.60	0.78	0.62	0.82	0.38	0.66
$W_{2,3}$		$v_{2,3}$	-0.00	1.00	0.00	-0.00	-0.00	-0.00	-0.00	-0.00	0.00
f_{min}-f_{max} (Hz)	18.75-25.00	En	5.2e-11	1.1e-07	8.2e-11	1.7e-10	4.2e-10	2.7e-10	5.7e-09	2.2e-11	2.8e-10
M($W_{2,3}$)	1.551	Az	172.18	14.95	116.79	-128.44	-164.40	-78.15	-57.70	39.54	-21.94
$\log_{10}(E_{out}/E_{in})$	-0.246	In	56.08	85.84	88.58	88.55	69.95	42.46	84.65	72.60	83.39
		Rc	0.37	0.61	0.35	0.42	0.50	0.35	0.51	0.20	0.60
		Pl	0.54	0.74	0.51	0.59	0.73	0.55	0.74	0.21	0.67

Table 4.2. continued

Signal	*Time*	*Sta*	*ECBD*	*ECPN*	*ECZM*	*EMNR*	*EMPL*	*EPDN*	*ESLN*	*ESPC*	*ESVO*
$P^{(2)}$	11/24 11:00										
$W_{7,2}$		$v_{7,2}$	0.01	0.91	-0.01	0.04	0.01	-0.41	0.10	-0.01	0.00
f_{min}-f_{max} (Hz)	0.39-0.59	En	4.3e-08	1.2e-06	2.2e-08	3.1e-07	6.2e-08	9.6e-07	3.3e-07	5.9e-08	4.5e-07
M($W_{7,2}$)	1.711	Lag	2.48	-3.36	1.66	0.82	2.58	-2.20	-3.02	1.26	-0.24
$\log_{10}(E_{out}/E_{in})$	-0.195	Az	-7.49	60.04	-177.54	158.66	99.02	41.19	45.44	67.17	16.29
		In	74.80	80.12	67.54	84.03	85.98	85.21	76.69	89.68	85.40
		Rc	0.64	0.87	0.43	0.54	0.79	0.71	0.66	0.74	0.82
		Pl	0.69	0.87	0.41	0.65	0.84	0.92	0.86	0.88	0.80
$W_{7,12}$		$v_{7,12}$	-0.00	-0.97	0.01	0.01	-0.01	0.24	-0.04	-0.00	0.01
f_{min}-f_{max} (Hz)	2.34-2.54	En	1.4e-07	1.7e-05	1e-07	6.1e-07	2.9e-07	7.1e-06	2.9e-06	1.6e-07	2.8e-06
M($W_{7,12}$)	0.737	Lag	2.22	-3.04	-0.10	3.50	0.12	-3.08	-2.44	3.20	-0.34
$\log_{10}(E_{out}/E_{in})$	-0.260	Az	64.77	-144.15	3.73	100.47	170.22	-88.64	74.39	-41.48	157.16
		In	89.73	87.39	85.65	87.67	89.60	73.77	89.42	74.27	89.77
		Rc	0.55	0.58	0.64	0.67	0.57	0.69	0.75	0.33	0.56
		Pl	0.75	0.88	0.65	0.81	0.81	0.78	0.75	0.52	0.80
$P^{(2)}$	11/24 11:30										
$W_{7,2}$		$v_{7,2}$	-0.00	-0.93	-0.00	-0.00	0.01	0.34	-0.12	0.02	0.09
f_{min}-f_{max} (Hz)	0.39-0.59	En	4e-08	9.7e-07	2.3e-08	2.7e-07	6e-08	6.6e-07	2.9e-07	5.4e-08	4e-07
M($W_{7,2}$)	1.718	Lag	2.38	-3.00	1.78	0.76	2.26	-2.20	-3.20	1.62	-0.38
$\log_{10}(E_{out}/E_{in})$	-0.225	Az	-6.54	59.74	176.70	156.10	102.23	33.19	54.68	-109.44	11.55
		In	76.95	80.48	72.08	85.01	86.20	85.49	78.02	89.52	86.95
		Rc	0.69	0.84	0.54	0.58	0.80	0.63	0.59	0.74	0.77
		Pl	0.74	0.87	0.45	0.68	0.85	0.92	0.83	0.87	0.77
$P^{(3)}$	11/24 11:00										
$W_{7,3}$		$v_{7,3}$	0.00	-0.07	0.01	-0.01	0.01	0.99	-0.14	0.00	0.00
f_{min}-f_{max} (Hz)	0.59-0.78	En	1.3e-07	4.2e-06	1.4e-07	8.6e-07	2.7e-07	7.8e-06	2e-06	2.2e-07	1.1e-06
M($W_{7,3}$)	1.098	Lag	1.18	-2.60	2.00	-0.18	1.88	-2.52	-2.08	1.12	1.20
$\log_{10}(E_{out}/E_{in})$	-0.010	Az	-47.88	64.24	163.35	-19.51	108.22	48.75	72.21	68.21	0.29
		In	89.06	86.14	84.63	83.58	89.85	86.43	81.92	82.67	89.16
		Rc	0.68	0.82	0.78	0.69	0.78	0.87	0.77	0.71	0.50
		Pl	0.75	0.90	0.76	0.84	0.87	0.96	0.87	0.84	0.61

Table 4.2. continued

Signal	*Time*	*Sta*	*ECBD*	*ECPN*	*ECZM*	*EMNR*	*EMPL*	*EPDN*	*ESLN*	*ESPC*	*ESVO*
$W_{7,4}$		$v_{7,4}$	0.01	-0.01	-0.01	0.02	0.01	-0.98	0.22	-0.00	0.03
f_{min}-f_{max} (Hz)	0.78-0.98	En	1.7e-07	7.7e-06	2.8e-07	1.8e-06	5e-07	2.3e-05	3.2e-06	4.3e-07	2.4e-06
M($W_{7,4}$)	0.637	Lag	0.52	-3.60	2.20	2.36	3.24	-2.98	-2.80	0.28	0.80
$\log_{10}(E_{out}/E_{in})$	-0.522	Az	126.78	60.64	161.20	-32.30	-76.96	-119.36	82.76	61.82	-9.69
		In	83.48	89.24	87.50	87.60	85.81	89.62	84.98	87.96	88.36
		Rc	0.46	0.74	0.82	0.70	0.79	0.93	0.68	0.72	0.61
		Pl	0.65	0.91	0.76	0.90	0.84	0.98	0.90	0.86	0.64
$W_{7,7}$		$v_{7,7}$	0.00	-0.25	0.00	-0.02	-0.01	0.97	-0.04	0.00	0.04
f_{min}-f_{max} (Hz)	1.37-1.56	En	7.9e-07	4.5e-05	3.6e-07	4.1e-06	1.2e-06	5e-05	4.5e-06	9.8e-07	9.1e-06
M($W_{7,7}$)	1.302	Az	-87.90	-109.89	-16.52	62.01	-44.43	-94.19	167.26	45.83	-21.10
$\log_{10}(E_{out}/E_{in})$	-0.297	In	89.96	86.27	89.50	81.98	82.65	89.23	86.67	79.70	83.63
		Rc	0.59	0.79	0.52	0.63	0.66	0.89	0.56	0.52	0.69
		Pl	0.60	0.94	0.72	0.77	0.73	0.90	0.82	0.77	0.81
		Rc	0.55	0.69	0.29	0.40	0.67	0.45	0.45	0.36	0.60
		Pl	0.84	0.71	0.33	0.60	0.78	0.62	0.82	0.38	0.66
$P^{(4)}$	11/24 11:00										
$W_{7,5}$		$v_{7,5}$	-0.02	-0.31	0.01	-0.02	-0.01	-0.94	0.16	-0.01	0.01
f_{min}-f_{max} (Hz)	0.98-1.17	En	7.3e-07	2.1e-05	3.3e-07	4.3e-06	1.5e-06	2.7e-05	5.5e-06	9.2e-07	7e-06
M($W_{7,5}$)	1.452	Lag	1.00	-2.70	0.86	4.10	2.62	-1.92	-3.10	2.22	-3.08
$\log_{10}(E_{out}/E_{in})$	-0.552	Az	-8.51	-117.41	-18.68	-83.80	-76.29	62.44	-14.12	67.41	30.97
		In	78.94	82.97	82.54	83.08	88.52	87.67	85.85	81.96	87.10
		Rc	0.70	0.73	0.54	0.71	0.83	0.70	0.67	0.79	0.72
		Pl	0.70	0.92	0.75	0.84	0.88	0.97	0.78	0.79	0.74
$W_{7,8}$		$v_{7,8}$	0.00	-0.37	0.00	-0.01	-0.01	-0.93	-0.01	-0.00	0.05
f_{min}-f_{max} (Hz)	1.56-1.76	En	6.4e-07	4.1e-05	3.3e-07	3e-06	9.4e-07	4.7e-05	3.7e-06	8.8e-07	7.3e-06
M($W_{7,8}$)	1.173	Az	93.95	-104.05	-21.27	71.99	-38.52	85.64	165.43	59.67	-24.53
$\log_{10}(E_{out}/E_{in})$	-0.024	In	88.24	85.54	86.37	85.71	81.87	89.01	85.07	78.64	85.11
		Rc	0.53	0.79	0.58	0.63	0.57	0.89	0.56	0.48	0.64
		Pl	0.62	0.94	0.70	0.71	0.72	0.89	0.82	0.72	0.79

Table 4.2. continued

Signal	*Time*	*Sta*	*ECBD*	*ECPN*	*ECZM*	*EMNR*	*EMPL*	*EPDN*	*ESLN*	*ESPC*	*ESVO*
P(5)	11/24 11:30										
$W_{7,3}$		$v_{7,3}$	0.00	0.14	-0.00	-0.01	-0.00	-0.92	0.36	0.00	0.02
f_{min}-f_{max} (Hz)	0.59-0.78	En	1.2e-07	4.2e-06	1.3e-07	7.4e-07	2.4e-07	6.4e-06	2e-06	2.3e-07	1.2e-06
M($W_{7,3}$)	1.083	Lag	2.48	-2.26	2.48	-1.32	1.76	-2.06	-1.38	0.06	0.24
$\log_{10}(E_{out}/E_{in})$	-0.028	Az	-48.76	65.70	164.53	-16.09	110.72	47.64	72.59	70.35	165.11
		In	87.44	85.83	84.18	84.37	89.98	86.68	83.21	82.90	88.83
		Rc	0.70	0.82	0.74	0.67	0.77	0.86	0.78	0.75	0.47
		Pl	0.76	0.90	0.75	0.84	0.86	0.96	0.87	0.84	0.60
$W_{7,4}$		$v_{7,4}$	0.01	-0.09	0.00	-0.00	-0.00	-0.98	0.20	0.01	0.02
f_{min}-f_{max} (Hz)	0.78-0.98	En	1.8e-07	7.4e-06	2.5e-07	1.6e-06	4.4e-07	1.8e-05	3.2e-06	3.9e-07	2.6e-06
M($W_{7,4}$)	0.822	Lag	2.10	-2.82	3.06	0.08	3.36	-2.32	-2.36	-0.08	-1.00
$\log_{10}(E_{out}/E_{in})$	-0.487	Az	120.63	64.02	163.03	-28.64	-75.37	-122.17	86.60	60.46	161.53
		In	83.96	88.10	88.63	87.21	85.11	89.41	87.63	88.00	87.87
		Rc	0.53	0.74	0.78	0.69	0.77	0.93	0.67	0.72	0.62
		Pl	0.69	0.90	0.73	0.88	0.83	0.97	0.90	0.85	0.64
P(6)	11/24 11:00										
$W_{7,6}$		$v_{7,6}$	-0.00	-0.52	0.00	0.02	0.00	-0.83	-0.18	-0.02	0.05
f_{min}-f_{max} (Hz)	1.17-1.37	En	6.7e-07	3.4e-05	5.5e-07	3.5e-06	1.2e-06	3.6e-05	7.2e-06	1.2e-06	7e-06
M($W_{7,6}$)	1.344	Lag	1.56	-2.62	0.20	2.88	2.36	-1.96	-2.24	1.42	-1.60
$\log_{10}(E_{out}/E_{in})$	-0.475	Az	39.57	-119.05	47.64	-48.58	118.98	3.61	172.42	56.76	-157.66
		In	83.11	84.65	89.06	87.95	88.74	87.19	86.80	76.99	85.77
		Rc	0.45	0.71	0.67	0.43	0.67	0.62	0.77	0.66	0.64
		Pl	0.60	0.93	0.76	0.67	0.76	0.95	0.85	0.75	0.72
P(6)	11/24 11:30										
$W_{7,5}$		$v_{7,5}$	0.00	-0.57	-0.01	-0.02	-0.02	-0.80	-0.17	-0.01	0.06
f_{min}-f_{max} (Hz)	0.98-1.17	En	5e-07	1.7e-05	3.1e-07	3.4e-06	1.3e-06	1.9e-05	4.7e-06	8.3e-07	5.8e-06
M($W_{7,5}$)	1.383	Az	-11.88	-115.60	-4.37	-73.50	-75.67	53.10	-25.22	65.46	24.78
$\log_{10}(E_{out}/E_{in})$	-0.531	In	82.29	85.49	84.54	83.19	89.34	88.93	87.13	81.43	85.72
		Rc	0.65	0.74	0.60	0.67	0.85	0.68	0.68	0.80	0.67
		Pl	0.66	0.90	0.75	0.84	0.88	0.96	0.80	0.79	0.69

Table 4.2. continued

Signal	*Time*	*Sta*	*ECBD*	*ECPN*	*ECZM*	*EMNR*	*EMPL*	*EPDN*	*ESLN*	*ESPC*	*ESVO*
$W_{7,6}$		$v_{7,6}$	-0.00	-0.29	-0.00	0.03	0.01	-0.95	-0.14	-0.00	0.03
f_{min}-f_{max} (Hz)	1.17-1.37	En	5.2e-07	2.8e-05	5e-07	3.2e-06	1e-06	3e-05	6.1e-06	9.7e-07	5.9e-06
M($W_{7,6}$)	1.459	Lag	0.52	-2.66	-0.84	1.64	4.22	-2.20	-3.34	2.70	-0.06
$\log_{10}(E_{out}/E_{in})$	-0.503	Az	30.60	-117.38	41.12	-43.64	117.79	9.19	168.50	54.94	-156.21
		In	84.28	85.59	89.18	84.54	87.35	87.51	87.44	77.85	88.79
		Rc	0.41	0.70	0.72	0.53	0.68	0.60	0.76	0.63	0.63
		Pl	0.55	0.92	0.76	0.70	0.76	0.95	0.84	0.71	0.69
$W_{7,7}$		$v_{7,7}$	-0.01	-0.35	-0.01	-0.03	-0.01	-0.93	-0.05	0.01	0.06
f_{min}-f_{max} (Hz)	1.37-1.56	En	7.1e-07	3.7e-05	3e-07	3.3e-06	8.7e-07	4.3e-05	4.1e-06	8.5e-07	7.9e-06
M($W_{7,7}$)	1.222	Az	-90.45	-106.24	164.93	63.03	-53.24	89.79	162.81	37.26	-18.20
$\log_{10}(E_{out}/E_{in})$	-0.278	In	89.25	86.57	89.13	80.97	85.97	88.82	85.57	78.93	84.52
		Rc	0.61	0.77	0.54	0.61	0.61	0.89	0.60	0.49	0.70
		Pl	0.62	0.94	0.69	0.79	0.70	0.91	0.81	0.76	0.81
$W_{7,8}$		$v_{7,8}$	-0.01	-0.55	0.01	-0.02	-0.01	-0.83	-0.01	-0.00	0.06
f_{min}-f_{max} (Hz)	1.56-1.76	En	5.7e-07	3.4e-05	2.8e-07	2.5e-06	7.6e-07	3.7e-05	3.5e-06	7.5e-07	6.4e-06
M($W_{7,8}$)	1.178	Az	-89.10	-100.45	-17.28	72.62	-49.04	90.49	166.67	49.96	-19.99
$\log_{10}(E_{out}/E_{in})$	-0.051	In	89.88	85.28	89.32	85.31	84.51	88.33	84.63	77.26	86.13
		Rc	0.55	0.77	0.58	0.62	0.53	0.88	0.60	0.45	0.64
		Pl	0.63	0.94	0.68	0.71	0.69	0.90	0.81	0.72	0.79

Notes to Chapter III

Allard, P., Behncke, B., D'Amico, S., Neri, M., Gambino, S., 2006. Mount Etna 1993–2005: Anatomy of an evolving eruptive cycle, *Earth-Science Rev. 78*, 85-114.

Battaglia, J., K. Aki, Ferrazzini, V., 2005. Location of tremor sources and estimation of lava output using tremor source amplitude on the Piton de la Fournaise volcano: 1. Location of tremor sources, *J. Volcanol. Geotherm. Res.*, 147, 268-290.

Chouet, B., 1996. Long-Period volcano seismicity: its source and use in eruption forecasting. *Nature* 380, 309-316.

Del Carlo, P. Vezzosi, L., Coltelli, M., 2004. Last 100 ka tephrostratigraphic record of Mount Etna, in *Mt. Etna: Volcano Laboratory*, A. Bonaccorso, ed., 77-89, *AGU Geophysical Monograph Series* 143.

Di Grazia, G., S. Falsaperla, Langer, H., 2006. Volcanic tremor location during the 2004 Mount Etna lava effusion, *Geophys. Res. Lett*., 33, L04304, doi:10.1029/2005GL025177 .

Francis, P., Oppenheimer, C., Stevenson, D., 1993. Endogenous growth of persistently active volcanoes, *Nature* 366, 554 - 557, doi:10.1038/366554a0.

Gottschämmer, E., Surono, I., 2000. Locating tremor and shock sources at Bromo Volcano. *J. Volcanol. Geotherm. Res.* 101, 199-209.

Jaupart, C., Vergniolle, S., 1988. Laboratory models of Hawaiian and Strombolian eruptions, *Nature* 331, 58-60.

Patanè, D., Di Grazia, G., Cannata, A., Montalto, P., Boschi, E. 2008. The shallow magma pathway geometry at Mt. Etna volcano. *Geochem. Geophys. Geosys.* 9, doi: 10.1029/2008GC002131.

Saccorotti, G., Lockmer, I., Bean, C.J. Di Grazia, G., Patanè, D., 2007. Analysis of sustained long-period activity at Etna Volcano, Italy, *J. Volcanol. Geotherm. Res.* 160, 340-354.

Woods, A.W., Cardoso, S.S. 1997. Bubble–melt separation as a trigger for basaltic volcanic eruptions, *Nature* 385, 518-520.

V. Conclusions

In the past, volcanic tremor was usually analyzed in some region of the frequency spectrum that could be represented by a single source. The research presented here is a first attempt at quantitatively decomposing continuous volcanic tremor, using a quantitative, semi-automated algorithm to segregate subbands of the frequency spectrum that might correspond to different seismic sources. In this way it is a first attempt to treat volcanic tremor as a composite signal, formed by multiple seismic sources whose seismic spectra sometimes overlap.

The method of subband decomposition and reconstruction, or *SDR*, makes only one assumption about the nature of volcanic tremor: that some parts of its frequency spectrum are more strongly dominated by a single signal than other parts. From this single assumption, using only basic principles of wavelet analysis, it has been demonstrated that continuous volcanic tremor can be quantitatively decomposed into subbands in a way that preserves many properties that are classically used to describe volcanic tremor (see e.g. Konstantinou and Schlindwein 2002). These properties, in turn, can be used to constrain the seismic sources that generate many of the recovered signals. We have shown that the observed and inferred properties of these recovered signals differ dramatically, even in adjacent subbands of the frequency spectrum, in ways that cannot be discerned by a human eye, nor by *ad hoc* assumptions about the nature of the data. This was shown to be true even at quiescent volcanoes, such as Erta 'Ale, Ethiopia, and detectible even at

volcanoes where broadband non-volcanic seismic noise often masks volcanogenic signals, such as Mount Erebus, Antarctica.

The *SDR* method offers a great deal of insight into the physical sources of the tremor at each volcano, and could potentially help to resolve some of the competing methods for tremor generation. For example, I was able to constrain the source of many recovered signals at Erta ‘Ale, Ethiopia, and to examine their relationships to physical processes in e.g. the deep lava lake, the shallow lava lake, and fumaroles in the north crater. In addition to identifying many simultaneously active seismic sources, this paints a much clearer picture of the physical processes; in this case, the controversy resolved is what conceptual model drove the cyclical convection of the lava lake in 2002 (Harris 2008, Harris et al. 2005). Based on the polarization and frequency content of a persistent recovered signal, I have argued that the continuous tremor was always dominated by a recovered signal corresponding to fresh magma propagating through a conduit that fed the lava lake. By elimination, this implies that the cyclical nature of the lava lake convection reported in Harris et al. (2005) was driven by cooling and crusting of magma at the lava lake surface, i.e. the second model of Harris (2008). This example demonstrates that even with 3 seismic stations in a non-ideal configuration, *SDR* can sometimes answer fundamental questions about the nature and causes of volcanic tremor. Presumably, this method could be applied identically to other systems whose tremor exhibits similar spectral transitions, e.g. Ambrym, Vanuatu, (Carniel et al. 2003) or Stromboli, Italy (Ripepe et al. 2002).

Resolving these spectral transitions is not the only potential application of this work. The methods developed herein, and the recovered signals found by *SDR*, can also help differentiate between competing source models for volcanic tremor at specific systems. In fact, as I have shown, these models need not be in competition; several different sources of the tremor can exist simultaneously. For example, using data recorded at Erta 'Ale in 2003, and simple energy-based location methods (Gottschämmer and Surono 2000), *SDR* was used to demonstrate the existence of simultaneous shallow and deep tremor sources in the active lava lake. The shallower signals correlated to recovered signals found by applying *SDR* to seismo-acoustic data, confirming a very shallow source, while the deeper signals had no significant correlations. From this, and from the properties of the recovered signals, I could infer that the shallower signals were most likely generated by a process such as forced bubble coalescence (Ripepe and Gordeev 1999), while the deeper signals were most likely generated by a crack resonating in response to magma feeding through it, into the lava lake (Chouet 1996). Thus these differing models of tremor sources are not in conflict; they appear to be active at the same volcanic system, at the same time. They are merely difficult to separate.

Additionally, again using the example of Erta 'Ale, I was able to show that at least one signal with no relation to any surface feature still had a meaningful geological interpretation: a distributed, subsurface tremor centroid, located between the two craters, was inferred to originate from propagation of magma through a conduit system that (once) connected the two craters. The existence of such a

conduit system had been inferred from similar properties of Erta 'Ale's past and present lava lakes (Oppenheimer and Francis 1998, Tazieff 1994), but this is the first measurable seismic signal that corroborates the geologic observations. Furthermore, we were able to recover signals whose most likely sources were the fumaroles in and around the northern crater, which suggest that passive degassing occurred underneath much of the summit caldera in a system of connected conduits. Thus we assembled solid evidence that the magmatic system of Erta ‘Ale connected both craters at shallow depths within the summit caldera, even two years before a lava lake reappeared in the northern crater.

There are many potential applications of the method that are not fully explored. Perhaps the greatest among these is a direct consequence of the way that a recovered signal is defined: namely, that one can determine, in a straightforward and quantitative way, which recovered signals persist through time. As was shown, using test data from Erta 'Ale, Ethiopia, and Etna, Italy, the often-cumbersome process of locating a recovered signal is *not* necessary to track its persistence. As I showed, using data from both volcanoes, persistent recovered signals have no statistically significant change in their location. Thus, merely tracking the principal eigenvectors of recovered signals through time could enable volcanologists to quantitatively determine when the content of continuous volcanic tremor changes. At more explosive, silicic systems, this method could even provide a quantitative means of detecting signals that precede volcanic unrest, as the sample data from Mt. Etna suggested.

In fact, some evidence for this potential application of *SDR* already exists, as was show using data from Mt. Etna. This method recovered distinct low frequency signals in the range 0.39-0.59 Hz, consistent with those of discrete LF events at Etna (Patanè et al. 2008), which could have served as precursors to the unrest of 23-24 Nov 2006. The presence and evolution of such signals are consistent with models for choked fluid flow in a conduit (e.g. Chouet 1996), and thus could support the notion that injection of gas-rich magma into the conduit system drove the paroxysmal lava flows of 24 Nov 2006. However, using our method, the low-frequency energy was detectible in a straightforward way, 12h before the paroxysm began. Unfortunately, because predictions are easier to make after the fact, it is unknown how well SDR could detect precursors to unrest in real time. However, this result at least suggests that SDR holds some promise for eruption forecasting.

We learn from these case studies that the treatment of volcanic tremor as a single signal is an oversimplification that hinders our ability to understand the physical processes of active volcanoes. It is far more diagnostic to examine tremor as a composite of many sources, from which one can extract a wealth of information about the myriad physical processes of seismic signals at active volcanoes. The notion that background tremor has a single source is true in some cases, but may not be complete, nor even particularly useful (as the case study at Mt. Etna showed). Tremor could be a superposition of many transients and many signals on a quasi-static and quasi-continuous background. As has been shown, these secondary

signals could potentially prove more useful in understanding volcanic behavior (and forecasting unrest) than the continuous background signal.

My conclusions from this work are the following. First, it is not always true that a single model explains continuous volcanic tremor, nor that any single model necessarily explains continuous tremor in any time period. It is also not necessarily true that volcanic systems with simple conduit geometries will generate simple seismic signals. As was seen in particular at Erta 'Ale, it can be the case that each secondary signal is associated with a different part (and, often, a different surface expression) of volcanic activity. It is also not necessarily true that a static background signal will provide diagnostic information about unrest at a volcanic system. However, the composite signal that we call "continuous tremor" contains a wealth of information, which can be recovered and tracked using straightforward, quantitative, semi-automated wavelet methods. It can have multiple, simultaneously active sources, which can be resolved even when their centroids and frequency spectra are similar. The signals recovered in this way can correspond to geologic features and observable geophysical processes, and their inferred sources can provide a great deal of insight into the nature of volcanic tremor.

Notes to Chapter V

Chouet, B., 1996. Long-Period volcano seismicity: its source and use in eruption forecasting. *Nature* 380, 309-316.

Harris, A.J.L., 2008, Modeling lava lake heat loss, rheology, and convection, *Geophys. Res. Lett.*, 35, L07303, doi:10.1029/2008GL033190.

Harris, A.J.L., Carniel, R., Jones, J., 2005. Identification of variable convective regimes at Erta Ale Lava Lake. *J. Volcanol. Geotherm. Res.*, 142, 207-223.

Jones, J., Carniel, R., Harris, A.J.L., Malone, S., 2006. Seismic characteristics of variable convection at Erta `Ale lava lake, Ethiopia, *J. Volcanol. Geotherm. Res.* 153, 64-79.

Konstantinou, K.I., Schlindwein, V., 2002. Nature, wavefield properties and source mechanism of volcanic tremor: a review. *J. Volcanol. Geotherm. Res.* 119, 161-187.

Patanè, D., Di Grazia, G., Cannata, A., Montalto, P., Boschi, E. 2008. The shallow magma pathway geometry at Mt. Etna volcano. *Geochem. Geophys. Geosys.* 9, doi: 10.1029/2008GC002131.

Ripepe, M., Gordeev, E., 1999. Gas bubble dynamics model for shallow volcanic tremor at Stromboli, *J. Geophys. Res.* 104(B5), 10,639–10,654.

References

Acernese, F., Ciaramella, A., De Martino, S. Falanga, M., Godano, C., Tagliaferri, R., 2004. Polarization analysis of the independent components of low frequency events at Stromboli volcano (Aeolian Islands, Italy). *J. Volcanol. Geotherm. Res.* 137, 153-168.

Aki, K., 1957. Space and time spectra of stationary stochastic waves, with special reference to microtremors. *B. Earthq. Res. Inst. Tokyo Univ.* 25, 415-457.

Aki, K., 1992. State of the art in volcanic seismology. In: Gasparini, P., Scarpa, R., Aki, K. (Eds.), Volcanic Seismology. *IAVCEI Proc. Volcanol.* 3, 3-10.

Aki, K., Koyanagi, R.Y., 1981. Deep volcanic tremor and magma ascent mechanism under Kilauea, Hawaii. *J. Geophys. Res.* 86, 7095-7110.

Aki, K., Richards, P., 2002. Quantitative seismology, 2nd ed. New York: University science books.

Allard, P., Behncke, B., D'Amico, S., Neri, M., Gambino, S., 2006. Mount Etna 1993–2005: Anatomy of an evolving eruptive cycle, *Earth-Science Rev. 78*, 85-114.

Almendros, J., Ibanez, J.M., Alguacil, G., Del Pezzo, E., Ortiz, R., 1997. Array tracking of the volcanic tremor source at Deception Island, Antarctica. *Geophys. Res. Lett.* 24, 3069-3072.

Amelung, F., Oppenheimer, C., Segall, P., Zebker, H., 2000. Ground deformation near Gada 'Ale Volcano, Afar, observed by radar interferometry. *Geophys. Res. Lett.* 27, 3093-3096.

Anant, K.S., and Dowla, F.U., 1997. Wavelet transform methods for phase identification in three-component seismograms. *B. Seism. Soc. Am.* 87, 1598-1612.

Aster, R., McIntosh, W., Kyle, P., Esser, R., Bartel, B., Dunbar, N., Johns, B., Johnson, J., Karstens, R., Curnik, C., McGowan, N., McNamara, S., Meertens, C., Pauly, B., Richmond, M., Ruiz, M., 2004. Real-time data received from Mount Erebus Volcano, Antarctica, *Eos Trans. AGU 85*, 97-100.

Aster, R., Zandomeneghi, D., Mah, S., McNamara, S., Henderson, D.B., Knox, H., Jones, K., 2008. Moment tensor inversion of very long period seismic signals from Strombolian eruptions of Erebus Volcano, *J. Volcanol. Geotherm. Res. 177*, 635-647.

Bajope, B., Mahinda, K., Alean, J., Caillet, M., Carniel, R, Fulle, M., Vetsch, P., 2006. Continuous ash plumes and active lava lake, *B. Glob. Volc. Net.* 31:01.

Barberi, F., Varet, J., 1970. The Erta 'Ale volcanic range, *B. Volc.* 34, 848-917.

Bardintzeff, J.-M., Gaudru, H., 2004. On 4-5 December 2004 visitors noted active hornitos but solidified lava lake, *B. Glob. Volc. Net.* 29:11.

Battaglia, J., K. Aki, Ferrazzini, V., 2005. Location of tremor sources and estimation of lava output using tremor source amplitude on the Piton de la Fournaise volcano: 1. Location of tremor sources, *J. Volcanol. Geotherm. Res.*, 147, 268-290.

Benoit, J., McNutt, S.R., 1997. New constraints on the source processes of volcanic tremor at Arenal volcano, Costa Rica, using broadband seismic data. *Geophys. Res. Lett.* 24, 449-452.

Bevington, P., Robinson, D., 2002. Data reduction and error analysis for the physical sciences. New York: McGraw-Hill, 3rd ed.

Burg, J.P., 1967. Maximum entropy spectral analysis. In: Childers (Ed.), Modern Spectral Analysis. New York: IEEE Press, pp. 34-41.

Calder, E.S., Harris, A.J.K., Peña, P., Pilger, P., Flynn, L.P., Fuentealba, G., Moreno, H., 2004. Combined thermal and seismic analysis of the Villarrica volcano lava lake, Chile. *Revista Geológica de Chile* 31(2), 259-272.

Carniel, R., Di Cecca, M., Rouland, D. 2003. Ambrym, Vanuatu (July-August 2000): spectral and dynamical transitions on the hours-to-days timescale. *J. Volcanol. Geotherm. Res.* 128, 1-13.

Chouet, B.A., 1992. A seismic model for the source of long period events and harmonic tremor. In: Gasparini, P., Scarpa, R., Aki, K. (Eds.), Volcanic Seismology. *IAVCEI Proc. Volcanol.* 3, 133-156.

Chouet, B., 1996. Long-Period volcano seismicity: its source and use in eruption forecasting. *Nature* 380, 309-316.

Chouet, B.A., De Luca, G., Milana, G., Dawson, P., Martini, M., Scarpa, R., 1998. Shallow velocity structure of Stromboli volcano, Italy, derived from small aperture array measurements of Strombolian tremor. *B. Seism. Soc. Am.* 88, 653-666.

Chui, C.K., 1997. Wavelets: a mathematical tool for signal processing. *SIAM*, Philadelphia, PA, USA.

Coifman, R.R., Wickerhauser, M.V., 1992. Entropy-based algorithms for best basis selection. *IEEE Trans. Inf. Theory* 38, 713-718.

Coifman, R.R., Donoho, D.L., 1995. Translation-invariant de-noising. In *Wavelets and Statistics* (Lecture Notes in Statistics, v. 103), A. Antoniadis and G. Oppenheim, eds. New York: Springer-Verlag, pp.125-150.

Dainelli, G., Marinelli, O., 1907. Vulcani attivi della Dancalia. *Rivista Geografica Italiana* 13, 261-270.

Daubechies, L., 1992. Ten lectures on wavelets. *SIAM*, Philadelphia, PA, USA.

De Martino, S. Falanga, M., Scarpa, R., Godano, C., 2005. Very-long-period volcanic tremor at Stromboli, Italy. *B. Seism. Soc. Am.*, 95:1186-1192.

Del Carlo, P. Vezzosi, L., Coltelli, M., 2004. Last 100 ka tephrostratigraphic record of Mount Etna, in *Mt. Etna: Volcano Laboratory*, A. Bonaccorso, ed., 77-89, *AGU Geophysical Monograph Series* 143.

Di Grazia, G., S. Falsaperla, Langer, H., 2006. Volcanic tremor location during the 2004 Mount Etna lava effusion, *Geophys. Res. Lett*., 33, L04304, doi:10.1029/2005GL025177 .

Falsaperla, S., Langer, H., Spampinato, S., 1998. Statistical analyses and characteristics of volcanic tremor on Stromboli Volcano (Italy). *B. Volc.* 60(2), 75-88.

Fehler, M.C., 1983. Observations of volcanic tremor at Mt. St Helens volcano. *J. Geophys. Res.* 88, 3476-3484.

Ferrucci, F., Godano, C., Pino, N.A., 1990. Approach to the volcanic tremor by covariance analysis: Application to the1989 eruption of Mt Etna (Sicily). *Geophys. Res. Lett.* 17, 2425-2428.

Francis, P., Oppenheimer, C., Stevenson, D., 1993. Endogenous growth of persistently active volcanoes, *Nature* 366, 554 - 557, doi:10.1038/366554a0.

Furumoto, M., Kunitomo, T., Inoue, H., Yamada, I., Yamaoka, K., Ikami, A. Fukao, Y., 1990. Twin sources of high-frequency volcanic tremor of Izu-Oshima Volcano, Japan. *Geophys. Res. Lett.* 17(1): doi: 10.1029/89GL03678. issn: 0094-8276.

Furumoto, M., Kunimoto, T., Inoue, H., Yamaoka, K., 1992. Seismic image of the volcanic tremor source at Izu-Oshima volcano, Japan. In: Gasparini, P., Scarpa, R., Aki, K. (Eds.), Volcanic Seismology. *IAVCEI Proc. Volcanol.* 3, 201-211.

Giggenbach, W.F., Kyle, P.R., Lyon, G.L., 1973. Present volcanic activity on Mt. Erebus, Ross Island, Antarctica. *Geology* 1, 135–156.

Goldstein, P., Chouet, B., 1994. Array measurements and modeling of sources of shallow volcanic tremor at Kilauea volcano, Hawaii. *J. Geophys. Res.* 99, 2637-2652.

Gottschämmer, E., Surono, I., 2000. Locating tremor and shock sources at Bromo Volcano. *J. Volcanol. Geotherm. Res.* 101, 199-209.

Grandjean, V., 2006. Molten lava lake observations as late as 3 January 2006, *Bull. Glob. Volc. Net.* 31:03.

Greenhall, C.A., 1991. Recipes for degrees of freedom of frequency stability estimators. *IEEE Trans. Inst. Measurement*, 40, 994-999.

Gutenberg, B., Richter, C.,1956. Earthquake magnitude, intensity, energy, and acceleration, *B. Seism. Soc. Am.* 46, 105-145.

Hamaguchi, H., Nishimura, T., Zana, N., 1992. Process of the 1977 Nyiragongo eruption inferred from the analysis of long-period earthquakes and volcanic tremors. *Tectonophysics* 209, 241-254.

Harrington, R.M., Brodsky, E.E., 2007. Volcanic hybrid earthquakes that are brittle-failure events. *Geophys. Res. Lett.* 34, L06308, doi:10.10129/2006GL028714.

Harris, A.J.L., 2008, Modeling lava lake heat loss, rheology, and convection, *Geophys. Res. Lett.*, 35, L07303, doi:10.1029/2008GL033190.

Harris, A.J.L., Stevenson, D.S., 1997. Thermal observations of degassing open conduits and fumaroles at Stromboli and Vulcano using remotely sensed data. *J. Volcanol. Geotherm. Res.* 76, 175-198.

Harris, A.J.L., Carniel, R., Jones, J., 2005. Identification of variable convective regimes at Erta Ale Lava Lake. *J. Volcanol. Geotherm. Res.*, 142, 207-223.

Harris, A.J.L., Flynn, L.P., Rothery, D.A., Oppenheimer, C., Sherman, S.B., 1999. Mass flux measurements at active lava lakes: Implications for magma recycling. *J. Geophys. Res.* 104 (B4), 7117-7136.

Hofstetter, A.S., Malone, S.D., 1986. Observations of volcanic tremor at Mt. St Helens in April and May 1980. *B. Seism. Soc. Am.* 76, 923-938.

Hyvärinen, A., Karhunen, J, Oja, E., 2000. Independent component analysis. New York: John Wiley and Sons.

Jain, Anil, M. Narasimha Murty, and Patrick Flynn, 1999. Data clustering: A review. *ACM Computing Surveys* 31 (3), 264-323.

Jaupart, C., Vergniolle, S., 1988. Laboratory models of Hawaiian and Strombolian eruptions, *Nature* 331, 58-60.

Jones, J., Carniel, R., Harris, A.J.L., Malone, S., 2006. Seismic characteristics of variable convection at Erta `Ale lava lake, Ethiopia, *J. Volcanol. Geotherm. Res.* 153, 64-79.

Julian, B.R., 1994. Volcanic tremor: nonlinear excitation by fluid flow. *J. Geophys. Res.* 99, 11859-11877.

Jurkevics, 1988. Polarization analysis of three-component array data. *B. Seis. Soc. Am.* 78, 1725-1743.

Kaminuma, K., 1994. The seismic activity of Mount Erebus in 1981–1990. *In*: Kyle, P.R. (Ed.), *Volcanological and Environmental Studies of Mount Erebus, Antarctica*. Antarctic Research Series, American Geophysical Union, Washington DC, pp. 35–50.

Kawakatsu, H., Kaneshima, S., Matsubayashi, H., Ohminato, T., Sudo, Y., Tsutsui, T., Uhira, K., Yamasato, H., Legrand, D., 2000. Aso94: Aso seismic

observation with broadband instruments. *J. Volcanol. Geotherm. Res.* 101, 129-154.

Kienle, J., Kyle, P.R., Estes, S., Takanami, R., Dibble, P.R., 1981. Seismicity of Mt. Erebus, 1980–81. *Antarct. J. US* 16 (5), 35–36.

Knight, R.L., Dibble, R.R., Aster, R.C., Kyle, P.R., Ameko, A.K., 1996. Digital recording of the Seismicity of Mount Erebus Volcano, November 1994–June 1996. *Antarct. J. US* 31 (2), 41–43.

Konstantinou, K.I., Schlindwein, V., 2002. Nature, wavefield properties and source mechanism of volcanic tremor: a review. *J. Volcanol. Geotherm. Res.* 119, 161-187.

Kyle, P.R., 1994. Volcanological and environmental studies of Mount Erebus, Antarctica. AGU Antarctic Research Series, 66, 162 pp.

Lay, T., Wallace, T.C., 1995. Modern global seismology. New York: Academic press.

Liang, J., Parks, T.W., 1996. A translation-invariant wavelet representation algorithm with applications. *IEEE Trans. Sig. Processing*, 44, 225-232.

Le Guern, F., 1987. Mechanism of energy transfer in the lava lake of Nyiragongo (Zaire), 1959-1977. *J. Volcanol. Geotherm. Res.* 31, 17-31.

Lilly, J.M., Park, J., 1995. Multiwavelet spectral and polarization analyses of seismic records. *Geophys. J. Int* 122, 1001-1021.

Mallat, S.G., 1999. A wavelet tour of signal processing. New York: Academic Press.

Martini, M., 1969. Studio di prodotti fumarolici di alcuni vulcani della catena dell'Erta Ale (Etiopia). *Rend. Soc. Min. Ital.* 25, 79-92.

McCoy, E.J., Percival, D.B., Walden, A.T., 1995. On the phase of least-asymmetric scaling and wavelet filters. *Technical Report* TR-95-15, Statistics Section, Imperial College of Science, Technology and Medicine, London, UK.

McNutt, S.R., 1996. Seismic monitoring and eruption forecasting of volcanoes : A review of the state-of-the-art and case histories. In: Scarpa, Tilling (Eds.), Monitoring and Mitigation of Volcanic Hazards. Springer, Berlin, pp. 100-146.

Minakami, T., 1960. Fundamental research for predicting volcanic eruptions (Part 1). *B. Earthq. Res. Inst. Univ. Tokyo* 38, 497-544.

Montalbetti, J.F., Kanasewich, K.R., 1970. Enhancement of teleseismic body phases with a polarisation filter. *Geophys. J. R. Astron. Soc.* 21, 119-129.

Nason, G.P., Silverman, B.W., 1995. The stationary wavelet transform and some statistical applications. In *Wavelets and Statistics* (Lecture Notes in Statistics, v. 103), A. Antoniadis and G. Oppenheim, eds. New York: Springer-Verlag, 281-299.

Neidel, N., Tanner, M.T., 1971. Semblance and other coherency measures for multichannel data. *Geophys.* 36, 483-497.

Nishimura, T., Hamaguchi, H., Ueki, S., 1995. Source mechanisms of volcanic tremor and low-frequency earthquakes associated with the 1988-89 eruptive activity of Mt Tokachi, Hokkaido, Japan. *Geophys. J. Int.* 121, 444-458.

Omori, F., 1894. On the aftershocks of earthquakes, *J. Coll. Sci. Imp. Univ. Tokyo* 7, 111-216.

Oppenheimer, C., Francis, P., 1998. Implications of longeval lava lakes for geomorphological and plutonic processes at Erta 'Ale volcano, north Afar. *J. Volcanol. Geotherm. Res.* 80, 101-111.

Oppenheimer, C., Francis, P, 1997. Remote sensing of heat, lava and fumarole emissions from Erta 'Ale volcano, Ethiopia. *Int. J. Rem. Sensing* 18, 1661-1692.

Oweiss, K.G., Anderson, D.J., 2007. Tracking signal subspace invariance for blind separation and classification of nonorthogonal sources in correlated noise. *EURASIP Journal on Advances in Signal Processing*, 2007 (37485).

Patanè, D., Di Grazia, G., Cannata, A., Montalto, P., Boschi, E. 2008. The shallow magma pathway geometry at Mt. Etna volcano. *Geochem. Geophys. Geosys.* 9, doi: 10.1029/2008GC002131.

Patrick, M.P., Smellie, J.L., Harris, A.J.L., Garbeil, H., Pilger, E., 2004. First recorded eruption of Mount Belinda volcano, South Sandwich Islands. *B. Volc.* 67(5), 415-422.

Pearson, K., 1901. On lines and planes of closest fit to systems of points in space. *Philosophical Magazine* 2 (6), 559–572.

Percival, D.B., Guttorp, P., 1994. Long-memory processes, the Allan variance and wavelets. In *Wavelets in Geophyics*, E. Foufoula-Georgious and P. Kumar, *eds*. San Diego: Academic Press, 325-344.

Percival, D.B., Mojfeld, H., 1997. Analysis of subtidal coastal sea level fluctuations using wavelets. *Journ. Am. Stat. Assoc*, 92, 868-880.

Percival, D.B., Walden, A.T., 2000. Wavelet methods for time series analysis, Cambridge University Press, Cambridge, U.K.

Power, J.A., Lahr, J.C., Page, R.A., Chouet, B.A., Stephens, C.D., Harlow, D.H., Murray, T.L., Davies, J.N., 1994. Seismic evolution of the 1989-90 eruption sequence of Redoubt volcano, Alaska. *J. Volcanol. Geotherm. Res.* 62, 69-94.

Ripepe, M., Poggi, P., Braun, T., Gordeev, E., 1996. Infrasonic waves and volcanic tremor at Stromboli, *Geophys. Res. Lett.* 23(2), 181–184.

Ripepe, M., Gordeev, E., 1999. Gas bubble dynamics model for shallow volcanic tremor at Stromboli, *J. Geophys. Res.* 104(B5), 10,639–10,654.

Ripepe M., Harris, A. J. L. Carniel, R. 2002. Thermal, seismic and infrasonic evidences of variable degassing rates at Stromboli volcano, *J. Volcanol. Geotherm. Res.*118 (3-4), 285-297.

Rivallin, P., Mougin, D., 2008. Trip report of Pierrette Rivallin and Dédé Mougin: *LAVE Bulletin* 79, May 2008.

Rowe, C., Aster, R., Kyle, P., Dibble, R., Schlue, J., 2000. Seismic and acoustic observations at Mount Erebus Volcano, Ross Island, Antarctica, 1994–1998. *J. Volcanol. Geotherm. Res.* 101, 105–128.

Rymer, H., van Wyk de Vries, B., Stix, J., Williams-Jones, G., 1998. Pit crater structure and processes governing persistent activity at Masaya Volcano, Nicaragua. *B. Volc.* 59, 345-355.

Saccorotti, G., Lockmer, I., Bean, C.J. Di Grazia, G., Patanè, D., 2007. Analysis of sustained long-period activity at Etna Volcano, Italy, *J. Volcanol. Geotherm. Res.* 160, 340-354.

Shaw, P.J.A., 2003. Multivariate statistics for the Environmental Sciences. Hodder-Arnold.

Shensa, M.J., 1992. The discrete wavelet transform: wedding the a Trous and Mallat algorithms. *IEEE Trans. Signal Processing*, 40, 2464-2482.

Sherburn, S., Scott, B.J., Nishi, Y., Sughihara, M., 1998. Seismicity at White Island volcano, New Zealand: a revised classification and inferences about source mechanism. *J. Volcanol. Geotherm. Res.* 83, 287-312.

Strang, G., 1993. Wavelet transforms versus Fourier transforms. *B. Am. Math. Soc.* 28(2), 288-305.

Swanson, D.A., Duffield, W.A., Jackson, D.B., Peterson, D.W., 1979. Chronological narrative of the 1969-71 Mauna Ulu eruption of Kilauea volcano, Hawaii. *USGS Prof. Pap.* 1056, 55 pp.

Tazieff, H., 1994. Permanent lava lakes: observed facts and induced mechanisms, *J. Volcanol. Geotherm. Res.* 63(1-2), pp. 3-11.

Thompson, G., McNutt, S.R., Tytgat, G., 2002. Three distinct regimes of volcanic tremor associated with the eruption of Shishaldin Volcano, Alaska 1999. *B. Volc.* 64(8), 535-547.

Vandecar, J.C., Crosson, R., 1990. Determination of teleseismic relative phase arrival times using multi-channel cross-correlation and least squares. *B. Seis. Soc. Am.* 80(1), 150-169.

Vidale, J., 1986. Complex polarization analysis of particle motion. *B. Seis. Soc. Am.* 76(5), 1393-1405.

Walden, A.D., Cristan, A.C., 1998. The phase-corrected undecimated discrete wavelet packet transform and the recurrence of high latitude interplanetary shock waves. *Proceedings of the Royal Society of London*, Series A, 454, 2243-2266.

Wasserman, J., 1997. Locating the sources of volcanic explosions and volcanic tremor at Stromboli volcano (Italy) using beam-forming on diffraction hyperboloids. *Phys. Earth & Plan. Int.* 104, 271-281.

Wegler, U., Seidl, D., 1997. Kinematic parameters of the tremor wavefield at Mt. Etna (Sicily). *Geophys. Res. Lett.* 24, 759-762

Witter, J.B., 2003. Convection of magma in volcanic conduits as a degassing mechanism at active volcanoes, *Ph.D. Thesis, Univ. Washington, Seattle, WA, USA.*

Woods, A.W., Cardoso, S.S. 1997. Bubble–melt separation as a trigger for basaltic volcanic eruptions, *Nature* 385, 518-520.

Wright, R., Flynn, L.P., 2004, Space-based estimate of the volcanic heat flux into the atmosphere during 2001 and 2002. *Geology* 32, p. 189-192.

Yirgu, G., Kirkos, W., Philpotts, A., MODIS/MODVOLC Thermal Alerts Team, 2005. Agitated lava lake during time of September 2005 earthquake swarm ~ 100 km S, *Bull. G. Volc. Net.* 30:09.